

MOLECULAR AND FUNCTIONAL CHARACTERIZATION
OF CARDIAC $Ca_v3.2$ T-TYPE CALCIUM CHANNELS

by

Laurence Sahagun David

BSc Biology (Magna Cum Laude), Centro Escolar University, 1993

MET, Simon Fraser University, 2003

A THESIS SUBMITTED IN PARTIAL FULFILLMENT OF THE
REQUIREMENTS FOR THE DEGREE OF

DOCTOR OF PHILOSOPHY

in

THE FACULTY OF GRADUATE STUDIES

(NEUROSCIENCE)

THE UNIVERSITY OF BRITISH COLUMBIA

(VANCOUVER)

JULY 2011

© Laurence Sahagun David, 2011

ABSTRACT

T-type calcium (Ca^{2+}) channels contribute to the normal development of the heart and are also implicated in pathophysiological states such as cardiac hypertrophy. Functionally distinct Ca_v3 T-type Ca^{2+} channel isoforms can be generated by alternative splicing from each of three different Ca_v3 genes ($\text{Ca}_v3.1$, $\text{Ca}_v3.2$ and $\text{Ca}_v3.3$), although it remains to be described whether specific splice variants are associated with developmental stages and pathological conditions. Using full length cDNA generated from rat cardiac tissues, this study identified ten major regions of alternative splicing and systematically identified alternative splice variants of cardiac $\text{Ca}_v3.2$ channels. Quantitative real-time PCR analysis on the mRNA expression of the most common variants revealed preferential expression of $\text{Ca}_v3.2(-25)$ splice variant channels in the newborn rat heart, whereas in the adult heart approximately equal levels of expression of both (+25) and (-25) exon variants was observed. In the adult stage of hypertensive rats, an increase in overall $\text{Ca}_v3.2$ mRNA expression and a shift towards the expression of $\text{Ca}_v3.2(+25)$ containing channels as the predominant form was observed. This is the first evidence to show that cardiac $\text{Ca}_v3.2$ is subject to considerable splicing. Moreover, this thesis is also the first study to show developmental and pathological changes in expression of specific splice variants of the $\text{Ca}_v3.2$ channels.

The biophysical characteristics of cloned $\text{Ca}_v3.2$ splice variants and T-type Ca^{2+} currents from dissociated cultured newborn ventricular myocytes were investigated using whole cell patch clamp analysis. This study showed variant-specific voltage-dependent facilitation (VDF) of $\text{Ca}_v3.2$ channels attributed to the exclusion of exon 25 in $\text{Ca}_v3.2$ transcripts. Lastly, this thesis is the first to provide evidence on VDF of T-type currents in rat ventricular myocytes.

PREFACE

A version of Chapter 2 has been published in the journal *Channels* (David, L.S., Garcia, E., Cain, S.C., Thau, E.M., Tyson, J.R., Snutch, T.P. 2010. Splice-variant changes of the Ca_v3.2 T-type calcium channel mediate voltage-dependent facilitation and associate with cardiac hypertrophy and development. *Channels* (Austin). 4(5):375-389). I designed all experiments and analyzed all results with input and feedback from my collaborators. I performed all screening and cloning of all splice variants in this thesis. Elana Thau helped me in generating cDNA libraries. Dr. Esperanza Garcia and Dr. Stuart Cain contributed to the whole cell recordings; Dr. John Tyson performed qRT-PCR and western blot analysis. I wrote the entire manuscript with subsequent editing from Dr. Terry Snutch and other authors. In Chapter 3, I also designed all experiments and analyzed all experimental results. I performed whole cell recordings and qRT-PCR analysis utilized in this chapter. Dr. Esperanza Garcia and Dr. Anamika Singh contributed to the whole cell recordings of cardiac myocytes. I wrote all of Chapter 3.

I also contributed to the electrophysiology section and cloned the Ca_v3.2 T-type Ca²⁺ channel splice variants used in Appendix 5 (Powell, K.L., Cain, S.M., Ng, C., Sirdesai, S., David, L.S., Kyi, M., Garcia, E., Tyson, JR, Reid, C.A., Bahlo, M., Foote, S.J., Snutch, T.P., O'Brien, T.J. 2009. A Ca_v3.2 T-type calcium channel point mutation has splice-variant-specific effects on function and segregates with seizure expression in a polygenic rat model of absence epilepsy. *The Journal of Neuroscience*. 29(2):371-380). In Appendix 3 (Nelson, M.T., Joksovic, P.M., Su, P., Kang, H-W., Van Deusen, A., Baumgart, J.P., David, L.S., Snutch, T.P., Barrett, P.Q., Lee, J-H., Zorumski, C.F., Perez-Reyes, E., and Todorovic, S.M. 2007. Molecular mechanisms of subtype-specific inhibition of neuronal T-type calcium channels by ascorbate. *The Journal of Neuroscience*. 27(46), 12577- 12583), I cloned the rat thalamic Ca_v3.2 utilized in the paper. I participated in the molecular biology section of Appendix 2 (Hildebrand, M.E., David, L.S., Hamid, J., Mulatz, K.,

Garcia, E., Zamponi, G.W. and Snutch, T.P. 2007. Selective inhibition of Ca_v3.3 T-type calcium channels by G_{αq/11}-coupled muscarinic acetylcholine receptors. *Journal of Biological Chemistry*. 282(29), 21043-21055) and Appendix 4 (Adams, P.J., Garcia, E., David, L.S., Mulatz, K.J., Spacey, S.D., Snutch, T.P. 2009. Ca_v2.1 P/Q-type calcium channel alternative splicing affects the functional impact of familial hemiplegic migraine mutations: Implications for calcium channelopathies. *Channels (Austin)*. 3(2):110-121). I also contributed to writing the review article shown in Appendix 1 (Snutch, T.P. and David, L.S. 2006. T-type calcium channels: An emerging therapeutic target for the treatment of pain. *Drug Discovery Research*. 67:404-415).

All animal procedures were performed in accordance with Canadian Council on Animal Care guidelines for animal research (UBC Animal Certificate Numbers A04-1003 and A08-0005).

TABLE OF CONTENTS

ABSTRACT	ii
PREFACE	iii
TABLE OF CONTENTS	v
LIST OF TABLES	ix
LIST OF FIGURES	x
LIST OF ABBREVIATIONS	xii
ACKNOWLEDGEMENTS	xvi
DEDICATION	xvii
1 INTRODUCTION	1
1.1 Calcium channels overview	1
1.1.1 Classes and nomenclature	1
1.1.2 Calcium channel biochemical composition	6
1.2 T-type calcium channels	8
1.2.1 T-type calcium channel expression	8
1.2.2 Biophysical properties	10
1.2.3 T-type channel pharmacology	11
1.2.4 Modulation of T-type calcium channels	16
1.3 Alternative splicing	22
1.3.1 Overview of calcium channel alternative splicing	23
1.3.2 Alternative splicing of T-type calcium channels	31
1.4 T-type calcium channels and the heart	34
1.4.1 Expression, functional roles and modulation	34
1.4.2 Developmental regulation and association in cardiac diseases	37
1.5 Voltage-dependent facilitation of calcium channels	41
1.5.1 Voltage-dependent facilitation of high voltage-activated calcium channels	41
1.5.2 Voltage-dependent facilitation of T-type channels	43
1.6 Thesis hypotheses and objectives	47
1.6.1 Hypothesis 1	47
1.6.2 Hypothesis 2	47

1.6.4 Hypothesis 3.....	48
1.6.5 Objectives.....	48
2 SPLICE-VARIANT CHANGES OF THE Ca_v3.2 T-TYPE CALCIUM CHANNEL MEDIATE VOLTAGE-DEPENDENT FACILITATION AND ASSOCIATE WITH CARDIAC HYPERTROPHY AND DEVELOPMENT.....	50
2.1 Introduction.....	50
2.2 Results	53
2.2.1 Alternative splicing generates multiple Ca _v 3.2 T-type variants with differential expression across development	53
2.2.2 Exclusion of exon 25 confers voltage-dependent facilitation and accelerates recovery from inactivation	67
2.2.3 The effect of cAMP and Gβ ₂ γ ₂ on Ca _v 3.2 voltage-dependent facilitation	77
2.2.4 Differential expression of Ca _v 3.2 exon 25 variants in hypertension-associated cardiac hypertrophy	79
2.3 Discussion.....	82
2.3.1 Splice variant specific expression of cardiac Ca _v 3.2 Ca ²⁺ channels in development and hypertrophy.....	82
2.3.2 Ca _v 3.2(-25) channels display faster recovery from inactivation and voltage- dependent facilitation	84
2.3.3 The magnitude of VDF of Ca _v 3.2(-25) splice variant currents is reduced by Gβ ₂ γ ₂	86
2.3.4 Potential relevance to cardiac pathophysiology	87
2.4 Materials and methods	88
2.4.1 Animals and tissue preparation	88
2.4.2 Histological staining.....	89
2.4.3 RT-PCR and short amplicon scanning	90
2.4.4 Construction of cDNA libraries and full length splice variant screening.....	93
2.4.5 Cloning of full-length Ca _v 3.2 alternative splice variants.....	93
2.4.6 Western blot analysis.....	94
2.4.7 Quantitative real-time-PCR (qRT-PCR)	95
2.4.8 Whole cell electrophysiology of transfected HEK cells	98
3 VOLTAGE-DEPENDENT FACILITATION OF T-TYPE CALCIUM CURRENTS IN NEONATAL RAT VENTRICULAR MYOCYTES.....	101
3.1 Introduction.....	101
3.2 Results	102
3.2.1 Expression of Ca ²⁺ channels in neonatal rat ventricular myocytes.....	102
3.2.2 Biophysical properties of T-type Ca ²⁺ currents in isolated ventricular myocytes	104
3.2.3 Voltage-dependent facilitation of T-type Ca ²⁺ currents in rat ventricular myocytes.....	109

3.3 Discussion.....	111
3.3.1 T-type Ca²⁺ channels are expressed in neonatal rat ventricular myocytes	111
3.3.2 Voltage-dependent facilitation of NRVM I_{CaT} is correlated with Ca_v3.2(-25) splice variant expression	112
3.3.3 Potential significance of voltage-dependent facilitation of T-type Ca²⁺ currents in neonatal ventricle	113
3.4 Materials and methods	117
3.4.1 Animals and reagents	117
3.4.2 Isolation of neonatal rat ventricular myocytes.....	117
3.4.3 RNA extraction and quantitative Real-Time-PCR (qRT-PCR).....	119
3.4.4 Whole cell patch clamp analysis of isolated neonatal ventricular myocytes	120
4 CONCLUSION	124
4.1 Overall significance.....	124
4.1.1 Identification and characterization of cardiac Ca_v3.2 alternative splice variants	124
4.1.2 Developmental and pathological expression of Ca_v3.2 alternative splice variants	126
4.2 Splice variant specific expression of Ca_v3.2 T-type Ca²⁺ channels during development and hypertrophy.....	129
4.2.1 Working hypothesis	129
4.2.2 Potential limitations	136
4.3. Voltage-dependent facilitation of Ca_v3.2 T-type channels	137
4.3.1 Working hypothesis	137
4.3.2 Potential limitations	139
4.4 Conclusion	140
4.4.1 General conclusions	140
4.4.2 Potential relevance of Ca_v3.2 alternative splicing in cardiac development and hypertrophy	141
4.4.3 Future directions.....	142
REFERENCES.....	145
APPENDIX 1: T-TYPE CALCIUM CHANNELS: AN EMERGING THERAPEUTIC TARGET FOR THE TREATMENT OF PAIN.....	167
APPENDIX 2: SELECTIVE INHIBITION OF Ca_v3.3 T-TYPE CALCIUM CHANNELS BY G_{αq11}-COUPLED MUSCARINIC ACETYLCHOLINE RECEPTORS	179
APPENDIX 3: MOLECULAR MECHANISMS OF SUBTYPE-SPECIFIC INHIBITION OF NEURONAL T-TYPE CALCIUM CHANNELS BY ASCORBATE	192

APPENDIX 4: Ca_v2.1 P/Q-TYPE CALCIUM CHANNEL ALTERNATIVE SPLICING AFFECTS THE FUNCTIONAL IMPACT OF FAMILIAL HEMIPLEGIC MIGRAINE MUTATIONS: IMPLICATIONS FOR CALCIUM CHANNELOPATHIES..... 199

APPENDIX 5: A Ca_v3.2 T-TYPE CALCIUM CHANNEL POINT MUTATION HAS SPLICE-VARIANT SPECIFIC EFFECTS ON FUNCTION AND SEGREGATES WITH SEIZURE EXPRESSION IN POLYGENIC RAT MODEL OF ABSENCE EPILEPSY . 211

LIST OF TABLES

Table 1.1. Neurological agents known to inhibit T-type currents.	13
Table 2.1. Identified cardiac Ca _v 3.2 T-type Ca ²⁺ channel variants.....	61
Table 2.2. Gating properties of Ca _v 3.2 alternative splice variants.	71
Table 2.3. Deactivation and recovery from inactivation of Ca _v 3.2 alternative splice variants.	74
Table 2.4. Primers utilized for exon scanning amplification.	92
Table 2.5. Oligonucleotide primers for qRT-PCR.....	97
Table 3.1. Biophysical properties of T-type Ca ²⁺ currents in isolated neonatal rat ventricular myocytes	105

LIST OF FIGURES

Figure 1.1. Calcium channel classifications	5
Figure 1.2. Topographical illustration of the α_1 calcium channel subunit.	7
Figure 1.3. Effectors with identified modulation sites in the $\text{Ca}_v3.2$ T-type channel	21
Figure 1.4 Mechanisms of modulation of $\text{Ca}_v3.2$ T-type Ca^{2+} channels by G protein-coupled receptors (GPCRs).	22
Figure 1.5. Patterns of alternative splicing in eukaryotic mRNA	29
Figure 1.6. Functionally relevant alternative splicing events in HVA channels.	30
Figure 1.7. Functionally relevant alternative splicing events in T-type channels.	33
Figure 1.8. Proposed mechanisms underlying the facilitation of native T-type calcium currents	46
Figure 2.1. Ca^{2+} channel expression in rat cardiac tissues and identification of $\text{Ca}_v3.2$ alternative splice variants.....	55
Figure 2.2. Topology of $\text{Ca}_v3.2$ channel showing the location of all in-frame and truncated carboxyl terminal variants.	59
Figure 2.3. Differential expression of $\text{Ca}_v3.2$ T-type Ca^{2+} channel alternative splice variants in newborn and adult cardiac tissues.	64
Figure 2.4. Spatial and developmental changes in the expression of $\text{Ca}_v3.2(+25)$ and $\text{Ca}_v3.2(-25)$ exon splice variants.	66
Figure 2.5. Representative data on the voltage-dependent properties of $\text{Ca}_v3.2$ alternative splice variants.	70
Figure 2.6. Alternative splicing affects the time course of recovery from inactivation and voltage-dependent facilitation of $\text{Ca}_v3.2$ T-type macroscopic currents.	72
Figure 2.7. The voltage-dependent facilitation of $\text{Ca}_v3.2(-25)$ T-type Ca^{2+} channels does not depend upon Ca^{2+}	75
Figure 2.8. Voltage-dependent facilitation differs in T-type Ca^{2+} channel isoforms.	76
Figure 2.9. The effect of $\text{G}\beta\gamma$ and cAMP on voltage-dependent facilitation (VDF) of cardiac $\text{Ca}_v3.2$ exon 25 alternative splice variants	78
Figure 2.10. Alteration of $\text{Ca}_v3.2(+25)$ and (-25) splice variant expression is associated with the hypertrophic SHR pathological phenotype.	81

Figure 3.1. Expression of HVA and LVA Ca²⁺ channels in dissociated neonatal rat ventricular myocytes (NRVM).....	103
Figure 3.2. Pharmacological and biophysical isolation of T-type Ca²⁺ currents in newborn ventricular myocytes.....	106
Figure 3.3. The potentiated recovery from inactivation properties of NRVM T-type Ca²⁺ currents is comparable to the recombinant Ca_v3.2(-25) alternative splice variant.	108
Figure 3.4. Neonatal rat ventricular myocytes display VDF properties which is correlated with high level of Ca_v3.2 minus exon 25 alternative splice variant.	110
Figure 3.5. Potential contribution of Ca_v3.2 T-type Ca²⁺ channel VDF in neonatal rat ventricle.....	116
Figure 4.1. Hypothetical pathway of the signaling mechanism potentially involved in the regulation of expression of Ca_v3.2 exon 25 splice variants.....	135

LIST OF ABBREVIATIONS

ANP: atrial natriuretic peptide

AOB: aortic banded heart

AngII: angiotensin II

AP: action potentials

AT₁: angiotensin II type I receptor

AV: atrioventricular

Ba²⁺: barium

Ca²⁺: calcium

CaM: calmodulin

CaMKII: calcium/calmodulin-dependent protein kinase II

CDF: calcium-dependent facilitation

CDI: calcium-dependent inactivation

CICR: calcium-induced calcium release

C-terminus: carboxyl terminus

D: aspartate

DADs: delayed afterdepolarizations

DHP: dihydropyridines

DNA: deoxyribonucleic acid

DRG: dorsal root ganglion

DTNB: 5, 5' dithio-bis(2-nitrobenzoic acid)

DTT: dithiothreitol

E: glutamate

EADs: early afterdepolarizations

E-C coupling: excitation-contraction coupling

ECG: electrocardiogram

ET-1: endothelin 1

FHM-1: familial hemiplegic migraine-1

GPCR: G protein-coupled receptors

GST: glutathione S-transferase

HCN: hyperpolarization-activated cyclic nucleotide gated channels

HDAC: histone deacetylase

HVA: high voltage-activated

HEK: human embryonic kidney

LVA: low voltage-activated

Mg: magnesium

mg: milligram

μg: microgram

mM: millimolar

μM: micromolar

ms: millisecond

mV: millivolt

Na: sodium

Na/Ca: sodium/calcium exchanger

NFAT: nuclear factor of activated T-cells

nM: nanomolar

NRSE: neuron-restrictive silencer element

NRSF: neuron-restrictive silencer factor

ORF: open reading frame

P: proline

PA: polyadenylation

PF: Purkinje fibers

PIP₂: phosphatidylinositol bisphosphate

PIP₃: phosphatidylinositol triphosphate

PKA: protein kinase A

PKC: protein kinase C

PMI: post-myocardial infarcted heart

R: arginine

Redox: reduction – oxidation

RT-PCR: reverse transcription polymerase chain reaction

RyR: ryanodine receptors

s: second

SA: sinoatrial

SHR: Spontaneously Hypertensive rats

Sr: strontium

τ_{act} : time constant of activation

TBA: tetrabutylammonium

TEA: tetraethylammonium

τ_{inact} : time constant of inactivation

UTR: untranslated region

V_{50act} : half activation potential

$V_{50inact}$: half inactivation potential

VDF: voltage-dependent facilitation

VDI: voltage-dependent inactivation

WKY: Wistar Kyoto rats

ACKNOWLEDGEMENTS

I would like to express my sincere gratitude to my supervisor, Terry Snutch for his support, understanding, guidance and direction throughout my PhD studies. Special thanks to Esperanza Garcia for teaching me electrophysiology and for her guidance, encouragement and comments in this thesis. Thank you to Dr. John Tyson for his support in molecular biology and feedback on this thesis. I would like to thank my supervisory committee, Vanessa Auld, Edwin Moore, and Brian MacVicar for their direction and advice.

Thank you to all past and present members of Snutch lab. It has been a pleasure collaborating and working with you all. I am also thankful to the Heart and Stroke Foundation of Canada and UBC W.C. Koerner Fellowship for providing me with doctoral research funding during my PhD studies.

To all my friends, thank you for your support and encouragement. I would like to thank my children for inspiring me to finish my PhD. Lastly to my late wife Con, thanks for the support, love and inspiration. This is for you!

DEDICATION

In my wife's loving memory

To my sons, Tophy and Troy

And To my Saviour, Jesus Christ

1 INTRODUCTION

Calcium (Ca^{2+}) ions crucially contribute to numerous physiological processes and cells have evolved multiple mechanisms to finely control Ca^{2+} transport. Amongst these modes of transport, voltage-gated Ca^{2+} channels play a major role in the cellular physiology and pathology of many tissues including the heart. In particular, cardiac T-type Ca^{2+} channels are thought to play significant roles during cardiac development and disease. These include contributions to cardiac pacemaking, automaticity, conduction and excitation-contraction (E-C) coupling. This thesis focused on the identification, profiling and functional characterization of alternative splice variants of $\text{Ca}_v3.2$ T-type channels, one of the two major T-type isoforms expressed in the mammalian heart.

1.1 Calcium channels overview

Voltage-gated Ca^{2+} channels are ubiquitously expressed throughout cells and tissues and are involved in numerous physiological processes including neuronal firing, cardiac excitability, hormone secretion, gene expression, and cell growth and proliferation. They are also implicated in the pathogenesis in over a dozen distinct diseases of the nervous and cardiovascular systems. Phenotypically, Ca^{2+} channels are divided into two major classes – the high voltage-activated (HVA) and low voltage-activated (LVA) Ca^{2+} channels. Detailed description of various classes and biochemical composition of Ca^{2+} channels are discussed in this section.

1.1.1 Classes and nomenclature

There are ten known genes that encode distinct α_1 pore-forming subunits in the Ca^{2+} channel family (Figure 1.1). Historically, identification of Ca^{2+} channels by several laboratories

over the years has led to numerous ways of naming the channels. These include; phenomenological nomenclature HVA versus LVA and consist of the L; T; N; P/Q; and R; types), clone nomenclature (α_{1A} , α_{1B} , α_{1C} , α_{1H} , etc.), and gene nomenclature (for example *CACNA1A*, *CACNA1G*, *CACNA1H*, *CACNA1I*) (Lory et al., 1997; Hille, 2001). In 2000, a more systematic nomenclature was adopted based on the well defined potassium channel nomenclature (Chandy and Gutman, 1993; Ertel et al., 2000). Under this naming system, Ca^{2+} channels were named using the chemical symbol of the principal permeating ion (Ca) with the principal regulator (voltage) indicated as a subscript (Ca_v) (Ertel et al., 2000; Catterall et al., 2003). The numerical identifier corresponds to the Ca_v channel α_1 subunit gene family (i.e., 1, 2 and 3) and the order of discovery of the α_1 subunit within that family (Figure 1.1).

According to this nomenclature, the Ca_v1 family includes $\text{Ca}_v1.1$, $\text{Ca}_v1.2$, $\text{Ca}_v1.3$ and $\text{Ca}_v1.4$ which correspond to α_{1S} , α_{1C} , α_{1D} , and α_{1F} , respectively. All Ca_v1 Ca^{2+} channels mediate L-type Ca^{2+} currents. On the other hand, the Ca_v2 family ($\text{Ca}_v2.1$, $\text{Ca}_v2.2$ and $\text{Ca}_v2.3$ previously α_{1A} , α_{1B} , and α_{1E}) mediate P/Q-, N- and R-type currents, respectively. Lastly, T-type Ca^{2+} channels belong to the Ca_v3 family which includes $\text{Ca}_v3.1$, $\text{Ca}_v3.2$ and $\text{Ca}_v3.3$ (previously α_{1G} , α_{1H} , and α_{1I} , respectively). Brief descriptions of the expression, functional roles, and biophysical and pharmacological properties of the ten Ca^{2+} channel subtypes are discussed in this section.

The Ca_v1 channel subfamily are generally characterized by large single channel conductances, minimal voltage-dependent inactivation and significant Ca^{2+} -dependent inactivation (Hille, 2001; Snutch et al., 2005). Pharmacologically, Ca_v1 channels are potently blocked by phenylalkylamines, benzothiazapines and dihydropyridines (DHPs) (Fleckenstein, 1983; Fox et al., 1987; Hockerman et al., 1997). $\text{Ca}_v1.1$ channels are primarily expressed in skeletal muscles where they act as the voltage-sensor for E-C coupling (Rios and Brum, 1987;

Tanabe et al., 1988; Bean, 1989a; Tsien et al., 1991; Miller, 1992). $Ca_v1.2$ channels are expressed in the nervous system with high level of expression detected in the olfactory bulb, cerebellum, striatum, thalamus, hypothalamus and cortex and low levels in medulla, pons and spinal cord (Snutch et al., 1991; Hell et al., 1993). $Ca_v1.2$ channels are the main Ca^{2+} channels in the heart and smooth muscles where they are known to define the shape of the action potentials (APs) and to mediate excitation and contraction (Reuter et al., 1988; Tanabe et al., 1990; Bers and Perez-Reyes, 1999; Bers, 2001). $Ca_v1.3$ channels are present in the cell bodies and proximal dendrites of the central neurons as well as in endocrine, amacrine and cochlear hair cells (Hell et al., 1993; Ihara et al., 1995; Kollmar et al., 1997; Morgans, 1999; Habermann et al., 2003; Liu et al., 2004). In the heart, $Ca_v1.3$ channels are present in atria and sino-atrial (SA) nodes where they are reported to contribute to cardiac pacemaking (Zhang et al., 2002; Mangoni et al., 2003; Mangoni and Nargeot, 2008). Lastly, $Ca_v1.4$ channels are known to have important roles in neurotransmitter release in retinal photoreceptors and bipolar cells (Koschak et al., 2003; Baumann et al., 2004; McRory et al., 2004).

Ca_v2 channels are primarily expressed in the central and peripheral nervous systems. They are primarily involved in the release of neurotransmitters in response to presynaptic APs. These channels are known to bind directly with several proteins of the presynaptic exocytotic machinery and may form part of the docking complex for synaptic vesicles (Catterall, 2000). Pharmacologically, they are relatively insensitive to DHPs but are specifically blocked with high affinity by peptide toxins from spiders and marine snails (Miljanich and Ramachandran, 1995).

$Ca_v2.1$ channels are highly expressed in the mammalian brain and peripheral nervous system (Mori et al., 1991; Starr et al., 1991) where they play an important role in neurotransmission. They are known to be potently blocked by the peptide ω -agatoxin IVA from funnel web spider venom (Randall and Tsien, 1995). The $Ca_v2.2$ channels conduct N-type Ca^{2+}

currents and are potently blocked by the peptides ω -conotoxin GVIA and ω -conotoxin MVIIA and MVIIC (McCleskey et al., 1987; Catterall et al., 2003). N-type channels play important roles in the sensation and transmission of pain signals (McGivern and McDonough, 2004; Swayne and Bourinet, 2008; Zamponi et al., 2009). $Ca_v2.3$ channels conduct R-type currents and are blocked by the synthetic peptide SNX-482 (Newcomb et al., 1998). They are expressed in the nervous, endocrine, male reproductive and gastrointestinal systems (Grabsch et al., 1999; Westenbroek and Babcock, 1999; Lu et al., 2004; Jing et al., 2005; Wakamori and Imoto, 2009). These channels play important roles in neurotransmitter release and synaptic plasticity (Kubota et al., 2001; Breustedt et al., 2003; Dietrich et al., 2003), pain sensing (Saegusa et al., 2000), hormone secretion and glucose homeostasis (Pereverzev et al., 2002).

Ca_v3 T-type channels are generally insensitive to L-type blockers and to toxins that block Ca_v2 channels. The three types, $Ca_v3.1$, $Ca_v3.2$ and $Ca_v3.3$, are expressed throughout the body including nervous tissue, heart, kidney, smooth muscle, sperm, uterus and endocrine organs (reviewed in (Perez-Reyes, 2003)). The biophysical properties, functional and pathological roles of T-type Ca^{2+} channels are discussed in more detail in subsequent sections.

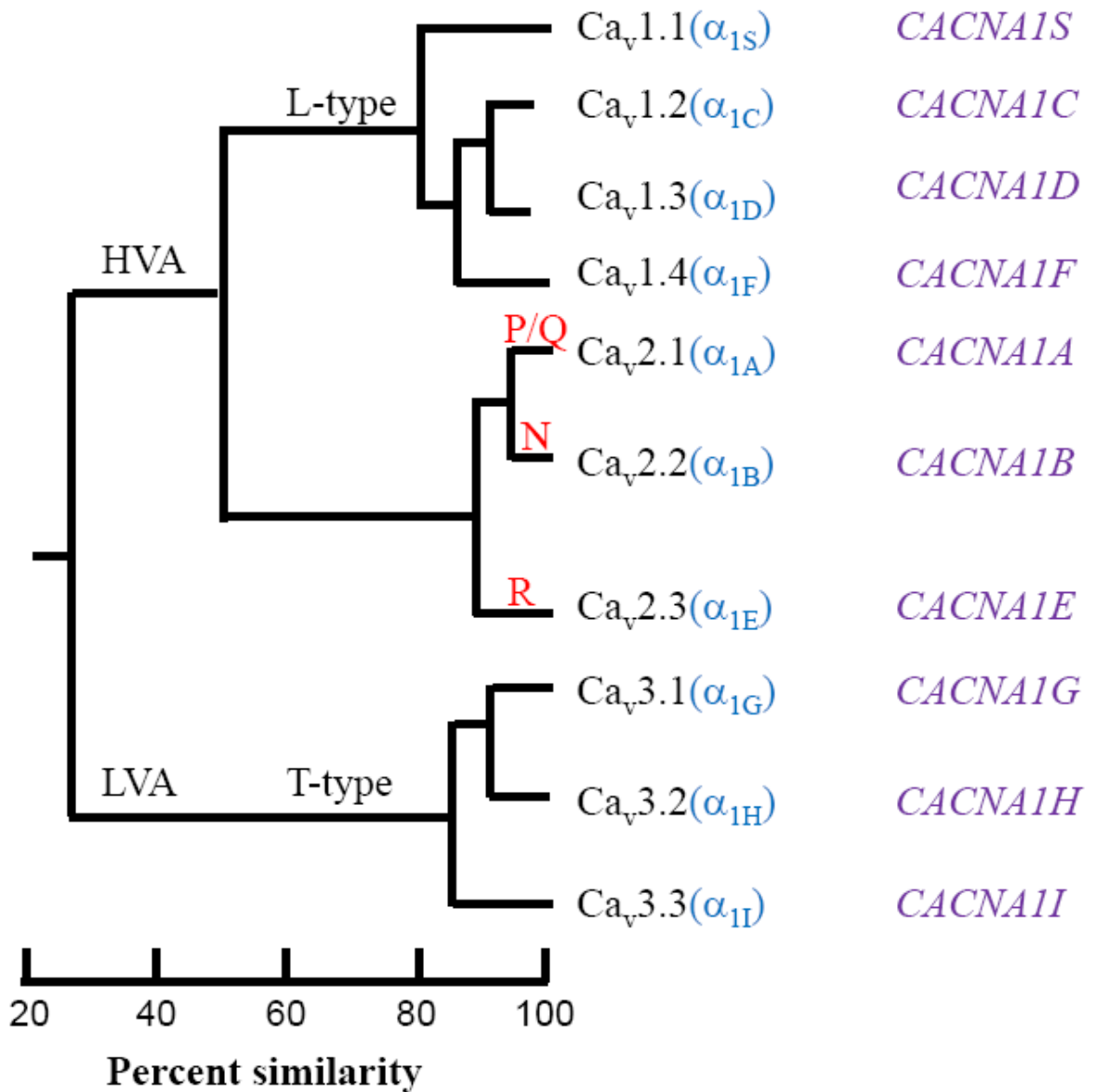


Figure 1.1. Calcium channel classifications.

Voltage-gated Ca^{2+} channels are divided into major classes – the high voltage-activated (HVA) and low voltage-activated (LVA) channels. HVA channels are further subdivided into Ca_v1 and Ca_v2 subfamilies and LVA comprises the Ca_v3 subfamily. The Ca_v nomenclature (black) is currently the official naming system for voltage-gated Ca^{2+} channels. Voltage-gated Ca^{2+} channels are also named according to the type of Ca^{2+} currents recorded from native tissues for instance L-, N-, P/Q-, R and T-types. Clone nomenclatures for example α_{1A} or α_{1E} are shown in blue. The official gene names are listed in the right panel of the figure (purple) (Lory et al., 1997; Ertel et al., 2000; Hille, 2001).

1.1.2 Calcium channel biochemical composition

Insight into the molecular basis for the differences in the functional properties of Ca^{2+} channels initially required the identification of channel protein structure. The protein composition of Ca^{2+} channels was first determined from the pioneering studies by Campbell, Catterall, Hoffman and Glossmann laboratories (Striessnig et al., 1987; Takahashi et al., 1987; Ruth et al., 1989; Jay et al., 1990). The transverse tubule membranes of skeletal muscle served as the primary biochemical preparation for studying the Ca^{2+} channel structure. Initial purification studies from this preparation revealed that skeletal L-type Ca^{2+} channels contain α_1 , β and γ subunits (Curtis and Catterall, 1984). Subsequent studies of these L-type channels revealed a more complex protein and it is now known that they are a large multimeric complex containing an equal stoichiometric ratio of α_1 pore-forming subunit and auxiliary subunits α_2 , δ , β , and γ (Hosey et al., 1987; Leung et al., 1987; Striessnig et al., 1987; Takahashi et al., 1987; Catterall, 2000).

The amino acid composition of the Ca^{2+} channel α_1 subunits revealed similarities to the predicted transmembrane structures of the pore-forming α_1 subunits of sodium (Na^+) channels (Tanabe et al., 1987). The amino acid sequences are organized into four homologous domains (I – IV) with each domain containing six transmembrane segments (S1 to S6), and a pore-forming loop between transmembrane segments S5 and S6 (Catterall, 2000) (Figure 1.2). The fourth segment (S4) contains five to six positively charged arginine and lysine residues, and serves as the major voltage sensor component. The pore-forming loop is responsible for the selectivity and permeation properties of the channels (Kim et al., 1993). The transmembrane segments and pore regions of all 10 Ca_v subunits are well conserved. Overall, amino acid sequences of α_1 subunits are over 70% identical within a channel subfamily while less than 40% identical between channel subfamilies (reviewed in (Ertel et al., 2000; Catterall et al., 2003). Of Ca_v members, the

T-type channels exhibit the least amount of sequence identity compared to other classes.

Analysis of the T-type channel amino acid sequences revealed a lack of the structural motif for the β subunit binding site conserved across HVA Ca_v I-II linker. Hence, the association of auxiliary subunits typically present among HVA channels is unlikely to play a significant role in native T-type channels (Dolphin et al., 1999; Dubel et al., 2004).

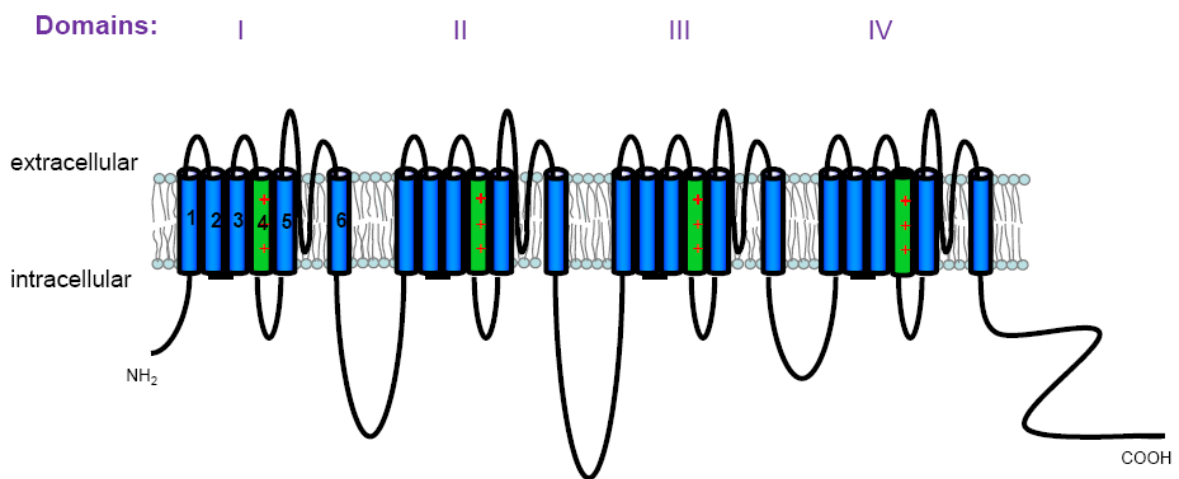


Figure 1.2. Topographical illustration of the α_1 calcium channel subunit.

All ten Ca^{2+} channel α_1 subunits have four homologous domains (labeled I to IV). Each domain is composed of six transmembrane segments (labeled 1 to 6 in domain I). The loop located between segments 5 and 6 forms the channel pore-forming loop. The 4th transmembrane segments (green) are formed by positively charged amino acids and formed the voltage sensor. The amino (NH₂), C-terminus (COOH) and interdomain linkers are all intracellular.

1.2 T-type calcium channels

The Ca_v3 T-type channels are widely expressed throughout the body including the heart, nervous tissue, kidney, smooth muscle and many endocrine organs. Some of the important roles that T-type channels contribute are neuronal firing, hormonal secretion and smooth muscle contraction. Importantly, they are also implicated in the pathophysiology of certain diseases such as epilepsy, chronic pain, hypertension and cardiac hypertrophy. In general, the biophysical properties of T-type channels recorded from various cell types are similar although differences have been noted in their kinetic properties, second-messenger-dependent modulation and sensitivity to pharmacological agents (Perez-Reyes, 2003, 2006). These differences can largely be explained by the existence of three main types of T-type channels: $Ca_v3.1$, $Ca_v3.2$ and $Ca_v3.3$ isoforms encoded by *CACNA1G*, *CACNA1H*, and *CACNA1I*, respectively (Figure 1.1). Extensive studies using Northern and dot blots, *in situ* hybridization and RT-PCR have been used to characterize the expression of the three Ca_v3 channels in various cells and tissues (Cribbs et al., 1998; Perez-Reyes et al., 1998; Talley et al., 1999; McRory et al., 2001; Perez-Reyes, 2003; Yunker and McEnery, 2003). Discussion in this section focuses on the general tissue expression, biophysical, pharmacological and modulation of T-type channel isoforms. More detailed discussions on the expression, properties, functional and pathological roles of T-type channels in the cardiovascular system are presented in section 1.4.

1.2.1 T-type calcium channel expression

All Ca_v3 channels are present in the central and peripheral nervous systems. $Ca_v3.1$ channels are highly expressed in inferior olivary neurons, thalamic relay neurons, cerebellar Purkinje neurons, subthalamic nucleus, the hippocampus, olfactory bulb, caudal thalamus, amygdala, cerebral cortex, brainstem and spinal cord (Talley et al., 1999; Monteil et al., 2000a;

McRory et al., 2001). $Ca_v3.2$ channels are reported in thalamic reticular neurons, olfactory tubercles, subthalamic nucleus, basal ganglia, hippocampus, olfactory bulb, caudal thalamus, sympathetic ganglion neurons, and dorsal root ganglia (White et al., 1989; Talley et al., 1999; McRory et al., 2001; Lee et al., 2002). $Ca_v3.3$ has been shown to be present in subthalamic nucleus, thalamic reticular neurons, basal ganglia, olfactory tubercles, nucleus accumbens and the striatum (Huguenard, 1999; Lee et al., 1999b; Talley et al., 1999; Monteil et al., 2000b; McRory et al., 2001).

T-type channels have also been found in the reproductive tissues such as the testes (Jagannathan et al., 2002; Son et al., 2002) and the uterus (Ohkubo et al., 2005). They are also reported to be present in adrenal glands (Enyeart et al., 1993; Mlinar et al., 1993; Chen et al., 1999; Schrier et al., 2001), pituitary glands (Talley et al., 1999) and in β -cells of the Islets of Langerhans in the pancreas (Ashcroft et al., 1990; Sala and Matteson, 1990; Parsey and Matteson, 1993).

Both $Ca_v3.1$ and $Ca_v3.2$ channels are expressed in the kidneys with $Ca_v3.2$ being predominantly present in renal smooth muscles and $Ca_v3.1$ in the renal tubules (Cribbs et al., 1998; Williams et al., 1999; Andreasen et al., 2000; Hansen et al., 2001). T-type Ca^{2+} currents (I_{CaT}) have been recorded in embryonic and newborn skeletal muscles (Beam and Knudson, 1988; Gono and Hasegawa, 1988; Berthier et al., 2002). I_{CaT} has also been recorded in smooth muscle myocytes cells isolated from the colon (Koh et al., 2001), coronary arteries (Ganitkevich and Isenberg, 1991; Mishra and Hermsmeyer, 1994; Quignard et al., 1997), aortas (Akaike et al., 1989), cerebral arteries (Hirst et al., 1986) and bronchi (Yamakage et al., 2001). RT-PCR analysis of smooth muscle myocytes has revealed the presence of both $Ca_v3.1$ and $Ca_v3.2$ channels (Gustafsson et al., 2001). Cardiac T-type channels consist of two main types: $Ca_v3.1$ and $Ca_v3.2$ (see Section 1.4).

1.2.2 Biophysical properties

The differential expression of Ca_v3 channels in diverse cell types suggests that these Ca²⁺ channels perform unique physiological functions. For example, in the nervous system all three T-type isoforms are present whereas in the heart only Ca_v3.1 and Ca_v3.2 channels are expressed. This differential expression likely account for differences in the electrophysiological properties observed for native T-type currents recorded from various cell types.

T-type channels have single channel conductances ranging between 6 and 8 pS in the presence of isotonic (110 mM) Ca²⁺ or barium (Ba²⁺) (Carbone and Lux, 1984; Droogmans and Nilius, 1989), ~5 pS in 10 mM Ca²⁺ (Balke et al., 1992) and 1 pS in 2 mM Ca²⁺ (Huguenard, 1996) demonstrating Ca²⁺-concentration-dependent ionic conduction in the T-type channel pore. The conduction of divalent ions differs in all three isoforms. In recombinant Ca_v3.1 channels, the current amplitude is larger in the presence of Ca²⁺ than in Ba²⁺. On the other hand, Ca²⁺ currents are smaller than Ba²⁺ currents in Ca_v3.2 channels while for Ca_v3.3 currents are approximately equal with Ba²⁺ and Ca²⁺ (McRory et al., 2001; Kaku et al., 2003).

The threshold for activation of T-type channels has been reported to be between -75 and -60 mV with half-maximal activation between -45 and -40 mV (McDonald et al., 1994; Huguenard, 1996; Perez-Reyes et al., 1998; Klockner et al., 1999; Kozlov et al., 1999; Perez-Reyes, 2003; Lacinova, 2005; Talavera and Nilius, 2006). At threshold potentials, T-type currents initially activate and inactivate slowly and then become faster with stronger depolarizations (Randall and Tsien, 1997; Perez-Reyes, 2003). T-type half maximal inactivation is generally between -80 and -60 mV (Vassort and Alvarez, 1994; Huguenard, 1996; Klockner et al., 1999; Talavera and Nilius, 2006). The overlapping activation and inactivation potential of T-type channels generates currents at steady state conditions called “window” currents (Vassort

and Alvarez, 1994; Chemin et al., 2000; Perez-Reyes, 2003; Talavera and Nilius, 2006). The magnitude of window currents has been estimated in heterologous expression system (Chemin et al., 2000).

In terms of activation and inactivation kinetics, comparison of the three T-type isoforms has revealed that recombinant Ca_v3.1 and Ca_v3.2 channels exhibit comparable properties, while the Ca_v3.3 subtype possesses distinct kinetics (Perez-Reyes et al., 1998; Klockner et al., 1999; Klugbauer et al., 1999; Kozlov et al., 1999; Lee et al., 1999b; Williams et al., 1999; McRory et al., 2001). The Ca_v3.1 and Ca_v3.2 isoforms have faster activation and inactivation kinetics, while the Ca_v3.3 channel activation and inactivation kinetics are both significantly slower. All three T-type isoforms have characteristically slower deactivation kinetics compared to the HVA channels with Ca_v3.3 being fastest and Ca_v3.1 the slowest (Klockner et al., 1999; Kozlov et al., 1999; Serrano et al., 1999; Monteil et al., 2000b; Perez-Reyes, 2003; Talavera and Nilius, 2006). The rates of recovery from inactivation of T-type channels are also faster than any of the HVA channels with Ca_v3.1 possessing the fastest time constants followed by Ca_v3.3 and slowest for Ca_v3.2 (Klockner et al., 1999; Chemin et al., 2002). Overall, the unique kinetic properties of T-type channels can serve as a valuable tool in distinguishing T-type isoforms, particularly in native cells and tissues. More importantly, their unique properties are predicted to distinctly affect intracellular Ca²⁺ influx and affect Ca²⁺ homeostasis and cellular physiology.

1.2.3 T-type channel pharmacology

With the successful cloning of the three Ca²⁺ channel genes encoding for T-type isoforms, our knowledge and understanding of the pharmacology of these channels has greatly improved. This section discusses current information concerning the pharmacology of T-type channels in both native and recombinant channels with emphasis given to neurological and

cardiovascular agents, toxins and polyvalent ions (for reviews see (Perez-Reyes, 2003; Yunker, 2003; Lacinova, 2005; Snutch and David, 2006) (Appendix 1). Although, these agents selectively target T-type channels for therapeutic purposes, these agents also block other ion channels. An understanding of the pharmacological properties of T-type channels allows the isolation of their relative contribution in native systems from that of other conductances. For example, in the heart the application of a specific blocker for Ca_v3.1 channels would permit studying the properties of Ca_v3.2 (and vice versa).

A number of neurological agents have been shown to block T-type channels at therapeutically-relevant levels (Table 1.1). These include antiepileptics (e.g., zonisamide, ethosuximide, and methyl-phenyl-succinimide(MPS) (Coulter et al., 1990; Kostyuk et al., 1992; Suzuki et al., 1992; Kito et al., 1996; Todorovic et al., 2000; Gomora et al., 2001), anticonvulsant (phenytoin) (Todorovic et al., 2000), diphenylbutylpiperidines neuroleptics (e.g., pimozide, flunarizine and penfluridol) (Enyeart et al., 1990a; Enyeart et al., 1990b; Opler and Feinberg, 1991; Santi et al., 2002), butyrophenone antipsychotic (haloperidol) (Santi et al., 2002) and general anaesthetics (e.g., isoflurane and propofol) (Todorovic and Lingle, 1998; Todorovic et al., 2000; Camara et al., 2001). The efficacy of these agents in blocking T-type channels indicates that T-type channels are important therapeutic targets for the treatment and management of a number of neurological conditions including epilepsy, pain and psychosis and possibly towards the management of cardiovascular disorders. Considering that T-type channels are upregulated in cardiac hypertrophy (Section 1.4.2), it would be relevant to investigate whether these agents affect the activity of T-type channels in the hypertrophic state.

Table 1.1. Neurological agents known to inhibit T-type currents.

Pharmacological agent	Tissue/Cell	T-type	IC ₅₀ (μM)	Reference
Zonisamide	cortical neurons	I _{CaT}	~500	Suzuki et al., 1992
	neuroblastoma cells	I _{CaT}	~50	Kito et al., 1996
Ethosuximide	ventrobasal thalamic neurons	I _{CaT}	200	Coulter et al., 1990
	dorsal root ganglia	I _{CaT}	7	Kostyuk et al., 1992
	heterologous expression (HEK cells)	Ca _v 3.1	12000	Gomora et al., 2001
		Ca _v 3.2	22000	Todorovic et al., 2000
MPS	ventrobasal thalamic neurons	I _{CaT}	1100	Coulter et al., 1990
	dorsal root ganglia	I _{CaT}	190	Todorovic et al., 2000
	heterologous expression (HEK cells)	Ca _v 3.1	1950	Gomora et al., 2001
		Ca _v 3.2	3000	Gomora et al., 2001
		Ca _v 3.3	1820	Gomora et al., 2001
Phenytoin	dorsal root ganglia	I _{CaT}	8	Todorovic et al., 2000
	heterologous expression (HEK cells)	Ca _v 3.1	140	Todorovic et al., 2000
		Ca _v 3.2	8.3	Todorovic et al., 2000
Pimozide	heterologous expression (HEK cells)	Ca _v 3.1	0.04	Santi et al., 2002
		Ca _v 3.2	0.06	Santi et al., 2002
		Ca _v 3.3	0.04	Santi et al., 2002
Penfluridol	heterologous expression (HEK cells)	Ca _v 3.1	0.11	Santi et al., 2002
		Ca _v 3.2	0.07	Santi et al., 2002
		Ca _v 3.3	0.10	Santi et al., 2002
Flunarizine	heterologous expression (HEK cells)	Ca _v 3.1	0.53	Santi et al., 2002
		Ca _v 3.2	3.5	Santi et al., 2002
		Ca _v 3.3	0.84	Santi et al., 2002
Haloperidol	heterologous expression (HEK cells)	Ca _v 3.1	1.2	Santi et al., 2002
		Ca _v 3.2	1.4	Santi et al., 2002
		Ca _v 3.3	1.3	Santi et al., 2002
Isoflurane	dorsal root ganglia	I _{CaT}	303	Todorovic & Lingle, 1998
	atrial myocytes	I _{CaT}	230	Camara et al., 2001
Propofol	heterologous expression (HEK cells)	Ca _v 3.1	21	Todorovic et al., 2000
		Ca _v 3.2	27	Todorovic et al., 2000

In general, T-type channels have been implicated in the pathogenesis of a number of cardiovascular diseases (Vassort and Alvarez, 1994; Vassort et al., 2006). The inhibition of T-type channels has been reported to have clinical importance in the treatment and management of a variety of cardiovascular diseases including hypertension and arrhythmia. Mibefradil is widely used as an antihypertensive drug and chronic stable angina pectoris agent (Perez-Reyes, 2003; Yunker, 2003; Snutch and David, 2006). This drug blocks both HVA and LVA Ca channels with

approximate IC_{50} values between 0.3 μ M and 20 μ M for HVA and 1 μ M for LVA channels (Jimenez et al., 2000). The mechanism of the T-type channel blockade by mibefradil was originally thought to be state-dependent; however, in a study by Martin and co-authors mibefradil was shown to be insensitive to voltage, ruling out state dependence as the mechanism of drug action (Martin et al., 2000). Efonidipine, an orally active antihypertensive and antianginal agent, has also been reported to block both HVA and LVA channels (Masumiya et al., 1997; Masumiya et al., 1998). It inhibits both cloned T-type channels expressed in baby hamster kidney (BHK) cells and in *Xenopus* oocytes, as well as native I_{CaT} in cardiac myocytes (Furukawa et al., 2004; Tanaka et al., 2004; Tanaka et al., 2008). The R(-)-enantiomer of efonidipine was reported to be more selective to block native myocardial I_{CaT} than I_{CaL} (85% inhibition of I_{CaT} versus no effect on I_{CaL} at 1 μ M) (Tanaka et al., 2004). Bepridil, another widely used antiarrhythmic and antianginal agent is reported to inhibit cloned $Ca_v3.2$ channels with an IC_{50} of ~400 nM (Uchino et al., 2005). In addition to the above compounds, recent studies have made progress towards the design and synthesis potentially selective T-type channel blockers (Yang et al., 2008; Uebele et al., 2009).

Divalent inorganic ions (e.g., Ni^{2+} , Zn^{2+} , Co^{2+}) were some of the first agents used to inhibit native I_{CaT} (Yunker, 2003). The high sensitivity of I_{CaT} to block by Ni^{2+} was considered one of the defining characteristics of these Ca^{2+} channels. In confirmation, whole cell patch clamp analysis of cloned Ca_v3 channel isoforms expressed in both HEK-293 cells and *Xenopus* oocytes showed sensitivity to inhibition by Ni^{2+} with IC_{50} values ranging from 12 to 250 μ M in HEK-293 cells and from 5.7 to 167 μ M in oocytes (Lee et al., 1999a). Among the three T-type isoforms, $Ca_v3.2$ is the most sensitive to Ni^{2+} . Using chimeric channels and site-directed mutagenesis, the structural determinant for inhibition was identified to be dependent on a histidine residue (H^{191}) in the $Ca_v3.2$ S3 and S4 loop of domain I and which is predicted to help

form a Ni²⁺ binding pocket on the extracellular surface of the channel (Kang et al., 2006; Kang et al., 2010). Both Ca_v3.1 and Ca_v3.3 channels have a glutamine residue instead of histidine at this site making them less sensitive to Ni²⁺. Trivalent cations (e.g. Y³⁺, Er³⁺, Gd³⁺, La³⁺) also inhibit Ca_v3.1 channels with Y³⁺ being the most potent blocker when recorded in 2 mM Ba²⁺ (IC₅₀ = 28 nM) (Beedle et al., 2002).

While toxins derived from numerous invertebrates have been utilized in the study of various HVA Ca²⁺ channels (Doering and Zamponi, 2003) relatively little is known about the sensitivity of T-type channels to peptide toxins. Kurtoxin, a peptide isolated from scorpions (*Parabuthus transvaalicus*), was reported to block both recombinant Ca_v3.1 and Ca_v3.2 channels (Chuang et al., 1998) and I_{CaT} recorded from thalamic neurons (Sidach and Mintz, 2002). In both cases, the kurtoxin effect was voltage-dependent and involved a modification of channel gating. Recently, two independent groups of investigators reported two peptide toxins isolated from the tarantula, *Thrixopelma pruriens*, to potently inhibit cloned Ca_v3.1 and Ca_v3.2 channels (Edgerton et al., 2010; Ohkubo et al., 2010). ProTx-I blocked Ca_v3.1 and Ca_v3.2 channels with 160-fold higher potency towards Ca_v3.1 (IC₅₀ values of approximately 0.2 μM for Ca_v3.1 and 32 μM for Ca_v3.2). Likewise, ProTx-II potently inhibited Ca_v3.1 channels (IC₅₀ value of 0.8 μM) and was found to induce a positive shift in the voltage-dependence of activation and to decrease the maximum macroscopic conductance (Edgerton et al., 2010). In this regard, the application of either ProTx-I or ProTx-II could be used to study Ca_v3.2 currents in isolation, particularly in cardiac myocytes. Although significant progress has been made concerning the pharmacology of T-type channels, the identification of T-type isoform-specific blocker remains to be described. Eventually, this will allow for the better characterization of T-type channel properties in cells expressing multiple T-type isoforms and their alternative splice variants.

1.2.4 Modulation of T-type calcium channels

Besides the effects of pharmacological agents on T-type channel functional states, T-type channels are also regulated by interactions with various signaling molecules. T-type channels are subject to considerable subtype specific regulation by activation of various G-protein coupled receptors (GPCRs) and second messengers. For example, Rho kinase has been shown to inhibit $Ca_v3.1$ channels (Iftinca et al., 2007) while the activation of M1 muscarinic acetylcholine receptors selectively inhibits recombinant $Ca_v3.3$ T-type channels (Hildebrand et al., 2007) (Appendix 2). The M1 receptor inhibition is mediated by $G_{\alpha q/\alpha 11}$ -linked pathways independent of the involvement of downstream signaling pathways such as protein kinase C (PKC), serine/threonine kinases, tyrosine kinase, phosphatases, and phosphoinositide-3-kinase. GPCR-mediated regulation effects on T-type channel activity are predicted to alter Ca^{2+} entry and cellular excitability. For example, in the nervous and cardiovascular systems the inhibition of T-type channels by GPCRs could potentially reduce neuronal firing or cardiac automaticity. As this thesis focuses on $Ca_v3.2$ channels, discussion will mainly focus on the modulation of $Ca_v3.2$ by direct effectors with known modulation sites and activators of GPCRs (Figures 1.3 and 1.4).

The contributions of Barrett and colleagues provided an initial understanding of $Ca_v3.2$ channel regulation. The $G\beta\gamma$ -mediated inhibition of I_{CaT} via activation of dopamine D_1 receptors was initially reported in rat adrenal zona glomerulosa (Drolet et al., 1997). This observation was further explored via co-expression of specific $G\beta\gamma$ proteins with recombinant T-type isoforms in HEK-293 cells and it was determined that $Ca_v3.2$ but not $Ca_v3.1$ channels are specifically inhibited by $G\beta\gamma$ and only with $G\beta\gamma$ dimers containing the $G\beta_2$ subunits (Wolfe et al., 2003; Hu et al., 2009). Experiments using chimeric $Ca_v3.2$ - $Ca_v3.1$ channels and fusion proteins demonstrated that $G\beta\gamma$ subunits directly bind to the domain II-III linker of the $Ca_v3.2$ subunit (Figure 1.3). The $G\beta\gamma$ -mediated inhibition of $Ca_v3.2$ was shown to be voltage-independent and to

be specific for $G\beta_2\gamma_2$ dimers (Wolfe et al., 2003; DePuy et al., 2006). A cluster of 4 amino acids (P140, V178, G179 and A181) within $G\beta_2$ were identified as critical sites for $G\beta_2\gamma_2$ inhibition and this region has also been shown to underlie the CaMKII-mediated potentiation of $Ca_v3.2$ channels (DePuy et al., 2006).

Barrett's group also showed that the $G\beta\gamma$ -dependent inhibition of $Ca_v3.2$ could be mediated by activation of the dopamine (D_1) receptor (Figure 1.4) (Hu et al., 2009). They also showed that the $G\beta\gamma$ inhibition of $Ca_v3.2$ channels is dependent on phosphorylation by protein kinase A (PKA) at Ser¹¹⁰⁷ in the $Ca_v3.2$ II – III cytoplasmic loop. The $G\beta\gamma$ -mediated inhibition of recombinant $Ca_v3.2$ channels has also been reported via activation of the corticotrophin-releasing factor receptor 1 (CRF-1) (Tao et al., 2008) (Figure 1.4). Protein kinase pathways were shown not to be involved in this regulation but rather were found to be dependent upon the activation of the cholera-toxin sensitive G_{α_s} pathway. Together, $G\beta\gamma$ regulation of $Ca_v3.2$ channels occurs through either direct binding of $G\beta\gamma$ or via activation of certain second messenger cascades. Interestingly, agonists of the CRF receptors are known to regulate sleep rhythms and T-type channels play a key role in generating thalamic oscillations; therefore it is tempting to speculate that the CRF mediated changes on T-type channel gating might play a role in regulating sleep patterns (Zoumakis et al., 2006; Tao et al., 2008; Iftinca and Zamponi, 2009)

Calcium/calmodulin-dependent protein kinase II (CaMKII) has also been implicated in I_{CaT} regulation. In canine Purkinje cells and ventricular myocytes I_{CaT} has been shown to be regulated by intracellular Ca^{2+} (Tseng and Boyden, 1991). In bovine adrenal glomerulosa cells I_{CaT} can be potentiated by increases in intracellular Ca^{2+} dependent upon CaMKII phosphorylation (Lu et al., 1994). Barrett and colleagues demonstrated that CaMKII activation underlies the Ca^{2+} -mediated potentiation of recombinant $Ca_v3.2$ currents expressed in HEK-293 cells (Wolfe et al., 2002). Using chimeric $Ca_v3.2$ - $Ca_v3.1$ channels, site-directed mutagenesis

and glutathione S-transferase (GST) fusion proteins, the same group identified the domain II – III linker as a critical region within Ca_v3.2 for mediating CaMKII modulation (Figure 1.3). An ¹¹⁹³LRRAESL¹¹⁹⁹ recognition motif located in the domain II – III intracellular linker was implicated as the critical site for CaMKII-dependent modulation of Ca_v3.2 channels (Welsby et al., 2003). Specifically, the authors attributed the phosphorylation of a serine residue (Ser¹¹⁹⁸) in the domain II – III linker as the site of CaMKII potentiation (Figure 1.3). CaMKII modulation of native Ca_v3.2 channels was further explored using adrenal glomerulosa cells. Barrett and colleagues demonstrated that activation of the angiotensin II (Ang II) receptor resulted in CaMKII phosphorylation of native Ca_v3.2 channels (Yao et al., 2006). Ang II receptor activation increases cytosolic Ca²⁺ levels to enhance synthesis and secretion of aldosterone, an identified early pathogenic stimulus that adversely influences cardiovascular homeostasis (Yao et al., 2006). In this regard, CaMKII potentiation of Ca_v3.2 channels is functionally relevant in Ang II mediated increase in aldosterone release which in turn could alter cardiovascular Ca²⁺ homeostasis. Hence, disruption of CaMKII signaling complex in the zona glomerulosa may provide a new therapeutic approach to regulating the production of aldosterone and to the control of cardiovascular disease progression (Yao et al., 2006).

PKA has also been demonstrated to potentiate recombinant Ca_v3.2 channels (Figure 1.3). Macroscopic currents from Ca_v3.2 channels are augmented by PKA activity when expressed in *Xenopus* oocytes and the effect can be mimicked by serotonin when co-expressed with the 5HT₇ receptor (Kim et al., 2006). Using chimeric Ca_v3.2 and Na_v1.4 subunits, a sodium channel which is not known to be regulated by PKA (Smith and Goldin, 1996), the authors identified the II-III intracellular linker as being required for the PKA-mediated potentiation of the Ca_v3.2 channels (Kim et al., 2006). In CHO and HEK mammalian cell lines, PKA-mediated potentiation of exogenous Ca_v3.2 currents has been reported to occur at physiological temperature (~30 – 37°C)

but not at room temperature ($\sim 22 - 27^{\circ}\text{C}$) (Chemin et al., 2007). The PKA-mediated potentiation is contrary to the reported PKA-dependent inhibition of $\text{Ca}_v3.2$ currents in bovine adrenal glomerulosa cells (Hu et al., 2009).

Protein kinase C (PKC) has also been shown to modulate $\text{Ca}_v3.2$ channels via activation of certain GPCRs (Figures 1.4). For example, activation of the neurokinin I (NK1) receptor inhibits $\text{Ca}_v3.2$ currents via the sequential activation of $\text{G}_{\alpha q/11}$, phospholipase $\text{C}\beta$ (PLC β) and PKC (Rangel et al., 2010) (Figure 1.4). The NK1-mediated inhibition of $\text{Ca}_v3.2$ can be occluded by co-expression with either a dominant-negative form of $\text{G}_{\alpha q}$ or regulators of G-protein signaling proteins (such as RGS2 and RGS3T), as well as by bath application of inhibitors of PLC β (U73122) and PKC (bisindolylmaleimide I).

$\text{Ca}_v3.2$ channels are also regulated by nitrous oxide and redox agents (e.g. L-cysteine, dithiothreitol (DTT), 5,5' dithio-bis(2-nitrobenzoic acid) (DTNB)) (Todorovic et al., 2001a; Todorovic et al., 2001b; Joksovic et al., 2006; Nelson et al., 2007b; Nelson et al., 2007a; Bartels et al., 2009) (Appendix 3). The putative extracellular loop connecting the third and fourth segments of domain I (IS3-IS4) of $\text{Ca}_v3.2$ channels is implicated as the site of modulation by nitrous oxide and redox agents (Figure 1.3). In particular, using chimeric channels and site-directed mutagenesis, the structural determinant for redox modulation was identified to be dependent upon a distinct histidine residue (H^{191}). The endogenous redox agent ascorbate (vitamin C) has also been shown to inhibit recombinant $\text{Ca}_v3.2$ channels in HEK cells and in DRG and nRT neurons, revealing a novel mechanism of the action of vitamin C in the peripheral and central nervous systems and may function as endogenous modulator of neuronal excitability (Nelson et al., 2007b) (Appendix 3). Considering that $\text{Ca}_v3.2$ channels are upregulated in the adult diseased heart (Section 1.4.2), the effects of vitamin C might have a protective role in cardiac disease progression.

While the modulation of Ca_v3.2 channels by various effectors is starting to be well understood, multiple possible transduction pathways have been proposed (Figure 1.4). Conflicting reports on the modulation of cardiac I_{CaT} (Ca_v3.1 and Ca_v3.2) by GPCRs have been communicated by a number of researchers (reviewed in (Chemin et al., 2006; Vassort et al., 2006; Kang et al., 2007; Salazar et al., 2007) and briefly discussed in Section 1.4.1). The variety of reports can possibly be explained by the existence of multiple splice variants of cardiac Ca_v3.1 and Ca_v3.2 channels (Section 1.3 and Chapter 2). To date, no study has reported the effect of Ca_v3.2 splice variation on the modulation of Ca_v3.2 channels by GPCRs. Exploring the possibility of splice-variant differential modulation by GPCRs and elucidating the potential mechanisms may explain the reported complexity of GPCR-mediated regulation of cardiac I_{CaT}. It is important to note that the expression of both cardiac Ca_v3.2 alternative splice variants, GPCRs, as well as their downstream effectors are altered in diseased hearts ((Kang et al., 2007; Salazar et al., 2007; Sato and Ishikawa, 2010) and Chapter 2). Thus, studying GPCR modulation of Ca_v3.2 variants may contribute to uncovering mechanisms underlying cardiovascular disease as well as in the development of novel therapeutic approaches.

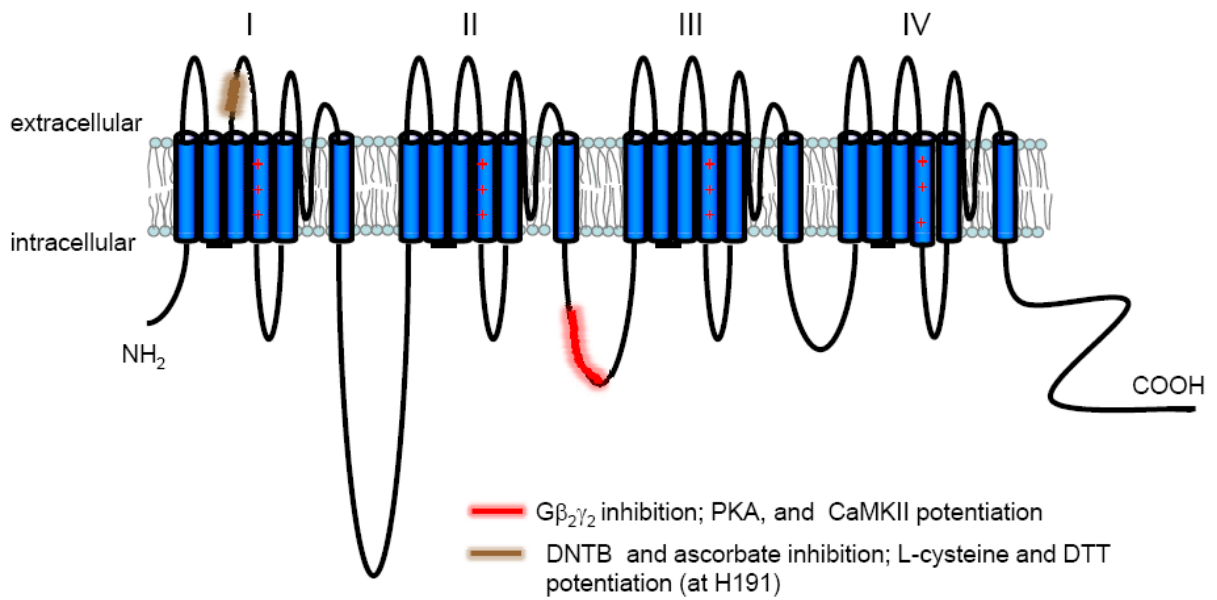


Figure 1.3. Effectors with identified modulation sites in the $Ca_v3.2$ T-type channel.

There are critical sites in the $Ca_v3.2$ channel known to be directly regulated by various effectors. Redox agents are known to act on H191 of IS3 – IS4 (brown line). The redox agent ascorbate causes inhibition, while reducing agents such as L-cysteine and DTT mediate potentiation. $Ca_v3.2$ channels are inhibited by Gβ₂γ₂ binding to the II – III linker (red line), while phosphorylation by CaMKII (at Ser₁₁₉₈) at the site within the II-III linker causes potentiation of $Ca_v3.2$ T-type channels.

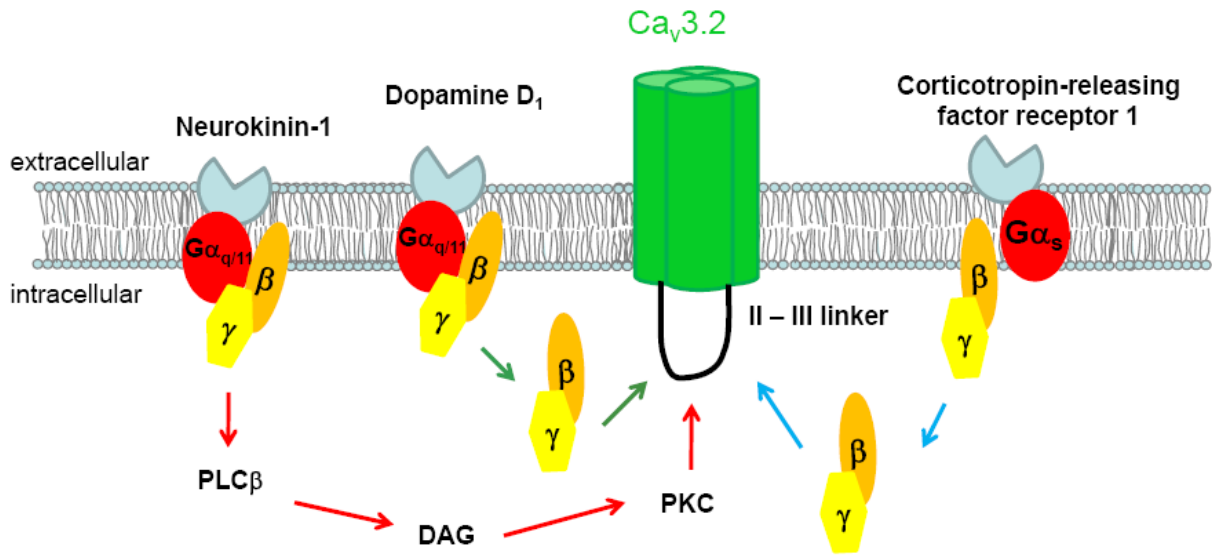


Figure 1.4. Mechanisms of modulation of Ca_v3.2 T-type Ca²⁺ channels by G protein-coupled receptors (GPCRs).

Ca_v3.2 channels are modulated by GPCRs activating G-proteins and related second messenger signaling pathways. The neurokinin I receptor inhibits Ca_v3.2 channel activity via PKC phosphorylation. Dopamine D₁ receptor activation (G_{αq/11}) inhibits channel activation via a direct action of G $\beta\gamma$ whereas corticotropin-releasing factor 1 (CRF-1) receptor activation inhibits channel activity via G_{αs} but not involving PLC β . CRF-1-mediated inhibition is thought to be caused by G $\beta\gamma$ binding to Ca_v3.2. The pathways leading to G $\beta\gamma$ inhibition of Ca_v3.2 channels generally occur via activation of G_{αq/11} and G_{αs} proteins.

1.3 Alternative splicing

Alternative splicing of voltage-gated Ca²⁺ channels is an important mechanism for increasing the functional repertoire of these channels. In the cardiovascular system, it is known that alternative splicing of various Ca²⁺ handling proteins profoundly affects Ca²⁺-mediated signaling processes in both normal and diseased myocytes (Ladd et al., 2005; Liao et al., 2005; Wang et al., 2006; Liao et al., 2009a).

In general, alternative splicing is the major source of protein diversity amongst organisms (Maniatis and Tasic, 2002; Black, 2003; Stamm et al., 2005; Blencowe, 2006). In typical

multiexonic mRNA splicing patterns can be altered via several distinct mechanisms (Figure 1.5). Most exons are constitutive; they are always either spliced out or included in the final mRNA. An alternatively spliced exon that is sometimes included or excluded is called a cassette exon (Figure 1.5A). In some cases, multiple cassette exons are mutually exclusive (Figure 1.5B), producing mRNAs that always include one of several possible exons but not all. Altering the position of one of the splice sites leads to shorter or longer exons (Figures 1.5C and 1.5D). Further, terminal exons can also be switched through the use of alternative promoter (5' end) and alternative polyadenylation (PA) (3') sites (Figures 1.5E and 1.5F). Overall, alternative splicing leads to three structural changes: introduction of stop codons, changes in the protein structure and/or changes in the 5' and 3' untranslated (UTR) regions (for reviews see (Black, 2003; Stamm et al., 2005; Blencowe, 2006)). This section focuses on the identification and expression of the alternative splice variants of voltage-gated Ca^{2+} channels and their relevance to physiology and pathophysiology.

1.3.1 Overview of calcium channel alternative splicing

Alternative splicing is a versatile process and along with transcriptional regulators can generate complex genetic alterations to modulate cellular responses to developmental, physiological and pathological signals (Lopez, 1998; Garcia-Blanco et al., 2004; Gray et al., 2007). In Ca^{2+} channels, alternative splicing occurs at sites important for biophysical properties, trafficking, post-translational modification and coupling to downstream signaling pathways (Gray et al., 2007). The expression of alternative splice variants can be highly variable depending on tissue type, cell type, developmental stage and disease state.

The HVA channels are subjected to extensive alternative splicing. Figure 1.6 illustrates some of the more common alternatively spliced regions of the $\text{Ca}_v1.2$, $\text{Ca}_v2.1$ and $\text{Ca}_v2.2$

channels. Functionally distinct alternative splice variants of neuronal Ca_v2.1 P/Q-type channels have been identified (Soong et al., 2002; Chang et al., 2007). Nine exons at seven loci in the *CACNA1A* gene were found to be alternatively spliced including one pair of mutually exclusive exons (37a and 37b) at the C-terminus which are important for Ca²⁺-dependent modulation mediated by calmodulin (EF hand) (Soong et al., 2002; Chaudhuri et al., 2004). The EF-hand-like domain controls the activity-dependent enhancement of Ca_v2.1 channel gating mediated by calmodulin, a phenomenon referred to as Ca²⁺-dependent facilitation (CDF). Alternative splicing in the EF-hand-like domain acts as a molecular switch for CDF of Ca_v2.1 channels and in mammalian brain occurs in an age- and gender-dependent manner (Chaudhuri et al., 2004; Chang et al., 2007). In both humans and rodents the exon 37b variant is predominantly expressed in early brain development and switches to the exon 37a variant in the adult brain. It is hypothesized that the regulation of expression of alternative splice variants of Ca_v2.1 channels potentially contributes to neurophysiological specialization during brain development.

The use of an alternative 3' acceptor site in a *CACNA1A* intron upstream of the last exon (exon 47) introduces a stop codon at the beginning of exon 47 (Soong et al., 2002). As a result, the Ca_v2.1 channel can exist in long (+47) or short (-47) isoforms. The Snutch laboratory explored the biophysical properties of the two C-terminus variants and the effects of introduced FHM-1 mutations and found that FHM-1 mutations have splice-dependent effects on voltage-dependent gating and kinetic properties (Adams et al., 2009) (Appendix 4). This result suggests a potential role of alternative splicing *CACNA1A* gene in the molecular pathophysiology of FHM-1.

Alternative splicing of Ca_v2.2 N-type channels has also been reported by Lipscombe and others (Bell et al., 2004; Thaler et al., 2004; Castiglioni et al., 2006; Lipscombe and Raingo, 2007; Raingo et al., 2007). The *CACNA1B* gene has at least two sites of alternative splicing, the

domain II – III intracellular loop region (exon 18a) and the C-terminus (exons e37a and e37b). Alternative splicing in the domain II – III linker affects sensitivity to inactivation during trains of action potential waveforms. Compared with Ca_v2.2 channels lacking e18a, the presence of e18a prevents the channel from entering into closed-state inactivation, leading to sustained Ca²⁺ influx (Thaler et al., 2004). N-type channels have been shown to play a significant role in pain processing and exon 37a appears preferentially expressed in nociceptive neurons of DRG (Bell et al., 2004). The presence of e37a produces larger whole cell N-type currents in nociceptive neurons, while exon e37b yields smaller currents. Moreover, a tyrosine residue within the alternative exon e37a has been shown to play a role in N-type channel G-protein-dependent inhibition in nociceptive neurons (Raingo et al., 2007). The inclusion of e37a in Ca_v2.2 appears to create an inhibitory pathway that is voltage-independent and that substantially increases the sensitivity of N-type channels to opiates. It has been suggested that the Ca_v2.2 exon e37a variant could be used as therapeutic target for pain management (Raingo et al., 2007).

The alternative splicing of Ca_v1.2 L-type channels has been studied extensively, with reports showing events related to development (Diebold et al., 1992; Tang et al., 2009), disease pathology (Tiwari et al., 2006; Wang et al., 2006; Tang et al., 2008; Liao et al., 2009b) and tissue-specificity (Liao et al., 2004; Tang et al., 2004; Liao et al., 2005; Tang et al., 2007; Tang et al., 2008) expression. Alternative splicing in the *CACNA1C* exons 31, 32, and 33 encoding for the IVS3 and IVS3 - S4 regions has been shown to be both tissue and developmentally regulated. The predominant splice combination for the fetal heart and brain appears to be the exclusion of exon 31 and the inclusion of exons 32 and 33 (-31, +32, +33). In the adult heart, the -31, +32, +33 combination decreases while -31, +32, -33 variant channel increase. Thus, overall exon 33 is downregulated in the adult heart. In adult brain, the -31, +32, -33 combination is lower than in adult heart suggesting tissue-specific expression. Relevant to cardiac pathology, aberrant

expression of exons 31, 32 and 33 has been reported in infarcted and failing hearts (Gidh-Jain et al., 1995; Yang et al., 2000; Liao et al., 2009b). Alternative splicing in the IVS3-IVS4 region affects the voltage-dependence of channel activation, revealing a positive shift in the voltage-dependence of activation correlated with increasing IVS3-IVS4 linker length (Tang et al., 2004). In the heart, splice variation in the IVS3-IVS4 region could potentially influence the shape and duration of ventricular APs. This suggests that Ca_v1.2 splice variation may play roles in the maintenance of muscle excitability and contractility and to also contribute to arrhythmogenesis.

Smooth and cardiac muscle specific expression of Ca_v1.2 variants have also been reported by Soong's laboratory (Liao et al., 2004; Liao et al., 2005; Tang et al., 2007). Mutually exclusive exons 8a and 8 encoding the Ca_v1.2 IS6 region are distributed differentially in heart and smooth muscles (Welling et al., 1997; Liao et al., 2005). The L-type IS6 segment determines channel sensitivity to DHPs, widely used Ca_v1.2 antagonists to treat cardiovascular disorders (Welling et al., 1997). The smooth muscle exon 8 variant was shown to be more sensitive to inhibition by DHPs compared with exon 8a variant channels. The role of exons 8 and 8a in the severity of disorder associated with Timothy syndrome has also been reported (Splawski et al., 2004; Splawski et al., 2005). Timothy syndrome is a congenital disease affecting various organs, and due to severe cardiac arrhythmia patients do not usually reach adulthood (Liao et al., 2009a). Interestingly, *CACNA1C* mutations in these patients have only been identified in one of the alternatively splice exons allowing the other exon to function normally. Of note, patients with mutation in cardiac exon 8a experience severe cardiac arrhythmia while patients with mutation in smooth muscle exon 8 have a longer life span (Splawski et al., 2004; Splawski et al., 2005; Liao et al., 2009a).

The level of expression of Ca_v1.2 channels containing exons 9* and 21 was reported to be higher in the aorta than the heart whereas exon 22 was reported to be more common in the heart

than in aorta (Liao et al., 2004; Liao et al., 2005; Tang et al., 2007). Exon 9* is highly expressed in the smooth muscle layer of arteries and whole cell recordings of the exon 9* containing Ca_v1.2 channels revealed a hyperpolarizing shift in the voltage-dependence of activation relative to Ca_v1.2 lacking exon 9* (Liao et al., 2004). Exon 9* is located in the Ca_v1.2 I-II linker immediately downstream of the β subunit binding site. Alternative splicing in this region could potentially affect β subunit regulation of Ca_v1.2 channel function and it remains to be tested whether the addition of 25 amino acids encoded by Ca_v1.2 exon 9* affects the binding and modulation of different β subunits on Ca_v1.2. Further, a possible role for the high expression of exon 9* in the arteries is to allow the activation of the channels with slight depolarization and to generate sufficient tension for blood vessels to function (Liao et al., 2005). The process would contribute to Ca²⁺ influx that presumably triggers greater myogenic tone or more prolonged contraction of the blood vessels (Jaggar et al., 1998).

Exons 21 and 22 are mutually exclusive exons encoding for the Ca_v1.2 IIIS2 region. The expression of these exons is either included or excluded in the Ca_v1.2 transcripts. In the aorta, the level of expression of exon 21 is about three-fold higher than exon 22. Interestingly, in human atherosclerotic patients, upregulation of expression of exon 22 was observed (Tiwari et al., 2006). In addition, the expression of exon 22 was found to have potential association with vascular smooth muscle proliferation. Relevant to cardiac hypertrophy, comparative studies of Ca_v1.2 alternative splicing between hypertrophic Spontaneously Hypertensive Rats (SHR) and normotensive Wistar Kyoto (WKY) rats has revealed significant changes in patterns of expression of alternative spliced variants (Tang et al., 2008; Liao et al., 2009a). The proportion of aberrant Ca_v1.2 transcript including both exons 21 and 22 (+21/+22) is higher in hypertrophic SHR than in normotensive WKY. Conversely, in WKY the inclusion of either exon 21 or exon 22 forms the IIIS2 transmembrane segment. The presence of both exons 21 and 22 creates

dominant negative effect (i.e. unable to conduct currents) on Ca_v1.2 channels while the presence of either exon 21 or 22 produces different biophysical and pharmacological properties (Soldatov et al., 1995; Zuhlke et al., 1998; Tiwari et al., 2006; Tang et al., 2008). As Ca_v1.2 exons (+21/+22) containing channels are predominantly expressed in hypertrophic heart perhaps these channels contribute to the altered electrical activity observed in cardiac hypertrophy. Lastly, exon 22 containing channels are reported to be more sensitive to blocking by DHPs than exon 21 containing Ca_v1.2 channels (Soldatov et al., 1995; Zuhlke et al., 1998). Thus, perhaps DHPs can be effectively used for management and treatment of atherosclerosis as this disorder is associated with an upregulation of exon 22 containing alternative splice variants.

Overall, alternative splicing of the HVA channel genes changes channel protein sequence and generates novel functional and nonfunctional isoforms. The spatial and temporal expression of alternatively spliced variants likely contributes to the physiological specialization of the splice variant isoforms. In certain pathological states the amount and pattern of expression of splice variants are also altered. Questions now remain as to whether these changes in expression are causes or effects of the disease. Understanding splice variant expression changes during the normal course of development and in disease progression is a major goal of future research in defining the contributions of alternative splicing to physiology and pathophysiology.

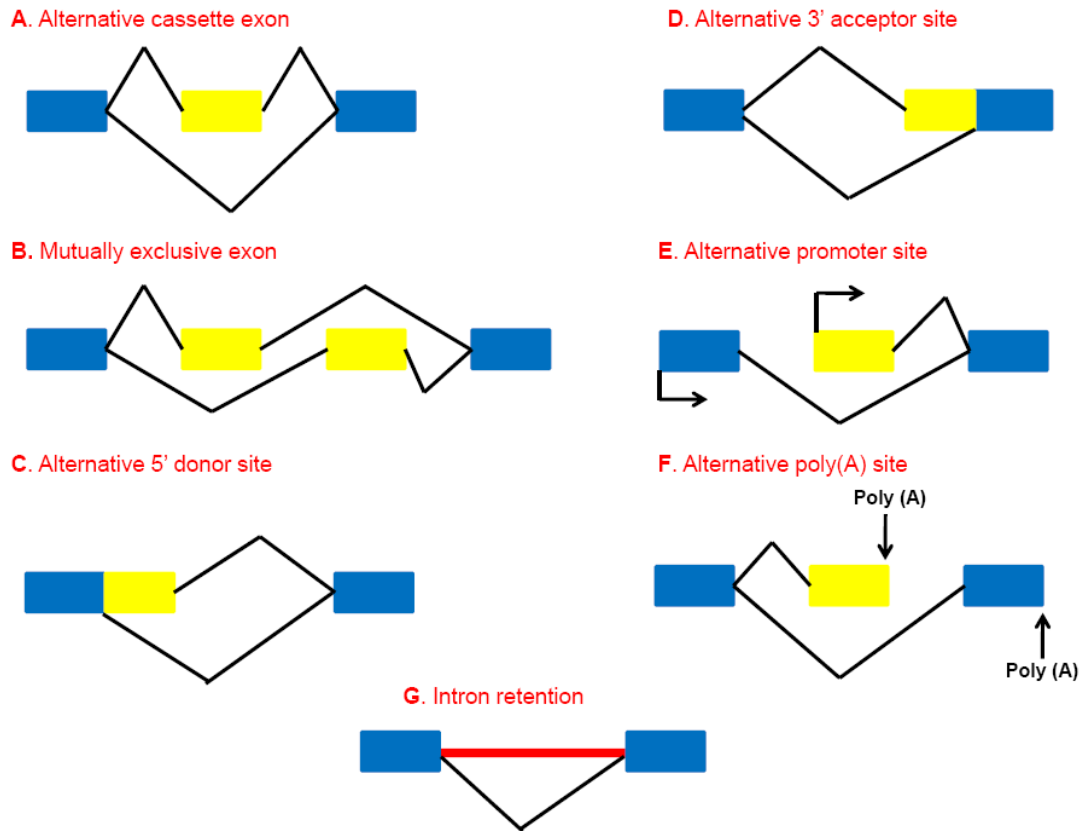


Figure 1.5. Patterns of alternative splicing in eukaryotic mRNA.

Patterns of alternative splicing that are responsible for the generation of distinct transcripts. The types of alternative splicing are depicted above each cartoon. Blue boxes represent constitutive exons, yellow boxes denote alternative exons, bent arrows and vertical arrows correspond to alternative promoter and poly (A) sites, respectively.

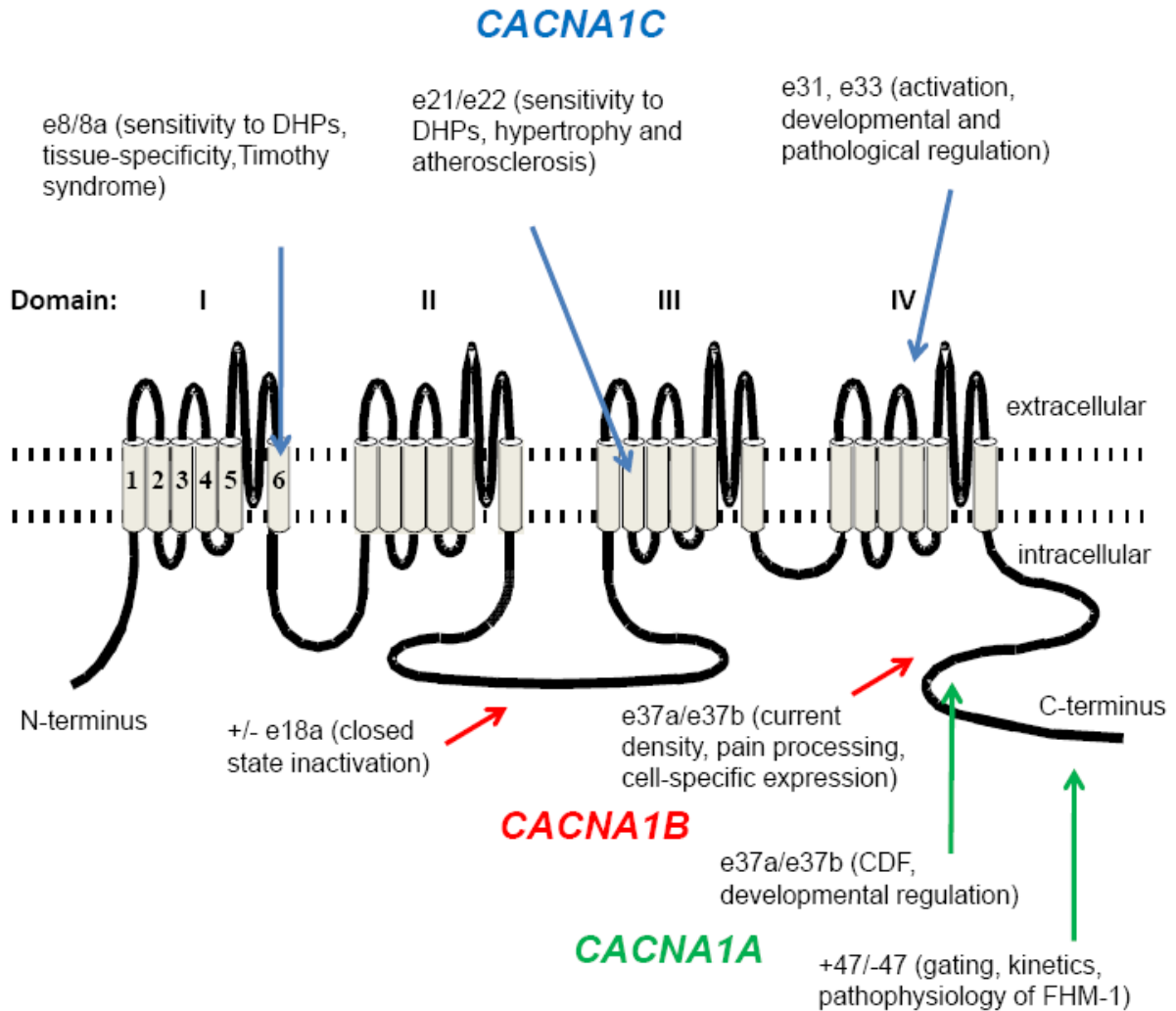


Figure 1.6. Functionally relevant alternative splicing events in HVA channels. The diagram shows functional domains (arrows) that are altered in $Ca_v1.2$, $Ca_v2.1$ and $Ca_v2.2$ channels as a result of alternative splicing events in *CACNA1C* (blue), *CACNA1B* (red) and *CACNA1A* (green) genes, respectively. Alternative splice variants in these regions are reported to contribute to the differential channel biophysical properties and are also implicated in the pathophysiology of cardiovascular and neurological disorders (Chaudhuri et al., 2004; Thaler et al., 2004; Splawski et al., 2005; Tiwari et al., 2006; Chang et al., 2007; Raingo et al., 2007; Tang et al., 2008).

1.3.2 Alternative splicing of T-type calcium channels

T-type channel genes are known to be subject to alternative splicing (Figure 1.7). Using short amplicon PCR colony screening, Mittman and colleagues initially identified two and six alternative splice sites for the human $Ca_v3.3$ and $Ca_v3.1$ channels, respectively. Alternative splicing of the human $Ca_v3.3$ channel gene was found to occur at two sites, one being the variable inclusion of exon 9 (35 amino acids) in the domain I – II linker and the other the use of an alternate acceptor in exon 33, leading to variable inclusion of 13 amino acids in the C-terminus (Mittman et al., 1999a; Mittman et al., 1999b). The splicing events affected channel activation and inactivation kinetics interdependently, suggesting a possible direct interaction between the two regions (Murbartian et al., 2004). Rat brain $Ca_v3.3$ channels were also reported to be alternatively spliced with all six splice variants located in the C-terminus between exons 33 and 34 (Murbartian et al., 2002). The electrophysiological properties of the variants displayed similar voltage-dependent gating, but differed in their kinetic properties.

Initial study of alternative splicing in the human brain $Ca_v3.1$ revealed broad splicing across exons 14, 25, 26, 34, 35 and 38 (Mittman et al., 1999a; Monteil et al., 2000a). Further studies using fetal and adult human brain cDNA libraries revealed nine additional sites of splice variation (Emerick et al., 2006). The majority of functional $Ca_v3.1$ channel splicing occurs in cytoplasmic channel regions. The C-terminus variants (exons 34, 35 and 38) were shown to affect channel gating and kinetic properties. Likewise, alternative splicing in exons 25 and 26 that encode for the $Ca_v3.1$ domain III – IV linker also affects gating, activation and inactivation kinetics as well as relative expression during development. Fetal brain transcripts predominantly express cassette exon 26 over the alternate donor exon 25C. In contrast, in the adult brain the relative expression of exon 25C is greater than exon 26. Structurally, exon 25C introduces a consensus phosphorylation site for PKA suggesting that variants resulting from alternative

splicing in the III – IV linker could be differentially regulated by cAMP-dependent mechanisms. In regards to regulation of expression of splice variants, the reciprocal relationship between cellular and molecular diversity in the developing brain suggests that splicing progresses with cell differentiation from nearly independent (stochastic) and unbiased splicing in fetal transcripts to strongly concerted (deterministic) splicing in adult transcripts (Emerick et al., 2006). Ca_v3.1 alternative splice variants involving the III – IV linker were also reported in embryonic day 14 mouse heart (Cribbs et al., 2001) and human gliomas (Latour et al., 2004). Latour et al. demonstrated changes in the relative mRNA expression of Ca_v3.1 transcripts between normal brain tissues and glioma biopsies suggesting potential contribution of alternative splicing to the pathophysiology of tumors (Latour et al., 2004).

Alternative splicing of Ca_v3.2 T-type channels has thus far been reported in human testes (Jagannathan et al., 2002), uterus (Ohkubo et al., 2005) and fetal brain (Zhong et al., 2006) as well as in rat thalamus (Powell et al., 2009) (Appendix 5). Using a human fetal brain cDNA library, Zhong and co-workers utilized partial length cDNA (from exon 19 to the 3'-UTR) and overlapping short PCR amplicons to screen for alternative splice variants of Ca_v3.2 channels (Zhong et al., 2006). The authors identified 12 – 14 alternative splice sites within the Ca_v3.2 open reading frame (ORF), potentially generating both functional and non-functional transcripts. The majority of functional Ca_v3.2 splicing occurs in cytoplasmic regions and was found to affect both current kinetics and voltage-dependence of gating (Ohkubo et al., 2005; Zhong et al., 2006; Powell et al., 2009) (Appendix 5).

The role of neuronal Ca_v3.2 T-type channel alternative splice variants in the pathophysiology of epilepsy was investigated by the Snutch and O'Brien groups (Powell et al., 2009) (Appendix 5). The work demonstrated that the functional effects of a Ca_v3.2 R1584P mutation in genetic absence epilepsy rats from the Strasbourg (GAERS) model are dependent

upon alternative splicing of exon 25. To date, $Ca_v3.2$ alternative splicing in the heart has not been explored. In part, this thesis studied cardiac $Ca_v3.2$ alternative splicing and the differential expression of alternative splice variants during maturation and cardiac hypertrophy (Chapter 2).

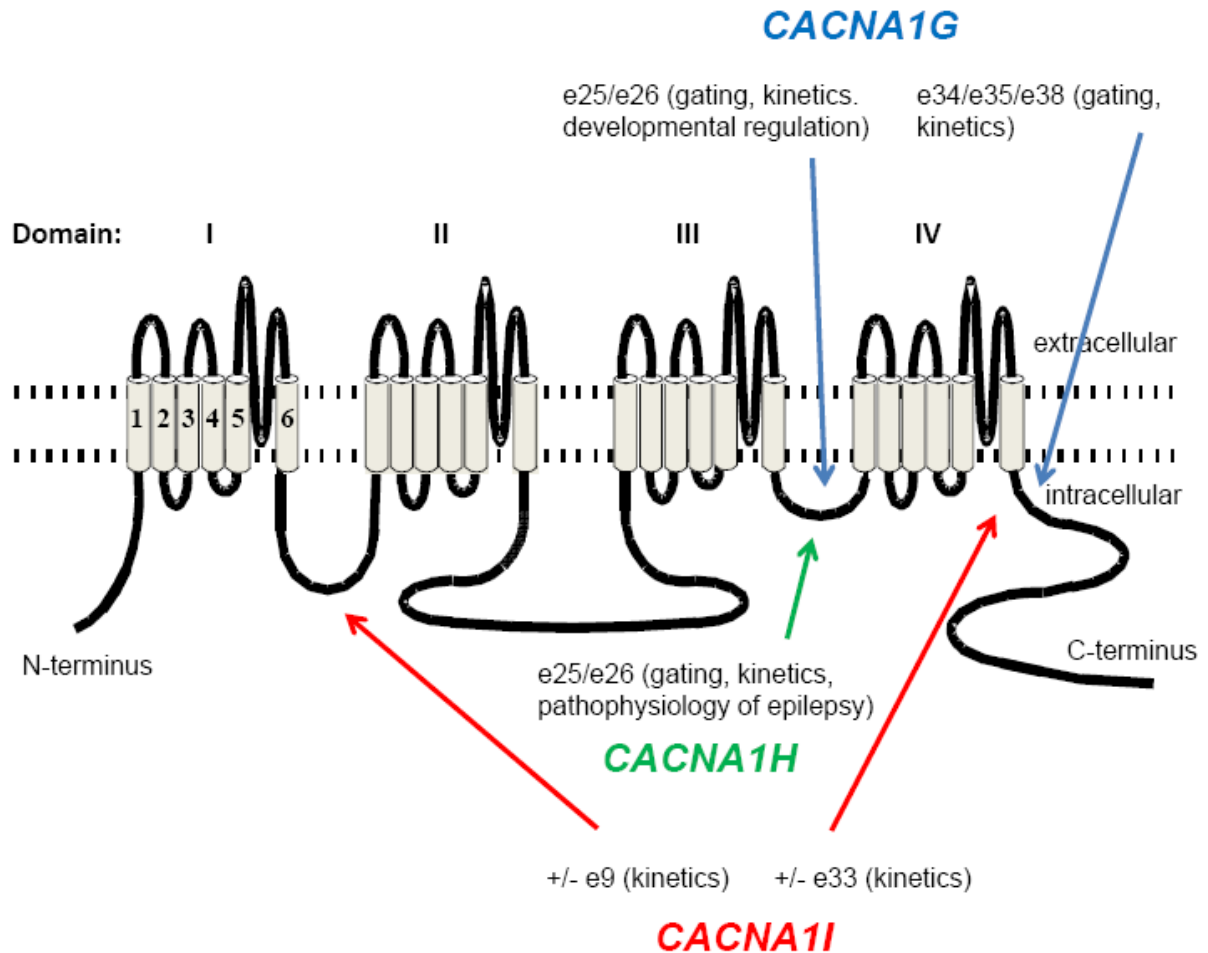


Figure 1.7. Functionally relevant alternative splicing events in T-type channels. The diagram shows functional domains (arrows) that are altered in $Ca_v3.1$, $Ca_v3.2$ and $Ca_v3.3$ channels as a consequence of different splicing events in *CACNA1G* (blue), *CACNA1H* (green) and *CACNA1I* (red) genes, respectively. Alternative splicing in these regions results in differential channel biophysical properties. Importantly, $Ca_v3.2$ alternative splice variants in the III – IV linker have been implicated in the pathophysiology of epilepsy (Zhong et al., 2006; Powell et al., 2009).

1.4 T-type calcium channels and the heart

Cardiac voltage-gated Ca^{2+} channels are known to contribute to the control of electrical activity of normal and diseased myocardium. Critically, they also play important roles in cardiac pacemaking, conduction, E-C coupling and the genesis of arrhythmias. Two distinct Ca^{2+} channel families have been identified in the heart: L- and T-type channels. L-type channels are ubiquitously expressed in the heart and are known to play important roles concerning E-C coupling and pacemaking (Bers, 2001; Bers, 2002; Mangoni et al., 2003). On the other hand, the functional role of T-type channels in cardiac physiology is not entirely clear. This section discusses the expression, modulation and physiological roles of cardiac T-type channels.

1.4.1 Expression, functional roles and modulation

There are two major T-type channel isoforms expressed in the heart; the $\text{Ca}_v3.1$ and $\text{Ca}_v3.2$ types (Cribbs et al., 1998; Demir et al., 1999; Cribbs et al., 2001; Perez-Reyes, 2003; Mangoni et al., 2006b; Rosati et al., 2007). In the adult heart, the expression of both T-type isoforms appears restricted to the SA node, atrio-ventricular node (AV) and Purkinje fibers (PF) (Hagiwara et al., 1988; Shorofsky and January, 1992; Xu and Best, 1992; Zhou and Lipsius, 1994; Bohn et al., 2000; Leuranguer et al., 2000; Marionneau et al., 2005; Mangoni et al., 2006b; Rosati et al., 2007).

I_{CaT} has been implicated in playing a role in generating pacemaker depolarization and in contributing to automaticity (Nilius, 1986; Hagiwara et al., 1988; Zhou and Lipsius, 1994; Ono and Iijima, 2005). Cardiac automaticity is a complex physiological function requiring the coordinated activity of the primary pacemaker center (SA node) and that of the conduction system (AV node and PF network) (Boyett et al., 2000; Moorman and Christoffels, 2003; Efimov et al., 2004; Mangoni et al., 2006a; Mangoni and Nargeot, 2008). Automaticity is initiated in the

SA node by primary pacemaker cells which propagate the impulse to the atria spreading to the AV node and PF enabling contraction of the entire myocardium (Mangoni et al., 2006a). Using pharmacological tools, the contribution of I_{CaT} in cardiac pacemaking was studied in SA node (Protas and Robinson, 2000; Madle et al., 2001). Using mibefradil to block I_{CaT} in the SA node, the authors showed a dose-dependent reduction of pacemaker activity, observed as the reduction in the slope of the later phase of diastolic depolarization. A similar concentration-dependent reduction of pacemaker activity was also observed with efonidipine (Masumiya et al., 1998). Further, Ca^{2+} influx through T-type channels in atrial myocytes triggers the release of Ca^{2+} from the SR which in turn activates Na/Ca exchanger currents ($I_{Na/Ca}$) leading to increased Na^+ influx and therefore promotes automaticity (Huser et al., 2000). Taken together, the results from these studies support the notion that T-type channels play important roles in cardiac pacemaking and automaticity.

L-type Ca^{2+} currents (I_{CaL}) are considered to be the primary trigger for SR Ca^{2+} release to induce E-C coupling in normal adult hearts. However, the involvement of I_{CaT} in SR Ca^{2+} release in amphibian and mammalian hearts was suggested initially by Morad and Cleeman (Morad and Cleemann, 1987) and supported by later studies using adult guinea pig ventricular myocytes (Sipido et al., 1998). The contribution of I_{CaT} to SR Ca^{2+} release was shown to be eliminated when 50 μ M Ni^{2+} was added to block T-type channels. In another study examining canine cardiac Purkinje cells it was observed that I_{CaT} is capable of initiating contraction via inducing Ca^{2+} release from SR (Zhou and January, 1998).

In immature hearts, cardiac contractility has been reported to be dependent mainly on transsarcolemmal Ca^{2+} influx contributed by I_{CaT} and I_{CaL} and reversed mode $I_{Na/Ca}$ (Nuss and Marban, 1994; Wetzel and Klitzner, 1996; Haddock et al., 1999; Kitchens et al., 2003; Escobar et al., 2004; Tohse et al., 2004). T-tubules and SR are not fully developed in immature hearts and

I_{CaT} supplies most of the Ca^{2+} that triggers the contraction in the immature myocardium. In support, Ca^{2+} flux and contraction were increased in adult mouse ventricular myocytes overexpressing $Ca_v3.1$ T-type channels (Jaleel et al., 2008). Collectively, these studies suggest the notion that T-type channels play a role in E-C coupling, particularly in the developing heart.

Cardiac T-type channels have also been reported to play important roles in the secretion of hormones. Atrial natriuretic peptide (ANP) hormone has been shown to be important in the control of blood pressure as well as in salt and water excretion and an increase in intracellular Ca^{2+} concentration in atria and ventricles stimulates ANP secretion (Thibault et al., 1999). The role of T-type channels in the secretion of atrial ANP has been described in rabbit and rat hearts wherein an increase in Ca^{2+} flux via T-type channels stimulates atrial myocytic ANP release (Leuranguer et al., 2000; Wen et al., 2000).

Cardiac I_{CaT} is also subject to modulation by G-protein-coupled receptors. In frog atrial myocytes, activators of β -adrenergic receptors facilitate cardiac I_{CaT} (Alvarez and Vassort, 1992; Alvarez et al., 1996; Alvarez et al., 2000). Further, atrial myocyte I_{CaT} is tonically inhibited by $G_{\alpha i}$ proteins. Several hormones implicated in playing important roles in cardiac remodelling including endothelin-1 (ET-1) (Furukawa et al., 1992; Izumi et al., 2003), Ang II (Ferron et al., 2003), aldosterone (Okoshi et al., 2004; Lalevee et al., 2005) and corticosteroids (Maturana et al., 2009) have been demonstrated to enhance cardiac I_{CaT} and T-type channel mRNA expression. In addition, estrogen and testosterone have been reported to affect cardiac myocyte I_{CaT} and T-type channel mRNA expression as long term pretreatment (24 to 30 hours) with testosterone on cultured ventricular myocytes increased I_{CaT} density attributed to upregulation of $Ca_v3.1$ and $Ca_v3.2$ mRNA expression and conversely, acute pretreatment (< 10 minutes) of testosterone decreased I_{CaT} (Michels et al., 2006). Contrary to the effect of long term testosterone treatment, 24 hour estrogen pretreatment resulted in decreased cardiac myocyte I_{CaT} and downregulation of

Ca_v3.2 mRNA (Marni et al., 2009). This suggests that chronic treatment of estrogen and testosterone produce differential effects on the heart, and may which have cardiac implications in hormone replacement therapy.

1.4.2 Developmental regulation and association in cardiac diseases

The expression of the two main cardiac T-type isoforms is known to be differentially regulated during development. Ca_v3.2 mRNA is highly expressed in the prenatal stage and reduced after birth. In the adult ventricle neither Ca_v3.1 nor Ca_v3.2 mRNA are detected (Leuranguer et al., 2000; Ferron et al., 2002; Larsen et al., 2002). In rat atria, the level of Ca_v3.1 mRNA expression is consistently high throughout development while Ca_v3.2 mRNA is highest in embryonic tissue to 3 weeks postnatal but becomes undetectable after 5 weeks (Larsen et al., 2002; Larsen et al., 2005).

In murine hearts, developmental changes in Ca_v3.2/Ca_v3.1 mRNA expression have been shown by several investigators. Using quantitative RT-PCR analysis on mouse cardiac ventricles, predominant Ca_v3.2 mRNA expression during the whole embryonic stage has been observed while in adults Ca_v3.1 mRNA expression was shown to be higher than Ca_v3.2 although regardless there was no detectable I_{CaT} in ventricular myocytes (Niwa et al., 2004; Mizuta et al., 2005; Yasui et al., 2005).

While I_{CaT} has not been recorded in the human heart, both Ca_v3.1 (Monteil et al., 2000a) and Ca_v3.2 (Cribbs et al., 1998) transcripts have been identified. Downregulation of Ca_v3.2 expression was also reported in human ventricular myocytes (Qu and Boutjdir, 2001). The reduction in expression of Ca_v3.2 mRNA could be attributed to regulation by the transcriptional repressor neuron-restrictive silencer factor (NRSF), a neuron-restrictive silencer element (NRSE) binding protein. Kuwahara and colleagues demonstrated a negative correlation of expression

between NRSF and $Ca_v3.2$ in adult and embryonic mouse ventricles (Kuwahara et al., 2003; Kuwahara et al., 2005). The authors reported that the level of NRSF expression was higher in the adult ventricle than in embryonic and fetal ventricles whereas the opposite pattern was observed in $Ca_v3.2$ mRNA (Kuwahara et al., 2001; Kuwahara et al., 2003). They also reported that the first intron of the *CACNA1H* gene contains NRSE-like sequences (93 – 97% identity) and are well conserved among different mammalian species (Kuwahara et al., 2003; Kuwahara et al., 2005). Taken together, the presence of high amount of NRSF in the adult ventricle perhaps represses $Ca_v3.2$ channel expression and may be the reason why $Ca_v3.2$ is much reduced or absent in adult mammalian ventricles.

T-type channels have been reported to be associated with the pathophysiology of a number of cardiovascular diseases (Lory et al., 2006; Cribbs, 2010; Ono and Iijima, 2010). Even before the cloning of T-type channels, I_{CaT} was recorded in the diseased myocardium and it had been suggested that the re-appearance of I_{CaT} in diseased hearts contributes to Ca^{2+} overload and the genesis of arrhythmias (Nuss and Houser, 1993; Sen and Smith, 1994; Bkaily et al., 1997; Cribbs, 2010). I_{CaT} is re-expressed in hypertrophied ventricles and shows relatively high Ni^{2+} sensitivity suggesting $Ca_v3.2$ as the underlying the re-expressed T-type isoform (Martinez et al., 1999). Further, in post-myocardial infarcted hearts (PMI) upregulation of $Ca_v3.1$ and $Ca_v3.2$ mRNA is reported (Huang et al., 2000; Yasui et al., 2005) and in the failing heart of Dahl-sensitive (DS) rats both I_{CaT} and $Ca_v3.1$ mRNA re-appear (Izumi et al., 2003). Thus, re-expression of T-type channels may contribute to the molecular remodeling of the diseased heart.

Although, T-type channels are implicated in cardiac hypertrophy and the pathogenesis associated with Ca^{2+} overload and arrhythmia, the mechanisms involved in the association of T-type channels with cardiac remodeling remains debatable. Ang II treatment has been extensively used to study cardiac hypertrophy in cultured cardiac myocytes. Ang II induces hypertrophy in

cardiac myocytes via binding to G-protein-coupled Ang II Type I (AT₁) receptors (see (Molkentin and Dorn, 2001; Dorn and Force, 2005; Heineke and Molkentin, 2006) for reviews). In frog atrial myocytes Ang II increases I_{CaT} (Bonvallet and Rougier, 1989) and in rat ventricular myocytes AngII both increases I_{CaT} and Ca_v3.1 mRNA expression (Ferron et al., 2003). On the other hand, activation of the AT₁ receptor by Ang II in neonatal rat ventricular myocytes enhanced I_{CaT} concomitant with increased expression of both Ca_v3.1 and Ca_v3.2 mRNA (Morishima et al., 2009). Recently, Chiang et al. have provided strong evidence implicating the involvement of Ca_v3.2 T-type channels in the pathogenesis of cardiac hypertrophy (Chiang et al., 2009). Pressure-overload cardiac hypertrophy was suppressed in Ca_v3.2 knockout mice (Ca_v3.2^{-/-}) but not in mice deficient for Ca_v3.1 (Ca_v3.1^{-/-}). Importantly, Ang II-induced cardiac hypertrophy was suppressed in Ca_v3.2^{-/-} mice further implicating Ca_v3.2 channels as a key component in Ang II hypertrophic signaling. The authors also identified calcineurin/NFAT-dependent pathways as signaling mechanisms responsible for the Ca_v3.2-dependent cardiac hypertrophy (Chiang et al., 2009). However, in another study examining the role of T-type channels in cardiac hypertrophy, an enhancement of cardiac hypertrophy in aortic banded Ca_v3.1^{-/-} mice was reported (Nakayama et al., 2009). The authors also showed that the enhanced hypertrophy in Ca_v3.1^{-/-} was rescued with the Ca_v3.1 transgene and dependent upon NOS3-mediated signaling mechanisms. Taken together, the results from the T-type channel knockout models suggest that Ca_v3.1 and Ca_v3.2 channels contribute differential roles in cardiac hypertrophy.

Mineralocorticoid and glucocorticoid hormones have also been implicated in cardiac hypertrophy and remodeling (Rossier et al., 2010). Interestingly, these hormones induce the expression of Ca_v3.2 mRNA and mediate positive chronotropic effect in ventricular myocytes (Rossier et al., 2003; Lalevee et al., 2005; Rossier et al., 2008; Maturana et al., 2009). It was

suggested that positive chronotropism as a result of increased $Ca_v3.2$ channel activity may predispose the ventricle to arrhythmia. In another report, the expression of $Ca_v3.1$ mRNA in neonatal rat ventricular myocytes was upregulated by dexamethasone treatment (BenMohamed et al., 2009).

Enhancement of I_{CaT} activity in cultured neonatal ventricular myocytes by ET-1, a vasoactive peptide associated with cardiac hypertrophy has been reported (Furukawa et al., 1992). Additionally, increases in I_{CaT} and $Ca_v3.1$ mRNA levels were found to be correlated with upregulated ET-1 in failing rat hearts, an observation implicating T-type channels in ET-1-induced cardiac remodeling (Izumi et al., 2003). Monocrotaline (MCT), a pyrrolizidine alkaloid, induces right ventricular hypertrophy and also upregulates I_{CaT} as well as $Ca_v3.1$ and $Ca_v3.2$ mRNA expression (Takebayashi et al., 2006). However, in a separate study, MCT-induced cardiac hypertrophy showed no significant changes in expression of $Ca_v3.1$ and $Ca_v3.2$ mRNA (Koyama et al., 2009). Interestingly, although the mRNA levels were not altered, an increase in I_{CaT} was observed, an indication that altered I_{CaT} may contribute to right atrial electrical remodeling. In chronic hypoxia in neonatal rat ventricular myocytes, downregulation of I_{CaT} and $Ca_v3.1$ mRNA expression has been observed; however, upon reoxygenation recorded currents and channel expression are restored (Pluteanu and Cribbs, 2009). The authors suggested that T-type channels play a significant role in cardiac remodeling induced by hypoxia/reoxygenation injury. Overall, alteration in the expression of T-type channels appears to alter Ca^{2+} -mediated signaling processes in the diseased heart. These modifications may affect overall cardiac contractility and electrical activity.

Although recent progress has provided insight into the developmental and pathological regulation of expression of T-type channels, there remains much to learn concerning the mechanisms and the role of these channels in the normal and diseased heart. In addition, it also

remains to be determined whether alternative splicing of cardiac T-type channels contributes to cardiac development and pathophysiology.

1.5 Voltage-dependent facilitation of calcium channels

The influx of Ca^{2+} into cardiac myocytes through the voltage-gated Ca^{2+} channels can be influenced by channel modulation, pharmacological agents and voltage-dependent mechanisms. The potentiation of Ca^{2+} currents by a prepulse depolarization is known as voltage-dependent facilitation (VDF). Facilitation of Ca^{2+} currents has been reported for both HVA and LVA channels. There are several mechanisms suggested to underlie facilitation of voltage-gated Ca^{2+} channels and this section focuses on the potentiation of Ca^{2+} currents induced by depolarizing prepulses. The first part of this section focuses on VDF of HVA Ca^{2+} channels and the second centers on the VDF of T-type channels. The reported VDF mechanisms and potential contribution to normal and diseased cells are also discussed.

1.5.1 Voltage-dependent facilitation of high voltage-activated calcium channels

The Ca_v2 channels are well known to display VDF through a mechanism involving the voltage-dependent relief of tonic G-protein-dependent inhibition. G-protein-dependent inhibition is characterized by a positive shift in voltage-dependence of activation, the slowing of time courses of activation and inactivation, and a reduction of peak current amplitude (Bean, 1989b; Kasai and Aosaki, 1989; Lipscombe et al., 1989). Inhibited channels are described as being ``reluctant`` to open and converted by strong depolarization into a ``willing`` state, resulting in facilitated currents (Bean, 1989b; Elmslie et al., 1990; Ikeda, 1991; Patil et al., 1996). This type of modulation has shown to be more common to N-type than P/Q-type Ca^{2+} channels (Colecraft

et al., 2000; Lee and Elmslie, 2000). Reports from various groups have demonstrated that VDF via removal of G-protein-mediated inhibition occurs specifically through G $\beta\gamma$ complexes (Bourinet et al., 1996; Herlitze et al., 1996; Ikeda, 1996; Meza and Adams, 1998). In one study, the structural determinants underlying the interaction between G $\beta\gamma$ and Ca²⁺ channels was investigated using chimeric Ca_v2.2 - Ca_v2.1 channels and the domain I and the C-terminus proposed to serve as major interaction sites for G $\beta\gamma$ (Zhang et al., 1996). Other studies used a combination of electrophysiological, molecular and biochemical techniques and identified the domain I – II linker of the Ca_v2 subunit as the critical region for G $\beta\gamma$ interaction (Pragnell et al., 1994; De Waard et al., 1995; Witcher et al., 1995; De Waard et al., 1997; Herlitze et al., 1997; Zamponi et al., 1997). Whole cell patch clamp analysis of N-type currents and inclusion of purified G $\beta\gamma$ in the patch pipette showed direct evidence for the physical dissociation of a single G $\beta\gamma$ underlying the prepulse-induced facilitation (Zamponi and Snutch, 1998). In general, the facilitation of N- and P/Q-type currents plays important roles in neurotransmitter release and synaptic plasticity (Brody and Yue, 2000; Colecraft et al., 2000; Currie and Fox, 2002).

VDF of L-type currents has also been described in skeletal muscle (Sculptoreanu et al., 1993a), chromaffin cells (Artalejo et al., 1992), neurons (Bourinet et al., 1994; Sculptoreanu et al., 1995; Calin-Jageman et al., 2007) and cardiac cells (Pietrobon and Hess, 1990; Sculptoreanu et al., 1993b; Xiao et al., 1994; Kamp et al., 2000; Blaich et al., 2010). Distinct from Ca_v2 channels, the VDF observed for L-type currents has been shown to be dependent upon phosphorylation by PKA (Sculptoreanu et al., 1993b; Sculptoreanu et al., 1993a; Xiao et al., 1994; Sculptoreanu et al., 1995) or by CaMKII (Xiao et al., 1994; Blaich et al., 2010). L-type channel VDF is characterized by a negative shift in voltage-dependent activation ascribed to an increase in open probability. Relevant to cardiac physiology, the facilitation of L-type currents has been suggested to contribute to the increase in cardiac muscle contractile force (Lee, 1987;

Fedida et al., 1988a, b). Prolonged APs, such as those observed in patients with bradycardia, could potentially lead to reactivation and facilitation of cardiac L-type Ca^{2+} channels. This would in turn result in an increase in myoplasmic Ca^{2+} promoting after-depolarizations and associated arrhythmias (January and Riddle, 1989; Kamp et al., 2000). Overall, changes in intracellular Ca^{2+} concentration as a result of VDF may lead to alteration in both inotropic and chronotropic properties of the normal and diseased heart.

1.5.2 Voltage-dependent facilitation of T-type channels

Among recombinant T-type channels, VDF has thus far been only shown for $\text{Ca}_v3.3$ channels (Klockner et al., 1999; Chemin et al., 2002; Gomora et al., 2002). Facilitated human $\text{Ca}_v3.3$ T-type channels show a significant increase in current amplitude (20 to 25%) after +100 mV prepulse. Conversely, no facilitation was observed for the rat $\text{Ca}_v3.1$ isoform and only weak facilitation (~5 %) for the human $\text{Ca}_v3.2$ subtype (Klockner et al., 1999). The structural determinants responsible for the human $\text{Ca}_v3.3$ VDF were found to be dependent upon the last 214 amino acids of the distal C-terminus (Gomora et al., 2002).

Prepulse-induced facilitation of native I_{CaT} has been observed in guinea pig coronary smooth muscle myocytes (Ganitkevich and Isenberg, 1991), frog atrial cells (Alvarez et al., 1996; Alvarez et al., 2000), rat bone marrow cells (Publicover et al., 1995) and mouse spermatogenic cells (Arnoult et al., 1997). The facilitation of I_{CaT} has variously been proposed to be due to voltage-dependent modulation, tyrosine phosphorylation, the voltage-dependent relief of tonic inhibition by G-proteins or PKA phosphorylation. Figure 1.6 illustrates the proposed underlying mechanisms of native I_{CaT} facilitation.

Facilitation of I_{CaT} involving a pure voltage mechanism has been proposed for guinea-pig coronary smooth muscle myocytes (Ganitkevich and Isenberg, 1991) and cultured rat bone

marrow cells (Publicover et al., 1995). I_{CaT} of guinea-pig smooth muscle myocytes was potentiated twofold by 200 ms prepulse to voltages above -30 mV and saturated at -10 mV. Potentiation of I_{CaT} by longer prepulses (10 s) shifted the voltage-dependency of facilitation to a more hyperpolarized potentials such that saturation occurred at -50 mV and varying the duration of the prepulse showed peak facilitation between 160 and 320 ms. Facilitated I_{CaT} inactivated faster than the unfacilitated currents. Facilitation of I_{CaT} in cultured bone cells was approximately 100% by a 750 ms prepulse to +150 mV. Compared with smooth muscle myocytes, stronger depolarizations were required and robust facilitation was only observed from potentials positive to 0 mV. Changing the duration of the prepulse showed that half maximal potentiation occurred at 250 ms and saturated at 1000 ms. The facilitation in these cells has been suggested to be due to both a shift in gating properties and recruitment of a population of quiescent channels (Ganitkevich and Isenberg, 1991; Publicover et al., 1995).

T-type currents from mouse spermatogenic cells are increased by strong depolarizing prepulses and involving removal of a tyrosine kinase tonic inhibition (Arnoult et al., 1997). The robust facilitation of I_{CaT} in spermatocytes was observed at prepulse potentials positive to -30 mV and the authors utilized membrane permeable inhibitors of tyrosine kinases (tryphostins A47 and A25) to explore the mechanism of facilitation in sperm cells. Tyrosine kinase inhibitors increased basal I_{CaT} and had no effect on facilitated currents while application of phenylarsine oxide (protein tyrosine phosphatase inhibitor) resulted in inhibition of the basal current and prevented facilitation. Thus, facilitation in spermatogenic I_{CaT} is dependent upon the voltage-dependent relief of tyrosine kinase-mediated inhibition.

Relevant to the heart, facilitation of I_{CaT} in frog atrial myocytes was shown to be regulated by both G_{α_s} and G_{α_i} proteins (Alvarez et al., 1996). I_{CaT} was stimulated by β -adrenergic agonists to activate G_{α_s} increasing adenylyl cyclase activity and leading to cAMP synthesis. This

activity leads to activation of PKA and eventually phosphorylates native T-type channels. The cAMP/PKA-dependent phosphorylation leads to facilitation of I_{CaT} in atrial myocytes. The cAMP/PKA -dependent stimulation could be further enhanced by depolarizing prepulses and prevented by the intracellular application of pertussis toxin (a $G\alpha_i$ inhibitor). Thus, the facilitation of I_{CaT} in frog atrial myocytes is a result of voltage-dependent relief of the $G\alpha_i$ -protein inhibitory tone (Alvarez et al., 1996). Interestingly, of the two cardiac T-type channel isoforms ($Ca_v3.1$ and $Ca_v3.2$), recombinant $Ca_v3.2$ T-type channels can be inhibited by G-proteins ascribed to the $Ca_v3.2$ channel direct interaction with $G\beta\gamma$ subunits (Wolfe et al., 2003; DePuy et al., 2006). Thus, the tonic inhibition observed in atrial cardiac myocytes might be due to direct binding of $G\beta\gamma$ subunits to native cardiovascular $Ca_v3.2$ channels.

Overall, the role of VDF of T-type channels in the cardiovascular system has not been elucidated. Given that cardiac T-type channels are predominantly expressed in the developing and disease hearts (Section 1.4), it is possible that the VDF of T-type channels plays distinct roles at different developmental stages and pathological conditions. For example, in the immature heart VDF may contribute to the contractility and beating frequency whereas in the diseased heart it may participate in sustaining arrhythmic electrical activity.

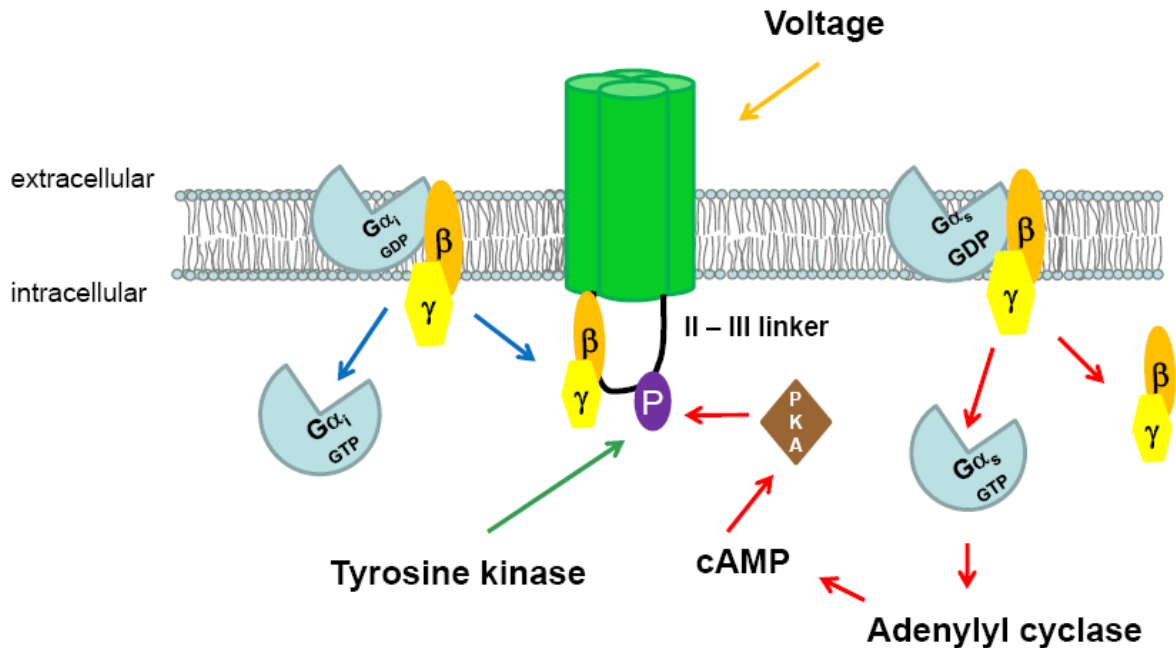


Figure 1.8. Proposed mechanisms underlying the facilitation of native T-type calcium currents.

Multiple molecular mechanisms have been suggested to underlie facilitation of native T-type Ca^{2+} currents. Facilitation has been proposed to be due to (1) voltage-dependent change in gating mode (orange arrow); (2) voltage-dependent relief of $\text{G}\beta\gamma$ -mediated inhibition (blue arrow), application of strong depolarizing prepulses removes the inhibition by $\text{G}\beta\gamma$ resulting to enhancement (facilitated) of Ca^{2+} currents during the test pulse; (3) removal of tonic inhibition due to tyrosine kinase phosphorylation (green arrow) or (4) increase in intracellular cAMP and phosphorylation by PKA as a result of $\text{G}\alpha_s$ activation (red arrow).

1.6 Thesis hypotheses and objectives

1.6.1 Hypothesis 1

While there are ten genes encoding Ca^{2+} channel α_1 subunits, it is predicted that there are perhaps 1000 times as many splice variants, likely with their own distinct functional properties and spatial and temporal expression patterns (Lipscombe et al., 2002; Gray et al., 2007). The structural differences resulting from alternative splicing can affect channel biophysics, drug affinity, trafficking, intracellular localization, protein stability, post translational modification, modulation and coupling to downstream signaling pathways (Stamm et al., 2005; Gray et al., 2007). All T-type channel isoforms are subject to alternative splicing with reports showing changes in expression patterns in different developmental stages and disease states. Specifically, alternative splice variants of $\text{Ca}_v3.2$ T-type channels have been reported in the brain and in reproductive tissues and associated with disorders such as absence epilepsy (Jagannathan et al., 2002; Ohkubo et al., 2005; Zhong et al., 2006; Powell et al., 2009). Currently, there has been no description of $\text{Ca}_v3.2$ alternative splicing in the heart. In this thesis, I specifically hypothesize:

That alternative splicing in rat cardiac $\text{Ca}_v3.2$ T-type channels is a mechanism to generate functionally distinct $\text{Ca}_v3.2$ channels.

1.6.2 Hypothesis 2

Recent trends in alternative splicing research have been directed to profiling functionally relevant transcripts and their role in normal physiology and diseases, particularly on how variants are coordinated on a global level to achieve cell- and tissue-specific functions (Blencowe, 2006). Regulation during development, by environmental stimuli or cellular activity has been shown to contribute to changes in splice variant expression patterns (Diebold et al., 1992; Liao et al., 2004;

Schultz Jel et al., 2004; Emerick et al., 2006). Such regulation is likely intended to adapt and compensate in response to changes in the gene expression patterns of other proteins during maturation and in pathological states or to refine electrical properties of ion channels in response to the cascade of changes in the cells and tissues. Of note, developmental and pathological regulation of the expression of a number of alternative splice variants of various cardiac Ca^{2+} handling proteins such as $\text{CaMII}\delta$, cardiac troponin T and $\text{Ca}_v1.2$ channels have been reported (Tang et al., 2004; Ladd et al., 2005; Xu et al., 2005; Tiwari et al., 2006; Tang et al., 2008) In this thesis, I specifically hypothesize:

That there is a differential expression of $\text{Ca}_v3.2$ splice variants between neonatal and adult hearts as well as between adult normotensive and hypertensive SHR rats.

1.6.4 Hypothesis 3

Biophysical characterization of native cardiac I_{CaT} has been studied in Purkinje fibers, SA node, atria and ventricle. However, there has been no description on the correlation between the electrophysiological properties of native I_{CaT} and the expression of alternative splice variants of T-type channels in cultured newborn rat ventricular myocytes. In this thesis, I specifically hypothesize:

That there is a correlation between the level of expression of T-type channel alternative splice variants and the biophysical properties of newborn rat ventricular myocytes I_{CaT} .

1.6.5 Objectives

The following thesis objectives were formulated to address the above hypotheses:

1. To generate both short amplicon and full length $Ca_v3.2$ specific cDNA libraries to determine the molecular profile of cardiac $Ca_v3.2$ T-type channel alternative splice variants.
2. To examine the differential expression of splice variants in ventricular tissue from newborn and adult rats and to compare the relative abundance of splice variants between hypertrophic SHR and age- and sex- matched normotensive WKY rats.
3. To generate selected full-length $Ca_v3.2$ alternative splice variants and to functionally characterize their biophysical properties after transient expression in HEK- 293 cells.
4. To investigate if the $Ca_v3.2$ variants are differentially affected by G-protein subunits co-expression or intracellular cAMP.
5. To characterize native T-type currents in neonatal rat ventricular myocytes.

2 SPLICE-VARIANT CHANGES OF THE Ca_v3.2 T-TYPE CALCIUM CHANNEL MEDIATE VOLTAGE-DEPENDENT FACILITATION AND ASSOCIATE WITH CARDIAC HYPERTROPHY AND DEVELOPMENT

2.1 Introduction

Alternative splicing is a ubiquitous post-transcriptional mechanism for generating diversity from individual genes and significantly expands the functional repertoire of eukaryotic cells (Black, 2003; Stetefeld and Ruegg, 2005). Greater than half of known human genes are subject to alternative splicing (Modrek and Lee, 2002) and splice-variant expression patterns often correlate with specific developmental stages as well as specific physiological and pathophysiological states (Diebold et al., 1992; Lopez, 1998; Chang et al., 2007; Adams et al., 2009) (Appendix 4). Cardiovascular diseases have been associated with altered regulation of alternative splicing and changes in the expression ratio of functionally relevant proteins, including some voltage-activated Ca²⁺ channels (Warnecke et al., 1999; Tiwari et al., 2006; Shang et al., 2007; Kong et al., 2010). The expression of distinct Ca²⁺ channel subtypes contributes to mechanical and electrophysiological functioning of different regions of the heart (Mangoni et al., 2003; Hatano et al., 2006). However, the identification and temporal and spatial expression patterns of alternatively spliced variants of most Ca²⁺ channel family members expressed in cardiac tissue has yet to be reported. Low voltage-activated T-type currents play a critical role in spontaneous diastolic depolarization (Mangoni et al., 2006b) and have also been

*A version of this chapter has been published. David, L.S., Garcia, E., Cain, S.C., Thau, E.M., Tyson, J.R., Snutch, T.P. 2010. Splice-variant changes of the Ca_v3.2 T-type calcium channel mediate voltage-dependent facilitation and associate with cardiac hypertrophy and development. *Channels (Austin)*. 4(5):375-389.

suggested to regulate the cell cycle and differentiation of cardiac myocytes (Vassort et al., 2006). Of the three genes encoding T-type channels in mammals, the $Ca_v3.1$ and $Ca_v3.2$ isoforms have been identified as underlying cardiac I_{CaT} (Perez-Reyes, 2003; Rosati et al., 2007; Mangoni and Nargeot, 2008). Both the $Ca_v3.1$ and $Ca_v3.2$ T-types are expressed in atrial and ventricular tissues during embryonic and neonatal periods (Cribbs et al., 2001; Ferron et al., 2002; Niwa et al., 2004) but by the adult stage $Ca_v3.2$ levels become significantly reduced and $Ca_v3.1$ becomes the predominant cardiac isoform, albeit mainly being restricted to pacemaker cells (Qu and Boutjdir, 2001; Mangoni and Nargeot, 2008). In addition to developmental regulation, there is an overall increase in functional I_{CaT} under pathological conditions such as post-myocardial infarction and cardiac hypertrophy and both $Ca_v3.1$ and $Ca_v3.2$ T-type Ca^{2+} channels have been reported to be re-expressed in adult ventricle of diseased hearts (Nuss and Houser, 1993; Martinez et al., 1999; Huang et al., 2000; Yasui et al., 2005; Takebayashi et al., 2006). Specific expression of the $Ca_v3.2$ T-type channel has also been associated with the pathogenesis of pressure overload-induced cardiac hypertrophy in mice (Chiang et al., 2009).

All three T-type Ca^{2+} channel genes are known to be subject to alternative splicing (Mittman et al., 1999b; Monteil et al., 2000a; Chemin et al., 2001a; Chemin et al., 2001b; Cribbs et al., 2001; Jagannathan et al., 2002; Murbartian et al., 2002; Ohkubo et al., 2005; Emerick et al., 2006; Zhong et al., 2006). In human fetal and adult brains, $Ca_v3.1$ was shown to have 15 sites subject to alternative splicing (Monteil et al., 2000a; Emerick et al., 2006), while two sites of alternative splicing have been reported to date for the human $Ca_v3.3$ channel (Mittman et al., 1999b; Chemin et al., 2001b). Examining human fetal brain and partial length splice-variant analysis, $Ca_v3.2$ channels were shown to be alternatively spliced at 12 to 14 sites (Zhong et al., 2006). Human uterine and testicular $Ca_v3.2$ T- Ca^{2+} channels have similarly been found to be alternatively spliced, particularly in the domain III-IV linker region (Jagannathan et al., 2002;

Ohkubo et al., 2005). In a number of these instances, alternative splicing has been shown to affect T-type channel biophysical properties (Jagannathan et al., 2002; Ohkubo et al., 2005; Zhong et al., 2006). To date, there has been no report concerning cardiac Ca_v3.2 T-type channel alternative splicing. A goal of the current study was to describe structural and functional composition of Ca_v3.2 channel variation in cardiac tissue from newborn rats and to then compare that with the splice-variant profile from adult heart. Additionally, this study hypothesized that under certain pathological conditions there might be changes in Ca_v3.2 T-type channels in both overall expression and the level of specific splice variants. Profiling of splice variants was performed using both short amplicon scanning and full-length cDNA screening, and combined with quantitative RT-PCR (qRT-PCR) using cardiac samples from newborn and adult male Wistar rats, as well as from hypertrophic SHR and age and sex-matched normotensive WKY animals. The study demonstrates developmental changes in the expression pattern of the most abundant alternatively spliced Ca_v3.2 transcripts in rat atrial and ventricular tissues. Furthermore, altered transcript ratios of the predominant Ca_v3.2 isoforms in the left ventricle of adult SHR were found to correlate with histopathological signs and the expression of molecular markers of pathological hypertrophy. In addition to a switch in variants with a distinct recovery from inactivation, this study finds that a major characteristic of Ca_v3.2 splicing is the generation of T-type Ca²⁺ channels that exhibit voltage-dependent facilitation (VDF).

2.2 Results

2.2.1 Alternative splicing generates multiple $\text{Ca}_v3.2$ T-type variants with differential expression across development

Utilizing subtype-specific probes and both qRT-PCR and Western blot analyses, the expression of the $\text{Ca}_v3.1$, $\text{Ca}_v3.2$ and $\text{Ca}_v3.3$ T-type isoforms as well as the high voltage-activated (HVA) $\text{Ca}_v1.2$ L-type and $\text{Ca}_v2.2$ N-type Ca^{2+} channels was determined in neonatal (P0) and adult atria and ventricle (relative to actin B). Figure 2.1A and 2.1B shows that the $\text{Ca}_v3.1$ and $\text{Ca}_v3.2$ T-types and $\text{Ca}_v1.2$ L-type Ca^{2+} channels were robustly expressed at the mRNA and protein levels in both cardiac chambers of neonate heart. Contrastingly, in adult animals the expression of both T-type isoforms was significantly lower in the ventricle while the level of expression of the $\text{Ca}_v1.2$ L-type remained high in both adult heart chambers. Neither the $\text{Ca}_v3.3$ T-type nor $\text{Ca}_v2.2$ N-type channels were expressed at appreciable levels in neonate or adult heart chambers (Figure 2.1A).

The rat $\text{Ca}_v3.2$ genomic locus spans ~110, 000 kb on chromosome 10 (NCBI, NC 005109; Ensembl, ENSRNOT00000048392). In order to identify $\text{Ca}_v3.2$ splice variants expressed in neonate heart, comprehensive transcript screening was initially performed using short amplicon scanning (Figure 2.1C). The reference $\text{Ca}_v3.2$ transcript used in this study corresponds to a transcript containing 35 exons across 7862 bp and encoding 2365 amino acids (Ensembl, ENSRNOT00000048392). Distinct from previous reports examining limited portions of the $\text{Ca}_v3.2$ channel for variability (Jagannathan et al., 2002; Ohkubo et al., 2005; Zhong et al., 2006), the entire open reading frame (ORF) of rat cardiac $\text{Ca}_v3.2$ transcripts was subject to systematic splice-variant analysis. In the present study, a total of 11 overlapping PCR amplifications each covering at least two exons and generating products between ~450 and ~1070 base pairs were subcloned and between 40 and 203 individual cDNAs from each of the

amplicon reactions were subject to DNA sequence analysis (Figure 2.1C). Sequences were searched against available databases and aligned with rat Ca_v3.2 genomic (NCBI, NC 005109 and Ensembl, ENSRNOT00000048392) and cDNA (NM_153814) sequences.

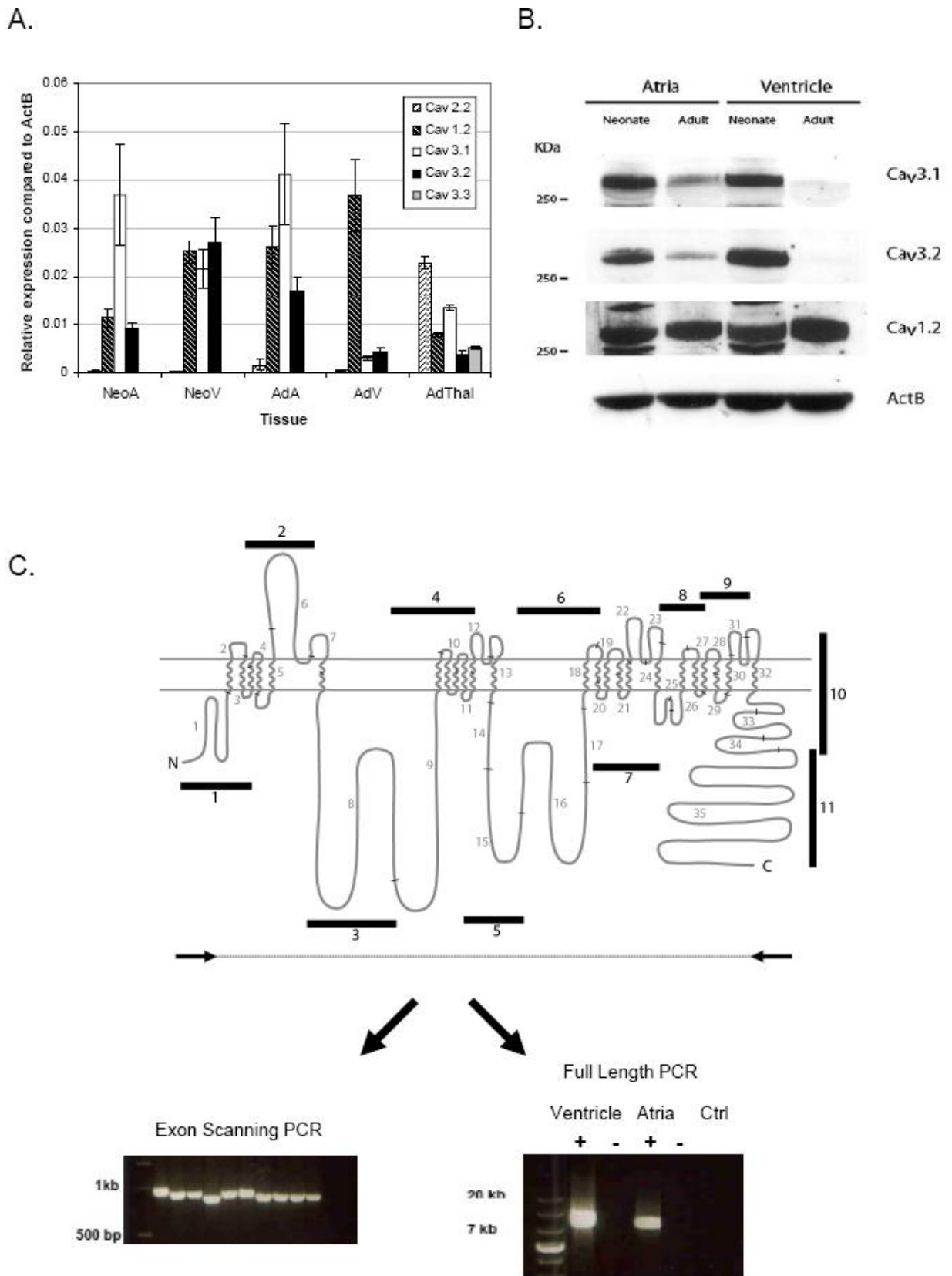


Figure 2.1. Ca^{2+} channel expression in rat cardiac tissues and identification of $\text{Ca}_v3.2$ alternative splice variants.

Panel (A) shows the relative mRNA expression of the T-type Ca_v3 , and the high-voltage activated $Ca_v1.2$ and $Ca_v2.2$ channels obtained using qRT-PCR to compare the overall level of isoform expression between newborn and adult cardiac tissues. Adult thalamic tissue is shown for comparison. Cardiac tissue displays high levels of expression of $Ca_v1.2$ and T-type $Ca_v3.1$ and $Ca_v3.2$, whereas neuronal $Ca_v2.2$ is negligible. Both $Ca_v3.1$ and $Ca_v3.2$ channels are expressed in cardiac tissues but a significant reduction was observed in adult ventricles, compared to newborn cardiac chambers. qRT-PCR reactions were run in triplicate and averages were determined. Relative amounts were compared to actin B and means were calculated. All experiments were done using 3-6 rats. Error bars show mean \pm standard error. (B) Western blot analysis showing a significant level of $Ca_v1.2$ isoform protein expression at both developmental stages, whereas $Ca_v3.1$ and $Ca_v3.2$ are prominently expressed only in newborn tissues. In the adult heart T-type channel proteins are moderately expressed in atria and at much lower levels in the ventricle. Panel (C) is a schematic of the $Ca_v3.2$ protein sequence to illustrate the strategy used to identify alternative splice variants. Numbers along the peptide sequence indicate the exon number (total of 35), and numbers on filled bars correspond to the short amplicon overlapping PCR reaction sequences used for exon scanning (bottom left). Horizontal arrows at N- and C-terminus of the channel correspond to the full-length amplification (bottom right). See Section 2.4.4 for details.

Twenty five in-frame/carboxyl variants occur at 10 distinct sites in the Ca_v3.2 protein (Figure 2.2 and Table 2.1). Analysis of 392 short amplicon cDNAs generated from neonate atrial RNA identified six in-frame and truncated C-terminus variants compared to the parental Ca_v3.2 channel: called 8a/9a, 20a, -25, 35a, 35c and Δ210 (Figure 2.2). Further analysis of 557 short amplicon cDNAs from neonate ventricle identified 14 in-frame variants and truncated C-terminus compared to the parental Ca_v3.2 channel, ten of which were unique to the neonate ventricular RNA: called variants 1a, -7, 8b, 8c, 28a/29a, 33b/34a, 35b, 35e, Δ214 and Δ304, and four of which had also been identified in neonate atria (8a/9a, 20a, -25, Δ210; Figure 2.2). In order to put the individual amplicon variants into context, full-length Ca_v3.2 cDNA was amplified from both atria and ventricle neonate RNA and 56 individually isolated full-length ventricle cDNAs and 50 full-length atria cDNAs were subject to complete DNA sequencing. In addition to placing some of the amplicon variants into their larger expression context, the full-length analyses identified a further eight Ca_v3.2 channel in-frame variants: called 1b, 7a/8d, 9c, 20b, 24a, 33a, 34b and 35d (Figure 2.2).

Alternative splicing mechanisms associated with the identified variants are suggested to include deletion and insertion of cassette exons, alternative donor/splice sites, splicing within exons, and retained introns (Black, 2003). In the amino-terminus, in-frame deletions within exon 1 result in removal of either 16 amino acids (variant 1a) or 8 amino acids (variant 1b). Further downstream, the domain I-II linker region possesses a high degree of variation with five distinct isoforms identified; variants 8b, 8c, 7a/8d, 8a/9a and 9c. An example of a canonical cassette-type exon is the inclusion (+) or exclusion (-) of exon 25 encoding residues in the domain III – IV linker, notable as a site of splice variation previously implicated in regulating voltage-dependent properties of Ca_v3.2 channels (Jagannathan et al., 2002; Ohkubo et al., 2005; Zhong et al., 2006;

Powell et al., 2009) (Appendix 5). In this same region, further neonate cardiac variation results from the partial insertion of 24 nucleotides to the end of exon 24 (called variant 24a).

In domain III, splicing due to an alternate splice acceptor site internal to exon 20 (variant 20a) leads to a 15 amino acid deletion in the cytoplasmic IIS2 – IIS3 region and the partial insertion of intron 20 (20b) confers a 7 amino acid insertion (SPLPGCR) in domain IIS3 (Figure 2.2). In domain IV, the use of alternate donor and acceptor splice sites in exons 28 and 29 respectively results in an in-frame deletion of 39 amino acids in domain IVS4 (called 28a/29a). The most extensively spliced region in Ca_v3.2 channels expressed in neonate heart occurs at the carboxyl-terminus and including the parental variant could result in up to 12 distinct carboxyl-terminal isoforms. The newly identified variants include 33a, Δ214, Δ210, Δ304, 33b/34a, 34b, 35a, 35b, 35c, 35d and 35e. The first four of these terminate at the same stop codon (last four amino acids, DEPV) whereas the remaining seven result in alternative carboxyl stop sites, all of which except 33a are shorter versions of the canonical C-terminus. The 33a splice variant contains the longest C-terminus due to inclusion of 5 additional amino acids (PPSPQ) at the proximal end.

There are several contextually noteworthy aspects evident from the 106 full-length Ca_v3.2 cDNAs analyzed. Variants 1b, 7a/8d, 9c, 20a, 24a, 33a and Δ214 always occurred in combination with the (-)25 exon splice variant whereas the 34b isoform occurred in combination with the (+)25 variant. Further, variant 35a was found in combination with either of the (+) or (-) exon 25 splice isoforms. In the full-length Ca_v3.2 cDNA there were a number of combinations of individual exonic variants: e.g., 20b/-25/33a and 20a/-25/35d. Generally, across both the amplicon and full-length analyses the majority of the Ca_v3.2 variants were found to be expressed in either atria or ventricle with a smaller portion being expressed in both chambers (8a/9a, 20a, +/-25, 35a and Δ210).

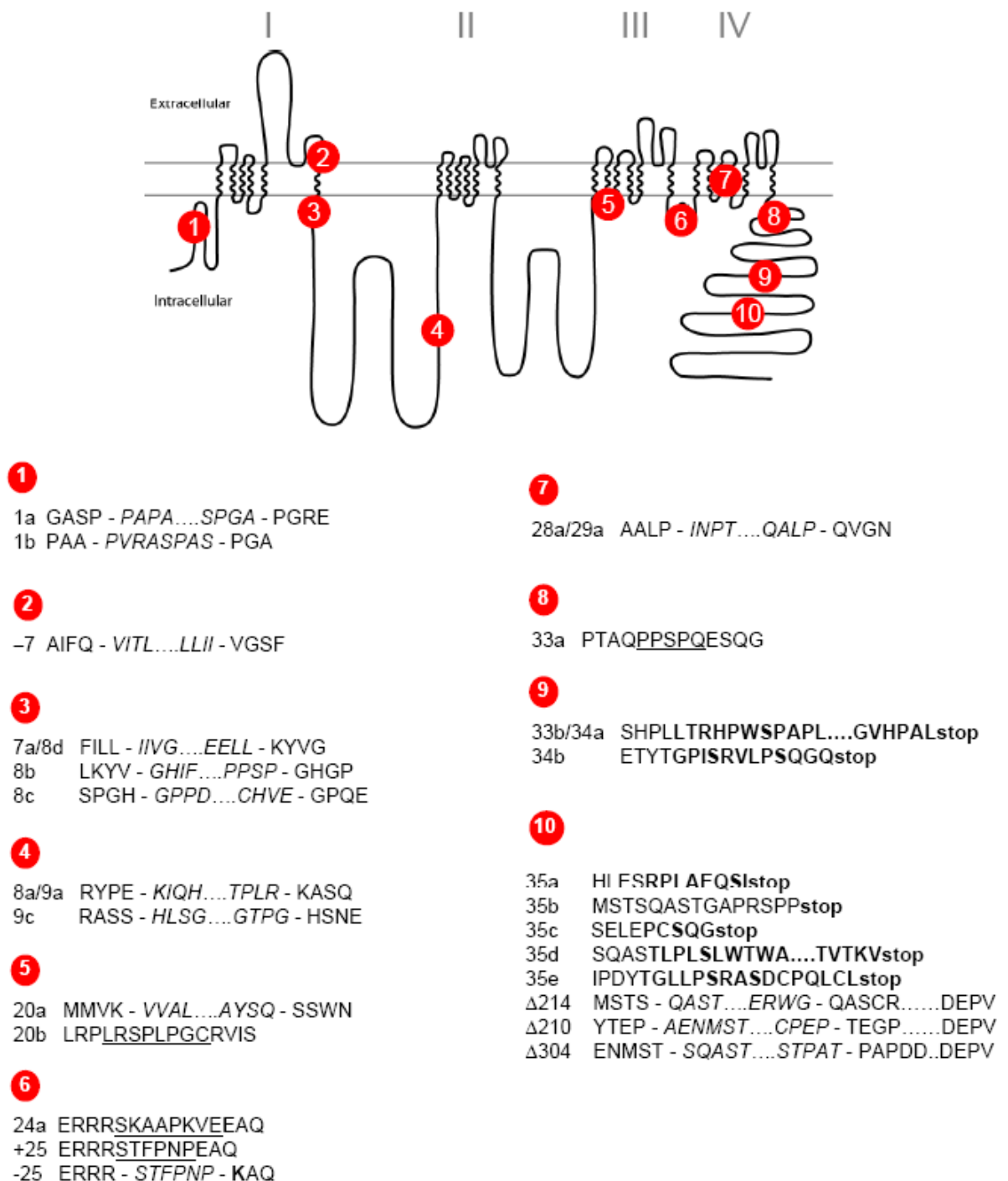


Figure 2.2. Topology of Ca_v3.2 channel showing the location of all in-frame and truncated carboxyl terminal variants.

Twenty five identified in-frame and truncated carboxyl-terminus Ca_v3.2 variants are located at 10 different sites as indicated in the diagram. The amino acid sequences (single letter code) resulting from each alteration are depicted below. Alternative splice variants are named after the alternatively spliced exons and letters after the exon number correspond to the different variants in that particular exon. (-) and (+) correspond to the absence and the presence of the indicated

exon. The symbol Δ followed by a number (n) refer to a deletion n amino acid. When alternative splicing affects consecutive exons, the variants are named using both exon designations separated by a slash. All sequences were aligned using published rat Ca_v3.2 genomic and mRNA sequences (NCBI, NC 005109; Ensembl, ENSRNOT00000048392; and NM_153814). Italicized, underlined and bold indicate deletion, insertion and alternative sequences, respectively. A dash (-) in the peptide sequences correspond to the start and end of deleted amino acids. Out of frame splice variants resulting into premature chain termination, hemichannels or interdomain truncations are not shown.

Table 2.1. Identified cardiac Ca_v3.2 T-type Ca²⁺ channel variants.

Italicized, underlined and bold indicate deletion, insertion and alternative sequences, respectively. A slash (-) in the peptide sequences correspond to the start and end of deleted amino acids. Sequences were aligned using published rat Ca_v3.2 genomic and mRNA sequences. The variants reported here are in-frame insertions and deletions as well as in-frame truncations in the carboxyl-terminus.

Location	Variant	Nucleotide Sequence	Peptide Sequence
1	1a 1b	<i>gccg - ccggcccc.....ctggggcg - ccgg</i> <i>cgcc - ggtgagg.....gcgagccc - tggg</i>	GASP - PAPA.....SPGA - PGRE PAA – PVRASPAS - PGA
2	-7	<i>tcttcag - gtcacac....tcaccatt - gtggctc</i>	AIFQ - VITL.....LLII - NGSF
3	7a/8d 8b 8c	<i>cctcctca - tcattgtg....gctcctca - agtatgta</i> <i>aagtatgt - aggccaca..ccatcccc - aggccatg</i> <i>aggccatg - gccacca..cgtggagg - ggccgcag</i>	FILL - IIVG.....EELL - KYVG LK YV - GHIF.....PPSP - GHGP SPGH - GPPDCHVE - GPQE
4	8a/9a 9c	<i>ccctatga - gaagatcc...ccactgcg - gaaggcct</i> <i>agcctcta - gccacctg.....cacaccag - gccacagc</i>	RPYE - KIQHTPLR - KASQ RASS - HLSG.....GTPG - HSNE
5	20a 20b	<i>tggtgaag - gtgtagc...acctacag - agcagttg</i> <i>ctctgagatcccctctgcctgggtcagggctcat</i>	MMVK - VVAL.....AYLQ - SSWN LRPLRSPLPGCRVIS
6	24a +25 -25	<i>gcgcaggagtaagcggcccccaaggtggaggaggcccag</i> <i>gcgcaggagcactttcccacccagaggcccag</i> <i>gcgcagga – gcactttcccacccag - aggcccag</i>	ERRRRSKAAPKVEEAQR ERRRRSTFPNPEAQ ERRRR – STFPNP - KAQ
7	28a/29a	<i>gccctgcc - catcaatc...gctctgcc - tcaggtag</i>	AALP - INPT.....QALP - QVGN
8	33a	<i>cagcagcgcctcctcaccagaaagcca</i>	PTAQPPSPQESQG
9	33b/34a 34b	<i>cccactgc - aggaagtg..tcacctctgc - tcactgcc</i> <i>ctacacag - gcccggt.....ctttccag - gtcccacagc</i>	SHPLLTRHPWSPAPL...GVHPALstop ETYTGPISRVLP SQGQstop
10	35a 35b 35c 35d 35e Δ214 Δ210 Δ304	<i>cctagagtc - ggggaagt...ctggggcc - aggcctct</i> <i>tcccctcc - gtgctccc....tgccctcc - atagggac</i> <i>ctcgaacc - agctcttg....gaggggacc - ctgtagcc</i> <i>gcatcaac - aggtgcc...tcccac - tttgcctt</i> <i>cagactacacag - agcc...gctggggccag - gcctct</i> <i>cacgagcc - aggcatac...ctggggcc - aggcctct</i> <i>cagagcct - gctgaaaa...cagagcct - acagaagg</i> <i>atgtccac - gagccagg...ccagccac - tcctgcc</i>	HLESRPLAEQSIstop MSTSQASTGAPRSPstop SELEPCSQGstop SQASTLPLSLWTWA...TVTKVstop IPDYTGLLPSRASDCPQLCLstop MSTS - QAST.....ERWG – QASCR....DEPV YTEP - AENMST...CPEP – TEGP.....DEPV ENMST - SQAST...STPAT – PAPDD...DEPV

From the combined short amplicon scanning and full-length cDNA analyses, six distinct variant regions were chosen for more in-depth expression analysis in newborn and adult heart chambers by qRT-PCR: Ca_v3.2(8b) in the domain I – II linker, Ca_v3.2(20a) between domain IIS2 and IIS3, Ca_v3.2(±25) in the domain III – IV linker and three carboxyl-terminal variants - Ca_v3.2(33a), Ca_v3.2(Δ214) and Ca_v3.2(35a) located at the proximal, middle and distal portions of the C-terminus (Figure 2.3).

In T-type channels the cytoplasmic regions mentioned above have been implicated in gating (Chemin et al., 2001a; Vitko et al., 2007), surface expression (Vitko et al., 2007) and G-protein-dependent regulation (Wolfe et al., 2003; DePuy et al., 2006). For some variant positions the reference isoform predominates in both neonate and adult and in both chambers (Figure 2.3), while in other instances there is clear evidence that both variants are co-expressed at different levels (e.g., +/-25, 35a vs reference). Of the six Ca_v3.2 variants analyzed by qRT-PCR only the (+/-) exon 25 showed a significant difference in relative abundance across newborn and adult hearts and in both atria and ventricle (Figure 2.3C).

In the human brain, testis, and uterus the Ca_v3.2 exon 26, which is homologous to the exon 25 described here, has been previously implicated in affecting activation, channel availability and recovery from inactivation (Jagannathan et al., 2002; Ohkubo et al., 2005; Zhong et al., 2006). It was therefore of interest to target this variant region for more in-depth transcript copy number analyses in the heart. Figure 2.4 shows the transcript copy numbers of Ca_v3.2 (+25) and (-25) exon splice variants normalized to rat ActB. In neonate heart the exclusion of exon 25 occurred at a level 7 to 8 fold higher in atria and ventricle tissues compared to (+25) exon variant transcripts. Contrastingly, in adult atria the relative copies of (+25) exon variant transcripts were increased while adult ventricular (-25) transcripts decreased such that overall the ratio of (+25) to (-25) variants in both adult heart chambers was approximately equal (Figure 2.4). Taken

together, there appears to be a significant developmental- and chamber-specific mechanism regulating the relative expression of Ca_v3.2 (+25) and (-25) variant channels.

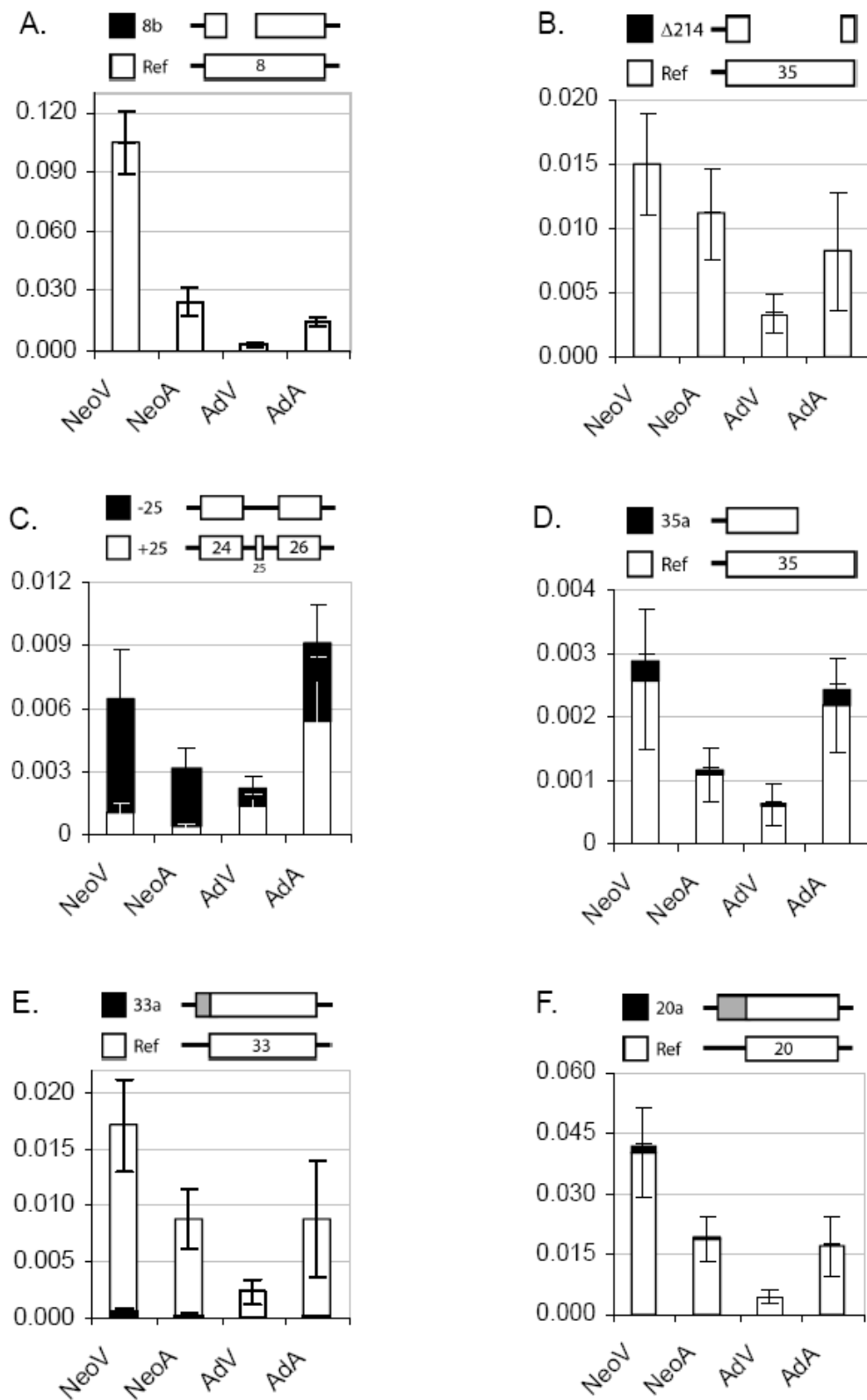


Figure 2.3. Differential expression of $Ca_v3.2$ T-type Ca^{2+} channel alternative splice variants in newborn and adult cardiac tissues.

Relative mRNA levels of Ca_v3.2 splice variants were obtained by qRT-PCR and compared at two developmental stages. Alternative splice variants 8b (**A**), Δ214 (**B**), -25 (**C**), 35a (**D**), 33a (**E**) and 20a (**F**) display different levels of expression in neonatal and adult atria and ventricle. The (-25) variant is the most abundant in neonate while both (+) and (-) exon 25 variants are present in approximately equal amounts in adult heart. Experiments were performed using 3 - 6 rats for each sample and qRT-PCR reactions were performed in triplicate. Error bars correspond to standard error. A schematic representation of each splice variant is shown in each graph. Gray box represents an alternative start to a given exon, gaps represent deletions, and open boxes the reference sequence of each exon. Y axis scale represents relative expression compared to ActB. NeoA (neonatal atria), NeoV (neonatal ventricle), AdA (adult atria), AdV (adult ventricle). Each variant probe was checked for specificity against its parental cDNA before qRT-PCR analysis.

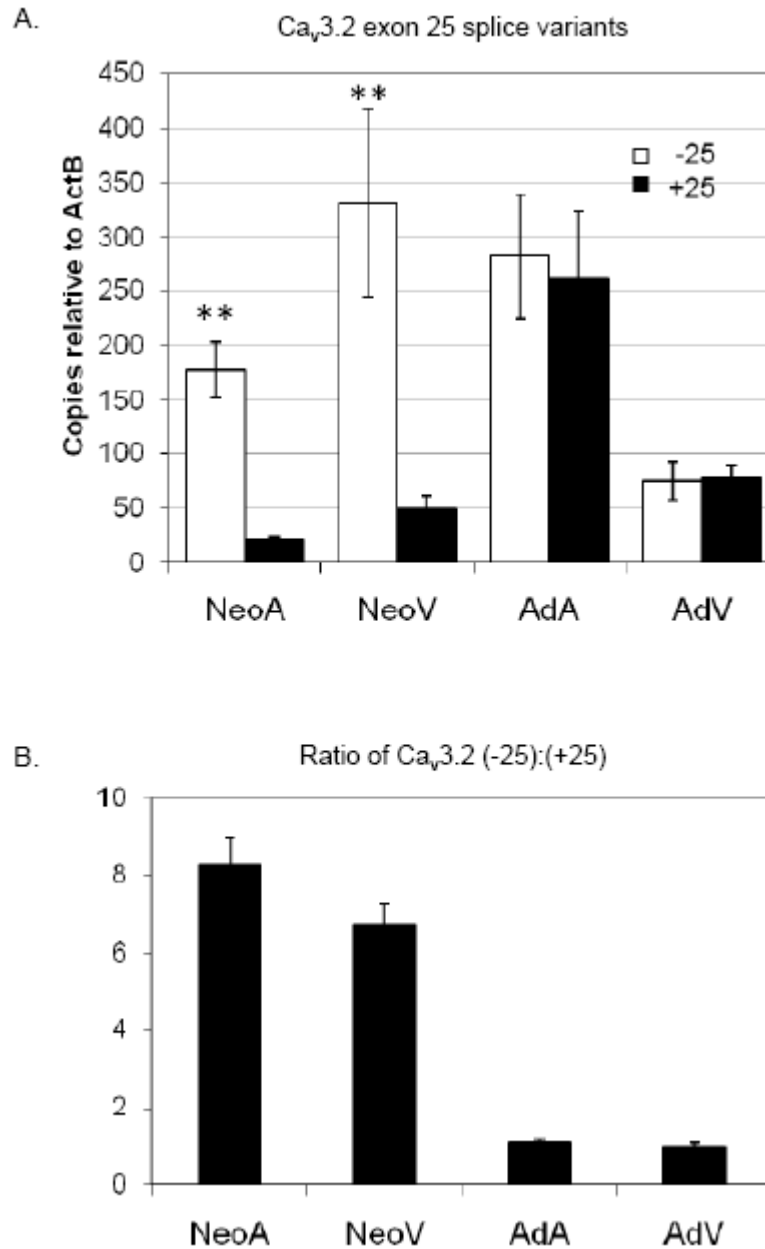


Figure 2.4. Spatial and developmental changes in the expression of $Ca_v3.2(+25)$ and $Ca_v3.2(-25)$ exon splice variants.

Panel (A) shows developmental differences in the relative number of transcript copies of $Ca_v3.2$ (+25) and (-25) splice variants. There is preferential expression of (-25) $Ca_v3.2$ variant channels compared to (+25) alternative splice variant in newborn ventricle and atria. Approximately the same level of mRNA expression of both exon 25 variants was observed in adult heart. The developmental shift in the proportion of exon 25 variants expressed in cardiac chambers is shown on panel B. (B) A ~7 to 8 fold difference in the ratio of (-25) over (+25) exon variant copy number was obtained using specific qRT-PCR probes and titration against quantified cDNA clones from each respective variant and then normalized relative to rActB levels. Error bars show standard error. T-tests were performed to measure significant differences. ** $p < 0.01$. NeoA(neonatal atria), NeoV(neonatal ventricle), AdA(adult atria), AdV(adult ventricle).

2.2.2 Exclusion of exon 25 confers voltage-dependent facilitation and accelerates recovery from inactivation

The full-length cDNA screening revealed that Ca_v3.2 channel variants in neonate heart predominantly occur in the context of exclusion of exon 25 (also see Figures 2.3 and 2.4). In this regard, several full-length variants in the context of the (-25) isoform were analyzed following heterologous expression in HEK cells using whole-cell patch-clamp. Biophysical characterization was performed on the following variants identified by full-length cDNA screening: Ca_v3.2(-7/-25), Ca_v3.2(20a/-25), Ca_v3.2(20b/-25), Ca_v3.2(-25), Ca_v3.2(+25), Ca_v3.2(24a/-25), Ca_v3.2(33a/-25), Ca_v3.2(Δ214/-25), Ca_v3.2(35a/-25) and Ca_v3.2(35a/+25). This research also analyzed the Ca_v3.2(8b/-25) variant which was identified by short amplicon screening. Ca_v3.2(8b/-25) splice variant is located at the I - II linker, a region implicated in controlling gating and plasma membrane surface expression (Vitko et al., 2007).

Examination of current densities from macroscopic Ca²⁺ currents showed that Ca_v3.2(+25), Ca_v3.2(Δ214/-25), Ca_v3.2(35a/-25) and Ca_v3.2(8b/-25) variants had significantly higher current densities (30.34 ± 4.13 , 31.60 ± 5.95 , 38.39 ± 5.70 , 66.14 ± 17.45 pA/pF, respectively) compared with the Ca_v3.2(-25) variant (21.64 ± 1.88 pA/pF). The parameters of voltage-dependent gating properties are summarized in Table 2.2. Overall, exon 25 containing variant channels displayed small but significant differences in the voltage dependence of activation. Ca_v3.2(8b/-25) and Ca_v3.2(+25) showed ~10 mV and ~5 mV leftward shifts in the V_{50act} relative to Ca_v3.2(-25) (Figure 2.5A and Table 2.2). In regards to steady-state inactivation, a 10 mV hyperpolarizing shift was observed when Ca_v3.2(8b/-25) (V_{50inact} = -75.7 ± 0.3 mV) was compared with Ca_v3.2(-25) (V_{50inact} = -65.5 ± 0.3 mV)(Figure 2.5C and Table 2.2). The voltage-dependence of deactivation as well as the kinetics of Ca²⁺ currents generated by expressing the splice variants was also analyzed. The proximal C-terminus splice variant Ca_v3.2(33a/-25) and

the alternative exon 24 variant Ca_v3.2(24a/-25) were only the two alternative splice variants showing changes in the kinetics of activation and inactivation compared to Ca_v3.2(-25) (Table 2.2). Ca_v3.2(-7/-25) and Ca_v3.2 (20a/-25) did not yield measurable Ca²⁺ currents whereas Ca_v3.2(20b/-25) showed low level of expression. All eight fully characterized splice variants examined showed similar voltage-dependence of deactivation (Table 2.3).

The recovery from inactivation was investigated using a double pulse protocol (Fig. 2.6A inset) and time constants obtained by fitting a double exponential function are shown in Table 2.3. Ca_v3.2(-25) channels recovered significantly faster (~ 1 second) from inactivation than Ca_v3.2(+25) channels (~2.5 seconds; Figure 2.6A and Table 2.3). Interestingly, compared to Ca_v3.2(+25) channels, Ca_v3.2(-25) channels recover from inactivation to a level greater than 100%, suggesting facilitation (or potentiation) of this variant. The distal carboxyl-terminus variant Ca_v3.2(35a) also displayed significant potentiation when expressed in combination with Ca_v3.2(-25) but not when expressed in a Ca_v3.2(+25) background (Figure 2.6A), suggesting that exclusion of exon 25 residues located in the domain III – IV linker are a structural determinant for the observed facilitation. Additionally, the relative proportion of the channels recovering from fast (τ_1) and slow (τ_2) inactivation was estimated by obtaining the ratio between the current amplitude of each component and the total current amplitude. The fast inactivation component (relative A₁) is predominant in Ca_v3.2(-25) (Table 2.3). In contrast, the slow inactivation component (relative A₂) is higher in Ca_v3.2(+25) than Ca_v3.2(-25). Representative current traces of recovery from inactivation for Ca_v3.2(-25) and Ca_v3.2(+25) variants are shown in Figures 2.6B and 2.6C, respectively. In order to further investigate if the potentiation observed in Ca_v3.2(-25) variant could be attributed to VDF, two pulse protocols were used as shown in Figure 2.6D and 2.6F. Percentage of VDF (Figure 2.6E) was measured as the ratio of current magnitude evoked by a test pulse at -30 mV applied after a strong depolarizing prepulse

(+120mV) over the current magnitude in the absence of prepulse. The time course was determined by increasing the time intervals (from 300 ms to 1500 ms) between the prepulse and the test pulse (Figure 2.6D). Voltage dependence of facilitation was then explored by applying prepulses from -120 mV to +150 mV with a constant interpulse interval of 1200 ms (Figure 2.6F). The robust VDF displayed by $Ca_v3.2(-25)$ (50-60%) was absent in the $Ca_v3.2(+25)$ splice variant (Figure 2.6E). Furthermore, $Ca_v3.2(35a/-25)$ also showed facilitation properties (50 – 60%) (data not shown), consistent with an increase in fractional recovery (Figure 2.6A) when expressed in the $Ca_v3.2(-25)$ background, but not when expressed in combination with $Ca_v3.2(+25)$, suggesting that exclusion of exon 25 in the rat $Ca_v3.2$ III-IV linker region is associated with VDF. This property was also observed when Ba^{2+} was substituted for Ca^{2+} in the external recording solution. The degree of relative facilitation for both the $Ca_v3.2(-)$ and $(+)$ exon 25 splice variants showed no significant difference regardless of whether Ca^{2+} or Ba^{2+} was the charge carrier thereby affirming the facilitation as being voltage-dependent (Figure 2.7). The magnitude of facilitation elicited by strong depolarizing prepulses was also examined in stable cell lines expressing human $Ca_v3.1$ and $Ca_v3.3$ isoforms and compared with that observed for the $Ca_v3.2(+/-25)$ splice variant (Figure 2.8). Consistent with previous studies (Klockner et al., 1999; Gomora et al., 2002), $Ca_v3.3$ channels display an approximate 20% VDF, significantly smaller than that reported here for $Ca_v3.2(-25)$ variant channels. $Ca_v3.1$ T-type channel examined did not display VDF.

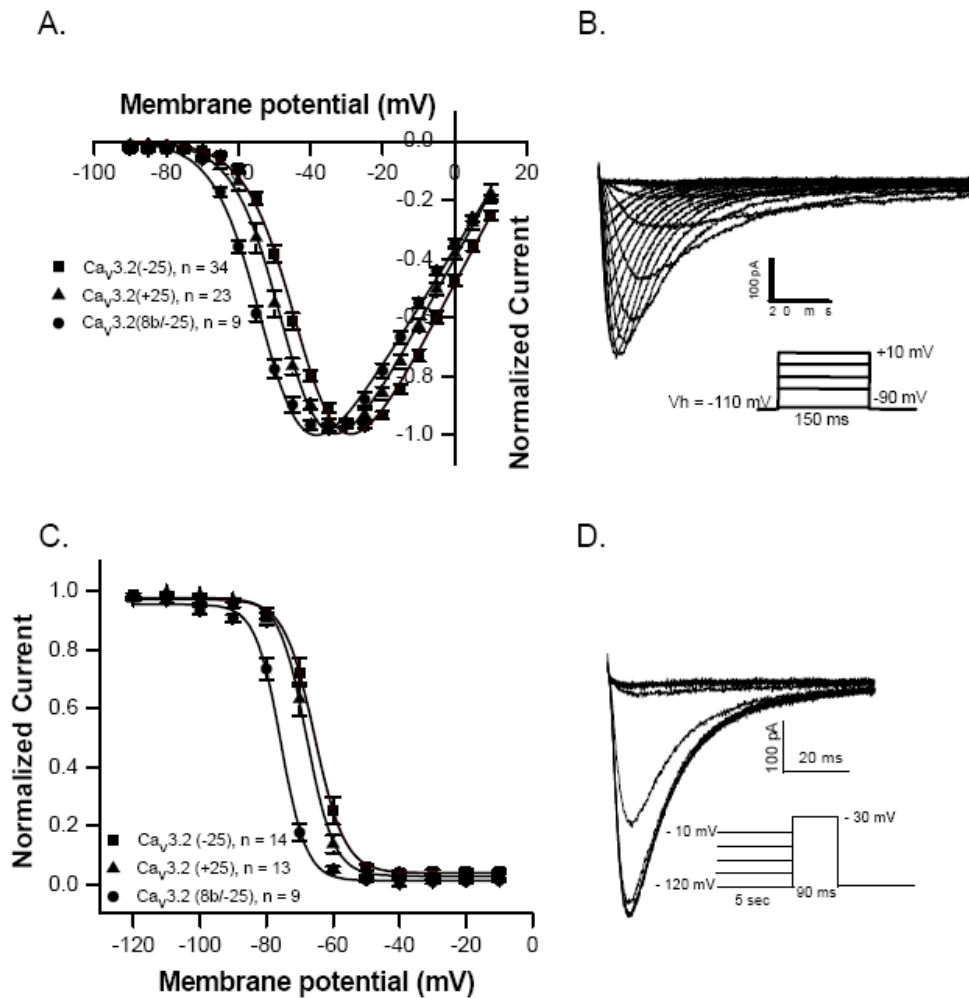


Figure 2.5. Representative data on the voltage-dependent properties of $Ca_v3.2$ alternative splice variants.

(A) Normalized current-voltage relationships (I-V) of $Ca_v3.2(+25)$ and $Ca_v3.2(8b/-25)$ compared with $Ca_v3.2(-25)$ alternative splice variants. The expression of exon 25 in the III – IV linker showed a 5 mV negative shift in I-V whereas deletion of 99 amino acid in the I – II linker resulted into 10 mV negative shift. (B) Representative traces and waveforms acquired from recording I-V relationships. The current-voltage (I-V) relationships were obtained by depolarizing the membrane with 150 msec test pulses from -90 to +10 mV at 5 mV steps ($V_h = -110$ mV). Voltage waveforms are shown as an inset. Normalized peak amplitude of Ca^{2+} currents was plotted against test pulse potential. Averaged values were fitted using a modified Boltzmann equation: $I = (G_{max} * (V_m - E_r)) / (1 + \exp((V_m - V_{50})/k))$, where G_{max} is the maximum value of membrane conductance, V_m is the test potential, E_r is the extrapolated reversal potential, V_{50} is the half-activation potential, and k the slope factor. (C) Steady state inactivation curves for the three variants indicating a 10 mV hyperpolarizing shift for $Ca_v3.2(8b/-25)$ and no significant difference for $Ca_v3.2(+25)$. Example of steady state inactivation recordings and waveforms are shown in (D). Steady state inactivation curves were obtained with a double pulse protocol with 5s conditioning prepulses from -120 to -10 mV in 10 mV increments. Averaged values for the normalized peak currents are plotted as a function of conditioning prepulse potential. *All variants were compared against $Ca_v3.2(-25)$ and significant differences were calculated using ANOVA $p < 0.05$.

Table 2.2. Gating properties of Ca_v3.2 alternative splice variants.

	Activation				Inactivation				
	V _{50act} (mV)	k(mV)	τ _{act} (ms)	n	V _{50inact} (mV)	k(mV)	n	τ _{inact} (ms)	n
Ca _v 3.2(-25)	-41.4 ± 0.5	-7.0 ± 0.3	21.8 ± 0.9	34	-65.5 ± 0.3	4.5 ± 0.2	14	5.6 ± 0.5	30
Ca _v 3.2(8b/-25)	-51.7 ± 0.4*	-6.5 ± 0.3	18.3 ± 0.9	9	-75.7 ± 0.3*	3.8 ± 0.2	9	4.5 ± 0.5	8
Ca _v 3.2(24a/-25)	-44.4 ± 0.4	-6.9 ± 0.3	25.0 ± 3.7	10	-69.0 ± 0.2	4.6 ± 0.2	7	8.1 ± 0.7*	8
Ca _v 3.2(33a/-25)	-39.2 ± 0.6	-7.7 ± 0.3	39.6 ± 5.5*	11	-63.9 ± 0.2	4.6 ± 0.2	7	3.8 ± 0.3*	8
Ca _v 3.2(Δ214/-25)	-41.2 ± 0.6	-7.7 ± 0.3	25.5 ± 2.5	12	-63.8 ± 0.3	4.8 ± 0.2	6	8.0 ± 1.1	10
Ca _v 3.2(35a/-25)	-44.4 ± 0.5	-6.2 ± 0.3	21.0 ± 2.5	14	-66.5 ± 0.2	4.2 ± 0.2	11	5.6 ± 0.8	15
Ca _v 3.2(35a/+25)	-46.6 ± 0.4*	-6.0 ± 0.3	19.5 ± 0.6	10	-68.3 ± 0.1	4.9 ± 0.1	10	5.5 ± 0.7	10
Ca _v 3.2(+25)	-45.7 ± 0.7*	-6.6 ± 0.3	19.5 ± 2.2	23	-67.9 ± 0.2	4.1 ± 0.2	13	5.5 ± 0.5	20

*All variants were compared against Ca_v3.2(-25) and significant differences were calculated using ANOVA p < 0.05. τ_{act} – time constant of activation; τ_{inact} – time constant of inactivation.

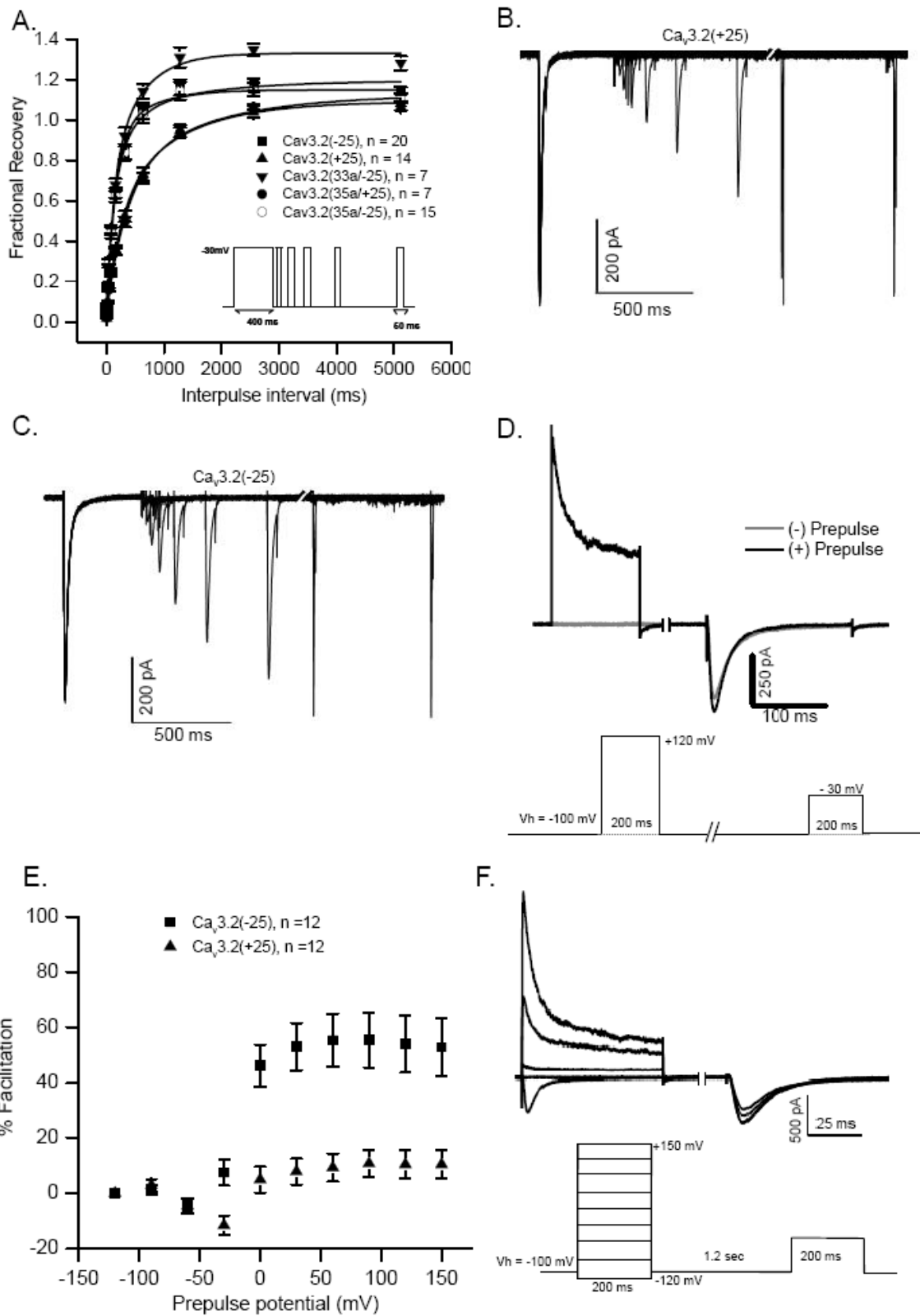


Figure 2.6. Alternative splicing affects the time course of recovery from inactivation and voltage-dependent facilitation of $Ca_v3.2$ T-type macroscopic currents.

(A) The splice variant generated by exclusion of exon 25 ($Ca_v3.2(-25)$, filled squares) displays a faster recovery from inactivation than the variant $Ca_v3.2(+25)$ variant (upright triangles) enabling $Ca_v3.2$ channels to recover to more than 100% after a prolonged depolarization. The contribution of carboxyl-tail domain on the recovery from inactivation was explored by expressing both the (+) and (-) 25 exon variants in combination with the (35a) variant. Maximal fraction and time course of recovery from inactivation of 35a/+25 (filled circles) and 35a/-25 (open circles) were determined by the exon 25 variant used as background. A significant increase in fractional recovery was observed when the variant 33a (a five amino acid insertion in the proximal C-terminus) was expressed in combination with the (-25) variant ($Ca_v3.2(33a/-25)$, inverted triangles). Recovery from inactivation was studied with a double-pulse protocol (**inset Panel A**) using a 400 ms prepulse to -30 mV from a holding potential of -110 mV. After the inactivating prepulse, a 50 ms test pulse to -30 mV was given after a varying time period (interpulse interval) between 5 and 5000 ms. The peak current from the test pulse was plotted as a ratio of maximum pre-pulse current versus interval between pulses. Average data were fitted with a double exponential function to obtain the time constants for the fast (τ_1) and slow (τ_2) components of recovery from inactivation. Representative traces are shown for $Ca_v3.2(+25)$ (**B**) and $Ca_v3.2(-25)$ (**C**). The time course of VDF was explored with the protocol shown in (**D**). A strong depolarization to +120 mV was applied from a holding potential of -100 mV and followed by a 200 ms test pulse to -30 mV with interpulse intervals of 300, 600, 900, 1200, 1500 ms. Representative traces illustrate VDF of $Ca_v3.2(-25)$ variant. (**E**) The current ratio was determined by dividing the current amplitude of the test pulses preceded by a prepulse by that of the test pulse without a prepulse. Robust voltage-dependent facilitation (VDF) was observed in the $Ca_v3.2(-25)$ splice variant (filled squares) compared with $Ca_v3.2(+25)$. VDF was observed with prepulses from 0 mV to +150 mV. Representative traces for $Ca_v3.2(-25)$ VDF and the protocol used are shown on panel (**F**). VDF was studied by applying a 200 ms test pulse to -30 mV following a series of depolarizing prepulses from -120 to +150 mV after a time interval of 1.2 sec.

Table 2.3. Deactivation and recovery from inactivation of Ca_v3.2 alternative splice variants.

	Deactivation		Recovery from Inactivation				
	$\tau_{\text{deact}}(\text{ms})$	n	$\tau_1(\text{ms})$	$\tau_2(\text{ms})$	Relative A ₁	Relative A ₂	n
Ca _v 3.2(-25)	17.7 ± 1.0	14	36.6 ± 12.3	325.0 ± 33.4	0.74 ± 0.03	0.26 ± 0.04	20
Ca _v 3.2(8b/-25)	22.2 ± 1.5	8	50.2 ± 24.2	306.1 ± 36.9	0.78 ± 0.13	0.22 ± 0.12	7
Ca _v 3.2(24a/-25)	23.9 ± 1.3	5	25.3 ± 13.9	532.2 ± 13.3*	0.07 ± 0.02*	0.93 ± 0.02*	10
Ca _v 3.2(33a/-25)	19.3 ± 1.4	7	47.3 ± 14.9	356.1 ± 33.5	0.75 ± 0.09	0.25 ± 0.09	7
Ca _v 3.2(Δ214/-25)	16.6 ± 0.9	5	36.9 ± 12.8	330.9 ± 30.6	0.76 ± 0.06	0.24 ± 0.06	6
Ca _v 3.2(35a/-25)	20.4 ± 1.1	8	32.5 ± 12.0	295.3 ± 27.9	0.77 ± 0.05	0.23 ± 0.05	15
Ca _v 3.2(35a/+25)	24.2 ± 1.7	10	31.8 ± 2.9	693.8 ± 9.9*	0.15 ± 0.01*	0.85 ± 0.01*	7
Ca _v 3.2(+25)	20.0 ± 0.8	12	32.3 ± 7.6	629.9 ± 25.0*	0.16 ± 0.01*	0.84 ± 0.01*	14

*All variants were compared against Ca_v3.2(-25) and significant differences were calculated using ANOVA $p < 0.05$.

τ_{deact} – time constant of deactivation, τ_1 – fast time constant of recovery from inactivation, τ_2 – slow time constant of recovery from inactivation. Relative A₁ – relative current amplitude at τ_1 . Relative A₂ – relative current amplitude at τ_2 . The recovery from inactivation was determined at $V_h = -110$ mV.

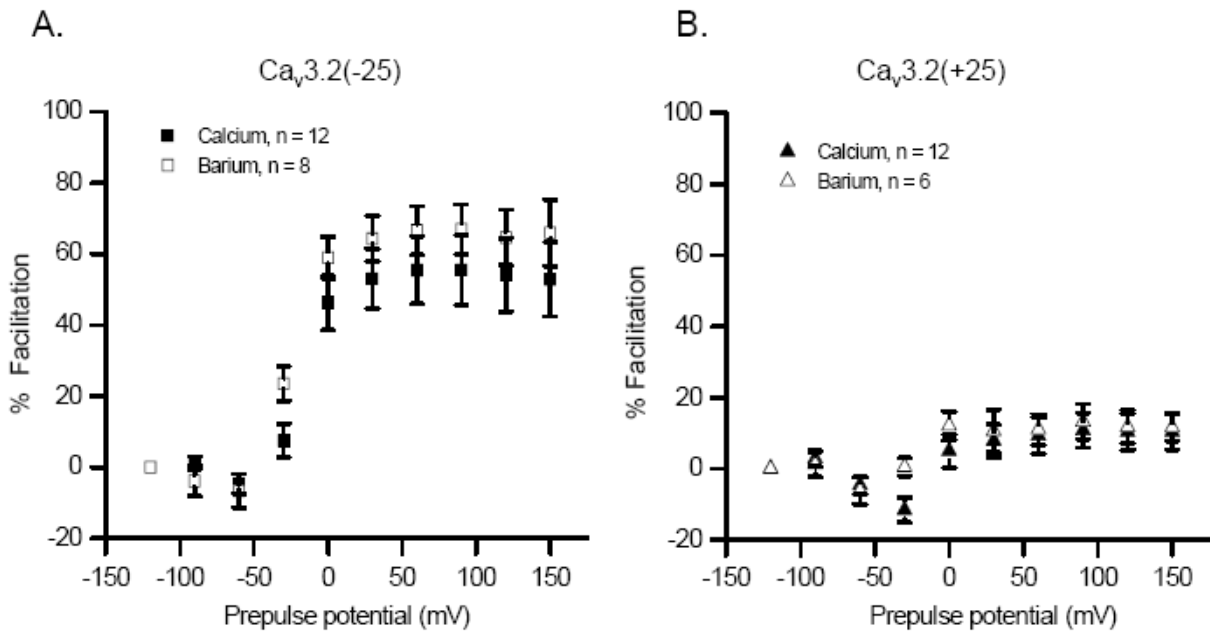


Figure 2.7. The voltage-dependent facilitation of Ca_v3.2(-25) T-type Ca²⁺ channels does not depend upon Ca²⁺.

The ionic sensitivity of voltage-dependent facilitation was explored using Ca²⁺ or Ba²⁺ as charge carriers in both the exon 25 (+) and (-) splice variants. The magnitude of relative facilitation observed in Ca_v3.2(-25) (**Panel A**) and Ca_v3.2(+25) (**Panel B**) showed no significant difference when currents were recorded in calcium (filled symbols) or barium (open symbols). Data were obtained using the pulse protocol shown in the insets of Figures 2.6D and 2.6F.

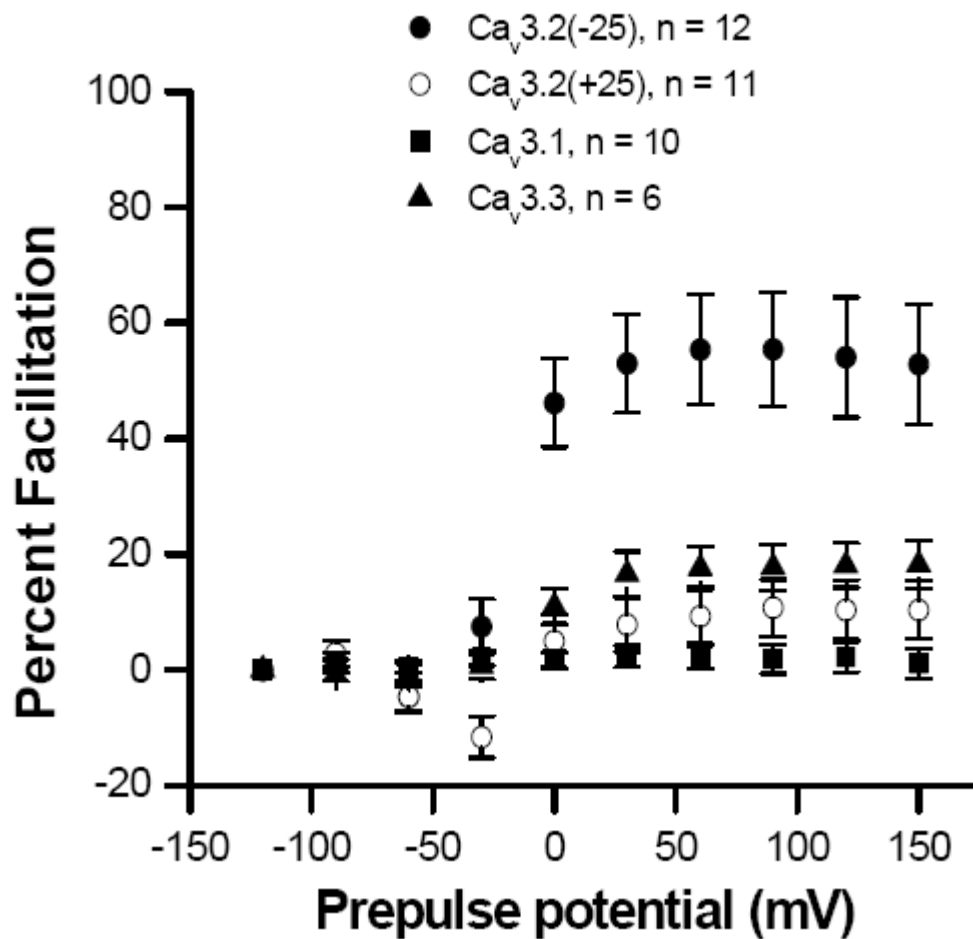


Figure 2.8. Voltage-dependent facilitation differs in T-type Ca²⁺ channel isoforms.

Percentage of facilitation as a function of prepulse potential was compared between different T-type channel isoforms. The absence of facilitation was characteristic of the Ca_v3.1 isoform (filled squares). Ca²⁺ currents through recombinant Ca_v3.2(+25) splice variant (open circles) facilitated approximately 5-7% compared to 20% observed in Ca_v3.3 isoform (filled triangles). Ca_v3.2(-25) splice variant (filled circles) displayed a robust facilitation (50 to 60%). VDF was calculated as the ratio of current magnitude evoked by a test pulse at -30 mV applied after strong depolarizing prepulses over the current magnitude in the absence of prepulse (see Figure 2.6 for pulse protocol). Stable cell lines expressing human Ca_v3.1 and Ca_v3.3 T-type channels were kindly provided by Neuromed Pharmaceuticals. HEK293 cells expressing Ca_v3.1 and Ca_v3.3 channels were maintained in DMEM containing zeocin (25 μg/mL) and hygromycin (300 μg/mL), respectively.

2.2.3 The effect of cAMP and G $\beta_2\gamma_2$ on Ca $_v$ 3.2 voltage-dependent facilitation

The inclusion of exon 25 in the Ca $_v$ 3.2 introduces a consensus phosphorylation site for PKA suggesting the possibility that Ca $_v$ 3.2 (\pm) exon 25 splice variants could be differentially regulated by cAMP-dependent mechanisms. In this regard, the effect of cAMP on the Ca $_v$ 3.2 VDF was examined. The effect of cAMP on VDF was studied in Ca $_v$ 3.2 (\pm) exon 25 alternative splice variants via perfusion with 10 μ M forskolin in combination with 10 mM IBMX (3-isobutyl-1-methylxanthine). Forskolin elevates cAMP via activation of adenylyl cyclase whereas IBMX prevents degradation of cAMP via inhibition of phosphodiesterase. Whole cell patch clamp analysis of HEK-293 cells on VDF of Ca $_v$ 3.2 exon 25 splice variants revealed absence of significant difference between the basal and facilitated currents in treated and control cells (Figures 2.9B and 2.9C). VDF of Ca $_v$ 3.2(-25) variant channel was not affected by the combined perfusion of forskolin and IBMX (Figures 2.9B and 2.9C). Similarly, a lack of VDF of forskolin/IBMX was also observed on Ca $_v$ 3.2(+25) variant channels (Figure 2.9C lower panel), an indication of the absence of regulation by cAMP.

Previous studies showed that Ca $_v$ 3.2 channels are inhibited by G $\beta\gamma$ specifically the G $\beta_2\gamma_2$ subunits (Drolet et al., 1997; Wolfe et al., 2003; DePuy et al., 2006). The effect of G $\beta\gamma$ on Ca $_v$ 3.2 VDF was investigated in this study. Figures 2.9D and 2.9E illustrate the effect of co-transfected G β_2 and G γ_2 on VDF of Ca $_v$ 3.2(-25) and Ca $_v$ 3.2(+25) splice variants, respectively. Co-transfection of G $\beta_2\gamma_2$ with the Ca $_v$ 3.2(-25) variant showed an ~50% reduction of VDF positive to -30 mV (Figure 2.9D). In contrast, Ca $_v$ 3.2(+25) co-transfected with G $\beta_2\gamma_2$ showed neither decreased nor increased VDF (Figure 2.9E).

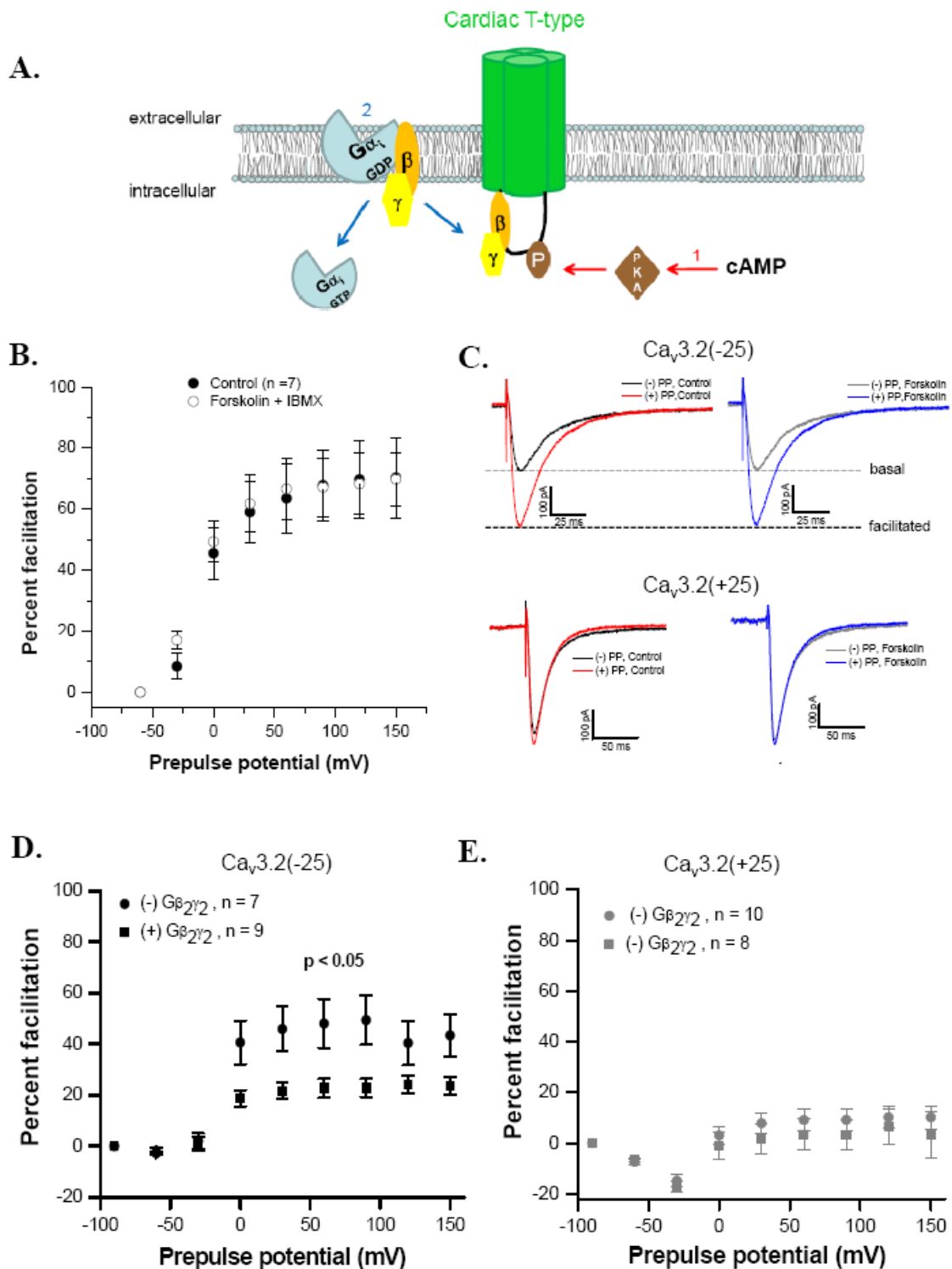


Figure 2.9. The effect of Gβγ and cAMP on voltage-dependent facilitation (VDF) of cardiac Ca_v3.2 exon 25 alternative splice variants.

(A) Schematic representation of G_{αi} activation and Gβγ binding as well as cAMP activation/PKA phosphorylation of Ca_v3.2 channel. (B) Forskolin treatment showed no effect on the VDF properties of Ca_v3.2(-25) alternative splice variants. (C) Representative traces for

Ca_v3.2(-25)(top panel) and Ca_v3.2(+25) (bottom panel) showed lack of effect by forskolin on basal and facilitated T-type Ca²⁺ currents. Black traces represent basal currents in control cells; gray traces represent basal current in forskolin treated cells; red traces represent facilitated currents in control cells and blue traces represent facilitated currents in forskolin treated cells. (D) Ca_v3.2(-25) showed reduction of VDF by Gβ₂γ₂ from potentials positive to 0 mV. (E) Gβ₂γ₂ showed no effect on Ca_v3.2(+25).

2.2.4 Differential expression of Ca_v3.2 exon 25 variants in hypertension-associated cardiac hypertrophy

Both the altered expression of T-type Ca²⁺ channels and electrical properties of cardiomyocytes have been reported to be associated with a number of cardiac disease states (Nuss and Houser, 1993; Martinez et al., 1999; Huang et al., 2000; Yasui et al., 2005; Takebayashi et al., 2006). In order to examine the expression profile of identified cardiac Ca_v3.2 splice variants in diseased heart, cardiac tissue from adult spontaneously hypertensive rats (SHR) was analyzed as described above. Figures 2.10C and 2.10D show a comparison of the quantitative mRNA analysis of Ca_v3.2(+/-25) splice isoforms in cardiac tissue from normotensive WKY and SHR rats. The hypertrophic phenotype of the SHR animals was confirmed using the two molecular markers SIAT7 (Cerutti et al., 2006) and Frzb (Zhao et al., 2004), known to be upregulated in pathological cardiac hypertrophy (Figure 2.10B). The pathological phenotype of SHR was further confirmed by the elevation in heart weight/body weight (HW/BW) ratio in SHR animals, compared to age- and sex-matched normotensive WKY rats (data not shown). Also, the occurrence of perivascular and focal interstitial fibrosis, determined using Masson's trichrome technique, was used as an indicator of pathological hypertrophy in ventricular tissue from SHR hearts (Figure 2.10A). The quantitative mRNA analysis of rat rSIAT7 and rFrzb showed a ~4 -5 fold increase of mRNA levels in hypertrophic

SHR compared to normotensive WKY left ventricle (Figure 2.10B). Importantly, a significant increase in the relative amount of $Ca_v3.2(+25)$ splice isoform compared to $Ca_v3.2(-25)$ (Figures 2.10C and 2.10D) results in a shift in the predominant exon 25 splice isoform expressed in hypertrophic SHR, suggesting a splice-specific upregulation of $Ca_v3.2$ mRNA transcripts during pathological hypertrophic heart remodeling, in addition to an overall increase in total $Ca_v3.2$ isoform expression.

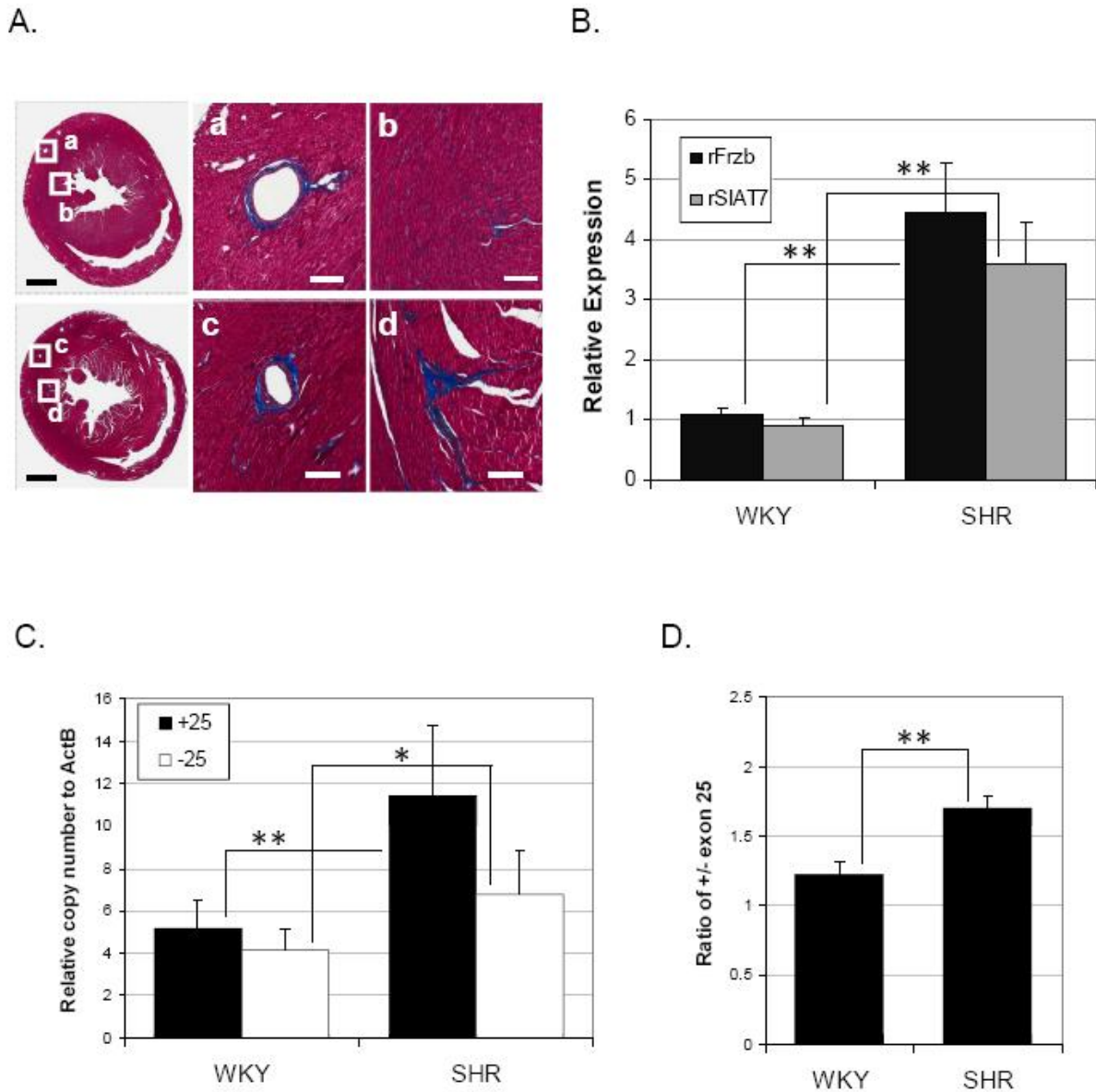


Figure 2.10. Alteration of Ca_v3.2(+25) and (-25) splice variant expression is associated with the hypertrophic SHR pathological phenotype.

(A) Histopathological markers in cardiac tissue from hypertrophic SHRs. Photomicrographs of ventricular sections of cardiac tissue stained with Masson's trichrome show perivascular (c) and interstitial (d) accumulation of fibrillar collagen in SHR heart (lower panels, c and d) compared to the age- and sex-matched normotensive WKY (upper panels, a and b). Leftmost panel calibration bar is 2 mm and a, b, c and d middle and right panels is 200 μ m. Cardiac tissue was embedded in paraffin, sectioned at 5 μ m and stained by the Masson's trichrome technique. (B) Real time PCR revealed the expression of the rat Frzb(rFrzb) and rat SIAT7(rSIAT7) hypertrophic markers relative to rActB in cDNA samples generated from left ventricle tissue from adult hypertrophic SHR or adult normotensive WKY. Five individual animals were sampled for each group. The same cDNA samples were used to measure expression of the Ca_v3.2

(+25) and (-25) exon splice variants in the SHR and WKY groups. (C) Transcript copies of (+25) and (-25) were calculated from each sample and normalized to rActB. Both variants were upregulated in hypertrophic SHR although the (+25) variant showed more pronounced upregulation indicating the preferential re-expression of (+25) splice variant in cardiac hypertrophy (D). Error bars indicate standard error. T-tests were performed to measure significant differences. **p<0.01, *p<0.05.

2.3 Discussion

The present study provides evidence for the differential regional and temporal expression of alternatively spliced Ca_v3.2 T-type Ca²⁺ channels in rat heart. Alternative splice variants span the entire Ca_v3.2 channel with the carboxyl-terminal region being the most extensively spliced domain. Examining cardiac regional and developmental expression patterns by qRT-PCR, the inclusion or exclusion of exon 25 in the domain III-IV linker generates the most distinct splice variant expression profile in cardiac Ca_v3.2 channels. Further, examining hypertrophic heart from adult SHR animals, a significant overall up-regulation of Ca_v3.2 expression was observed and occurred in the context of a change in the ratio of the exon (+/-) 25 splice variants. Heterologous expression analysis of predominant splice variants demonstrated distinct recovery from inactivation and VDF properties are associated with the exon (+/-) 25 containing variant channels. This thesis is the first comprehensive study across the full length Ca_v3.2 channel and which also demonstrates splice variation is correlated with cardiac development and the hypertrophic state.

2.3.1 Splice variant specific expression of cardiac Ca_v3.2 Ca²⁺ channels in development and hypertrophy

Alternative splicing of partial regions of Ca_v3.2 T-type channels has thus far been reported from human fetal brain, testicular and pregnant uterine tissue (Jagannathan et al., 2002;

Ohkubo et al., 2005; Zhong et al., 2006). This thesis examined the entire ORF of rat heart $Ca_v3.2$ channels using both short amplicon and full-length cDNA analyses and further examined predominant variants by qRT-PCR and exogenous expression. The results indicate that cardiac $Ca_v3.2$ channels are subject to extensive alternative splicing, particularly in predicted cytoplasmic regions where second messenger-dependent modulatory and protein-protein interaction sites are primarily located (e.g.(Wolfe et al., 2003; DePuy et al., 2006)). The cytoplasmic regions of T-type channels are known to affect channel gating (Chemin et al., 2001a; Vitko et al., 2007), trafficking to the membrane,(Vitko et al., 2007), G-protein dependent modulation (Wolfe et al., 2003; DePuy et al., 2006; Hildebrand et al., 2007) (Appendix 2), and regulation by a number of kinases (Arnoult et al., 1997; Welsby et al., 2003; Iftinca and Zamponi, 2009) suggesting that alternative splicing in these regions has the potential for affecting the modulation and functional diversity of cardiac $Ca_v3.2$ T-type channels.

The inclusion or exclusion of the cassette exon 25 encoding residues in the domain III - IV linker was the most common splicing event in cardiac samples. The exclusion of exon 25 is the predominant splice variant in newborn rat heart, being 7-8 fold higher than $Ca_v3.2(+25)$ variant channels in newborn cardiac tissue (Figure 2.4B). Contrastingly, in adult rat heart the expression of the two variants was approximately equal. A significant reduction in the expression of ventricular $Ca_v3.2(-25)$ splice-variant channels reported here might explain the overall down-regulation reported in previous studies for $Ca_v3.2$ isoform in the adult (Qu and Boutjdir, 2001; Yasui et al., 2005). However, in the atria, a significant amount of both $Ca_v3.2 (+)$ or $(-)$ exon 25 variants was detected (Figure 2.4A).

In order to determine whether $Ca_v3.2$ alternative splicing is altered during cardiac remodeling associated with diseased heart, the hypertrophic SHR model was examined. Previous studies have shown that $Ca_v3.2$ T-type channels are generally re-expressed in

hypertrophied heart (Nuss and Houser, 1993; Martinez et al., 1999; Takebayashi et al., 2006).

The current study addresses for the first time whether there are specific changes in the profile of $Ca_v3.2$ splice-variants in cardiac tissue from hypertension-associated hypertrophic heart.

Quantitative analysis showed a preferential expression of the inclusion of (+)25 exon containing variants in the adult hypertrophic heart (Figures. 2.10C and 2.10D). Moreover, the combined increase in expression levels of both exon 25 variants in hypertrophic ventricle could account for the disease-associated re-expression of T-type channels previously reported (Nuss and Houser, 1993; Martinez et al., 1999; Huang et al., 2000; Yasui et al., 2005; Takebayashi et al., 2006).

2.3.2 $Ca_v3.2(-25)$ channels display faster recovery from inactivation and voltage-dependent facilitation

Alternative splicing is known to confer distinct electrophysiological properties to T-type channels (Chemin et al., 2001a; Jagannathan et al., 2002; Ohkubo et al., 2005; Emerick et al., 2006; Zhong et al., 2006). This thesis demonstrated that the cardiac $Ca_v3.2$ channel shows significant variant-specific changes in recovery from inactivation and VDF in association with splicing of exon 25. When compared to $Ca_v3.2(+25)$ variant channels, results showed that both potentiated recovery from inactivation and robust VDF in the rat cardiac $Ca_v3.2$ when exon 25 is absent. The splice-variant specific VDF was also observed when macroscopic currents were recorded using Ba^{2+} as charge carrier, ruling out a direct Ca^{2+} -dependent facilitation process (Figure 2.7). Of note, native I_{CaT} from bullfrog atrial cells and guinea-pig coronary arterial myocytes have both been reported to display VDF properties (Ganitkevich and Isenberg, 1991; Alvarez et al., 1996; Alvarez et al., 2000). Conversely, Zhong and coworkers reported faster recovery kinetics associated with the homologous exon 26 region in the human fetal brain $Ca_v3.2$ channel although neither facilitation nor potentiation (>100% fractional recovery) were observed

(Zhong et al., 2006). VDF has been previously attributed to the cloned human Ca_v3.3 (Klockner et al., 1999; Gomora et al., 2002) albeit to a much lower degree (~ 20%) compared to that for the Ca_v3.2(-25) variant channel described here (Figures 2.6 and 2.8) (Klockner et al., 1999; Gomora et al., 2002).

It is well known that the mammalian heart undergoes significant functional and morphological changes during embryonic and postnatal development. The heart rate, configuration of action potential and excitation-contraction (E-C) coupling all differ considerably between postnatal and adult myocardial tissues (Wekstein, 1965; Adolph, 1971; Wahler et al., 1994; Ziman et al., 2010). In this regard, age-related differences in the relative expression of Ca_v3.2 splice variants displaying significantly different kinetic and gating properties could contribute to the developmental regulation of cardiac Ca²⁺ homeostasis. As a consequence, splice-specific T-type channel mediated Ca²⁺ entry could participate in the regulation of important processes in the developing heart such as cardiomyocyte growth, proliferation, hormone secretion and spontaneous activity (Leuranguer et al., 2000; Vassort et al., 2006). In neonate cardiomyocytes, the strong VDF and faster recovery from inactivation of Ca_v3.2(-25) channels may result in increased Ca²⁺ influx leading to increased electrical activity. Furthermore, predominant expression of Ca_v3.2(-25) (Figure 2.4) might be relevant for E-C coupling in immature myocardium which relies mainly on trans-sarcolemmal transport of Ca²⁺ for the activation of contractile machinery (Nuss and Marban, 1994; Haddock et al., 1999; Artman et al., 2000; Escobar et al., 2004). Although the physiological impact of Ca_v3.2 splice variation in different regions of the mammalian heart remains to be explored, our study demonstrates that alternative splicing can regulate the effect of strong depolarization on T-type Ca²⁺ channel gating properties as well as the time course of recovery from inactivation.

2.3.3 The magnitude of VDF of Ca_v3.2(-25) splice variant currents is reduced by Gβ₂γ₂

This thesis examined the potential cAMP regulation on the VDF of Ca_v3.2 exon 25 variants. This was undertaken by application of forskolin (an adenylyl cyclase stimulant) in combination with IBMX (a phosphodiesterase inhibitor) in HEK-293 cells transiently transfected with Ca_v3.2(-25) and Ca_v3.2(+25) alternative splice variants. Contrary to a previous report on the cAMP modulation of I_{CaT} VDF in atrial myocytes (Alvarez et al., 1996), this study showed lack of effect on VDF by cAMP (Figures 2.9B and 2.9C). In our study, I used a mammalian cell line (HEK cells) and recorded exogenous Ca_v3.2 currents at room temperature (~21°C). These experimental conditions may account for the lack of effect of cAMP on Ca_v3.2 currents as previous reports have shown temperature-dependence of kinase effects (Chemin et al., 2007). On the other hand, consistent with the findings in the current study, a lack of effect by cAMP on native I_{CaT} from various mammalian cardiovascular preparations has also been reported. These include a lack of effect on native I_{CaT} in rabbit SA node (Hagiwara et al., 1988), ear arteries (Benham and Tsien, 1988), guinea pig ventricular myocytes (Tytgat et al., 1988), dog atrial myocytes (Bean, 1985) and canine cardiac PF cells (Hirano et al., 1989; Tseng and Boyden, 1989). Taken together, further studies are necessary to explore the VDF of cardiac Ca_v3.2 alternative splice variants including whole cell patch clamp recording in a temperature controlled setting.

The VDF of I_{CaT} from frog atrial myocytes was reported to be due to voltage-dependent relief of tonic inhibition by G_{oi} proteins (Alvarez et al., 1996). The activation of G_{oi} proteins results in the release of Gβγ subunits allowing them to interact with ion channels (Logothetis et al., 1987). Among the three T-type isoforms, Ca_v3.2 channels are reported to be selectively inhibited by Gβ₂γ₂ (Wolfe et al., 2003; DePuy et al., 2006).

Since the $G\beta\gamma$ -mediated inhibition of $Ca_v3.2$ is specific to $G\beta_2\gamma_2$ subunits, the modulation of $G\beta\gamma$ to $Ca_v3.2$ (\pm) exon 25 alternative splice variant was investigated in the present study. To test the possibility that $G\beta\gamma$ subunits regulate $Ca_v3.2$ VDF in a splice-dependent manner, co-transfection of $G\beta_2$ and $G\gamma_2$ with $Ca_v3.2$ splice variants in HEK cells was performed. The results showed that there exists a splice-specific regulation of VDF by $G\beta_2\gamma_2$ (Figures 2.9D and 2.9E). In the presence of $G\beta_2\gamma_2$, the VDF of $Ca_v3.2(-25)$ was reduced by approximately 50% (Figure 2.9D), whereas $Ca_v3.2(+25)$ was not affected (Figure 2.9E). A lack of effect by $G\beta\gamma$ by strong depolarizing prepulses was also reported for the human $Ca_v3.2$ T-type channel containing exon 26 (Wolfe et al., 2003) which is homologous to the rat exon 25 (the cardiac $Ca_v3.2(+25)$ variant identified in this thesis). To date, there has been no report of the $G\beta\gamma$ -mediated inhibition of VDF of $Ca_v3.2$ channels hence this thesis is the first to report this type of modulation and further, that it occurs in splice-variant manner.

2.3.4 Potential relevance to cardiac pathophysiology

Splice variation associated with the cardiac HVA L-type channel encoded by $Ca_v1.2$ has been extensively studied. Of note pharmacologically, splice variation in the $Ca_v1.2$ IS6 segment accounts for the differential dihydropyridine sensitivity of L-type currents in smooth and cardiac tissues (Welling et al., 1997). Further, distinct $Ca_v1.2$ splice variants expressed in cardiac and smooth muscle contributes to the distinct biophysical properties of native L-type currents in these tissues (Liao et al., 2004; Tang et al., 2004; Liao et al., 2005; Tang et al., 2007). Similar to the results presented here for the $Ca_v3.2$ T-type channel, alternative splicing of the $Ca_v1.2$ L-type channel is also suggested to be involved in molecular remodeling associated with cardiovascular disease (Tiwari et al., 2006; Liao et al., 2009b).

It is tempting to speculate that the preferential up-regulation of Ca_v3.2(+25) channels in the heart of hypertrophic SHRs could potentially contribute to electrical remodeling in the hypertrophic ventricle. A higher level of expression of this particular splice variant with its hyperpolarized activation range and higher current density, could predispose the heart to pro-arrhythmic condition, contractile dysfunction and eventually heart failure. Interestingly, a recent study has found evidence implicating Ca_v3.2 T-type channel involvement in the pathogenesis of cardiac hypertrophy via the activation of calcineurin/nuclear factor of activated T cells (NFAT) pathway (Chiang et al., 2009). The preferential up-regulation of Ca_v3.2(+25) splice variant channels that I find correlated with cardiac hypertrophy in SHRs supports the notion that an enhanced Ca²⁺ flux associated with expression of this T-type variant might contribute to the hypertrophic signaling pathway.

In summary, this thesis finds that alternative splicing of Ca_v3.2 channel results in spatially and temporally expressed T-type cardiovascular variants and that in at least one instance are also associated with the hypertrophic state. The functional variability and compartmentalization of specific Ca_v3.2 splice variants potentially make significant contributions towards cardiac physiology and pathophysiology. In a broader context, it is apparent that examination of single splice variants should not be used to universally infer functional outcomes when looking across physiological and pathological conditions.

2.4 Materials and methods

2.4.1 Animals and tissue preparation

All animal procedures were performed in accordance with Canadian Council on Animal Care guidelines for animal research. Newborn (P0), adult male Wistar (Animal Care Center,

University of British Columbia, Canada) and four month old male spontaneously hypertensive rats (SHR) and Wistar Kyoto rats (WKY) (Charles River, Montreal, Canada) hearts were utilized in this study. Newborn and adult rats were anaesthetized using halothane (in closed chamber) and inactin (80 mg/kg i.p.), respectively. Rat heart chambers were dissected and washed in Krebs-Ringer solution containing (in mM) 120 NaCl, 4.8 KCl, 1.2 CaCl₂, 1.3 MgSO₄, 25.2 NaHCO₃, 5.8 glucose, 1.2 KH₂PO₄, 20 HEPES, pH 7.4. Krebs- Ringer solution was prepared in diethylpyrocarbonate(DEPC)-treated deionized water and filtered prior to use. The ratio of the heart weight (HW)/ body weight (BW) from SHR and WKY was calculated by dividing the total body weight (in grams) from the heart wet weight (in milligrams). All chemicals used in the study were purchased from Sigma-Aldrich Canada unless otherwise stated.

2.4.2 Histological staining

Four month old male SHR and WKY rats were anaesthetized using 80 mg/kg body weight inactin (Sigma, St. Louis, Mo.) administered intraperitoneally. Hearts were excised and washed through the aorta with Krebs-Ringer buffer then perfused with 10% cold buffered formalin. Hearts were fixed in formalin for at least 24 hours at 4°C. Samples were processed by Wax-It Histology Services (University of British Columbia, Vancouver, B.C., Canada). Briefly, cardiac tissues were embedded in paraffin, sectioned at 5 µm and stained using Masson's trichrome technique to detect interstitial fibrosis. The technique uses acid fuschin-xylydine ponceau for cytoplasmic staining (red), Weigert's hematoxylin for nuclear staining (black) and aniline blue for collagen. High resolution images were obtained by digital scanning of whole slides using Aperio's ScanScope system (Vista, CA).

2.4.3 RT-PCR and short amplicon scanning

Total RNA was prepared individually from five newborn, five SHR and five WKY rats. Each heart sample was homogenized in a sterile glass-Teflon homogenizer and 1 ml Trizol (Invitrogen). Homogenized samples were incubated at room temperature for 5 minutes followed by adding 200 μ L chloroform and incubated at room temperature for another 3 minutes. Samples were spun in table top centrifuge at 11,000 x g for 15 minutes at 4°C. The aqueous phase of the centrifugate was immediately transferred to a clean RNase-free eppendorf tube and 500 μ L of isopropanol was added. The centrifugate/isopropanol mixture was incubated at room temperature for 10 minutes to precipitate the RNA. After the incubation, samples were spun at 11,000 x g for 10 minutes at 4°C. The precipitate was washed with 75% ethanol and spun at 7,500 x g for 5 minutes. The supernatant was removed and the final pellets were dried briefly prior to suspension in DEPC-treated deionized water.

For cDNA synthesis, one microgram total RNA was initially treated with DNase to avoid genomic DNA contamination during reverse transcription (RT). Superscript II reverse transcriptase (Invitrogen) was used for the RT. A total of 20 μ l reaction volume was prepared containing DNase-treated total RNA, first strand buffer (1X), DTT (10 μ M), oligodT (0.5 μ g/L), dNTP mix (500 μ M), RNaseOUT (40 units) and RT (200 units).

Primer pairs were used to amplify small polymerase chain reaction amplicons covering overlapping regions of the entire Ca_v3.2 open reading frame. The oligonucleotides used in exon scanning are summarized in Table 2.4. There were 11 overlapping PCR amplifications with each reaction covering at least two exons and generating products of ~450 and ~1070 base pairs. PCR products were subcloned into the pGEM-T-Easy vector (Promega) and grown on agar plates for blue/white screening. Selected white colonies were grown into LB media and plasmid DNA from each culture was subjected to variant identification by size selection using agarose gel

electrophoresis. DNA sequencing was used to confirm variants and exon-exon junctions. DNA sequences were compared with published rat Ca_v3.2 cDNA sequences (NM_153814) and genomic sequences (ENSRNOT00000048392 and NC_005109).

Table 2.4. Primers utilized for exon scanning amplification.

Oligonucleotides	Scanning Reaction	Exons Spanned	Expected Product Size
LDH-1, ATGACCGAGGGCACGCTG LDH-2, CCCGCCATGACAATGAAG	1	1, 2, 3	545 bp
LDH-3, CCTGGGTGACACCTGGAA LDH-4, CTGGAAGATGGCAATCCAA	2	4, 5, 6	622 bp
LDH-5, CTCACAACGGTGCCATCA LDH-6, CTTGTTCTCCCACCACAT	3	7, 8	942 bp
LDH-7, CCCAGACCCTATGAGAAGA LDH-8, CTGAAGATGAAGATGAACAG	4	9, 10, 11	821 bp
LDH-9, CAACGTGGCCACCTTCTG LDH-10, CAGAGACTTCTGGTCCCC	5	12, 13, 14, 15	625 bp
LDH-11, CAAACCTGGACGTGGCCCA LDH-12, CTTCACCATCATCTCCAC	6	16, 17, 18, 19	806 bp
LDH-13, CTACATCTTCACAGCCAT LDH-14, CTGCTGGTCGATGCCAC	7	20, 21, 22, 23	571 bp
LDH-15, GGCTGGGTAAACATCATG LDH-16, CTGTCCTTGAAGAACCTC	8	24, 25, 26, 27	509 bp
LDH-17, GCTGCACTGAAGCTGGTG LDH-18, TCATAATCCCATTCCAG	9	28, 29, 30, 31	454 bp
LDH-19, CCTCACACTGTTCCGAGT LDH-20, CTGTCTGCAGAGTATCCG	10	32, 33, 34	628 bp
LDH-21, CCGCTCTCTGAGTCTCTC LDH-22, CACAGGCTCATCTCCACTG	11	35	1078 bp

2.4.4 Construction of cDNA libraries and full length splice variant screening

Full-length PCR was performed with ELONGASE Enzyme Mix using the oligonucleotides 5' - GATAAGCTTATGACCGAGGGCACG - 3' and 5'CGCTCTAGACTACACAGGCTCATC - 3'. The reaction volume was 50 μ L consisting of 2 μ L cDNA, 2 mM magnesium, 200 μ M each dNTP, 400 nM each primer, and 1 unit ELONGASE Enzyme Mix. PCR was run using the following cycle: 94.5°C 45 seconds, 94.5°C 20 seconds, 55°C 25 seconds, 68°C 8 minutes, 35 cycles and a final extension of 68°C for 15 minutes. The ~7 kb PCR product was purified and subcloned into the pGEM T-Easy vector. Individual splice variants from bacterial colonies obtained from short amplicon PCR products were identified via size differentiation using agarose gel electrophoresis. Between 40 and 200 colonies were screened in each of the 11 PCR reactions. For full length screening, positive full length clones were screened using *HindIII* and *SpeI* enzymes to release the ~7kb $Ca_v3.2$ fragment. The identification and confirmation of alternatively spliced variants were performed by DNA sequencing 56 atrial and 50 ventricular full length cDNAs. All DNA sequences were aligned against published mRNA and genomic sequences (Ensembl and PubMed).

2.4.5 Cloning of full-length $Ca_v3.2$ alternative splice variants

Eleven full-length splice variants were subcloned for subsequent biophysical characterization in HEK cells; $Ca_v3.2(-7/-25)$, $Ca_v3.2(8b/-25)$, $Ca_v3.2(20a/-25)$, $Ca_v3.2(20b/-25)$, $Ca_v3.2(24a/-25)$, $Ca_v3.2(-25)$, $Ca_v3.2(+25)$, $Ca_v3.2(33a/-25)$, $Ca_v3.2(\Delta 214/-25)$, $Ca_v3.2(35a/-25)$ and $Ca_v3.2(35a/+25)$. From the error-free full length cDNA subcloned in pGEM T-Easy vector, all $Ca_v3.2$ splice variants except $Ca_v3.2(8b/-25)$ were cloned by cutting the ~7 kb band with *HindIII* and *XbaI* restriction enzymes and moved to pCDNA3.1 zeo(+) (Invitrogen). Using $Ca_v3.2(-25)$ as template, $Ca_v3.2(8b/-25)$ was cloned using two-step overlapping PCR techniques.

Ca_v3.2(8b) alternative splice variant is a 99 amino acid deletion located in the I-II linker region within the *NheI* sites of Ca_v3.2(-25) in pCDNA3.1 zeo(+). All PCR reactions were done using Phusion Enzyme (Finnzymes, Espoo, Finland). Two overlapping PCR fragments namely *NheI* – 8b1 and 8b2 – *NheI4* were generated. *NheI* – 8b1 fragment was amplified with oligonucleotides RA1HLDHNhe1- 5' ggtctatataagcagagct 3' and RA1HLDH8b1 – 5' ctgagagctctggtggcccatggcctacatacttgaggagctcc 3', whereas, 8b2 – *NheI4* fragment with primers RA1HLDH8b2 – 5' ggagctcctcaagtatgtaggcatgggccaccagactctgag 3' and RA1HLDHNhe4 – 5' ttcaggctgaacttacagcc 3'. Products were then run in 0.8% agarose gel, excised and purified for subsequent annealing. The two fragments were annealed using the oligonucleotides RA1HLDHNhe1 – 5' ggtctatataagcagagct 3' and RA1HLDHNhe2 – 5' cgactcactatagggagac 3' to generate the 2.5 kb fragment possessing *NheI* sites for cutting. Annealed products were gel purified and the Ca_v3.2(-25) and the purified 8b *NheI* fragment were cut with *NheI* restriction enzymes for subsequent cloning. The 8b *NheI* fragment splice variant was cloned into the *NheI* cut Ca_v3.2(-25) in pCDNA3.1 zeo(+). The DNA sequence of each clone was determined prior to patch clamp analysis.

2.4.6 Western blot analysis

Protein sample extraction from heart tissue was performed by grinding frozen tissue in liquid nitrogen in extraction buffer (0.1M Tris pH 6.8, 2% sodium dodecyl sulfate (SDS), 10% Glycerol, 1% β-mercaptoethanol, 1x Proteinase inhibitor cocktail (Complete-EDTA free, Roche), 0.004% Bromophenol Blue) and followed by heating to 65°C for 10 minutes and trituration through a small gauge needle. Western Blot analysis was performed as follows: proteins were separated on NuPAGE Novex 4-12% Bis-Tris Midi gells (Invitrogen), followed by wet electro-transfer (20mmol/L Tris-base, 150mmol/L Glycine, 20% Methanol & 0.1% SDS)

onto nitrocellulose membrane (Hybond-ECL, GE Healthcare). Protein transfer was confirmed by Ponceau S staining, followed by membrane blocking with 2% skimmed milk in TBST (136 mM NaCl, 25 mM Tris-HCl (pH7.4), 2.8 mM KCl, 0.1% Tween). Antibody incubations were performed in TBST-2% milk for 1 hour and washed three times (5 minutes each) with Tris Buffered Saline(TBS) prior to incubation with secondary horseradish peroxidase(HRP) conjugated antibody. Final membrane washes were performed twice in TBST and once in TBS for 5 minute each. Proteins were detected using the SuperSignal West Pico Chemiluminescent kit (Thermo Scientific) on Hyperfilm ECL (GE Healthcare). The following antibodies used: Rabbit anti-rat Ca_v3.1 (1:10,000) (C-terminal region residues 1861-1934 (Q54898)), rabbit anti-rat Ca_v3.2 (1:5,000) (II-III linker region residues 11195-1273 (Q9EQ60)), rabbit anti-rat Ca_v1.2 (1:5,000) (C-terminal region residues 1725-11789 (P22002)), and mouse anti-ACTB (1:10,000) (Chemicon, MAB1501)

2.4.7 Quantitative real-time-PCR (qRT-PCR)

Two microgram (µg) of total RNA was used to synthesize cDNA using a High Capacity cDNA Reverse Transcription kit (Applied Biosystems). Real-time-PCR reactions were performed using Applied Biosystems reagents, an Applied Biosystems AB 7500 instrument and TaqMan probes generated against the respective cDNA targets. Primer mixes used for detection of specific splice variants are listed in Table 2.5. Splice-variant specificity was confirmed using full-length cDNAs and titration curves and enabled splice-variant copy number to be calculated. A rat actin B (rActB) primer set (Applied Biosystems AB 4352340E) was run in parallel with splice-variant specific probes in all samples as a control for total cDNA input to allow comparison. The rat molecular hypertrophic markers, SIAT7 (Rn01750492_m1) and Frzb (Rn01746979_m1) were obtained from Applied Biosystems. Relative amounts of different splice

variants were estimated after actin B normalization. In the case of the exon +/-25 splice variants, copy numbers for each variant in each sample were calculated and then compared with rActB. Target and control probe reactions were run in triplicate and averages were determined.

Table 2.5. Oligonucleotide primers for qRT-PCR.

Name	Probe	Forward	Reverse
H+8b*	CCTCAAGTATGTAGGCCACATCTTCCG	TCCAACGACAGCACTCT	GCATAAAGACGCAGGCTA
H-8b*	AGCTTCTCAGAGCCCGGCA	TCCAACGACAGCACTCT	GTGGCCCATGGCCTACATAC
H+20a	ATGCCTACCTACAGAGCAGT	TGGAGATGATGGTGAAGGTGGTA	CCCGTCCAGCACATTCCA
H-20a	CCAAGTCTTTCACCATC	CTACATCTTCACAGCCATCTTCGT	AGCCCGTCCAGCACATT
H+25	CCAACCCAGAGGCCAG	GCGCAGGAGCACTTTCC	GAGTGTGTGAATAGTCTGCGTAGTA
H-25	CTGGGCCTTCCTGCGCC	CGCCGGGAGGAGAAACG	GAGTGTGTGAATAGTCTGCGTAGTA
H+33a*	AGCACAGCCTCCCTCACCACAGGA	GCCCAGCCCCCACCTA	CATCCTGGACACAGATACTTTTCG
H-33a*	AAGGAGGCCCGCGAGGATGC	AAGCACCTGGAGGAGAGCAA	GGTACCTTGGCTTTCCTGTGC
H+35a	AAGAGGCCTGGCCCC	GGGACCCTGTAGCCAAGG	CAGAGGCTCAAAGGCAAAGTTG
H-35a	ACCTAGAGTCCAGGCCTC	TGGAAGTGGATAACGGAGAAAGC	CAGAGGCTCAAAGGCAAAGTTG
H+Δ214	CCAGGCCTCTTGCCGAGCA	GGGACCCTGTAGCCAAGG	GGCTCAAAGGCAAAGTTGGG
H-Δ214	ACGAGCCAGGCCTCT	CACAGAGCCTGCTGAAAATATGTC	GGCTCAAAGGCAAAGTTGGG

*No 3'-MGB; IB-FQ as 3'-Quencher; Source: Integrated DNA technologies (IDT). Rest from Applied Biosystems (AB). All forward oligos have 5' FAM.

2.4.8 Whole cell electrophysiology of transfected HEK cells

Human embryonic kidney cells (HEK293; Invitrogen, #11631-017) were grown in standard Dulbecco's modified Eagle's medium (DMEM) containing 10% heat inactivated fetal bovine serum, 50 units/ml penicillin and 50 $\mu\text{g}/\text{ml}$ streptomycin maintained at 37°C in a humidified incubator with 95% O₂ and 5% CO₂. Ca_v3.2 alternative splice variants were transfected using standard calcium phosphate transfection method and left overnight at 37°C incubator. As a reporter for transfection, CD8 was used at a molar ratio of 3:1. In separate experiments involving G $\beta\gamma$, cloned Ca_v3.2 (\pm) 25 variants were co-transfected with and without G $\beta_2\gamma_2$ subunits with a stoichiometric ratio of 3:3:3:1, for channel, G β_2 , G γ_2 , and CD8, respectively. Twelve to 18 hours later, media was replaced with fresh DMEM and cells were transferred to 28°C prior to whole cell patch clamp analysis.

Macroscopic currents were recorded using Axopatch 200B amplifiers (Axon Instruments, Foster City, CA) controlled and monitored with personal computers running with pClamp software version 9 (Axon Instruments). The external recording solution composed of the following (in mM) 2 CaCl₂, 1 MgCl₂, 92 CsCl, 10 glucose, 40 tetraethylammonium chloride, 10 HEPES, pH 7.4 and the internal pipette solution contained (in mM) 120 Cs-MeSO₃, 11 EGTA, 10 HEPES, 2 MgCl₂, 5 MgATP, pH 7.2. In some experiments using Ba²⁺ as the charge carrier, Ca²⁺ was replaced with iso-osmotic external recording solution containing Ba²⁺. In experiments involving testing the effect of cAMP, 10 μM forskolin and 10 mM IBMX were added to the external recording solution. Patch pipettes (borosilicate glass BF150-86-10; Sutter instruments, Novato, CA) were pulled using a Sutter P-87 puller and fire polished with a Narashige (Tokyo, Japan) microforge with typical resistances of 3 – 6 M Ω when filled with internal solution. The bath was grounded via a 3 mM KCl bridge. Data were low pass filtered at 2 kHz except for

measurement of tail currents that were filtered at 5 kHz with built-in Bessel filter of the amplifier, with a sampling period of 10 kHz.

Voltage dependence of activation was studied by applying 150 ms depolarizing pulses from -90 mV to + 10 mV at 5 mV increments ($V_h = -110$ mV). Current-voltage (I-V) relationships were fitted with the modified Boltzmann equation : $I_m = (G_{max} \times (V_m - E_{rev})) / (1 + \exp((V_m - V_{50act})/k_{act}))$, where G_{max} is the maximum slope conductance; E_{rev} is the extrapolated reversal potential; V_m is the membrane potential, V_{50act} is the half activation potential; k_{act} is the slope factor of activation which reflects the voltage sensitivity. Current values were normalized to the maximum current. Steady-state inactivation was studied by applying 5 second prepulses from -120 mV to -10 mV followed by a test pulse to - 30 mV for 50 ms. The current magnitude obtained during each test pulse was normalized to the maximum current and plotted as a function of the pre-pulse potential. Steady state inactivation normalized data were fitted using Boltzmann equation ($I/I_{max} = (1 + \exp((V - V_{50inact})/k_{inac}))^{-1}$), where I_{max} is the maximum current; $V_{50inact}$ is the membrane potential at 50% of the channel are inactivated, k_{inac} is the slope factor of inactivation. The kinetics of activation (τ_{act}) and inactivation (τ_{inact}) were analyzed by fitting current recordings obtained from the I-V protocol with a single exponential standard equation $I = Ae^{-t/\tau}$, where A is the amplitude of the current at t_0 and τ is the time constant. Recovery from inactivation was determined by double pulse protocol, a prepulse to -30 mV for 400 ms was given and allowed to recover at different time intervals (interpulse interval) between 5 ms to 5 seconds before applying a test pulse to -30 mV for 50 ms ($V_h = -110$ mV). The peak current from the test pulse was plotted as ratio of maximum prepulse current versus interval between pulses. The data were fitted with a double exponential function ($I/I_{max} = A_0 + A1 * \exp(-t/\tau1) + A2 * \exp(-t/\tau2)$), where A_0 is the amplitude for inactivating component, A1 and A2 are the amplitudes for the fast and slow components of the exponential, and $\tau1$ and $\tau2$ are the time

constants for the fast and slow components, respectively. Relative current amplitude for fast component (relative A_1) was calculated using the formula $A_1 / (A_1 + A_2)$, whereas relative amplitude for slow component was estimated by using the formula $A_2 / (A_1 + A_2)$. Deactivation was also investigated by measuring tail currents, using -110 mV as holding potential and depolarizations to -30 mV after which the membrane was repolarized to different levels (-120 mV to -50 mV). The data was fitted with a single exponential function ($I = Ae^{-t/\tau}$), where A is the amplitude of the current, and τ is the time constant. Fittings were plotted as a function of the repolarization potential. Voltage-dependent facilitation was studied by applying a 200 ms test pulse to -30 mV following a series of depolarizing prepulses from -120 to +150 mV after a time interval of 1.2 seconds. The percentage facilitation was obtained by dividing the currents obtained from prepulses to currents recorded at -120 mV. Averaged percentage facilitation was plotted as a function of prepulse depolarization. All recordings were performed at room temperature (~22 - 24°C).

Data analysis was performed using Clampfit software version 9.0 (Axon Instruments). All plots and statistical analysis (ANOVA) were performed using the Microcal Origin software version 7.5 (Northampton, MA). Statistical significance was tested with Student's *t*-test with significance being determined at confidence interval of $p < 0.05$ and $p < 0.01$.

3 VOLTAGE-DEPENDENT FACILITATION OF T-TYPE CALCIUM CURRENTS IN NEONATAL RAT VENTRICULAR MYOCYTES

3.1 Introduction

T-type Ca^{2+} channels in developing hearts have been reported to contribute to pacemaking, spontaneous contractions and hormone secretion (Section 1.4). The exact contributions of T-type channels in the heart likely relies on the amount of Ca^{2+} influx necessary to regulate other myoplasmic proteins and affect the transmembrane potential of cardiac myocytes. Hence, studying the mechanisms underlying the regulation of I_{CaT} in the heart will provide a better understanding of the role of T-type channels in cardiac physiology and pathophysiology.

One mechanism of altering Ca^{2+} channel activity in the heart is through the voltage-induced facilitation of Ca^{2+} currents. Facilitation of I_{CaT} in the cardiovascular system has thus far been shown only in guinea-pig coronary arteries (Ganitkevich and Isenberg, 1991) and frog atrial cells (Alvarez et al., 1996; Alvarez et al., 2000). Facilitation in guinea-pig coronary myocytes is attributed to changes in voltage-dependent gating properties of I_{CaT} (Ganitkevich and Isenberg, 1991). On the other hand, in frog atrial cells facilitation of I_{CaT} results from voltage-dependent relief of tonic inhibition by tyrosine phosphorylation and $G_{\alpha i}$ proteins (Alvarez et al., 1996; Alvarez et al., 2000).

In Chapter 2, this thesis demonstrated that heterologously expressed cloned cardiac $\text{Ca}_v3.2$ channel displays VDF and in a splice variant specific manner. Chapter 2 also showed that the $\text{Ca}_v3.2(-25)$ variant is predominantly expressed in the newborn rat ventricle and I hypothesize that the native ventricular I_{CaT} displays VDF. In this chapter, I investigated whether I_{CaT} in

newborn rat ventricular myocytes displays VDF and whether VDF is correlated with the expression of the $Ca_v3.2(-25)$ alternative splice variant.

3.2 Results

3.2.1 Expression of Ca^{2+} channels in neonatal rat ventricular myocytes

Newborn rat ventricular myocytes (NRVM) were prepared from newborn (P0) Wistar rats by serial enzymatic digestion and maintained in culture for two days prior to RNA extraction and whole cell patch clamp recordings. Immediately after isolation the cells were spherical in appearance. The cells were allowed to attach overnight. Adherent cells were fusiform or triangular in shape (Figure 3.1A). After 1 to 2 days in culture, NRVMs demonstrated spontaneous contractile activity. Quantitative RT-PCR analysis was used to examine the expression of cardiac $Ca_v1.2$, $Ca_v3.1$ and $Ca_v3.2$ channels (Figure 3.1B). The mRNA expression of $Ca_v3.2$ was approximately 35% higher than $Ca_v3.1$ channels and approximately 50% higher than $Ca_v1.2$ channels. The functional expression of HVA and LVA channels in NRVM was investigated by recording macroscopic Ca^{2+} currents via whole cell patch clamp analysis. Figure 3.1C illustrates the I-V relationship for total Ca^{2+} currents recorded from a holding potential (V_h) of -90 mV. Figure 3.1E shows the I-V relationship for Ca^{2+} currents when T-type channels are inactivated (V_h of -50 mV)(I_{CaL}). Representative current traces for total Ca currents and I_{CaL} are shown in Figures 3.1D and 3.1F, respectively. L-type currents were evidently observed at more depolarized potentials and showed peak currents at 0 mV, consistent with that observed for L-type channels (Figure 3.1E). The I-V curve from a V_h of -90 mV showed a peak current at -30 mV with a second component observed at more positive potentials (Figure 3.1C). Overall, under

short term culture conditions, NRVM Ca^{2+} currents recorded from Vh of -90 mV appear mostly contributed by T-type channels and likely consisting of both $\text{Ca}_v3.1$ and $\text{Ca}_v3.2$ isoforms.

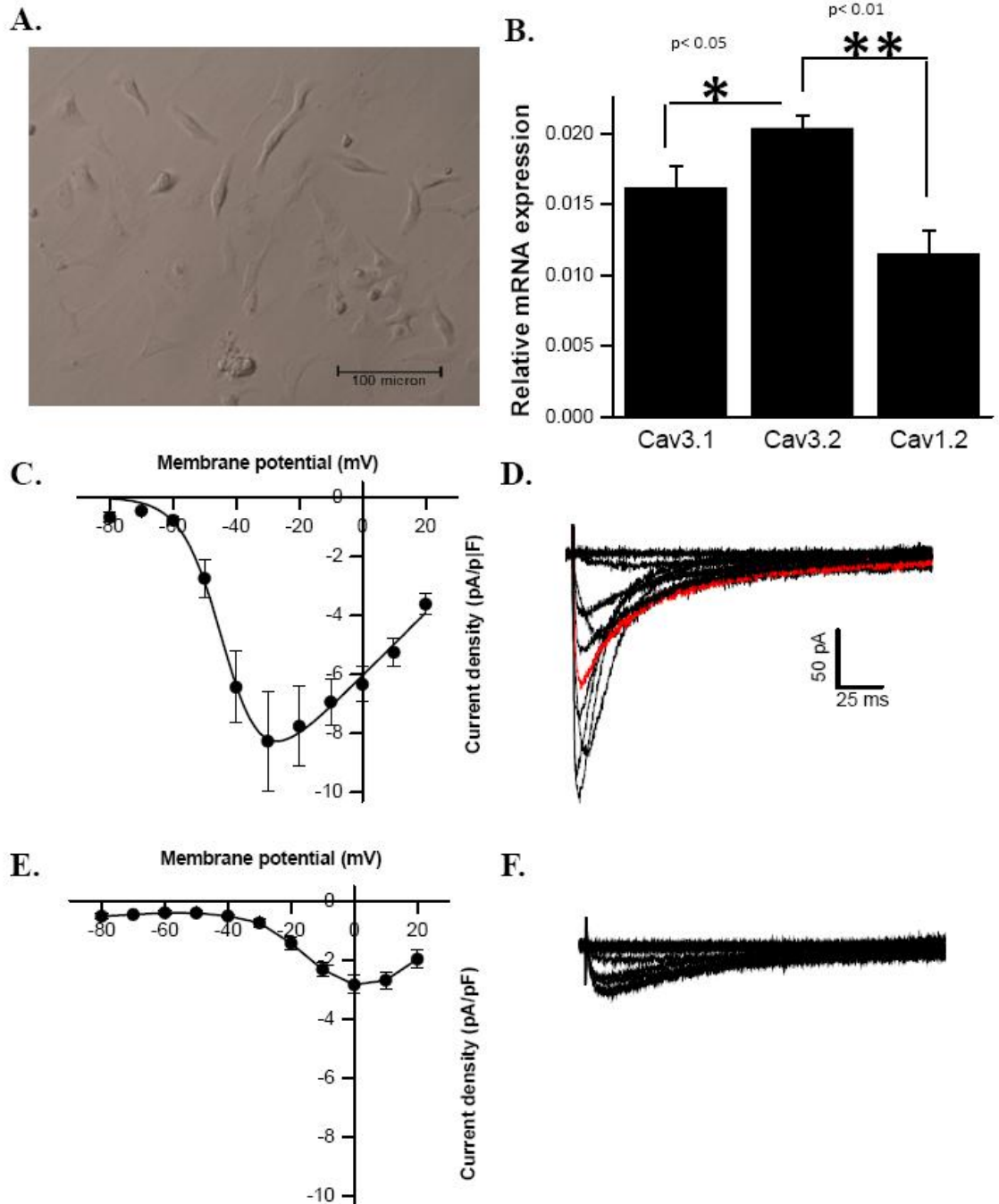


Figure 3.1. Expression of HVA and LVA Ca^{2+} channels in short-term cultured neonatal rat ventricular myocytes (NRVM).

(A) Neonatal rat ventricular myocytes (NRVM) 48 hours in culture. (B) qRT-PCR analysis for $\text{Ca}_v3.1$, $\text{Ca}_v3.2$ and $\text{Ca}_v1.2$ Ca^{2+} channels. The level of mRNA expression was calculated relative to rActB expression. The expression of $\text{Ca}_v3.2$ mRNA is significantly higher than $\text{Ca}_v3.1$ T-type and $\text{Ca}_v1.2$ L-type Ca^{2+} channels. Samples were from five individual total RNA preparations from five NRVM isolations. Values shown as mean \pm standard error. T-test was performed to measure significant differences. * $p < 0.05$ and ** $p < 0.01$. NRVM Ca currents were also recorded. (C) and (E) show the current-voltage (I - V) curves for total (L + T-type currents) and L-type Ca^{2+} currents recorded from NRVM, respectively. Representative traces for total (D) and L-type (F) macroscopic Ca^{2+} currents. Two populations of macroscopic Ca^{2+} currents exist in currents recorded from V_h of -90 mV as evidently observed in their kinetics of activation and inactivation (red trace). In V_h of -50 mV, macroscopic Ca^{2+} currents with fast activation and inactivation kinetics are eliminated. The I-V relationships of Ca^{2+} currents for ventricular myocytes were obtained by depolarizing the myocytes with 200 ms prepulse from -80 mV to +20 mV at 10 mV increments. A hyperpolarized holding potential of -90 mV recorded both Ca^{2+} currents whereas V_h of -50 mV revealed exclusively L-type.

3.2.2 Biophysical properties of T-type Ca^{2+} currents in isolated ventricular myocytes

To better isolate I_{CaT} from I_{CaL} , CdCl_2 (20 μM) was superfused to block I_{CaL} . Figure 3.2A illustrates representative current traces evoked by test pulses to -60 mV (black), -30 mV (red) and 0 mV (blue) and summarizes the subtraction strategy used in studying NRVM I_{CaT} . The top panel in Figure 3.2A shows current traces recorded from $V_h = -90$ mV -50 mV and the currents remaining after subtraction of the currents recorded from V_h of -90 mV to the currents recorded from $V_h = -50$ mV (in 2 mM Ca^{2+}). The kinetics of the subtracted currents in the absence of Cd^{2+} showed two distinct components of inactivation while Ca^{2+} currents recorded from V_h of -50 mV showed a single Cd^{2+} -sensitive component (Figure 3.2A top middle panel). The addition of Cd^{2+} totally eliminated I_{CaL} (Figure 3.2A bottom middle panel) thus the subtracted currents recorded in the presence of Cd^{2+} were taken as I_{CaT} .

I-V curves for subtracted currents in NRVM obtained in the presence and absence of Cd^{2+} in the external recording solution are shown in Figure 3.2B. Results showed a lack of significant difference between the V_{50} of activation of subtracted currents recorded in the

presence (-43.57 ± 1.06 mV, $n = 8$) and absence (-42.87 ± 0.68 mV, $n = 9$) of Cd^{2+} . Isolated I_{CaT} recorded with Cd^{2+} typically showed a “criss-crossing pattern” of current traces when recorded with the I-V protocol as illustrated in Figure 3.2C. The steady-state inactivation properties of NRVM I_{CaT} was studied by applying 5 second prepulses from -120 mV to -10 mV followed by a test pulse to -30 mV for 90 ms. Results showed that the $V_{50\text{inact}}$ of $\text{I}_{\text{CaT}} = -73.54 \pm 0.38$ mV ($n=7$) (Table 3.1). The kinetic properties were also analyzed and are summarized in Table 3.1.

Table 3.1. Biophysical properties of T-type Ca^{2+} currents in isolated neonatal rat ventricular myocytes.

Parameters	Mean \pm SE values	Number of cells
$V_{50\text{act}}$	-43.57 ± 1.06 mV	9
k_{act}	-5.90 ± 0.59 mV	9
$V_{50\text{inact}}$	-73.54 ± 0.38 mV	7
k_{inact}	4.47 ± 0.31 mV	7
τ_{act}	10.36 ± 1.59 ms	9
τ_{inact}	4.18 ± 0.92 ms	9
Recovery τ_1	21.81 ± 7.33 ms	6
Recovery τ_2	137.93 ± 50.62 ms	6

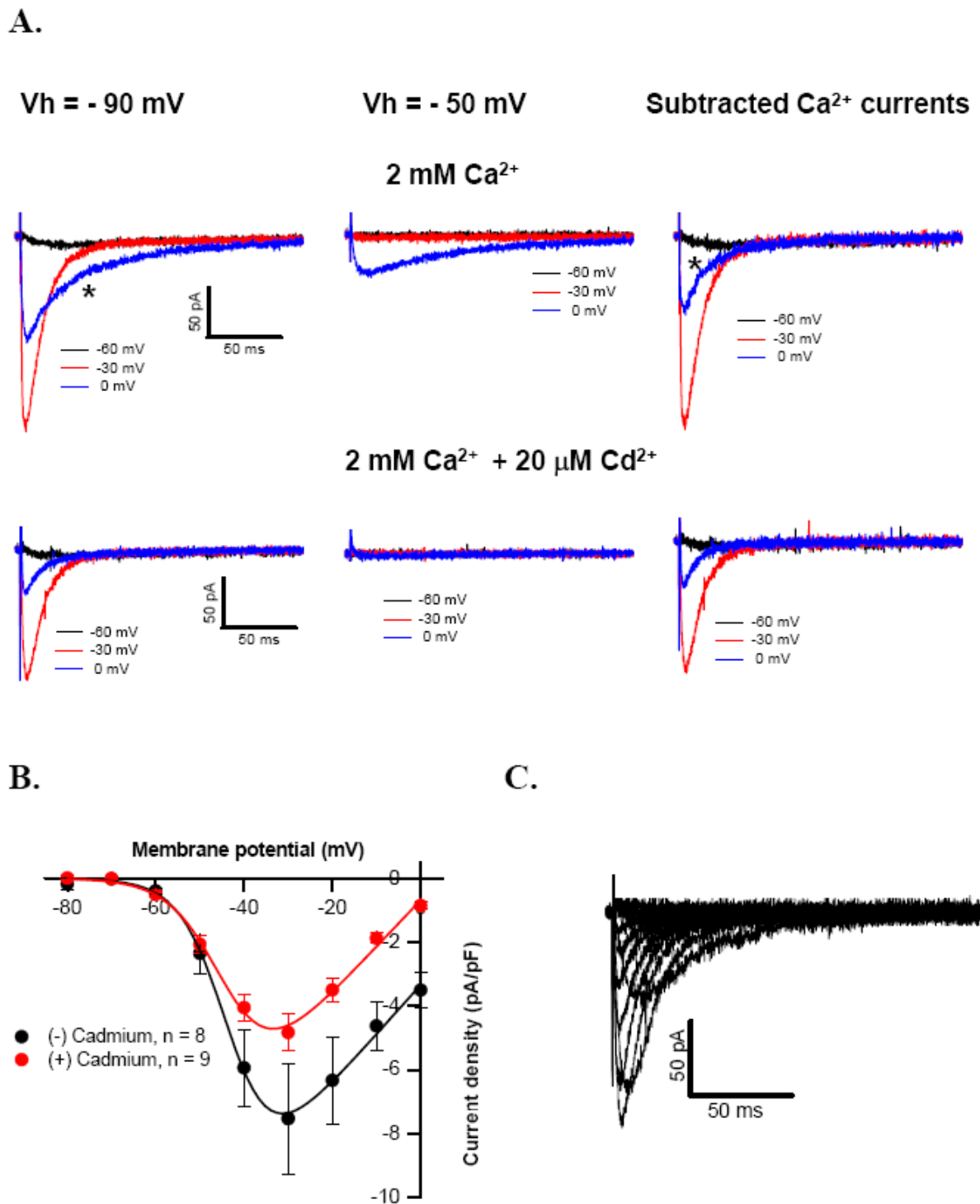


Figure 3.2. Pharmacological and biophysical isolation of T-type Ca²⁺ currents in newborn ventricular myocytes.

T-type Ca²⁺ currents (**A, right panel**) from newborn ventricular myocytes were isolated by subtracting currents recorded from Vh = -90 mV (**A, left panel**) to currents recorded from Vh = -50 mV (**A, middle panel**) in the presence (**A, lower panel**) and absence (**A, top panel**) of 20 μM CdCl₂. Macroscopic Ca²⁺ currents recorded without Cd²⁺ (Vh of -90 mV) revealed L- and T-type components as evidently observed in recorded currents at 0 mV (blue traces). L-type current components showed slow kinetics of inactivation (blue traces with asterisk). Typical I_{CaL}

was recorded from V_h of -50 mV using Ca^{2+} and was blocked when Cd^{2+} was added (**panel A, lower middle**). Pure I_{CaT} was obtained in the presence of 20 μM $CdCl_2$ (**A, lower right panel**). The inactivation kinetics observed in currents recorded at 0 mV in the presence of Cd^{2+} is faster than the current inactivation when Cd^{2+} is absent (blue traces in panel A, right). Panel **B** shows the I – V curves for NRVM I_{CaT} in the presence (red circle) and absence (black circle) of Cd^{2+} . The inclusion of Cd^{2+} reduced the subtracted current density without any significant change in V_{50} of activation. (**C**) Representative traces for I_{CaT} obtained from I – V protocol showed a criss-crossing pattern typically observed for whole cell recordings of T-type Ca^{2+} currents.

The recovery from inactivation of NRVM I_{CaT} was determined using a double pulse protocol. A prepulse to -30 mV for 400 ms was given and channels allowed to recover from inactivation at different time intervals (varying interpulse interval) between 5 ms to 5 seconds before applying a test pulse to -30 mV for 50 ms from V_h of -90 mV (Figure 3.3A, bottom panel). Fractional recovery was determined by calculating the amplitude ratio between the currents evoked by second pulse and the prepulse (Figure 3.3A top panel). Calculated ratios were plotted versus interval between pulses (Figure 3.3B). Results showed that the time constants of recovery were 21.81 ± 7.33 ms (n=6) and 137.93 ± 50.62 ms for τ_1 and τ_2 , respectively (Table 3.1). Of note, NRVM I_{CaT} displayed potentiated fractional recovery from inactivation (Figure 3.3B).

In order to examine if the observed potentiation of NRVM I_{CaT} was comparable to that observed in the recovery from inactivation profile for the recombinant $Ca_v3.2(-25)$ channel (Figure 2.6), an overlay of the NRVM I_{CaT} and $Ca_v3.2$ exon 25 splice variant recovery from inactivation data was performed. Results showed that both NRVM I_{CaT} and $Ca_v3.2(-25)$ currents revealed potentiated recovery from inactivation as well as faster recovery kinetics compared with $Ca_v3.2(+25)$ (Figure 3.3D). NRVM I_{CaT} and $Ca_v3.2(-25)$ showed a comparable level of potentiation until 1200 ms; however an interpulse greater than 3000 ms, the ratio of current magnitude reached a value close to that obtained for the $Ca_v3.2(+25)$ variant.

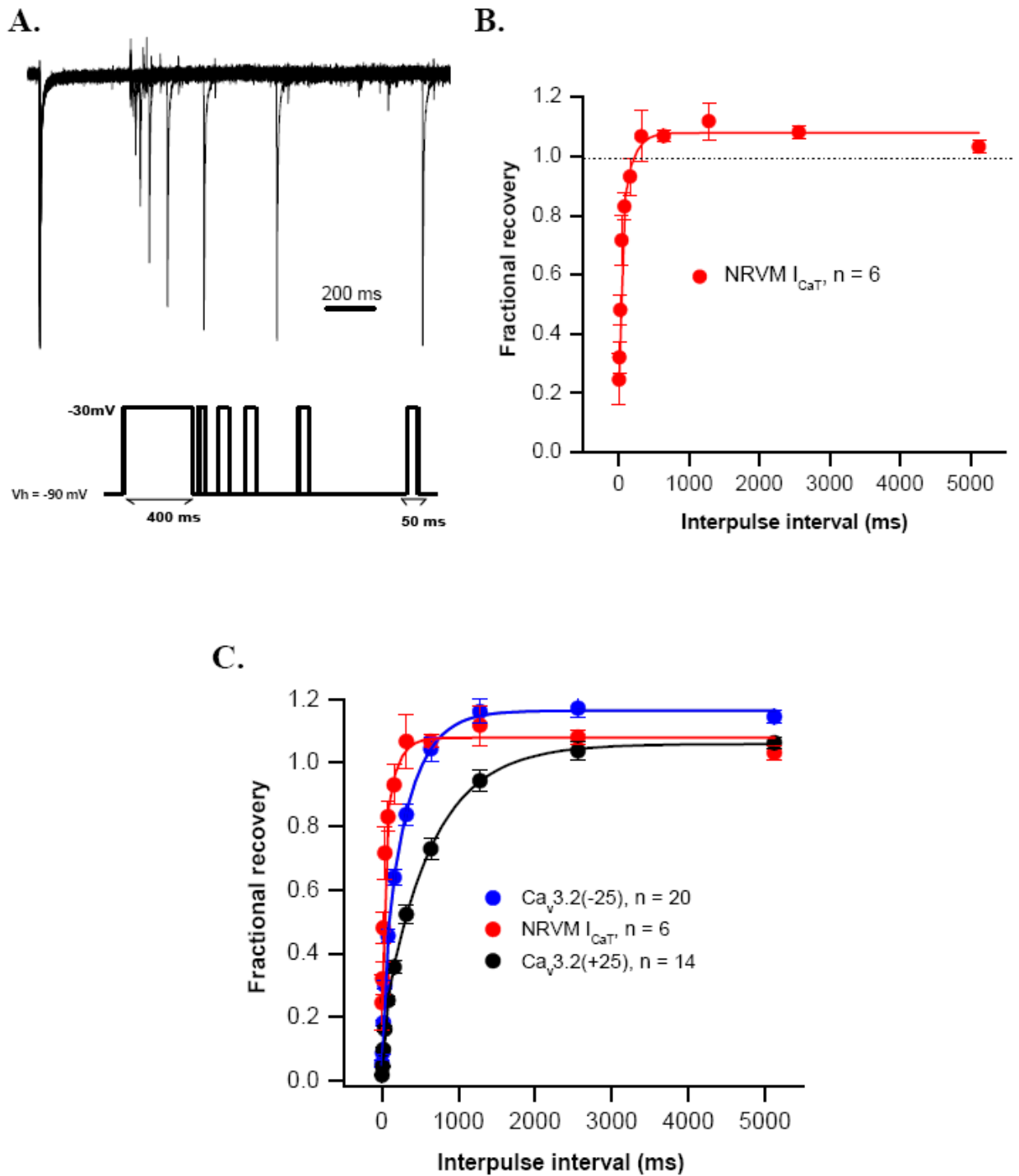


Figure 3.3. The potentiated recovery from inactivation properties of NRVM T-type Ca^{2+} currents is comparable to the recombinant $Ca_v3.2(-25)$ alternative splice variant. (A) Representative currents obtained from the first eight traces (5 ms to 640 ms) showed complete recovery from inactivation (**upper panel**). The recovery from inactivation was analyzed using double pulse protocol. A -30 mV prepulse was applied for 400 ms and channels were allowed to recover at different time interval before applying a second pulse to -30 mV for 50 ms (**bottom panel**). (B) I_{CaT} from newborn ventricular myocytes showed potentiated fractional recovery. (C) Overlay of recovery from inactivation profiles for $Ca_v3.2$ exon 25 alternative splice variants and NRVM I_{CaT} . Both $Ca_v3.2(-25)$ (blue circle) and

NRVM (red circle) I_{CaT} display potentiated fractional recovery but not $Ca_v3.2(+25)$ (black circle). The fractional recovery for NRVM at 3000 ms interpulse interval is comparable to $Ca_v3.2(+25)$. These results show that the potentiated recovery from inactivation property of NRVM I_{CaT} may be attributed to $Ca_v3.2$ minus exon 25 splice variant and the overall recovery from inactivation profile of NRVM could be a combination of both $Ca_v3.2(\pm)$ exon 25 splice variants. Fractional recovery was determined by calculating the amplitude ratio between the second pulse and the prepulse. Average data were fitted with a double exponential function to obtain the time constants for the fast (τ_1) and slow (τ_2) components of recovery from inactivation.

3.2.3 Voltage-dependent facilitation of T-type Ca^{2+} currents in rat ventricular myocytes.

The potentiated recovery from inactivation of I_{CaT} in ventricular myocytes was further explored using the same strategy used in studying the VDF properties of cloned $Ca_v3.2$ alternative splice variants. Briefly, the percentage of facilitation was obtained by dividing the currents obtained at test pulses preceded by prepulses by currents recorded from -90 mV (Figure 3.4B bottom panel). Average percentage NRVM I_{CaT} facilitation was plotted as a function of prepulse potential and VDF of NRVM I_{CaT} was observed from potentials positive to 0 mV (15 to 25%) (Figure 3.4A).

The magnitude of VDF of NRVM I_{CaT} was compared against recombinant $Ca_v3.1$ channels and $Ca_v3.2(\pm)$ exon 25 variants (Figure 3.4C). The recombinant $Ca_v3.1$ channels do not display VDF whereas $Ca_v3.2(-25)$ and NRVM I_{CaT} displayed VDF. Additionally, the VDF of NRVM I_{CaT} was greater than that for the VDF of $Ca_v3.2(+25)$ channel. To examine the correlation of expression of $Ca_v3.2$ exon 25 splice variants to the observed VDF, a qRT-PCR analysis was performed. Consistent with qRT-PCR data on newborn ventricular tissues (Figure 2.4), the level of mRNA expressed in newborn rat ventricular myocytes showed predominant expression of $Ca_v3.2(-25)$, with 4- to 5-fold higher expression than the $Ca_v3.2(+25)$ splice variant

(Figure 3.4D). This suggests that the observed VDF in newborn ventricular myocytes is predominantly contributed by $Ca_v3.2(-25)$ splice variant channels.

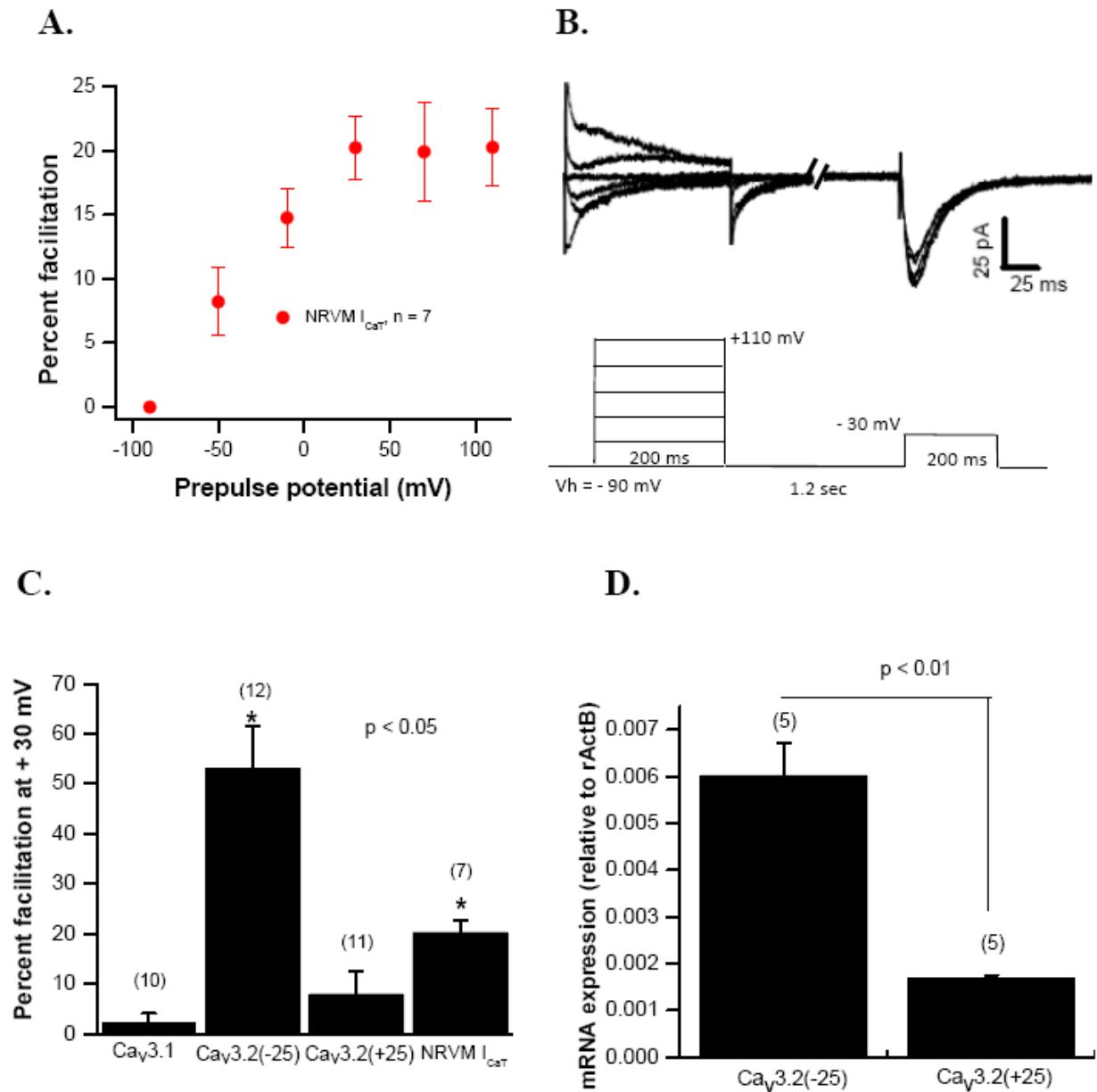


Figure 3.4. Neonatal rat ventricular myocytes display VDF properties which is correlated with high level of $Ca_v3.2$ minus exon 25 alternative splice variant.

(A) I_{CaT} in newborn rat ventricular myocytes display significant VDF. Panel B shows the representative current traces obtained from recording VDF from NRVM. The VDF of NRVM I_{CaT} was studied by applying a 200 ms test pulse to -30 mV following a series of depolarizing prepulses from -90 to +110 mV after a time interval of 1.2 seconds (Vh = -90 mV). The percentage of facilitation was obtained by dividing the currents obtained from prepulses to

currents recorded at -90 mV. Averaged percentage of facilitation was plotted as a function of prepulse potential. **(C)** Comparisons of the percentage VDF obtained from + 30 mV test potential. Both NRVM I_{CaT} and $Ca_v3.2(-25)$ currents display robust VDF but not $Ca_v3.2(+25)$ and $Ca_v3.1$. Thus, VDF in ventricular myocytes is perhaps contributed by I_{CaT} from $Ca_v3.2$ minus 25 containing channels. **(D)** qRT-PCR of $Ca_v3.2$ (\pm) exon 25 variants. The expression of minus 25 was shown to be 4 to 5 fold higher than $Ca_v3.2(+25)$ splice variants. Relative mRNA expression is compared against rat actin B (rActB) mRNA. Error bars represent standard error. T-test was performed to measure significant differences. * $p < 0.01$.

3.3 Discussion

3.3.1 T-type Ca^{2+} channels are expressed in neonatal rat ventricular myocytes

The mRNA expression of $Ca_v1.2$ L-type and cardiac T-type isoforms ($Ca_v3.1$ and $Ca_v3.2$ channels) was determined by qRT-PCR analysis. Consistent with our previous data on Ca^{2+} channels mRNA expression in heart tissue (Figures 2.1A and 2.1B), I demonstrated the expression of all three Ca^{2+} channels in short-term cultured NRVM (48 hours). The amount of $Ca_v3.2$ mRNA expressed in cultured NRVM is significantly greater than $Ca_v3.1$ and $Ca_v1.2$ channels (Figure 3.1). The expression of $Ca_v3.2$ is two-fold higher than $Ca_v1.2$, and about one-fold higher than $Ca_v3.1$. Collectively, the mRNA expression of both cardiac T-type channels is much greater than $Ca_v1.2$ channels. This is consistent with the relative contribution of I_{CaT} to the total Ca^{2+} currents recorded from NRVM where I_{CaL} contributed to approximately 35% of the total Ca^{2+} currents recorded in newborn ventricular myocytes compared to ~65% for I_{CaT} (Figures 3.1C and 3.1E). Our results are consistent with a previous report on the prominence of I_{CaT} over I_{CaL} in neonatal rat ventricular myocytes (Wang et al., 1991). Even when $Ca_v3.1$ and $Ca_v3.2$ channels are highly expressed during heart development (Section 1.4), knockout experiments have shown that silencing either of the *CACNAIG* and *CACNAIH* genes is not lethal indicating that individually the T-type isoforms are not indispensable or that a compensatory mechanism for T-type function exists in the knockouts (Kim et al., 2001; Chen et

al., 2003; Mangoni et al., 2006b). In this regard, it would be interesting to investigate whether a double knockout of $Ca_v3.1$ and $Ca_v3.2$ significantly alters heart development.

I_{CaT} in NRVM appears contributed by the expression of both $Ca_v3.1$ and $Ca_v3.2$ channels. Alternative splicing of $Ca_v3.1$ T-type channels in cultured ventricular myocytes has been reported (Cribbs et al., 2001), however, to our knowledge, alternative splicing of $Ca_v3.2$ channels in cultured NRVM has not been explored. In Chapter 2, I demonstrated the expression of alternative splice variants of $Ca_v3.2$ channels in newborn ventricular tissues. The III – IV linker variants encoding for the inclusion and exclusion of exon 25 variants are the most abundant $Ca_v3.2$ alternative splice variants in the newborn ventricle. In this chapter, I studied the expression of $Ca_v3.2$ (\pm) exon 25 variants in NRVM. Consistent with our data on neonatal ventricular tissues (Figure 2.4), I observed significant expression of $Ca_v3.2(-25)$ variants in short-term cultured newborn ventricular myocytes (Figure 3.4D).

3.3.2 Voltage-dependent facilitation of NRVM I_{CaT} is correlated with $Ca_v3.2(-25)$ splice variant expression

One of the objectives of this work was to examine whether I_{CaT} from newborn rat ventricular myocytes displays VDF. Our results presented in Chapter 2 demonstrated that cloned $Ca_v3.2$ channels exhibit both a potentiated fractional recovery from inactivation and VDF in splice variant specific manner (Figures 2.6, 2.7 and 2.8). In this chapter I examined the biophysical and VDF properties of NRVM I_{CaT} as well as correlated the expression profile of $Ca_v3.2(\pm)$ exon 25 splice variants to the observed properties.

Recovery from inactivation of NRVM I_{CaT} was investigated and showed a facilitated fractional recovery (Figure 3.3B). The recovery from inactivation of I_{CaT} from NRVM is more similar to the cloned $Ca_v3.2(-25)$ potentiated fractional recovery compared to cloned $Ca_v3.2(+25)$

fractional recovery (Figure 3.3C). VDF property was also examined in NRVM I_{CaT} . Comparative analysis of the VDF properties of NRVM I_{CaT} and the magnitude of facilitation of $Ca_v3.1$ channels and $Ca_v3.2$ (\pm) exon 25 alternative splice variants showed that both NRVM I_{CaT} and $Ca_v3.2(-25)$ displayed VDF but not the $Ca_v3.1$ or $Ca_v3.2(+25)$ isoforms (Figure 3.4C). Significantly, among recombinant $Ca_v3.1$ III – IV linker variants, a lack of potentiated fractional recovery (Chemin et al., 2001a; Latour et al., 2004) and VDF has also been reported (Klockner et al., 1999; Chemin et al., 2002; Gomora et al., 2002). Thus, the facilitation observed in dissociated NRVM is unlikely contributed by splice variants of $Ca_v3.1$ channels.

I also observed that the VDF of I_{CaT} in cultured NRVM is predominantly correlated to $Ca_v3.2(-25)$ variant expression. Hence, $Ca_v3.2(-25)$ containing channels likely contributes to the observed VDF of NRVM I_{CaT} . The magnitude of facilitation observed in NRVM is lesser than the recombinant $Ca_v3.2(-25)$ (Figure 3.4C). One possible explanation might be attributed to inhibition by endogenous regulatory proteins present in ventricular myocytes. For example, $G\beta\gamma$ might be tightly bound with $Ca_v3.2$ channels potentially leading to a lower relative VDF. In support of this potential mechanism, I demonstrated that the magnitude of VDF of recombinant $Ca_v3.2(-25)$ channels was reduced by $G\beta_2\gamma_2$ (Figure 2.9D). In the future, it would be interesting to determine whether disrupting the binding of endogenous $G\beta\gamma$ could increase the magnitude of facilitation of NRVM I_{CaT} .

3.3.3 Potential significance of voltage-dependent facilitation of T-type Ca^{2+} currents in neonatal ventricle

Prior to this research, VDF among T-type Ca^{2+} channels had been shown for recombinant $Ca_v3.3$ channels (Klockner et al., 1999; Chemin et al., 2002; Gomora et al., 2002) and native I_{CaT} in bone marrow cells as well in atrial and coronary smooth muscle myocytes (Ganitkevich and

Isenberg, 1991; Publicover et al., 1995; Alvarez et al., 1996). Here, I showed that the cloned rat cardiac $Ca_v3.2(-25)$ splice variant also displays prominent VDF (Chapter 2). Importantly, I also showed that cultured NRVM I_{CaT} exhibit VDF, correlated to the predominant expression of $Ca_v3.2(-25)$ variant in these cells (Figure 3.4).

The functional implication of I_{CaT} VDF in newborn ventricle remains to be described. In the following discussion, I will examine the potential contributions of $Ca_v3.2$ VDF in the neonatal ventricle and suggest potential experiments for future studies. Figure 3.5 illustrates some functional components of a typical neonatal rat ventricular myocytes (Gaughan et al., 1998). In newborn ventricle, the resting potential is between -70 mV and -60 mV, the AP duration of approximately is 350 ms and peaks at +30 mV. I observed that at +30 mV prepulse NRVM I_{CaT} display VDF (Figure 3.4). Taking into consideration the previously reported newborn ventricular electrical properties and our current data on I_{CaT} VDF in cultured NRVM, under physiological conditions VDF in newborn ventricle might occur which would potentially lead to an increase in intracellular Ca^{2+} .

T-tubules and SR are not fully developed in immature hearts and I_{CaT} supplies most of the Ca^{2+} that triggers the contraction in the immature myocardium (Nuss and Marban, 1994; Wetzel and Klitzner, 1996; Haddock et al., 1999; Artman et al., 2000; Escobar et al., 2004; Tohse et al., 2004). It is tempting to speculate that the VDF of $Ca_v3.2 I_{CaT}$ contributes to the Ca^{2+} flux leading to spontaneous beating and contractions of newborn ventricles. First, during the peak of the AP elevated Ca^{2+} from the VDF of $Ca_v3.2 I_{CaT}$ is predicted to directly activate the contractile machinery to induce contraction (Figure 3.5a). Secondly, elevated intracellular Ca^{2+} from VDF would directly trigger local Na/Ca exchangers to enter into reverse mode allowing Ca^{2+} flux to further increase contraction (Figure 3.5b). Because of their low threshold of activation, $Ca_v3.2$ channels activate early during the phase between two contractions and before the onset of the

next AP. The AP duration for neonatal rat ventricle is between 200 to 350 ms (Cohen and Lederer, 1988; Gaughan et al., 1998). Current work shows that both VDF and potentiated fractional recovery occurs after ~1000 ms interval, hence facilitation of native ventricular I_{CaT} might occur after at least three APs. The resulting increased in inward I_{Ca} would potentially result in an increase in intracellular Ca^{2+} concentration sufficient to trigger spontaneous contractions. Lastly, at rest the residual Ca^{2+} from the previous VDF would perhaps result in a relatively large inward Na/Ca exchanger component which would depolarize the ventricle to allow generation of the next AP (Figure 3.5c). This perhaps contributes to a more positive resting potential for the neonatal ventricle compared to the adult ventricle (Cohen and Lederer, 1988; Gaughan et al., 1998). Overall, it would be interesting to explore these potential contributions to further elucidate the role of $Ca_v3.2$ channels in postnatal heart development. Suggested future experiments include measurement of contractility and intracellular Ca^{2+} using a combination of confocal microscopy and patch-clamp techniques on $Ca_v3.2^{-/-}$ ventricular myocytes overexpressing exon 25 splice variants. Such studies may more clearly define the physiological roles of $Ca_v3.2$ exon 25 splice variant channels in the heart.

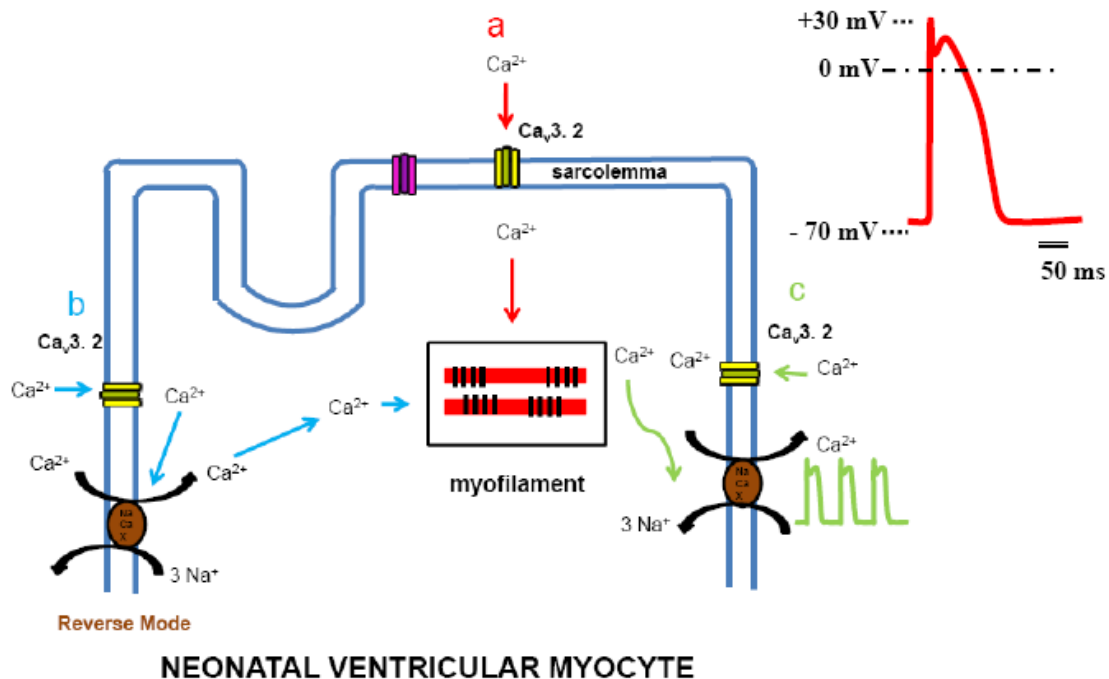


Figure 3.5. Potential contribution of $Ca_v3.2$ T-type Ca^{2+} channel VDF in neonatal rat ventricle.

A typical neonatal rat ventricular action potential is shown on the right. The resting potential is between -70 to -60 mV and peak AP is at +30 mV (Re-drawn from (Gaughan et al., 1998)). Proposed contributions of VDF of $Ca_v3.2$ T-type Ca^{2+} currents in neonatal ventricular myocytes. $Ca_v3.2$ T-type Ca^{2+} channels would contribute to activation of contractile machinery to induce spontaneous contraction and beating by (a) VDF of $Ca_v3.2$ channels would increase intracellular Ca^{2+} levels enough to directly activate myofilaments (red arrows), (b) Elevated Ca^{2+} would change the conformation of the local Na/Ca exchanger allowing it to go to reverse mode. This would increase intracellular Ca^{2+} enough to activate the contractile machinery (blue arrows) or (c) Residual Ca^{2+} from previous VDF would result in large inward Na/Ca exchanger currents. This would allow increase in Na^+ influx enough to depolarize the ventricle to generate the next action potential (green arrows).

3.4 Materials and methods

3.4.1 Animals and reagents

All animal procedures were performed in accordance with Canadian Council on Animal Care (CCAC) guidelines for animal research. Newborn (P0) Wistar-Kyoto rats were utilized in this research and purchased from University of British Columbia Animal Care Center, Vancouver, B.C., Canada.

All chemicals were purchased from Sigma (St. Louis, Missouri) unless otherwise stated. Culture media components were purchased from Invitrogen (Carlsbad, California).

3.4.2 Isolation of neonatal rat ventricular myocytes

One litter of newborn rats (8- 12 animals) was used per experiment. Ventricular myocytes were dissociated by serial enzymatic digestion as follows: P0 rats were cervically dislocated and then decapitated using a pair of scissors. The thorax of each animal was sterilized with 95% ethanol and an incision was made into the sternum to expose the heart. The beating heart was excised and immersed in sterile ice cold 1X ADS buffer containing (in mM) 116 NaCl, 20 HEPES, 0.5 NaH₂PO₄·H₂O, 5.4 KCl, 0.8 MgSO₄ and 5.5 glucose. All hearts were collected in a 60 mm Petri dish and washed.

Ventricles were isolated by removing the atria using curved forceps and a pair of curved small scissors. The isolated ventricles were then transferred into a new Petri dish and chopped into small pieces. Using a sterile 25 mL pipette the tissue pieces were transferred to a 50 mL Falcon tube. The ventricular tissues were allowed to settle at the bottom of the tube. Once settled ADS was removed using a sterile pipette.

Ventricular tissues were then subjected to serial enzymatic digestion using collagenase Type 2 (Worthington Biochemical Corporation, Lakewood, New Jersey) and pancreatin (Sigma, St. Louis, Missouri). Initial enzymatic digestion of ventricular tissues was performed by adding 8 mL of pre-warmed enzyme solution (0.6 mg/mL pancreatin and 100 Units/mL collagenase in 1X ADS buffer) and incubated in a shaking water bath at 37°C with a speed of 65 rpm for 5 minutes. After incubation, tissues were left to settle at the bottom of the tube and the supernatant was discarded using a sterile pipette and vacuumed. Ventricular tissues were then re-digested in enzyme solution and incubated in a shaking water bath at 37°C. Digested tissues were left to settle at the bottom and supernatant was transferred into a 50 mL Falcon tube containing sterile fetal bovine serum (Sigma, St. Louis, Missouri, 20% final concentration). The supernatant from this step contained the ventricular cell suspension. This supernatant was spun in a Hettich Universal 320R centrifuge at 1200 rpm for 6 minutes at 25°C. After centrifugation, the supernatant was discarded and the pellet was resuspended in sterile 6 mL pre-plating medium (PPM) containing (in %): 68 DMEM, 17 M199, 10 horse serum, 5 fetal bovine serum. Resuspended pellets were triturated and transferred in a sterile 50 mL falcon tube and equilibrated in the 37°C incubator aerated with 5 % CO₂. Prior to centrifugation ventricular tissues were re-digested with fresh enzyme solution and incubated in a shaking water bath. The digestion and centrifugation were repeated six to eight times. The ventricular cells harvested after centrifugation were pooled in the same 50 mL falcon tube containing PPM.

Immediately after finishing all the digestion steps, cells were spun at 1200 rpm for 6 minutes at 25°C and the pellet was resuspended in 15 mL PPM. The cell suspension was gently filtered through a sterile 70 µm Falcon cell strainer (BD Biosciences, Bedford, Massachusetts). The cell suspension was divided into three 60 mm Petri dishes containing 5 mL each and pre-plated for 60 – 90 minutes in a 37°C incubator allowing the fibroblast to be attached. After pre-

plating, the dishes were transferred to the sterile hood and were tapped on top of the hood bench to dislodge attached ventricular myocytes. Using a 10 ml pipette, the media containing the myocytes were transferred in a new sterile 50 mL falcon tube. Then the Petri dishes were washed with PPM to further harvest the myocytes that remained in the dish. Washing was repeated until there were no myocytes to transfer. The media used for washing was pooled to the original cell suspension. For electrophysiological studies, ventricular myocytes were seeded in 35 mm Petri dishes containing 12 mm glass coverslips coated with 15 $\mu\text{g/mL}$ laminin. NRVM were seeded at a density of 7.5×10^4 cells/mL. For qRT-PCR analysis, ventricular myocytes were grown in a 1% gelatin coated T25 flask at a density of 1.0×10^5 cells/mL. NRVM were incubated overnight at 37°C. The following day, media was replaced with pre-warmed sterile serum-free maintenance media containing 80% DMEM, 20% M199 and 1% (v/v) penicillin/streptomycin.

3.4.3 RNA extraction and quantitative Real-Time-PCR (qRT-PCR)

After 24 hours of incubation in serum free maintenance media, total RNA from cultured NRVM was prepared. Maintenance media were discarded using a sterile pipette and vacuumed. One mL of Trizol (Invitrogen) was added to the myocytes. Using an RNase-free plugged tip, myocytes were dislodged by pipetting up and down. NRVM/Trizol mixture was then transferred and homogenized in a sterile glass/Teflon homogenizer. Homogenized samples were incubated at room temperature (RT) for 5 minutes followed by adding 200 μL chloroform and incubated at RT for another 3 minutes. Samples were spun in a table top centrifuge at 11,000 x g for 15 minutes at 4°C. The aqueous phase of the centrifugate was immediately transferred to a clean RNase-free eppendorf tube and 500 μL of isopropanol was added. The centrifugate/isopropanol mixture was incubated at RT for 10 minutes to precipitate the RNA. After the incubation, samples were spun at 11,000 x g for 10 minutes at 4°C. The precipitate was washed with 75%

ethanol and spun at 7,500 x g for 5 minutes. The supernatant was removed and final pellets were dried briefly prior to suspension in DEPC-treated deionized water.

Total RNA was used to synthesize cDNA using a High Capacity cDNA Reverse Transcription kit (Applied Biosystems). Real-time-PCR reactions were performed using Applied Biosystems reagents; Applied Biosystems AB 7500 instrument and TaqMan probes generated against the respective cDNA targets. Primer mixes used for qRT-PCR analysis to determine the level of mRNA expression of Ca²⁺ channels were purchased from Applied Biosystems (Carlsbad, California). Relative mRNA amounts were estimated after actin B normalization. All qRT-PCR reactions were run in triplicate and averages were determined. A total of five RNA preparations from five NRVM isolations were utilized in determining the level of mRNA expression

3.4.4 Whole cell patch clamp analysis of isolated neonatal ventricular myocytes

Neonatal ventricular myocytes were maintained in serum-free maintenance media at 37°C in a humidified incubator with 95% O₂ and 5% CO₂ for 24 hours prior to whole cell patch clamp analysis. When the myocytes started beating which was normally 24 - 48 hours after isolation, NRVM were ready for biophysical characterization.

Macroscopic currents were recorded using Axopatch 200B amplifiers (Axon Instruments, Foster City, CA) controlled and monitored with personal computers running pClamp software version 9 (Axon Instruments). The external recording solution was composed of the following (in mM): 2 CaCl₂, 1 MgCl₂, 92 CsCl, 10 glucose, 40 tetraethylammonium chloride, 10 HEPES, osmolarity was adjusted to 310 mOsm with D-mannitol and pH to 7.4. The internal pipette solution contained (in mM): 120 Cs-MeSO₃, 11 EGTA, 10 HEPES, 2 MgCl₂, 5 MgATP, 0.3 NaGTP, osmolarity was adjusted to 290 mOsm with D-mannitol and pH to 7.2. 20 μM CdCl₂ was added to the external recording solution to eliminate the I_{CaL} component. Patch pipettes

(borosilicate glass BF150-86-10; Sutter instruments, Novato, CA) were pulled using a Sutter P-87 puller and fire polished with a Narashige (Tokyo, Japan) microforge with typical resistances of 3 – 6 M Ω when filled with internal solution. The bath was grounded via a 3 mM KCl bridge. Data were filtered at 2 kHz with the built-in Bessel filter of the amplifier. The amplifier was also used for capacitance and series resistance compensation between 75 to 85% on every cell. Leak subtraction of leakage current was performed during off-line analysis.

I-V relationships of ventricular myocytes were studied using two holding potentials to determine the contribution of T- and L-type Ca²⁺ currents in these cells. A hyperpolarized holding potential of -90 mV recorded both Ca²⁺ currents whereas V_h of -50 mV revealed exclusively I_{CaL}. The contribution of NRVM I_{CaT} was determined by subtracting recorded Ca²⁺ currents obtained from V_h -90 mV to V_h -50 mV both in the presence and absence of 20 μ M CdCl₂ (Figure 3.2). Voltage-dependent activation was studied by applying 200 ms depolarizing pulses from -80 mV to + 20 mV at 10 mV increments. Current densities (in pA/pF) were calculated by dividing the capacitance (in pF) of each myocyte from the current (in pA) obtained in each test potential. The values from the current densities were utilized to analyze the voltage-dependence of I_{CaT}. I-V relationships were fitted with the modified Boltzmann equation : $I_m = (G_{max} \times (V_m - E_{rev})) / (1 + \exp((V_m - V_{50act})/k_{act}))$, where G_{max} is the maximum slope conductance; E_{rev} is the extrapolated reversal potential; V_m is the membrane potential, V_{50act} is the half activation potential; k_{act} is the slope factor of activation which reflects the voltage sensitivity.

Steady-state inactivation of NRVM I_{CaT} was studied by applying 5 second prepulses from -120 mV to -10 mV followed by a test pulse to – 30 mV for 90 ms. The current magnitude obtained during each test pulse was normalized to the maximum current and plotted as a function of the pre-pulse potential. Steady state inactivation normalized data were fitted using the Boltzmann equation ($I/I_{max} = (1 + \exp((V - V_{50inact})/k_{inact}))^{-1}$), where I_{max} is the maximum current;

$V_{50\text{inact}}$ is the membrane potential at which 50% of the channels are inactivated, k_{inac} is the slope factor of inactivation.

NRVM I_{CaT} kinetics of activation (τ_{act}) and inactivation (τ_{inact}) were analyzed by fitting current recordings obtained from subtracted Ca^{2+} currents (Figure 3.2). To obtain the values for the activation and inactivation kinetics, current traces were fitted with a single exponential standard equation $I = Ae^{-t/\tau}$, where A is the amplitude of the current at t_0 , and τ is the time constant.

Recovery from inactivation was determined by double pulse protocol; a prepulse to -30 mV for 400 ms was given and allowed to recover at different time intervals (interpulse interval) between 5 ms to 5 seconds before applying a test pulse to -30 mV for 50 ms ($V_h = -90$ mV). The peak current from the test pulse was plotted as ratio of maximum prepulse current versus interval between pulses. The data were fitted with a double exponential function ($I/I_{\text{max}} = A_0 + A_1 \cdot \exp(-t/\tau_1) + A_2 \cdot \exp(-t/\tau_2)$), where A_0 is the amplitude for inactivating component, A_1 and A_2 are the amplitudes for the fast and slow components of the exponential, and τ_1 and τ_2 are the time constants for the fast and slow components.

The VDF property of NRVM I_{CaT} was studied by applying a 200 ms test pulse to -30 mV following a series of depolarizing prepulses from -90 to +110 mV after a time interval of 1.2 seconds. The percentage of facilitation was obtained by dividing the currents obtained from prepulses to currents recorded at -90 mV. Averaged percentage of facilitation was plotted as a function of prepulse depolarization. All recordings were performed at room temperature (~22 - 24°C).

Data analysis was performed using Clampfit software version 9.0 (Axon Instruments). All plots and statistical analysis (T-test and ANOVA) were performed using the Microcal Origin

software version 7.5 (Northampton, MA). Statistical significance was tested with Student's *t*-test with significance being determined at confidence interval of $p < 0.05$ and $p < 0.01$.

4 CONCLUSION

4.1 Overall significance

4.1.1 Identification and characterization of cardiac Ca_v3.2 alternative splice variants

Although Ca_v3.2 T-type channels had been reported to be expressed in the heart, alternative splicing of cardiac Ca_v3.2 channels has not yet been explored. Alternative splicing of transcript of the *CACNA1H* gene which encodes for the Ca_v3.2 T-type channel has thus far been shown in human fetal whole brain (Zhong et al., 2006), rat thalamus (David et al., 2008; Powell et al., 2009) (Appendix 5), testis (Jagannathan et al., 2002) and uterus (Ohkubo et al., 2005). Alternative splice variants of Ca_v3.2 channels have been implicated in the pathophysiology of epilepsy and sperm cell differentiation (Jagannathan et al., 2002; Zhong et al., 2006; Powell et al., 2009). However, prior to this research, the relevance of Ca_v3.2 alternative splicing had not been described for the developing or diseased heart. The elucidation of cardiac Ca_v3.2 alternative splice variants is predicted to provide important new insights into the contributions of Ca_v3.2 channels in cardiac development and disease progression.

The first major objective of this thesis was to explore whether cardiac Ca_v3.2 channels are subject to major alternative splicing. A second major objective was to functionally characterize the full-length splice variants using a heterologous expression system. This thesis utilized an experimental design that allowed comprehensive splice-variant screening via full length cDNA sequencing and colony PCR screening of possible cardiac Ca_v3.2 alternative splice variants (Chapter 2). Since Ca_v3.2 is predominantly expressed in the early stages of development, newborn (day 0) rat hearts were utilized for the splice variant screening.

This thesis described 25 in-frame/C-terminal alternative splice variants occurring at 10 distinct sites in the Ca_v3.2 protein (Figure 2.2 and Table 2.1). Additionally, this research found

21 out-of-frame splice variants (data not shown) which resulted in premature truncations (PCTs) predicted to encode in non-functional channels. Out of frame variants are predicted to elicit nonsense-mediated decay (NMD) and/or act as dominant negative regulators of wild type channels (Wielowieyski et al., 2001; Lejeune and Maquat, 2005; Zhong et al., 2006). NMD is an important mechanism to degrade abnormal mRNAs that encode potentially deleterious truncated proteins and to achieve proper levels of gene expression (Lejeune and Maquat, 2005). Truncated $Ca_v3.2$ channels have been shown to suppress the expression of wildtype channels suggesting a functional role for PCTs (Heron et al., 2004; Mezghrani et al., 2008). Compared with the previous studies on $Ca_v3.2$ alternative splicing which utilized partial length cDNA screening, this study employed full length cardiac $Ca_v3.2$ cDNA libraries which allowed analysis of the entire $Ca_v3.2$ ORF. Notably, most alternative splicing occurs at the cytoplasmic regions of the channel (8 sites) known to be critical for channel functional properties (Figure 2.2). The cytoplasmic regions of T-type channels are known to be implicated in regulation of channel biophysical properties as well as modulation by certain GPCRs and kinases (Arnoult et al., 1997; Chemin et al., 2001a; Welsby et al., 2003; Wolfe et al., 2003; Hildebrand et al., 2007; Vitko et al., 2007; Iftinca and Zamponi, 2009) (Appendix 2). The splice variants located in six different cytoplasmic regions were subjected to more in-depth analysis via qRT-PCR and whole cell patch clamp analysis.

Among the six distinct variant regions studied, $Ca_v3.2$ domain III – IV linker splice variants encoding for the inclusion or exclusion of exon 25 revealed notable expression and biophysical profiles. The level of mRNA expression of $Ca_v3.2(-25)$ channels was found to be higher than $Ca_v3.2(+25)$ channels in the newborn hearts (Figures 2.3, 2.4 and 3.4D). Furthermore, the two variants also showed distinct biophysical properties. Examination of cardiac $Ca_v3.2 (\pm)$ exon 25 splice variants demonstrated significant variant-specific changes in

recovery from inactivation and VDF. Exclusion of exon 25 resulted in Ca_v3.2 currents with robust VDF and faster time constants for recovery from inactivation compared with Ca_v3.2 plus exon 25 containing channels (Figures 2.6, 2.7, 2.8 and Table 2.3). This is the first study to report VDF of recombinant Ca_v3.2 channels. Another contribution of this research was the description of a differential effect on Ca_v3.2 VDF by Gβγ. Co-transfected Gβ₂γ₂ reduced the magnitude of VDF of Ca_v3.2(-25) by approximately 50% (Figure 2.9D). Gβ₂γ₂, however, did not have any effect on Ca_v3.2(+25) variant channels (Figure 2.9E). Overall, the study found evidence of extensive splicing in intracellular loops of cardiac Ca_v3.2 channels correlated with distinct biophysical properties.

4.1.2 Developmental and pathological expression of Ca_v3.2 alternative splice variants

Cardiovascular T-type Ca²⁺ channels have been shown to be prominently expressed during early stages of development, downregulated in the adult ventricles and upregulated or re-expressed in the adult diseased ventricles. The Ca_v3.1 and Ca_v3.2 isoforms are highly expressed in immature hearts (Cribbs et al., 2001; Ferron et al., 2002; Niwa et al., 2004) but in adult hearts the expression of Ca_v3.2 becomes significantly reduced and Ca_v3.1 becomes the predominant isoform but mainly being restricted to pacemaker cells (Qu and Boutjdir, 2001; Mangoni and Nargeot, 2008). However in the hypertrophic adult ventricle, both the functional I_{CaT} and mRNA expression of Ca_v3.2 have been shown to be upregulated (Martinez et al., 1999; Yasui et al., 2005). Additionally, specific expression of the Ca_v3.2 T-type isoform has also been associated with the pathogenesis of pressure overload-induced cardiac hypertrophy (Chiang et al., 2009). Although, regulation of Ca_v3.2 expression exists during development and disease, changes in the pattern of expression of Ca_v3.2 alternative splice variants have not been explored. The third

major objective of this thesis was to determine whether alteration in the pattern of expression of $Ca_v3.2$ alternative splice variants is associated with cardiac development and hypertrophy.

This study explored changes in the relative expression of $Ca_v3.2$ alternative splice variants in newborn and adult hearts (Chapter 2). I found that the relative expression of the domain III – IV linker variants ($Ca_v3.2 \pm 25$) showed significant differences in the pattern of expression in newborn versus adult hearts (Figure 2.3). In the newborn heart the exclusion of exon 25 is predominantly expressed occurring at a level 7 to 8 fold higher than (+) 25 exon variant transcripts. Interestingly, in the adult ventricle the overall ratio of (+25) to (-25) variants was approximately equal attributed to the reduction in the expression of the minus exon 25 variant (Figures 2.3 and 2.4). These findings are the first evidence that $Ca_v3.2$ alternative splicing is regulated in developing hearts. Interestingly, developmental regulation of expression of alternative splice variants of other Ca^{2+} handling proteins such as $CaMKII\delta$, cardiac troponin T and $Ca_v1.2$ channels have also been reported (Tang et al., 2004; Ladd et al., 2005; Xu et al., 2005). Therefore, understanding the overall functional significance of postnatal changes in cardiac splicing pattern of Ca^{2+} handling proteins would provide insight into the contribution of these proteins in postnatal heart development.

Ca^{2+} influx via transient receptor potential canonical (TRPC) channels (Wu et al., 2010; Eder and Molkenin, 2011), L-type channels (Chen et al., 2011) and T-type channels (Chiang et al., 2009; Nakayama et al., 2009; Cribbs, 2010) have all been implicated in cardiac hypertrophic responses. Increase of intracellular Ca^{2+} is thought to be critically involved in cardiac hypertrophic signalling in part through the Ca^{2+} -activated protein phosphatase calcineurin which leads to activation of the transcription factor NFAT (Houser and Molkenin, 2008). Interestingly, the $Ca_v3.2$ T-type channels have been shown to be involved in the pathogenesis of cardiac hypertrophy via calcineurin/NFAT pathway (Chiang et al., 2009). Moreover, upregulation of

Ca_v3.2 channels has also been demonstrated in pathological ventricular hypertrophy (Martinez et al., 1999; Yasui et al., 2005). Additionally, in Chapter 2 I provided evidence on extensive alternative splicing of cardiac Ca_v3.2 channels. This prompted me to study whether the expression of Ca_v3.2 alternative splice variants are altered in cardiac hypertrophy. The regulation of expression of Ca_v3.2 exon 25 splice variants was investigated in ventricular hypertrophic SHR animals. The SHR is a commonly-used model in studying cardiac hypertrophy since this model closely mimics the most common pathophysiological changes in the human cardiovascular system – hypertension, cardiac hypertrophy and heart failure (Doggrell and Brown, 1998; Chen-Izu et al., 2007; Tang et al., 2008). Age- and sex-matched normotensive WKY rats were used as controls. The hypertrophic phenotype of the SHR animals was confirmed using two molecular markers known to be upregulated in pathological hypertrophy (Figure 2.10A). In addition, histological staining indicative of tissue fibrosis resulting from cardiac hypertrophy was also determined (Figure 2.10B). Overall, our data were consistent with the phenotype of pathological ventricular hypertrophy. This thesis next determined if there are splice variant-specific changes in the expression of Ca_v3.2 exon 25 splice variants. An upregulation of overall expression of Ca_v3.2 channels was observed in hypertrophic SHR (Figure 2.10C), a result consistent with an increase in expression of Ca_v3.2 channels observed in the diseased ventricle by other investigators (Martinez et al., 1999; Yasui et al., 2005). More importantly, a significant increase in the relative amount of Ca_v3.2(+25) variant compared to Ca_v3.2(-25) was observed in hypertrophic SHR (Figures 2.10C and 2.10D) resulting in a shift in the predominant exon 25 splice isoform. Thus in pathological cardiac hypertrophy there appears to be a splice-specific upregulation of Ca_v3.2 alternative splice variants. The potential significance of this observation is discussed in subsequent section. Overall, the study provided evidence that splice-variant

specific changes in expression of $Ca_v3.2$ are associated with cardiac development and hypertrophy.

4.2 Splice variant specific expression of $Ca_v3.2$ T-type Ca^{2+} channels during development and hypertrophy

4.2.1 Working hypothesis

Several splice variants exist for each of ten Ca^{2+} channel genes with evidence showing developmental and pathophysiological changes in expression patterns. Alternative splicing generates isoforms that show significant ion channel properties, localization, enzymatic activity, protein stability and post-translational modification (Stamm et al., 2005) profoundly affecting animal physiology, development and pathophysiology (reviewed in (Lopez, 1998; Grabowski and Black, 2001; Stamm et al., 2005; Blencowe, 2006; Gray et al., 2007; Swayne and Bourinet, 2008). For example, alternative splicing in the *CACNA1A* genes has been demonstrated to alter the functional properties of $Ca_v2.1$ channels. It was reported that the expression of the mutually exclusive exons 37a and 37b (EF hand variants) determines the CDF property of $Ca_v2.1$ (Soong et al., 2002; Chaudhuri et al., 2004). The expression of these variants changes the functional properties of $Ca_v2.1$ channels by regulating the influx of Ca^{2+} to the cell. Interestingly, spatial and temporal regulation of expression EF hand variants was observed in human and rodent brains suggesting regional- and development-specific roles (Chang et al., 2007). Additionally, our laboratory has also shown that FHM-1 mutations introduced to the $Ca_v2.1$ (+/-) exon 47 have splice-dependent effects on voltage-dependent gating and kinetic properties suggesting a role of $Ca_v2.1$ alternative splicing in the molecular pathophysiology of FHM-1 (Adams et al., 2009) (Appendix 4).

Changes in the expression of Ca_v1.2 alternative splice variants during development and in disease states have been demonstrated by several groups of investigators (Section 1.3.1). For instance, the level of expression of exons 9* and 33 was reported to change during maturation. Compared to the fetal brain, downregulation of exon 9* and upregulation of exon 33 was observed in the adult brain (Tang et al., 2009). Conversely, compared to the fetal heart, higher expression of exon 9* and lower expression of exon 33 were observed in the adult heart (Tang et al., 2004). Relevant to cardiovascular diseases, changes in the level of expression of Ca_v1.2 of the mutually exclusive exons 21 and 22 have been reported in human atherosclerotic patients and hypertrophic SHR (Tiwari et al., 2006; Tang et al., 2008). Upregulation of exon 22 was observed in atherosclerosis whereas in cardiac hypertrophy the combination of both exons 21 and 22 are significantly expressed.

T-type channels are also subjected to alternative splicing (Section 1.3.2). Developmental regulation of expression of human Ca_v3.1 channels has been reported by Emerick et al. (Emerick et al., 2006). The authors reported a switch in the predominant expression of exon 25C and 26 variants between fetal and adult brains. Exon 26 is predominantly expressed in the fetal brain whereas exon 25C is preferentially expressed in the adult brain. The neuronal Ca_v3.2 channels have also been demonstrated to be subjected to alternative splicing (Zhong et al., 2006; David et al., 2008; Powell et al., 2009) (Appendix 5). Thus far, there is no report on developmental and pathological changes in the expression of Ca_v3.2 alternative splice variants. However, our laboratory demonstrated that the functional effects of introduced GAERS mutations are dependent on Ca_v3.2 alternative splice variants (Powell et al., 2009) (Appendix 5). Collectively, the results from the above studies provided evidence of alteration in the expression of alternative splice variants during development and disease. To date, alternative splicing in rat cardiac Ca_v3.2 channels has not been studied. This study worked on the hypothesis that the cardiac Ca_v3.2

channels are subjected to alternative splicing and that patterns of expression of alternative splice variants are altered during development and hypertrophy.

The results in Chapter 2 provided evidence of extensive splicing of cardiac Ca_v3.2 T-type channels. Importantly, I demonstrated an alteration in the predominant expression of Ca_v3.2 alternative splice variants during normal cardiac development and in pathophysiological state. I showed that the expression of Ca_v3.2 minus exon 25 is predominantly expressed in the newborn atria and ventricles. In the adult ventricle, I demonstrated that the expression of Ca_v3.2 minus exon 25 was significantly reduced resulting in approximately equal levels of both plus and minus exon 25 variants. However, in the adult hypertrophic ventricle from SHR, an overall upregulation of both splice variants was observed. Interestingly, I observed a shift towards the expression of Ca_v3.2 plus exon 25 variants as the predominant form. Overall, my observations support my hypothesis that changes in the expression of Ca_v3.2 alternative splice variants are associated with cardiac development and hypertrophy.

In general, the molecular mechanism underlying the downregulation and upregulation of Ca_v3.2 channel expression in the adult normal and diseased rat ventricles is not clearly understood. I speculate that downregulation of cardiac Ca_v3.2 expression during maturation could be explained by suppression by the transcriptional suppressor NRSE/NRSF. Previous reports showed that NRSF expression in the fetal heart is barely detectable but in adult heart significant expression was detected (Kuwahara et al., 2001; Kuwahara et al., 2003). With regard to the expression of Ca_v3.2 channels, significant expression was reported during the early stage of development and much reduced or undetected in the adult heart (Qu and Boutjdir, 2001; Ferron et al., 2002). This shows that the expression of Ca_v3.2 and NRSF is negatively correlated. This negative correlation was tested in transgenic mice expressed with a dominant negative mutant of NRSF (dnNRSF Tg). Compared with the wild type mice, Ca_v3.2 mRNA were

upregulated in dnNRSF Tg mice, suggesting that the absence of NRSF allowed Ca_v3.2 expression to proceed (Kuwahara et al., 2003; Kuwahara et al., 2005).

In this study, I also showed an upregulation of expression of Ca_v3.2 channels in hypertrophic ventricles from SHR. This is consistent with previous reports on upregulation of Ca_v3.2 expression in other models of cardiac hypertrophy (Martinez et al., 1999; Kuwahara et al., 2003; Yasui et al., 2005). Kuwahara and colleagues have reported negative correlation of expression of mouse cardiac Ca_v3.2 channels and the transcriptional repressor NRSF (Kuwahara et al., 2003; Kuwahara et al., 2005). In addition, the authors also observed that dnNRSF Tg mice have a cardiac hypertrophic phenotype suggestive of the involvement of NRSE/NRSF transcriptional regulator to the hypertrophic signalling pathways (Kuwahara et al., 2003; Kuwahara et al., 2005). Therefore, it is tempting to speculate that the upregulation of rat cardiac Ca_v3.2 expression in hypertrophic SHR could also be attributed to downregulation of NRSF.

Based upon my data on the quantitative mRNA expression analysis, I showed splice variant specific changes in the expression of cardiac Ca_v3.2 during development and pathological hypertrophy. This study provided evidence of changes in the pattern of expression of Ca_v3.2 exon 25 splice variants in developing and disease states. However, the pathways leading to the expression of specific splice variants in specific functional states are not explored in this thesis. Using the data obtained in this thesis and information from previous studies, I am proposing hypothetical pathways on the signalling mechanisms involved in the regulation of expression of rat cardiac Ca_v3.2 exon 25 splice variants (Figure 4.1). These proposed pathways would be potentially good research topics for future studies.

A number of transcription factors and splicing regulators have been reported to be involved in the regulation of expression of cardiac proteins in the developing and diseased heart (Tang et al., 2004; Ladd et al., 2005; Xu et al., 2005; Houser and Molkenin, 2008). Here, I will

discuss my suggestions on the potential involvement of a number of transcription and splicing regulators in controlling the preferential expression of a specific Ca_v3.2 exon 25 splice variant in the developing and diseased heart. One potential candidate is the regulation of expression by the fox family of splicing regulators. These proteins recognize the hexanucleotide TGCATG and bind to the intron adjacent to their target exon where they generally repress splicing when bound upstream of the exon but enhance splicing from a downstream binding site (Underwood et al., 2005; Zhang et al., 2008; Zhou and Lou, 2008; Yeo et al., 2009). Upon inspection of the rat Ca_v3.2 genomic sequence (ENSRNOT00000048392 and NC_005109), a fox binding site in Ca_v3.2 intron located and identified 14 base pairs downstream of exon 25 (Figure 4.1A). Based on the presence and location of a fox binding site in the Ca_v3.2 genomic sequence, I speculate that fox proteins are good candidates as potential regulators of expression of Ca_v3.2 exon 25 splice variants.

A differential pattern of fox protein expression exists in the developing mouse heart. In the adult mouse heart, the level of expression of fox-1 was shown to be ~10-fold higher than the newborn heart (Kalsotra et al., 2008). The presence of fox protein recognition site downstream of Ca_v3.2 exon 25 (Figure 4.1A) and the low level of fox protein expression in neonatal heart likely explain the observed low mRNA expression of Ca_v3.2(+25). Although a higher level of fox protein expression in the adult rat heart potentially increases the expression of the plus exon 25 variant, our data showed lack of increase in the expression of Ca_v3.2(+25) splice variant in the adult ventricle. This could be explained by an overall downregulation of Ca_v3.2 expression in the adult ventricle brought about by an increase in expression of NRSF. Taken together, NRSF/fox protein-mediated regulation of expression of Ca_v3.2 exon 25 splice variants may occur in developing rat hearts (Figure 4.1C).

A different signalling mechanism likely exists in pathological cardiac hypertrophy (Figure 4.1B) due to differential activity and expression of fox proteins and other transcription factors such as the class II histone deacetylase (HDAC) transcription factors. Compared to the newborn heart, fox proteins are prominently expressed in the adult heart. Previous studies have reported the involvement of fox proteins in the pathogenesis of human cardiac hypertrophy and failure (Hannenhalli et al., 2006). Thus, in the diseased adult ventricle, fox proteins may play an important role in cardiac disease progression. Additionally, NRSF and HDACs have also been shown to contribute to cardiac hypertrophy (Nakagawa et al., 2006; Bingham et al., 2007). Both groups demonstrated that NRSF-mediated repression has been shown to form a complex with HDAC (Nakagawa et al., 2006; Bingham et al., 2007) thereby repressing the expression of the cardiac fetal genes including the *CACNA1H* genes. However, in ET-1-induced ventricular hypertrophy this complex is disrupted due to increase in phosphorylation of HDACs (Bingham et al., 2007). Phosphorylation of HDACs leads to translocation of HDACs from the nucleus to the cytoplasm making them unable to form a complex with NRSF (Nakagawa et al., 2006). Once this binding is disrupted, de-repression of NRSF-mediated repression would allow the expression of fetal cardiac genes such as the *CACNA1H* genes. Therefore, I suggest that in hypertrophic SHR there exists an increase in fox protein and HDAC activities. This might explain why the Ca_v3.2(+25) alternative splice variant is preferentially expressed in hypertrophic SHR.

The hypothetical signalling mechanism proposed here (Figure 4.1) provides an opening for future studies on elucidating the signalling pathway involved in the splice-specific changes in expression of Ca_v3.2 alternative splice variants in normal heart development as well as in pathological cardiac hypertrophy. This would also potentially provide an understanding of the contribution of Ca_v3.2 T-type channels in normal cardiac physiology and remodelling.

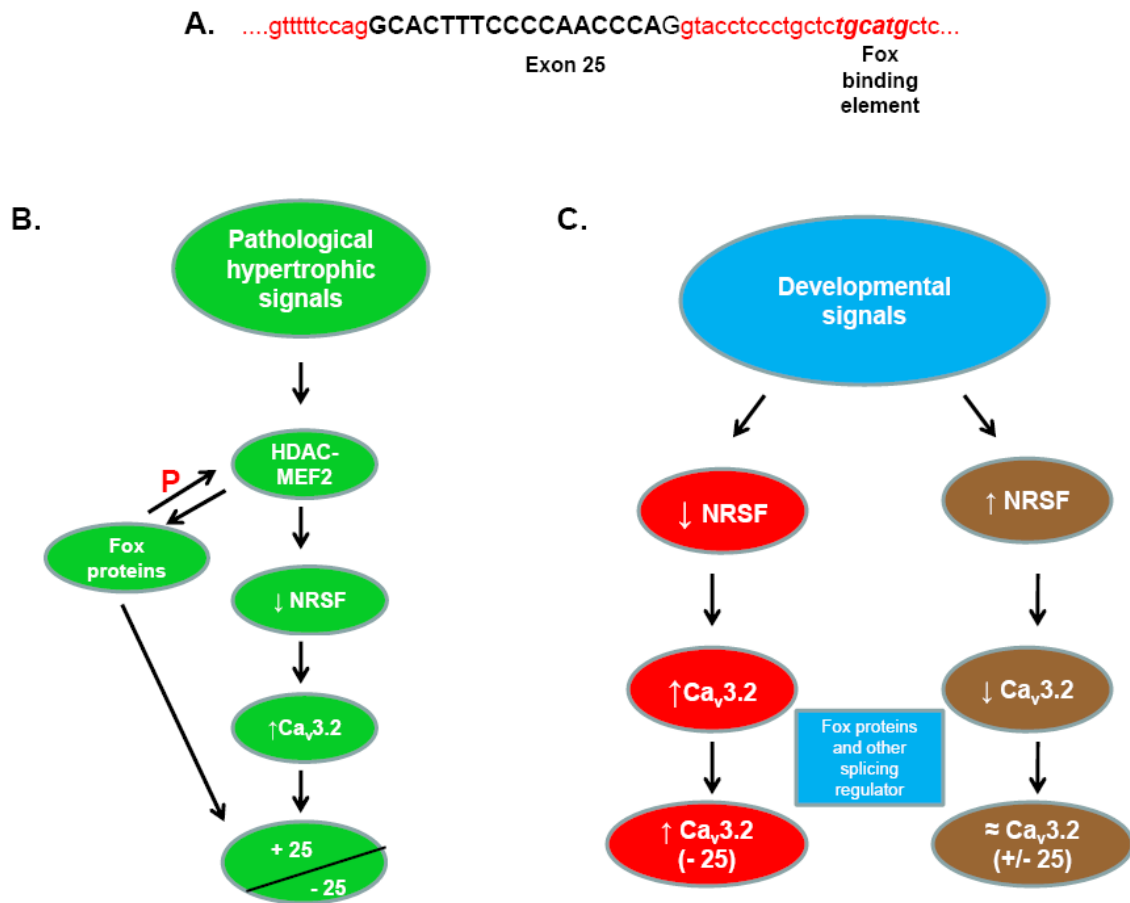


Figure 4.1. Hypothetical pathways of the signaling mechanism potentially involved in the regulation of expression of $Ca_v3.2$ exon 25 splice variants.

(A) Sequence analysis on the genomic sequence of $Ca_v3.2$ (ENSRNOT00000048392 and NC_005109) showing the presence of fox protein binding element downstream of $Ca_v3.2$ exon 25. (red, intron; black, exon). Fox binding element consensus sequence TGCATG was identified 14 base pairs downstream of exon 25. (B) Potential involvement of HDAC, NRSF and fox proteins in the pathological regulation of expression of $Ca_v3.2$. (C) Developmental regulation of expression of $Ca_v3.2$ channels (red oval, newborn; brown oval, adult). In this hypothetical model, it is suggested that the expression of $Ca_v3.2$ exon 25 splice variants is differentially regulated during normal cardiac development and pathological hypertrophy. The transcriptional repressor NRSF would regulate the expression of $Ca_v3.2$. Low level of NRSF would allow the expression of $Ca_v3.2$ whereas at high amount would repress $Ca_v3.2$ expression. Low level of fox proteins would allow the expression of minus exon 25 variants while keeping plus exon 25 variants at minimal. Conversely, in pathological cardiac hypertrophy, HDAC would de-repress NRSF-mediated repression of $Ca_v3.2$ allowing $Ca_v3.2$ to be upregulated or re-expressed. Fox proteins activity would increase in cardiac hypertrophy thereby increasing the expression of $Ca_v3.2$ exon 25 variants.

4.2.2 Potential limitations

Alternative splice variants were examined across the entire ORF of neonatal rat cardiac $Ca_v3.2$ T-type channels using a combination of overlapping short amplicon PCR screening and full length cDNA sequence analysis (Chapter 2). Approximately 1000 short amplicon and 106 full length cDNAs were utilized for splice variant screening. Although this thesis used a large sample size in the analysis, there remains the possibility that all potential splice variants were not recovered, particularly the less abundant variants. Regan et al. suggested that at least ~2300 clones are required to detect at least one of the lowest frequency splice variants (Regan et al., 2000). To address this, it would be ideal to utilize a large number of full length cDNA clones. In addition, instead of analyzing individual full length cDNA clone, an alternative option would be to perform high through-put sequencing of full length cDNA amplicon generated from RT-PCR. For 2 μ g total RNA, it was suggested that ~20,000 to 100,000 full length clones could be generated (Regan et al., 2000).

Although this thesis showed extensive alternative splicing in cardiac $Ca_v3.2$ T-type channels, analysis of full length screening in this study was focused on newborn (day 0) hearts. In the future, it would be interesting to perform a full inventory of the splice variant profile of $Ca_v3.2$ channel in adult normal and hypertrophic hearts. This would determine whether the utilization of $Ca_v3.2$ splice variants or their combinations are altered in pathological hypertrophy. In fact, Tang et al. have reported significant differential $Ca_v1.2$ splicing patterns in the hearts of 18 week-old hypertrophic SHR and normotensive WKY rats (Tang et al., 2008). While this thesis did not show full length cDNA screening of $Ca_v3.2$ splice variants in normotensive and hypertrophic hearts, this work provided strong evidence of changes in $Ca_v3.2$ splicing pattern by demonstrating alteration in the level of expression of the predominant exon 25 splice variants in the newborn, adult and hypertrophic ventricle (Chapter 2).

Differential expression of Ca_v3.2 exon 25 variants during development was demonstrated in this thesis. Two developmental stages were utilized i.e. newborn day 0 and four month old adults. In future studies, it will be interesting to characterize changes in Ca_v3.2 splicing pattern in other developmental stages; perhaps it would be better to include embryonic, fetal (before birth), and juvenile, in splice variant screening. Likewise, in a disease state, profiles of various stages of cardiac diseases (pre-hypertensive, hypertensive, pre-heart failure and heart failure) would be effective ways to determine potential changes in the expression of Ca_v3.2 splice variants.

4.3. Voltage-dependent facilitation of Ca_v3.2 T-type channels

4.3.1 Working hypothesis

As described in Chapter 2, I identified several splice variants of Ca_v3.2 channels. Thus, I further explored the hypothesis that alternative splice variants of Ca_v3.2 confer functionally distinct channels. I observed that the Ca_v3.2(-25) splice variant display potentiated recovery from inactivation. Previous reports showed that the recombinant Ca_v3.3 is the only T-type isoform displaying VDF (Klockner et al., 1999; Gomora et al., 2002). However, in the cardiovascular system VDF of native I_{CaT} has been shown in frog atrial and guinea pig coronary myocytes (Ganitkevich and Isenberg, 1991; Alvarez et al., 1996; Alvarez et al., 2000). Since among the three T-type isoforms the Ca_v3.1 and Ca_v3.2 channels are the only two T-type isoforms in the heart (Cribbs et al., 1998; Cribbs et al., 2001; Perez-Reyes, 2003) and I observed that Ca_v3.2 revealed potentiated recovery from inactivation, I hypothesized that cardiac Ca_v3.2 T-type channels display VDF.

The results in Chapter 2 showed that full-length cardiac Ca_v3.2 variants cloned in the minus exon 25 background display VDF and potentiated fractional recovery. The observed

magnitude of VDF for Ca_v3.2 minus exon 25 variant is between 50 and 60% (Figure 2.6). Thus, my data supports our hypothesis that cloned Ca_v3.2 channels display VDF. Moreover, I also observed significant expression of Ca_v3.2(-25) in newborn rat ventricular tissues (Figure 2.4). This led me to hypothesize that I_{CaT} in neonatal rat ventricles displays VDF. In Chapter 3, I worked on the hypothesis that native cardiac I_{CaT} displays VDF and this property is correlated with a high expression of Ca_v3.2(-25) alternative splice variant. I optimized a protocol design to dissociate NRVM and grow them in culture prior to whole cell patch clamp and qRT-PCR analyses. Indeed, biophysical analysis using prepulse-induced facilitation protocol recorded from NRVM in culture revealed significant VDF of neonatal ventricular I_{CaT} (Figures 3.4A and 3.4C). Importantly, the observed VDF in NRVM I_{CaT} is correlated with predominantly Ca_v3.2(-25) expression (Figure 3.4D).

VDF of NRVM I_{CaT} was compared with the VDF profiles of recombinant Ca_v3.1 and Ca_v3.2 variants. I observed that both NRVM I_{CaT} and Ca_v3.2(-25) displayed VDF, and lack of facilitation was observed for Ca_v3.2(+25) and Ca_v3.1 channels (Figure 3.4C). My observations are consistent with the lack of facilitation in Ca_v3.1 observed by several investigators (Klockner et al., 1999; Chemin et al., 2001a; Chemin et al., 2002; Gomora et al., 2002; Latour et al., 2004). In addition, preliminary results from our laboratory also showed that homologous exon 25 splice variant of Ca_v3.1 channels do not display VDF. However, it remains to be determined whether novel alternative splice variants of cardiac Ca_v3.1 may display VDF. The fact that I observed VDF of I_{CaT} in NRVM and recombinant Ca_v3.2(-25) but not in recombinant Ca_v3.1 affirms my hypothesis that NRVM I_{CaT} display VDF and attributed to the exclusion of exon 25.

4.3.2 Potential limitations

This thesis has proven that alternative splicing in Ca_v3.2 T-type channels confers distinct biophysical properties. This research is the first to demonstrate that the Ca_v3.2 channels display VDF property, dependent on the inclusion or exclusion of exon 25 in the Ca_v3.2 channel. Analysis of the Ca_v3.2 VDF was first undertaken in HEK 293 cells and subsequently determined in dissociated NRVM in culture. In Chapter 2, this work presented compelling evidence of splice-variant specific Ca_v3.2 VDF in HEK 293 cells. Eleven splice variants were cloned and biophysically characterized. Eight showed measurable Ca²⁺ currents. These eight splice variants are in combination with either plus or minus exon 25. This thesis demonstrated that only splice variants with minus exon 25 display VDF but not variants with plus exon 25. Based on significantly high levels of mRNA expression of Ca_v3.2(-25) in dissociated NRVM (Chapter 3), it is tempting to suggest that the VDF property of NRVM I_{CaT} is contributed to the expression of Ca_v3.2(-25) splice variant. Although this research demonstrated lack of Ca_v3.1 VDF, it would be ideal to record purely Ca_v3.2 I_{CaT} in NRVM. This is important to eliminate the contribution of Ca_v3.1 channel splice variants potentially displaying VDF. However, unpublished data in our laboratory (Garcia, E.G. personal communication) and reports from other groups (Chemin et al., 2001a; Chemin et al., 2002; Gomora et al., 2002; Latour et al., 2004) showed that Ca_v3.1 homologous exon 25 splice variants do not display VDF. Hence, it remains to be determined whether unidentified splice variants of Ca_v3.1 display VDF.

One potential limitation of this research is the analysis of splice-variant specific protein expression of Ca_v3.2 ± exon 25 variants. This is challenging as there is no available splice-variant specific antibody. It would be better if a target specific antibody could be made. This

would allow this research to study the protein expression and localization of specific splice variants not only in the ventricular myocytes but also in other regions of the heart.

In Chapter 2, I demonstrated an upregulation of the $Ca_v3.2$ channels in hypertrophic SHR. Although there is a preferential upregulation of $Ca_v3.2(+25)$ over $Ca_v3.2(-25)$ in hypertrophic SHR, it would be ideal to investigate whether I_{CaT} from dissociated ventricular myocytes from adult hypertrophic hearts display VDF. The fact that there is also a two-fold increase in $Ca_v3.2(-25)$ (Figure 2.10C) in hypertrophic SHR makes it a likely candidate to be tested-whether I_{CaT} from diseased ventricular myocytes display VDF.

A further potential limitation relates to the $G\beta_2\gamma_2$ -mediated inhibition of $Ca_v3.2(-25)$ VDF. The last part of Chapter 2 showed that co-transfection with $G\beta_2\gamma_2$ reduces the magnitude of facilitation of $Ca_v3.2(-25)$. The study did not show whether disrupting the binding of $G\beta_2\gamma_2$ to the $Ca_v3.2(-25)$ affects its VDF. In the future, it will be interesting to know whether disruption of the $G\beta\gamma$ binding sites via site-directed mutagenesis or deletion of the consensus binding sites in the $Ca_v3.2(-25)$ splice variant have an effect on VDF. In addition, it will be appealing to investigate whether buffering $G\beta\gamma$ via co-transfection of rod transducin ($G_{\alpha T}$) reverses $G\beta\gamma$ -mediated inhibition of VDF. $G_{\alpha T}$ has been reported to buffer $G\beta\gamma$ binding (Meza et al., 2007; Rangel et al., 2010). Thus, further studies are needed to explore the effects of $G\beta\gamma$ on the facilitation of $Ca_v3.2$.

4.4 Conclusion

4.4.1 General conclusions

Overall, this study has shown that cardiac $Ca_v3.2$ T-type channels are subjected to considerable splicing with the splice variants in the III – IV linker conferring for the presence or absence of exon 25 demonstrating the most notable molecular and biophysical profile. This work

also showed that there is a preferential expression of the Ca_v3.2(-25) splice variant in the newborn heart with a shift in the adult heart that results in equal levels of expression of both (+) and (-) exon 25 variants. This study also showed that in pathological cardiac hypertrophy the expression of Ca_v3.2 channels was upregulated with a shift towards the expression of Ca_v3.2(+25) as the predominant form. This thesis therefore concludes that changes in the pattern of expression of Ca_v3.2 III – IV linker exon 25 splice variants are associated with development and pathological cardiac hypertrophy.

Moreover, this thesis was the first to report VDF of Ca_v3.2 channels. This work showed that Ca_v3.2(-25) channel variant display robust VDF whereas lack of VDF was observed in Ca_v3.2(+25) channel variant. This current study also demonstrated that the VDF of I_{CaT} in neonatal rat ventricular myocytes was correlated with predominant expression of Ca_v3.2(-25) splice variant. Together, this thesis concludes that Ca_v3.2 alternative splicing confers splice variant-specific VDF.

In conclusion, this thesis showed that Ca_v3.2 alternative splicing generates significant T-type Ca²⁺ channel molecular and functional diversity with potential implications for cardiac development, physiology and pathophysiology.

4.4.2 Potential relevance of Ca_v3.2 alternative splicing in cardiac development and hypertrophy

The precise contribution of Ca_v3.2 T-type channels to the normal development and pathological hypertrophy of the mammalian hearts remains unresolved. This thesis showed for the first time that there are changes in splice variant patterns associated with ontogenic development and pathological hypertrophy. In one instance, the changes are associated with the expression of splice variants that mediate VDF. VDF of Ca_v3.2 channels would likely increase

intracellular Ca^{2+} thereby potentially contributing to the spontaneous contractility and conduction of APs of the newborn ventricle (Figure 3.5).

In hypertrophic hearts, the predominant splice variant was shifted to $\text{Ca}_v3.2(+25)$ although $\text{Ca}_v3.2(-25)$ was also upregulated. The upregulation of expression of $\text{Ca}_v3.2$ channels in cardiac hypertrophy could potentially contribute to an electrical remodelling in the hypertrophic ventricle. Importantly, the preferential expression of $\text{Ca}_v3.2(+25)$ could play a big role in cardiac remodelling. A higher level expression of this variant combined with its hyperpolarized activation range and higher current density, could predispose the heart to a proarrhythmogenic condition, contractile dysfunction and eventually heart failure. Interestingly, similar predominant expression of specific alternative splice variants was also observed in the $\text{Ca}_v1.2$ Ca^{2+} channels in patients with atherosclerosis (Tiwari et al., 2006).

Taken together, alternative splicing of $\text{Ca}_v3.2$ T-type channels could potentially play important roles in normal cardiac development and remodelling. The results from this study have proven that there is a differential expression of $\text{Ca}_v3.2$ alternative splice variants in the diseased heart. This may be important for the development of target specific drugs with the exclusive intention to act on a specific splice variant. This approach is essential for better managing of disease as well as minimizing potentially adverse side effects.

4.4.3 Future directions

An important future direction of this research would be to explore a more extensive developmental profiling of $\text{Ca}_v3.2$ alternative splice variants. Suggested experiments would include analysis of the splice variant profile in embryonic, fetal (before birth) and juvenile rats. Similar experimental procedures outlined in Chapter 2 would be necessary to determine the splice variant profile present in full length cDNA libraries. In order to increase the chances of

recovering rare splice variants, high through-put DNA sequencing is recommended. However, this approach would not give information on splice variant combinations present in the Ca_v3.2 full length transcripts. Thus, it is suggested that both high through-put DNA sequencing and full length splice variant screening should be undertaken to obtain a more detailed profile of the differential pattern of expression of Ca_v3.2 alternative splice variants during development.

With regard to pathological cardiac hypertrophy, suggested future experiments should include analysis on pre-hypertensive, hypertensive, pre-heart failure and heart failure disease states. The SHR model should be used in this experiment since this model was proven to have age-specific progression of the disease phenotype (Doggrell and Brown, 1998; Chen-Izu et al., 2007; Tang et al., 2008). As recommended above, high through-put DNA sequencing and full length screening would be interesting to explore differential patterns of alternative splicing in various pathological stages. Relevant to the signalling mechanisms involved in splice variant-specific developmental and pathological regulation of expression in cardiac Ca_v3.2 channels, an important future research would be to explore this thesis's proposed hypotheses on variant-specific regulation (Figure 4.1). To investigate this, quantitative RT-PCR analysis of the levels of expression of Ca_v3.2 (\pm) exon 25 variants, fox proteins, NRSF and HDAC is necessary in various stages of development and in disease states. In addition, measurement of the activities of the transcriptional regulators, HDAC and fox proteins, and other signalling molecules upstream and downstream of these regulators (Molkentin and Dorn, 2001; Dorn and Force, 2005; Heineke and Molkentin, 2006) would also be helpful to identify the regulation mechanism of cardiac Ca_v3.2 alternative splice variants.

An important future study will be to perform a biophysical characterization of I_{CaT} in adult hypertrophic SHR and compare with age- and sex matched normotensive WKY rats. Recording I_{CaT} from isolated adult ventricular myocytes would be important to determine the

electrophysiological characteristics of I_{CaT} in the hypertrophic heart. It would also be interesting to explore if VDF exists in hypertrophic myocytes as both $Ca_v3.2(-25)$ and $Ca_v3.2(+25)$ were found to both upregulated in hypertrophic SHR (Chapter 2). An additional potential future experiment is to explore the contributions of $Ca_v3.2$ exon 25 splice variant channels in pacemaker activity and contractility. Reports show that induction of $Ca_v3.2$ channels in cultured neonatal cardiomyocytes can lead to increased excitability (Levitsky and Lopez-Barneo, 2009) and accelerated spontaneous contractile activity in myocytes treated with corticosteroids (Lalevee et al., 2005; Maturana et al., 2009). Moreover, it was suggested that T-type channels play a role in E-C coupling in the newborn ventricle (Nuss and Marban, 1994; Wetzel and Klitzner, 1996; Haddock et al., 1999; Escobar et al., 2004; Tohse et al., 2004). Thus, it would be interesting to address whether $Ca_v3.2$ exon 25 splice variant channels play similar roles. Potential experiments include measurement of contractility, beating frequency and Ca^{2+} transients in $Ca_v3.2^{-/-}$ ventricular myocytes overexpressing exon 25 splice variants.

Relevant to G-protein mediated effects on VDF of $Ca_v3.2$ exon 25 variant channels, important future studies are to disrupt the binding site and/or to buffer $G\beta\gamma$ binding. These suggested future experiments could include site-directed mutagenesis to eliminate $G\beta\gamma$ binding consensus site or co-transfection of rod transducin ($G_{\alpha T}$) which is known to buffer $G\beta\gamma$ binding (Meza et al., 2007; Rangel et al., 2010).

REFERENCES

- Adams PJ, Garcia E, David LS, Mulatz KJ, Spacey SD, Snutch TP (2009) Ca_v2.1 P/Q-type calcium channel alternative splicing affects the functional impact of familial hemiplegic migraine mutations: implications for calcium channelopathies. *Channels (Austin)* 3:110-121.
- Adolph EF (1971) Ontogeny of heart-rate controls in hamster, rat, and guinea pig. *Am J Physiol* 220:1896-1902.
- Akaike N, Kostyuk PG, Osipchuk YV (1989) Dihydropyridine-sensitive low-threshold calcium channels in isolated rat hypothalamic neurones. *J Physiol* 412:181-195.
- Alvarez JL, Vassort G (1992) Properties of the low threshold Ca current in single frog atrial cardiomyocytes. A comparison with the high threshold Ca current. *J Gen Physiol* 100:519-545.
- Alvarez JL, Rubio LS, Vassort G (1996) Facilitation of T-type calcium current in bullfrog atrial cells: voltage-dependent relief of a G protein inhibitory tone. *J Physiol* 491 (Pt 2):321-334.
- Alvarez JL, Artiles A, Talavera K, Vassort G (2000) Modulation of voltage-dependent facilitation of the T-type Ca²⁺ current by sodium ion in isolated frog atrial cells. *Pflugers Arch* 441:39-48.
- Andreasen D, Jensen BL, Hansen PB, Kwon TH, Nielsen S, Skott O (2000) The alpha(1G)-subunit of a voltage-dependent Ca²⁺ channel is localized in rat distal nephron and collecting duct. *Am J Physiol Renal Physiol* 279:F997-1005.
- Arnoult C, Lemos JR, Florman HM (1997) Voltage-dependent modulation of T-type calcium channels by protein tyrosine phosphorylation. *Embo J* 16:1593-1599.
- Artalejo CR, Rossie S, Perlman RL, Fox AP (1992) Voltage-dependent phosphorylation may recruit Ca²⁺ current facilitation in chromaffin cells. *Nature* 358:63-66.
- Artman M, Henry G, Coetzee WA (2000) Cellular basis for age-related differences in cardiac excitation-contraction coupling. *Prog Pediatr Cardiol* 11:185-194.
- Ashcroft FM, Kelly RP, Smith PA (1990) Two types of Ca channel in rat pancreatic beta-cells. *Pflugers Arch* 415:504-506.
- Balke CW, Rose WC, Marban E, Wier WG (1992) Macroscopic and unitary properties of physiological ion flux through T-type Ca²⁺ channels in guinea-pig heart cells. *J Physiol* 456:247-265.
- Bartels P, Behnke K, Michels G, Groner F, Schneider T, Henry M, Barrett PQ, Kang HW, Lee JH, Wiesen MH, Matthes J, Herzig S (2009) Structural and biophysical determinants of single Ca_v3.1 and Ca_v3.2 T-type calcium channel inhibition by N₂O. *Cell Calcium* 46:293-302.
- Baumann L, Gerstner A, Zong X, Biel M, Wahl-Schott C (2004) Functional characterization of the L-type Ca²⁺ channel Cav1.4alpha1 from mouse retina. *Invest Ophthalmol Vis Sci* 45:708-713.
- Beam KG, Knudson CM (1988) Effect of postnatal development on calcium currents and slow charge movement in mammalian skeletal muscle. *J Gen Physiol* 91:799-815.
- Bean BP (1985) Two kinds of calcium channels in canine atrial cells. Differences in kinetics, selectivity, and pharmacology. *J Gen Physiol* 86:1-30.
- Bean BP (1989a) Classes of calcium channels in vertebrate cells. *Annu Rev Physiol* 51:367-384.

- Bean BP (1989b) Neurotransmitter inhibition of neuronal calcium currents by changes in channel voltage dependence. *Nature* 340:153-156.
- Beedle AM, Hamid J, Zamponi GW (2002) Inhibition of transiently expressed low- and high-voltage-activated calcium channels by trivalent metal cations. *J Membr Biol* 187:225-238.
- Bell TJ, Thaler C, Castiglioni AJ, Helton TD, Lipscombe D (2004) Cell-specific alternative splicing increases calcium channel current density in the pain pathway. *Neuron* 41:127-138.
- Benham CD, Tsien RW (1988) Noradrenaline modulation of calcium channels in single smooth muscle cells from rabbit ear artery. *J Physiol* 404:767-784.
- BenMohamed F, Ferron L, Ruchon Y, Gouadon E, Renaud JF, Capuano V (2009) Regulation of T-type Cav3.1 channels expression by synthetic glucocorticoid dexamethasone in neonatal cardiac myocytes. *Mol Cell Biochem* 320:173-183.
- Bers DM (2001) Excitation-contraction coupling and cardiac contractile force, 2nd Edition. Dordrecht, The Netherlands: Kluwer Academic Publishers.
- Bers DM (2002) Cardiac excitation-contraction coupling. *Nature* 415:198-205.
- Bers DM, Perez-Reyes E (1999) Ca channels in cardiac myocytes: structure and function in Ca influx and intracellular Ca release. *Cardiovasc Res* 42:339-360.
- Berthier C, Monteil A, Lory P, Strube C (2002) Alpha(1H) mRNA in single skeletal muscle fibres accounts for T-type calcium current transient expression during fetal development in mice. *J Physiol* 539:681-691.
- Bingham AJ, Ooi L, Kozera L, White E, Wood IC (2007) The repressor element 1-silencing transcription factor regulates heart-specific gene expression using multiple chromatin-modifying complexes. *Mol Cell Biol* 27:4082-4089.
- Bkaily G, Sculptoreanu A, Jacques D, Jasmin G (1997) Increases of T-type Ca²⁺ current in heart cells of the cardiomyopathic hamster. *Mol Cell Biochem* 176:199-204.
- Black DL (2003) Mechanisms of alternative pre-messenger RNA splicing. *Annu Rev Biochem* 72:291-336.
- Blaich A, Welling A, Fischer S, Wegener JW, Kostner K, Hofmann F, Moosmang S (2010) Facilitation of murine cardiac L-type Ca_v1.2 channel is modulated by calmodulin kinase II-dependent phosphorylation of S1512 and S1570. *Proc Natl Acad Sci U S A* 107:10285-10289.
- Blencowe BJ (2006) Alternative splicing: new insights from global analyses. *Cell* 126:37-47.
- Bohn G, Moosmang S, Conrad H, Ludwig A, Hofmann F, Klugbauer N (2000) Expression of T- and L-type calcium channel mRNA in murine sinoatrial node. *FEBS Lett* 481:73-76.
- Bonvallet R, Rougier O (1989) Existence of two calcium currents recorded at normal calcium concentrations in single frog atrial cells. *Cell Calcium* 10:499-508.
- Bourinet E, Soong TW, Stea A, Snutch TP (1996) Determinants of the G protein-dependent opioid modulation of neuronal calcium channels. *Proc Natl Acad Sci U S A* 93:1486-1491.
- Bourinet E, Charnet P, Tomlinson WJ, Stea A, Snutch TP, Nargeot J (1994) Voltage-dependent facilitation of a neuronal alpha 1C L-type calcium channel. *Embo J* 13:5032-5039.
- Boyett MR, Honjo H, Kodama I (2000) The sinoatrial node, a heterogeneous pacemaker structure. *Cardiovasc Res* 47:658-687.
- Breustedt J, Vogt KE, Miller RJ, Nicoll RA, Schmitz D (2003) Alpha1E-containing Ca²⁺ channels are involved in synaptic plasticity. *Proc Natl Acad Sci U S A* 100:12450-12455.
- Brody DL, Yue DT (2000) Relief of G-protein inhibition of calcium channels and short-term synaptic facilitation in cultured hippocampal neurons. *J Neurosci* 20:889-898.

- Calin-Jageman I, Yu K, Hall RA, Mei L, Lee A (2007) Erbin enhances voltage-dependent facilitation of $\text{Ca}_v1.3 \text{ Ca}^{2+}$ channels through relief of an autoinhibitory domain in the $\text{Ca}(v)1.3 \alpha 1$ subunit. *J Neurosci* 27:1374-1385.
- Camara AK, Begic Z, Kwok WM, Bosnjak ZJ (2001) Differential modulation of the cardiac L- and T-type calcium channel currents by isoflurane. *Anesthesiology* 95:515-524.
- Carbone E, Lux HD (1984) A low voltage-activated, fully inactivating Ca channel in vertebrate sensory neurones. *Nature* 310:501-502.
- Castiglioni AJ, Raingo J, Lipscombe D (2006) Alternative splicing in the C-terminus of $\text{CaV}2.2$ controls expression and gating of N-type calcium channels. *J Physiol* 576:119-134.
- Catterall WA (2000) Structure and regulation of voltage-gated Ca^{2+} channels. *Annu Rev Cell Dev Biol* 16:521-555.
- Catterall WA, Striessnig J, Snutch TP, Perez-Reyes E (2003) International Union of Pharmacology. XL. Compendium of voltage-gated ion channels: calcium channels. *Pharmacol Rev* 55:579-581.
- Cerutti C, Kurdi M, Bricca G, Hodroj W, Paultre C, Randon J, Gustin MP (2006) Transcriptional alterations in the left ventricle of three hypertensive rat models. *Physiol Genomics* 27:295-308.
- Chandy KG, Gutman GA (1993) Nomenclature for mammalian potassium channel genes. *Trends Pharmacol Sci* 14:434.
- Chang SY, Yong TF, Yu CY, Liang MC, Pletnikova O, Troncoso J, Burgunder JM, Soong TW (2007) Age and gender-dependent alternative splicing of P/Q-type calcium channel EF-hand. *Neurosci* 145:1026-1036.
- Chaudhuri D, Chang SY, DeMaria CD, Alvania RS, Soong TW, Yue DT (2004) Alternative splicing as a molecular switch for Ca^{2+} /calmodulin-dependent facilitation of P/Q-type Ca^{2+} channels. *J Neurosci* 24:6334-6342.
- Chemin J, Traboulsie A, Lory P (2006) Molecular pathways underlying the modulation of T-type calcium channels by neurotransmitters and hormones. *Cell Calcium* 40:121-134.
- Chemin J, Monteil A, Bourinet E, Nargeot J, Lory P (2001a) Alternatively spliced $\alpha(1G)$ ($\text{Ca}_v3.1$) intracellular loops promote specific T-type Ca^{2+} channel gating properties. *Biophys J* 80:1238-1250.
- Chemin J, Monteil A, Dubel S, Nargeot J, Lory P (2001b) The $\alpha 1I$ T-type calcium channel exhibits faster gating properties when overexpressed in neuroblastoma/glioma NG 108-15 cells. *Eur J Neurosci* 14:1678-1686.
- Chemin J, Monteil A, Perez-Reyes E, Bourinet E, Nargeot J, Lory P (2002) Specific contribution of human T-type calcium channel isoforms ($\alpha(1G)$, $\alpha(1H)$ and $\alpha(1I)$) to neuronal excitability. *J Physiol* 540:3-14.
- Chemin J, Monteil A, Briquaire C, Richard S, Perez-Reyes E, Nargeot J, Lory P (2000) Overexpression of T-type calcium channels in HEK-293 cells increases intracellular calcium without affecting cellular proliferation. *FEBS Lett* 478:166-172.
- Chemin J, Mezghrani A, Bidaud I, Dupasquier S, Marger F, Barrere C, Nargeot J, Lory P (2007) Temperature-dependent modulation of $\text{CaV}3$ T-type calcium channels by protein kinases C and A in mammalian cells. *J Biol Chem* 282:32710-32718.
- Chen-Izu Y, Chen L, Banyasz T, McCulle SL, Norton B, Scharf SM, Agarwal A, Patwardhan A, Izu LT, Balke CW (2007) Hypertension-induced remodeling of cardiac excitation-contraction coupling in ventricular myocytes occurs prior to hypertrophy development. *Am J Physiol Heart Circ Physiol* 293:H3301-H3310.
- Chen CC, Lamping KG, Nuno DW, Barresi R, Prouty SJ, Lavoie JL, Cribbs LL, England SK, Sigmund CD, Weiss RM, Williamson RA, Hill JA, Campbell KP (2003) Abnormal

- coronary function in mice deficient in $\alpha 1H$ T-type Ca^{2+} channels. *Science* 302:1416-1418.
- Chen X, Nakayama H, Zhang X, Ai X, Harris DM, Tang M, Zhang H, Szeto C, Stockbower K, Berretta RM, Eckhart AD, Koch WJ, Molkentin JD, Houser SR (2011) Calcium influx through $Ca_v1.2$ is a proximal signal for pathological cardiomyocyte hypertrophy. *J Mol Cell Cardiol* 50:460-470.
- Chen XL, Bayliss DA, Fern RJ, Barrett PQ (1999) A role for T-type Ca^{2+} channels in the synergistic control of aldosterone production by ANG II and K^+ . *Am J Physiol* 276:F674-F683.
- Chiang CS, Huang CH, Chieng H, Chang YT, Chang D, Chen JJ, Chen YC, Chen YH, Shin HS, Campbell KP, Chen CC (2009) The $Ca_v3.2$ T-type Ca^{2+} channel is required for pressure overload-induced cardiac hypertrophy in mice. *Circ Res* 104:522-530.
- Chuang RS, Jaffe H, Cribbs L, Perez-Reyes E, Swartz KJ (1998) Inhibition of T-type voltage-gated calcium channels by a new scorpion toxin. *Nat Neurosci* 1:668-674.
- Cohen NM, Lederer WJ (1988) Changes in the calcium current of rat heart ventricular myocytes during development. *J Physiol* 406:115-146.
- Colecraft HM, Patil PG, Yue DT (2000) Differential occurrence of reluctant openings in G-protein-inhibited N- and P/Q-type calcium channels. *J Gen Physiol* 115:175-192.
- Coulter DA, Huguenard JR, Prince DA (1990) Differential effects of petit mal anticonvulsants and convulsants on thalamic neurones: calcium current reduction. *Br J Pharmacol* 100:800-806.
- Cribbs L (2010) T-type calcium channel expression and function in the diseased heart. *Channels (Austin)* 4.
- Cribbs LL, Martin BL, Schroder EA, Keller BB, Delisle BP, Satin J (2001) Identification of the t-type calcium channel ($Ca_v3.1d$) in developing mouse heart. *Circ Res* 88:403-407.
- Cribbs LL, Lee JH, Yang J, Satin J, Zhang Y, Daud A, Barclay J, Williamson MP, Fox M, Rees M, Perez-Reyes E (1998) Cloning and characterization of $\alpha 1H$ from human heart, a member of the T-type Ca^{2+} channel gene family. *Circ Res* 83:103-109.
- Currie KP, Fox AP (2002) Differential facilitation of N- and P/Q-type calcium channels during trains of action potential-like waveforms. *J Physiol* 539:419-431.
- Curtis BM, Catterall WA (1984) Purification of the calcium antagonist receptor of the voltage-sensitive calcium channel from skeletal muscle transverse tubules. *Biochemistry* 23:2113-2118.
- David LS, Garcia E, Tyson JR, Thau EM, Cain SM, Snutch TP (2008) Identification and biophysical characterization of rat thalamic $Ca_v3.2$ T-type calcium channel alternatively spliced variants. In: *Society for Neuroscience Meeting*, p 32.33/D46. Washington Convention Center, Washington, D.C., USA.
- De Waard M, Witcher DR, Pragnell M, Liu H, Campbell KP (1995) Properties of the $\alpha 1$ - β anchoring site in voltage-dependent Ca^{2+} channels. *J Biol Chem* 270:12056-12064.
- De Waard M, Liu H, Walker D, Scott VE, Gurnett CA, Campbell KP (1997) Direct binding of G-protein betagamma complex to voltage-dependent calcium channels. *Nature* 385:446-450.
- Demir SS, Clark JW, Giles WR (1999) Parasympathetic modulation of sinoatrial node pacemaker activity in rabbit heart: a unifying model. *Am J Physiol* 276:H2221-H2244.
- DePuy SD, Yao J, Hu C, McIntire W, Bidaud I, Lory P, Rastinejad F, Gonzalez C, Garrison JC, Barrett PQ (2006) The molecular basis for T-type Ca^{2+} channel inhibition by G protein $\beta 2$ subunits. *Proc Natl Acad Sci U S A* 103:14590-14595.

- Diebold RJ, Koch WJ, Ellinor PT, Wang JJ, Muthuchamy M, Wiczorek DF, Schwartz A (1992) Mutually exclusive exon splicing of the cardiac calcium channel alpha 1 subunit gene generates developmentally regulated isoforms in the rat heart. *Proc Natl Acad Sci U S A* 89:1497-1501.
- Dietrich D, Kirschstein T, Kukley M, Pereverzev A, von der Brölie C, Schneider T, Beck H (2003) Functional specialization of presynaptic $\text{Ca}_v2.3$ Ca_{2+} channels. *Neuron* 39:483-496.
- Doering CJ, Zamponi GW (2003) Molecular pharmacology of high voltage-activated calcium channels. *J Bioenerg Biomembr* 35:491-505.
- Doggrell SA, Brown L (1998) Rat models of hypertension, cardiac hypertrophy and failure. *Cardiovasc Res* 39:89-105.
- Dolphin AC, Wyatt CN, Richards J, Beattie RE, Craig P, Lee JH, Cribbs LL, Volsen SG, Perez-Reyes E (1999) The effect of alpha2-delta and other accessory subunits on expression and properties of the calcium channel alpha1G. *J Physiol* 519 Pt 1:35-45.
- Dorn GW, 2nd, Force T (2005) Protein kinase cascades in the regulation of cardiac hypertrophy. *J Clin Invest* 115:527-537.
- Drolet P, Bilodeau L, Chorvatova A, Laflamme L, Gallo-Payet N, Payet MD (1997) Inhibition of the T-type Ca^{2+} current by the dopamine D1 receptor in rat adrenal glomerulosa cells: requirement of the combined action of the G betagamma protein subunit and cyclic adenosine 3',5'-monophosphate. *Mol Endocrinol* 11:503-514.
- Droogmans G, Nilius B (1989) Kinetic properties of the cardiac T-type calcium channel in the guinea-pig. *J Physiol* 419:627-650.
- Dubel SJ, Altier C, Chaumont S, Lory P, Bourinet E, Nargeot J (2004) Plasma membrane expression of T-type calcium channel alpha(1) subunits is modulated by high voltage-activated auxiliary subunits. *J Biol Chem* 279:29263-29269.
- Eder P, Molkenin JD (2011) TRPC channels as effectors of cardiac hypertrophy. *Circ Res* 108:265-272.
- Edgerton GB, Blumenthal KM, Hanck DA (2010) Inhibition of the activation pathway of the T-type calcium channel $\text{Ca}_v3.1$ by ProTxII. *Toxicon* 56:624-636.
- Efimov IR, Nikolski VP, Rothenberg F, Greener ID, Li J, Dobrzynski H, Boyett M (2004) Structure-function relationship in the AV junction. *Anat Rec A Discov Mol Cell Evol Biol* 280:952-965.
- Elmslie KS, Zhou W, Jones SW (1990) LHRH and GTP-gamma-S modify calcium current activation in bullfrog sympathetic neurons. *Neuron* 5:75-80.
- Emerick MC, Stein R, Kunze R, McNulty MM, Regan MR, Hanck DA, Agnew WS (2006) Profiling the array of $\text{Ca}_v3.1$ variants from the human T-type calcium channel gene *CACNA1G*: alternative structures, developmental expression, and biophysical variations. *Proteins* 64:320-342.
- Enyeart JJ, Mlinar B, Enyeart JA (1993) T-type Ca^{2+} channels are required for adrenocorticotropin-stimulated cortisol production by bovine adrenal zona fasciculata cells. *Mol Endocrinol* 7:1031-1040.
- Enyeart JJ, Biagi BA, Day RN, Sheu SS, Maurer RA (1990a) Blockade of low and high threshold Ca^{2+} channels by diphenylbutylpiperidine antipsychotics linked to inhibition of prolactin gene expression. *J Biol Chem* 265:16373-16379.
- Enyeart JJ, Dirksen RT, Sharma VK, Williford DJ, Sheu SS (1990b) Antipsychotic pimozide is a potent Ca^{2+} channel blocker in heart. *Mol Pharmacol* 37:752-757.

- Ertel EA, Campbell KP, Harpold MM, Hofmann F, Mori Y, Perez-Reyes E, Schwartz A, Snutch TP, Tanabe T, Birnbaumer L, Tsien RW, Catterall WA (2000) Nomenclature of voltage-gated calcium channels. *Neuron* 25:533-535.
- Escobar AL, Ribeiro-Costa R, Villalba-Galea C, Zoghbi ME, Perez CG, Mejia-Alvarez R (2004) Developmental changes of intracellular Ca²⁺ transients in beating rat hearts. *Am J Physiol Heart Circ Physiol* 286:H971-978.
- Fedida D, Noble D, Spindler AJ (1988a) Use-dependent reduction and facilitation of Ca²⁺ current in guinea-pig myocytes. *J Physiol* 405:439-460.
- Fedida D, Noble D, Spindler AJ (1988b) Mechanism of the use dependence of Ca²⁺ current in guinea-pig myocytes. *J Physiol* 405:461-475.
- Ferron L, Capuano V, Deroubaix E, Coulombe A, Renaud JF (2002) Functional and molecular characterization of a T-type Ca²⁺ channel during fetal and postnatal rat heart development. *J Mol Cell Cardiol* 34:533-546.
- Ferron L, Capuano V, Ruchon Y, Deroubaix E, Coulombe A, Renaud JF (2003) Angiotensin II signaling pathways mediate expression of cardiac T-type calcium channels. *Circ Res* 93:1241-1248.
- Fleckenstein A (1983) History of calcium antagonists. *Circ Res* 52:I3-16.
- Fox AP, Nowycky MC, Tsien RW (1987) Kinetic and pharmacological properties distinguishing three types of calcium currents in chick sensory neurones. *J Physiol* 394:149-172.
- Furukawa T, Miura R, Honda M, Kamiya N, Mori Y, Takeshita S, Isshiki T, Nukada T (2004) Identification of R(-)-isomer of efonidipine as a selective blocker of T-type Ca²⁺ channels. *Br J Pharmacol* 143:1050-1057.
- Furukawa T, Ito H, Nitta J, Tsujino M, Adachi S, Hiroe M, Marumo F, Sawanobori T, Hiraoka M (1992) Endothelin-1 enhances calcium entry through T-type calcium channels in cultured neonatal rat ventricular myocytes. *Circ Res* 71:1242-1253.
- Ganitkevich V, Isenberg G (1991) Stimulation-induced potentiation of T-type Ca²⁺ channel currents in myocytes from guinea-pig coronary artery. *J Physiol* 443:703-725.
- Garcia-Blanco MA, Baraniak AP, Lasda EL (2004) Alternative splicing in disease and therapy. *Nat Biotechnol* 22:535-546.
- Gaughan JP, Hefner CA, Houser SR (1998) Electrophysiological properties of neonatal rat ventricular myocytes with alpha1-adrenergic-induced hypertrophy. *Am J Physiol* 275:H577-590.
- Gidh-Jain M, Huang B, Jain P, Battula V, el-Sherif N (1995) Reemergence of the fetal pattern of L-type calcium channel gene expression in non infarcted myocardium during left ventricular remodeling. *Biochem Biophys Res Commun* 216:892-897.
- Gomora JC, Daud AN, Weiergraber M, Perez-Reyes E (2001) Block of cloned human T-type calcium channels by succinimide antiepileptic drugs. *Mol Pharmacol* 60:1121-1132.
- Gomora JC, Murbartian J, Arias JM, Lee JH, Perez-Reyes E (2002) Cloning and expression of the human T-type channel Ca_v3.3: insights into prepulse facilitation. *Biophys J* 83:229-241.
- Gonoi T, Hasegawa S (1988) Post-natal disappearance of transient calcium channels in mouse skeletal muscle: effects of denervation and culture. *J Physiol* 401:617-637.
- Grabowski PJ, Black DL (2001) Alternative RNA splicing in the nervous system. *Progress in Neurobiology* 65:289-308.
- Grabsch H, Pereverzev A, Weiergraber M, Schramm M, Henry M, Vajna R, Beattie RE, Volsen SG, Klockner U, Hescheler J, Schneider T (1999) Immunohistochemical detection of alpha1E voltage-gated Ca²⁺ channel isoforms in cerebellum, INS-1 cells, and neuroendocrine cells of the digestive system. *J Histochem Cytochem* 47:981-994.

- Gray AC, Raingo J, Lipscombe D (2007) Neuronal calcium channels: splicing for optimal performance. *Cell Calcium* 42:409-417.
- Gustafsson F, Andreasen D, Salomonsson M, Jensen BL, Holstein-Rathlou N (2001) Conducted vasoconstriction in rat mesenteric arterioles: role for dihydropyridine-insensitive Ca^{2+} channels. *Am J Physiol Heart Circ Physiol* 280:H582-H590.
- Habermann CJ, O'Brien BJ, Wassle H, Protti DA (2003) AII amacrine cells express L-type calcium channels at their output synapses. *J Neurosci* 23:6904-6913.
- Haddock PS, Coetzee WA, Cho E, Porter L, Katoh H, Bers DM, Jafri MS, Artman M (1999) Subcellular $[Ca^{2+}]_i$ Gradients During Excitation-Contraction Coupling in Newborn Rabbit Ventricular Myocytes. *Circ Res* 85:415-427.
- Hagiwara N, Irisawa H, Kameyama M (1988) Contribution of two types of calcium currents to the pacemaker potentials of rabbit sino-atrial node cells. *J Physiol* 395:233-253.
- Hannenhalli S, Putt ME, Gilmore JM, Wang J, Parmacek MS, Epstein JA, Morrissey EE, Margulies KB, Cappola TP (2006) Transcriptional genomics associates FOX transcription factors with human heart failure. *Circulation* 114:1269-1276.
- Hansen PB, Jensen BL, Andreasen D, Skott O (2001) Differential expression of T- and L-type voltage-dependent calcium channels in renal resistance vessels. *Circ Res* 89:630-638.
- Hatano S, Yamashita T, Sekiguchi A, Iwasaki Y, Nakazawa K, Sagara K, Iinuma H, Aizawa T, Fu LT (2006) Molecular and electrophysiological differences in the L-type Ca^{2+} channel of the atrium and ventricle of rat hearts. *Circ J* 70:610-614.
- Heineke J, Molkentin JD (2006) Regulation of cardiac hypertrophy by intracellular signalling pathways. *Nat Rev Mol Cell Biol* 7:589-600.
- Hell JW, Westenbroek RE, Warner C, Ahljanian MK, Prystay W, Gilbert MM, Snutch TP, Catterall WA (1993) Identification and differential subcellular localization of the neuronal class C and class D L-type calcium channel alpha 1 subunits. *J Cell Biol* 123:949-962.
- Herlitze S, Hockerman GH, Scheuer T, Catterall WA (1997) Molecular determinants of inactivation and G protein modulation in the intracellular loop connecting domains I and II of the calcium channel alpha1A subunit. *Proc Natl Acad Sci U S A* 94:1512-1516.
- Herlitze S, Garcia DE, Mackie K, Hille B, Scheuer T, Catterall WA (1996) Modulation of Ca^{2+} channels by G-protein beta gamma subunits. *Nature* 380:258-262.
- Heron SE, Phillips HA, Mulley JC, Mazarib A, Neufeld MY, Berkovic SF, Scheffer IE (2004) Genetic variation of *CACNA1H* in idiopathic generalized epilepsy. *Ann Neurol* 55:595-596.
- Hildebrand ME, David LS, Hamid J, Mulatz K, Garcia E, Zamponi GW, Snutch TP (2007) Selective inhibition of $Ca_v3.3$ T-type calcium channels by Galphaq/11-coupled muscarinic acetylcholine receptors. *J Biol Chem* 282:21043-21055.
- Hille B (2001) *Ion Channels of Excitable Membranes*, 3rd Edition. Sunderland, MA, U.S.A.: Sinauer Associates, Inc.
- Hirano Y, Fozzard HA, January CT (1989) Characteristics of L- and T-type Ca^{2+} currents in canine cardiac Purkinje cells. *Am J Physiol* 256:H1478-1492.
- Hirst GD, Silverberg GD, van Helden DF (1986) The action potential and underlying ionic currents in proximal rat middle cerebral arterioles. *J Physiol* 371:289-304.
- Hockerman GH, Peterson BZ, Johnson BD, Catterall WA (1997) Molecular determinants of drug binding and action on L-type calcium channels. *Annu Rev Pharmacol Toxicol* 37:361-396.
- Hosey MM, Barhanin J, Schmid A, Vandaele S, Ptasienski J, O'Callahan C, Cooper C, Lazdunski M (1987) Photoaffinity labelling and phosphorylation of a 165 kilodalton

- peptide associated with dihydropyridine and phenylalkylamine-sensitive calcium channels. *Biochem Biophys Res Commun* 147:1137-1145.
- Houser SR, Molkenin JD (2008) Does contractile Ca²⁺ control calcineurin-NFAT signaling and pathological hypertrophy in cardiac myocytes? *Sci Signal* 1:pe31.
- Hu C, Depuy SD, Yao J, McIntire WE, Barrett PQ (2009) Protein kinase A activity controls the regulation of T-type CaV3.2 channels by Gbetagamma dimers. *J Biol Chem* 284:7465-7473.
- Huang B, Qin D, Deng L, Boutjdir M, N E-S (2000) Reexpression of T-type Ca²⁺ channel gene and current in post-infarction remodeled rat left ventricle. *Cardiovasc Res* 46:442-449.
- Huguenard JR (1996) Low-threshold calcium currents in central nervous system neurons. *Annu Rev Physiol* 58:329-348.
- Huguenard JR (1999) Neuronal circuitry of thalamocortical epilepsy and mechanisms of antiabsence drug action. *Adv Neurol* 79:991-999.
- Huser J, Blatter LA, Lipsius SL (2000) Intracellular Ca²⁺ release contributes to automaticity in cat atrial pacemaker cells. *J Physiol* 524 Pt 2:415-422.
- Iftinca M, Hamid J, Chen L, Varela D, Tadayonnejad R, Altier C, Turner RW, Zamponi GW (2007) Regulation of T-type calcium channels by Rho-associated kinase. *Nat Neurosci* 10:854-860.
- Iftinca MC, Zamponi GW (2009) Regulation of neuronal T-type calcium channels. *Trends Pharmacol Sci* 30:32-40.
- Ihara Y, Yamada Y, Fujii Y, Gono T, Yano H, Yasuda K, Inagaki N, Seino Y, Seino S (1995) Molecular diversity and functional characterization of voltage-dependent calcium channels (*CACN4*) expressed in pancreatic beta-cells. *Mol Endocrinol* 9:121-130.
- Ikeda SR (1991) Double-pulse calcium channel current facilitation in adult rat sympathetic neurones. *J Physiol* 439:181-214.
- Ikeda SR (1996) Voltage-dependent modulation of N-type calcium channels by G-protein beta gamma subunits. *Nature* 380:255-258.
- Izumi T, Kihara Y, Sarai N, Yoneda T, Iwanaga Y, Inagaki K, Onozawa Y, Takenaka H, Kita T, Noma A (2003) Reinduction of T-type calcium channels by endothelin-1 in failing hearts in vivo and in adult rat ventricular myocytes in vitro. *Circulation* 108:2530-2535.
- Jagannathan S, Punt EL, Gu Y, Arnoult C, Sakkas D, Barratt CL, Publicover SJ (2002) Identification and localization of T-type voltage-operated calcium channel subunits in human male germ cells. Expression of multiple isoforms. *J Biol Chem* 277:8449-8456.
- Jaggar JH, Wellman GC, Heppner TJ, Porter VA, Perez GJ, Gollasch M, Kleppisch T, Rubart M, Stevenson AS, Lederer WJ, Knot HJ, Bonev AD, Nelson MT (1998) Ca²⁺ channels, ryanodine receptors and Ca²⁺-activated K⁺ channels: a functional unit for regulating arterial tone. *Acta Physiol Scand* 164:577-587.
- Jaleel N, Nakayama H, Chen X, Kubo H, MacDonnell S, Zhang H, Berretta R, Robbins J, Cribbs L, Molkenin JD, Houser SR (2008) Ca²⁺ Influx Through T- and L-Type Ca²⁺ Channels Have Different Effects on Myocyte Contractility and Induce Unique Cardiac Phenotypes. *Circ Res* 103:1109-1119.
- January CT, Riddle JM (1989) Early afterdepolarizations: mechanism of induction and block. A role for L-type Ca²⁺ current. *Circ Res* 64:977-990.
- Jay SD, Ellis SB, McCue AF, Williams ME, Vedvick TS, Harpold MM, Campbell KP (1990) Primary structure of the gamma subunit of the DHP-sensitive calcium channel from skeletal muscle. *Science* 248:490-492.

- Jimenez C, Bourinet E, Leuranguer V, Richard S, Snutch TP, Nargeot J (2000) Determinants of voltage-dependent inactivation affect Mibefradil block of calcium channels. *Neuropharmacology* 39:1-10.
- Jing X, Li DQ, Olofsson CS, Salehi A, Surve VV, Caballero J, Ivarsson R, Lundquist I, Pereverzev A, Schneider T, Rorsman P, Renstrom E (2005) $\text{Ca}_v2.3$ calcium channels control second-phase insulin release. *J Clin Invest* 115:146-154.
- Joksovic PM, Nelson MT, Jevtovic-Todorovic V, Patel MK, Perez-Reyes E, Campbell KP, Chen CC, Todorovic SM (2006) $\text{Ca}_v3.2$ is the major molecular substrate for redox regulation of T-type Ca^{2+} channels in the rat and mouse thalamus. *J Physiol* 574:415-430.
- Kaku T, Lee TS, Arita M, Hadama T, Ono K (2003) The gating and conductance properties of $\text{Ca}_v3.2$ low-voltage-activated T-type calcium channels. *Jpn J Physiol* 53:165-172.
- Kalsotra A, Xiao X, Ward AJ, Castle JC, Johnson JM, Burge CB, Cooper TA (2008) A postnatal switch of CELF and MBNL proteins reprograms alternative splicing in the developing heart. *Proc Natl Acad Sci U S A* 105:20333-20338.
- Kamp TJ, Hu H, Marban E (2000) Voltage-dependent facilitation of cardiac L-type Ca^{2+} channels expressed in HEK-293 cells requires beta-subunit. *Am J Physiol Heart Circ Physiol* 278:H126-136.
- Kang HW, Vitko I, Lee SS, Perez-Reyes E, Lee JH (2010) Structural determinants of the high affinity extracellular zinc binding site on $\text{Ca}_v3.2$ T-type calcium channels. *J Biol Chem* 285:3271-3281.
- Kang HW, Park JY, Jeong SW, Kim JA, Moon HJ, Perez-Reyes E, Lee JH (2006) A molecular determinant of nickel inhibition in $\text{Ca}_v3.2$ T-type calcium channels. *J Biol Chem* 281:4823-4830.
- Kang M, Chung KY, Walker JW (2007) G-protein coupled receptor signaling in myocardium: not for the faint of heart. *Physiology (Bethesda)* 22:174-184.
- Kasai H, Aosaki T (1989) Modulation of Ca-channel current by an adenosine analog mediated by a GTP-binding protein in chick sensory neurons. *Pflugers Arch* 414:145-149.
- Kim D, Song I, Keum S, Lee T, Jeong MJ, Kim SS, McEnery MW, Shin HS (2001) Lack of the burst firing of thalamocortical relay neurons and resistance to absence seizures in mice lacking alpha(1G) T-type Ca^{2+} channels. *Neuron* 31:35-45.
- Kim JA, Park JY, Kang HW, Huh SU, Jeong SW, Lee JH (2006) Augmentation of $\text{Ca}_v3.2$ T-type calcium channel activity by cAMP-dependent protein kinase A. *J Pharmacol Exp Ther* 318:230-237.
- Kim MS, Morii T, Sun LX, Imoto K, Mori Y (1993) Structural determinants of ion selectivity in brain calcium channel. *FEBS Lett* 318:145-148.
- Kitchens SA, Burch J, Creazzo TL (2003) T-type Ca^{2+} current contribution to Ca^{2+} -induced Ca^{2+} release in developing myocardium. *J Mol Cell Cardiol* 35:515-523.
- Kito M, Maehara M, Watanabe K (1996) Mechanisms of T-type calcium channel blockade by zonisamide. *Seizure* 5:115-119.
- Klockner U, Lee JH, Cribbs LL, Daud A, Hescheler J, Pereverzev A, Perez-Reyes E, Schneider T (1999) Comparison of the Ca^{2+} currents induced by expression of three cloned alpha1 subunits, alpha1G, alpha1H and alpha1I, of low-voltage-activated T-type Ca^{2+} channels. *Eur J Neurosci* 11:4171-4178.
- Klugbauer N, Lacinova L, Marais E, Hobom M, Hofmann F (1999) Molecular diversity of the calcium channel alpha2delta subunit. *J Neurosci* 19:684-691.
- Koh SD, Monaghan K, Ro S, Mason HS, Kenyon JL, Sanders KM (2001) Novel voltage-dependent non-selective cation conductance in murine colonic myocytes. *J Physiol* 533:341-355.

- Kollmar R, Montgomery LG, Fak J, Henry LJ, Hudspeth AJ (1997) Predominance of the alpha1D subunit in L-type voltage-gated Ca²⁺ channels of hair cells in the chicken's cochlea. *Proc Natl Acad Sci U S A* 94:14883-14888.
- Kong SW, Hu YW, Ho JW, Ikeda S, Polster S, John R, Hall JL, Bisping E, Pieske B, dos Remedios CG, Pu WT (2010) Heart failure-associated changes in RNA splicing of sarcomere genes. *Circ Cardiovasc Genet* 3:138-146.
- Koschak A, Reimer D, Walter D, Hoda JC, Heinzle T, Grabner M, Striessnig J (2003) Cav1.4alpha1 subunits can form slowly inactivating dihydropyridine-sensitive L-type Ca²⁺ channels lacking Ca²⁺-dependent inactivation. *J Neurosci* 23:6041-6049.
- Kostyuk PG, Molokanova EA, Pronchuk NF, Savchenko AN, Verkhatsky AN (1992) Different action of ethosuximide on low- and high-threshold calcium currents in rat sensory neurons. *Neuroscience* 51:755-758.
- Koyama T, Ono K, Watanabe H, Ohba T, Murakami M, Iino K, Ito H (2009) Molecular and Electrical Remodeling of L- and T-Type Ca²⁺ Channels in Rat Right Atrium With Monocrotaline-Induced Pulmonary Hypertension. *Circulation Journal* 73:256-263.
- Kozlov AS, McKenna F, Lee JH, Cribbs LL, Perez-Reyes E, Feltz A, Lambert RC (1999) Distinct kinetics of cloned T-type Ca²⁺ channels lead to differential Ca²⁺ entry and frequency-dependence during mock action potentials. *Eur J Neurosci* 11:4149-4158.
- Kubota M, Murakoshi T, Saegusa H, Kazuno A, Zong S, Hu Q, Noda T, Tanabe T (2001) Intact LTP and fear memory but impaired spatial memory in mice lacking Ca_v2.3 (alpha(IE)) channel. *Biochem Biophys Res Commun* 282:242-248.
- Kuwahara K, Takano M, Nakao K (2005) Pathophysiological significance of T-type Ca²⁺ channels: transcriptional regulation of T-type Ca²⁺ channel--regulation of CACNA1H by neuron-restrictive silencer factor. *J Pharmacol Sci* 99:211-213.
- Kuwahara K, Saito Y, Ogawa E, Takahashi N, Nakagawa Y, Naruse Y, Harada M, Hamanaka I, Izumi T, Miyamoto Y, Kishimoto I, Kawakami R, Nakanishi M, Mori N, Nakao K (2001) The neuron-restrictive silencer element-neuron-restrictive silencer factor system regulates basal and endothelin 1-inducible atrial natriuretic peptide gene expression in ventricular myocytes. *Mol Cell Biol* 21:2085-2097.
- Kuwahara K et al. (2003) NRSF regulates the fetal cardiac gene program and maintains normal cardiac structure and function. *Embo J* 22:6310-6321.
- Lacinova L (2005) Voltage-dependent calcium channels. *Gen Physiol Biophys* 24 Suppl 1:1-78.
- Ladd AN, Stenberg MG, Swanson MS, Cooper TA (2005) Dynamic balance between activation and repression regulates pre-mRNA alternative splicing during heart development. *Dev Dyn* 233:783-793.
- Lalevee N, Rebsamen MC, Barrere-Lemaire S, Perrier E, Nargeot J, Benitah JP, Rossier MF (2005) Aldosterone increases T-type calcium channel expression and in vitro beating frequency in neonatal rat cardiomyocytes. *Cardiovasc Res* 67:216-224.
- Larsen JK, Mitchell JW, Best PM (2002) Quantitative analysis of the expression and distribution of calcium channel alpha 1 subunit mRNA in the atria and ventricles of the rat heart. *J Mol Cell Cardiol* 34:519-532.
- Larsen JK, Chen CC, Best PM (2005) Disruption of growth hormone secretion alters Ca²⁺ current density and expression of Ca²⁺ channel and insulin-like growth factor genes in rat atria. *Am J Physiol Heart Circ Physiol* 288:H829-H838.
- Latour I, Louw DF, Beedle AM, Hamid J, Sutherland GR, Zamponi GW (2004) Expression of T-type calcium channel splice variants in human glioma. *Glia* 48:112-119.

- Lee HK, Elmslie KS (2000) Reluctant gating of single N-type calcium channels during neurotransmitter-induced inhibition in bullfrog sympathetic neurons. *J Neurosci* 20:3115-3128.
- Lee JH, Gomora JC, Cribbs LL, Perez-Reyes E (1999a) Nickel block of three cloned T-type calcium channels: low concentrations selectively block α_1H . *Biophys J* 77:3034-3042.
- Lee JH, Daud AN, Cribbs LL, Lacerda AE, Pereverzev A, Klockner U, Schneider T, Perez-Reyes E (1999b) Cloning and expression of a novel member of the low voltage-activated T-type calcium channel family. *J Neurosci* 19:1912-1921.
- Lee JH, Kim EG, Park BG, Kim KH, Cha SK, Kong ID, Lee JW, Jeong SW (2002) Identification of T-type α_1H Ca^{2+} channels ($Ca_v3.2$) in major pelvic ganglion neurons. *J Neurophysiol* 87:2844-2850.
- Lee KS (1987) Potentiation of the calcium-channel currents of internally perfused mammalian heart cells by repetitive depolarization. *Proc Natl Acad Sci U S A* 84:3941-3945.
- Lejeune F, Maquat LE (2005) Mechanistic links between nonsense-mediated mRNA decay and pre-mRNA splicing in mammalian cells. *Curr Opin Cell Biol* 17:309-315.
- Leung AT, Imagawa T, Campbell KP (1987) Structural characterization of the 1,4-dihydropyridine receptor of the voltage-dependent Ca^{2+} channel from rabbit skeletal muscle. Evidence for two distinct high molecular weight subunits. *J Biol Chem* 262:7943-7946.
- Leuranguer V, Monteil A, Bourinet E, Dayanithi G, Nargeot J (2000) T-type calcium currents in rat cardiomyocytes during postnatal development: contribution to hormone secretion. *Am J Physiol Heart Circ Physiol* 279:H2540-2548.
- Levitsky KL, Lopez-Barneo J (2009) Developmental change of T-type Ca^{2+} channel expression and its role in rat chromaffin cell responsiveness to acute hypoxia. *J Physiol* 587:1917-1929.
- Liao P, Zhang H, Soong T (2009a) Alternative splicing of voltage-gated calcium channels: from molecular biology to disease. *Pflügers Archiv European Journal of Physiology* 458:481-487.
- Liao P, Yong TF, Liang MC, Yue DT, Soong TW (2005) Splicing for alternative structures of $Ca_v1.2$ Ca^{2+} channels in cardiac and smooth muscles. *Cardiovasc Res* 68:197-203.
- Liao P, Li G, Yu de J, Yong TF, Wang JJ, Wang J, Soong TW (2009b) Molecular alteration of $Ca_v1.2$ calcium channel in chronic myocardial infarction. *Pflugers Arch* 458:701-711.
- Liao P, Yu D, Lu S, Tang Z, Liang MC, Zeng S, Lin W, Soong TW (2004) Smooth muscle-selective alternatively spliced exon generates functional variation in $Ca_v1.2$ calcium channels. *J Biol Chem* 279:50329-50335.
- Lipscombe D, Raingo J (2007) Alternative splicing matters: N-type calcium channels in nociceptors. *Channels (Austin)* 1:225-227.
- Lipscombe D, Kongsamut S, Tsien RW (1989) Alpha-adrenergic inhibition of sympathetic neurotransmitter release mediated by modulation of N-type calcium-channel gating. *Nature* 340:639-642.
- Lipscombe D, Pan JQ, Gray AC (2002) Functional diversity in neuronal voltage-gated calcium channels by alternative splicing of $Ca(v)\alpha_1$. *Mol Neurobiol* 26:21-44.
- Liu G, Hilliard N, Hockerman GH (2004) $Ca_v1.3$ is preferentially coupled to glucose-induced $[Ca^{2+}]_i$ oscillations in the pancreatic beta cell line INS-1. *Mol Pharmacol* 65:1269-1277.
- Logothetis DE, Kurachi Y, Galper J, Neer EJ, Clapham DE (1987) The beta gamma subunits of GTP-binding proteins activate the muscarinic K^+ channel in heart. *Nature* 325:321-326.

- Lopez AJ (1998) Alternative splicing of pre-mRNA: developmental consequences and mechanisms of regulation. *Annu Rev Genet* 32:279-305.
- Lory P, Ophoff RA, Nahmias J (1997) Towards a unified nomenclature describing voltage-gated calcium channel genes. *Hum Genet* 100:149-150.
- Lory P, Bidaud I, Chemin J (2006) T-type calcium channels in differentiation and proliferation. *Cell Calcium* 40:135-146.
- Lu HK, Fern RJ, Nee JJ, Barrett PQ (1994) Ca(2+)-dependent activation of T-type Ca²⁺ channels by calmodulin-dependent protein kinase II. *Am J Physiol* 267:F183-189.
- Lu ZJ, Pereverzev A, Liu HL, Weiergraber M, Henry M, Krieger A, Smyth N, Hescheler J, Schneider T (2004) Arrhythmia in isolated prenatal hearts after ablation of the Ca_v2.3 (alpha1E) subunit of voltage-gated Ca²⁺ channels. *Cell Physiol Biochem* 14:11-22.
- Madle A, Linhartova K, Koza J (2001) Effects of the T-type calcium channel blockade with oral mibefradil on the electrophysiologic properties of the human heart. *Med Sci Monit* 7:74-77.
- Mangoni ME, Nargeot J (2008) Genesis and regulation of the heart automaticity. *Physiol Rev* 88:919-982.
- Mangoni ME, Couette B, Marger L, Bourinet E, Striessnig J, Nargeot J (2006a) Voltage-dependent calcium channels and cardiac pacemaker activity: from ionic currents to genes. *Prog Biophys Mol Biol* 90:38-63.
- Mangoni ME, Couette B, Bourinet E, Platzer J, Reimer D, Striessnig J, Nargeot J (2003) Functional role of L-type Ca_v1.3 Ca²⁺ channels in cardiac pacemaker activity. *Proc Natl Acad Sci U S A* 100:5543-5548.
- Mangoni ME, Traboulsie A, Leoni AL, Couette B, Marger L, Le Quang K, Kupfer E, Cohen-Solal A, Vilar J, Shin HS, Escande D, Charpentier F, Nargeot J, Lory P (2006b) Bradycardia and slowing of the atrioventricular conduction in mice lacking Ca_v3.1/alpha1G T-type calcium channels. *Circ Res* 98:1422-1430.
- Maniatis T, Tasic B (2002) Alternative pre-mRNA splicing and proteome expansion in metazoans. *Nature* 418:236-243.
- Marionneau C, Couette B, Liu J, Li H, Mangoni ME, Nargeot J, Lei M, Escande D, Demolombe S (2005) Specific pattern of ionic channel gene expression associated with pacemaker activity in the mouse heart. *J Physiol* 562:223-234.
- Marni F, Wang Y, Morishima M, Shimaoka T, Uchino T, Zheng M, Kaku T, Ono K (2009) 17 beta-estradiol modulates expression of low-voltage-activated Ca(V)3.2 T-type calcium channel via extracellularly regulated kinase pathway in cardiomyocytes. *Endocrinology* 150:879-888.
- Martin RL, Lee JH, Cribbs LL, Perez-Reyes E, Hanck DA (2000) Mibefradil block of cloned T-type calcium channels. *J Pharmacol Exp Ther* 295:302-308.
- Martinez ML, Heredia MP, Delgado C (1999) Expression of T-type Ca²⁺ channels in ventricular cells from hypertrophied rat hearts. *J Mol Cell Cardiol* 31:1617-1625.
- Masumiya H, Tanaka H, Shigenobu K (1997) Effects of Ca²⁺ channel antagonists on sinus node: prolongation of late phase 4 depolarization by efonidipine. *Eur J Pharmacol* 335:15-21.
- Masumiya H, Shijuku T, Tanaka H, Shigenobu K (1998) Inhibition of myocardial L- and T-type Ca²⁺ currents by efonidipine: possible mechanism for its chronotropic effect. *Eur J Pharmacol* 349:351-357.
- Maturana A, Lenglet S, Python M, Kuroda SI, Rossier MF (2009) Role of the T-Type Calcium Channel Ca_v3.2 in the Chronotropic Action of Corticosteroids in Isolated Rat Ventricular Myocytes. *Endocrinology* 150:3726-3734.

- McCleskey EW, Fox AP, Feldman DH, Cruz LJ, Olivera BM, Tsien RW, Yoshikami D (1987) Omega-conotoxin: direct and persistent blockade of specific types of calcium channels in neurons but not muscle. *Proc Natl Acad Sci U S A* 84:4327-4331.
- McDonald TF, Pelzer S, Trautwein W, Pelzer DJ (1994) Regulation and modulation of calcium channels in cardiac, skeletal, and smooth muscle cells. *Physiol Rev* 74:365-507.
- McGivern JG, McDonough SI (2004) Voltage-gated calcium channels as targets for the treatment of chronic pain. *Curr Drug Targets CNS Neurol Disord* 3:457-478.
- McRory JE, Santi CM, Hamming KS, Mezeyova J, Sutton KG, Baillie DL, Stea A, Snutch TP (2001) Molecular and functional characterization of a family of rat brain T-type calcium channels. *J Biol Chem* 276:3999-4011.
- McRory JE, Hamid J, Doering CJ, Garcia E, Parker R, Hamming K, Chen L, Hildebrand M, Beedle AM, Feldcamp L, Zamponi GW, Snutch TP (2004) The CACNA1F gene encodes an L-type calcium channel with unique biophysical properties and tissue distribution. *J Neurosci* 24:1707-1718.
- Meza U, Adams B (1998) G-Protein-dependent facilitation of neuronal alpha1A, alpha1B, and alpha1E Ca channels. *J Neurosci* 18:5240-5252.
- Meza U, Thapliyal A, Bannister RA, Adams BA (2007) Neurokinin 1 receptors trigger overlapping stimulation and inhibition of CaV2.3 (R-type) calcium channels. *Mol Pharmacol* 71:284-293.
- Mezghrani A, Monteil A, Watschinger K, Sinnegger-Brauns MJ, Barrere C, Bourinet E, Nargeot J, Striessnig J, Lory P (2008) A destructive interaction mechanism accounts for dominant-negative effects of misfolded mutants of voltage-gated calcium channels. *J Neurosci* 28:4501-4511.
- Michels G, Er F, Eicks M, Herzig S, Hoppe UC (2006) Long-term and immediate effect of testosterone on single T-type calcium channel in neonatal rat cardiomyocytes. *Endocrinology* 147:5160-5169.
- Miljanich GP, Ramachandran J (1995) Antagonists of neuronal calcium channels: structure, function, and therapeutic implications. *Annu Rev Pharmacol Toxicol* 35:707-734.
- Miller RJ (1992) Voltage-sensitive Ca²⁺ channels. *J Biol Chem* 267:1403-1406.
- Mishra SK, Hermsmeyer K (1994) Inhibition of signal Ca²⁺ in dog coronary arterial vascular muscle cells by Ro 40-5967. *J Cardiovasc Pharmacol* 24:1-7.
- Mittman S, Guo J, Agnew WS (1999a) Structure and alternative splicing of the gene encoding alpha1G, a human brain T calcium channel alpha1 subunit. *Neurosci Lett* 274:143-146.
- Mittman S, Guo J, Emerick MC, Agnew WS (1999b) Structure and alternative splicing of the gene encoding alpha1I, a human brain T calcium channel alpha1 subunit. *Neurosci Lett* 269:121-124.
- Mizuta E, Miake J, Yano S, Furuichi H, Manabe K, Sasaki N, Igawa O, Hoshikawa Y, Shigemasa C, Nanba E, Ninomiya H, Hidaka K, Morisaki T, Tajima F, Hisatome I (2005) Subtype switching of T-type Ca²⁺ channels from Ca_v3.2 to Ca_v3.1 during differentiation of embryonic stem cells to cardiac cell lineage. *Circ J* 69:1284-1289.
- Mlinar B, Biagi BA, Enyeart JJ (1993) Voltage-gated transient currents in bovine adrenal fasciculata cells. I. T-type Ca²⁺ current. *J Gen Physiol* 102:217-237.
- Modrek B, Lee C (2002) A genomic view of alternative splicing. *Nat Genet* 30:13-19.
- Molkentin JD, Dorn GW, 2nd (2001) Cytoplasmic signaling pathways that regulate cardiac hypertrophy. *Annu Rev Physiol* 63:391-426.
- Monteil A, Chemin J, Bourinet E, Mennessier G, Lory P, Nargeot J (2000a) Molecular and functional properties of the human alpha(1G) subunit that forms T-type calcium channels. *J Biol Chem* 275:6090-6100.

- Monteil A, Chemin J, Leuranguer V, Altier C, Mennessier G, Bourinet E, Lory P, Nargeot J (2000b) Specific properties of T-type calcium channels generated by the human alpha 1I subunit. *J Biol Chem* 275:16530-16535.
- Moorman AF, Christoffels VM (2003) Cardiac chamber formation: development, genes, and evolution. *Physiol Rev* 83:1223-1267.
- Morad M, Cleemann L (1987) Role of Ca²⁺ channel in development of tension in heart muscle. *J Mol Cell Cardiol* 19:527-553.
- Morgans CW (1999) Calcium channel heterogeneity among cone photoreceptors in the tree shrew retina. *Eur J Neurosci* 11:2989-2993.
- Mori Y, Friedrich T, Kim MS, Mikami A, Nakai J, Ruth P, Bosse E, Hofmann F, Flockerzi V, Furuichi T, et al. (1991) Primary structure and functional expression from complementary DNA of a brain calcium channel. *Nature* 350:398-402.
- Morishima M, Wang Y, Akiyoshi Y, Miyamoto S, Ono K (2009) Telmisartan, an angiotensin II type 1 receptor antagonist, attenuates T-type Ca²⁺ channel expression in neonatal rat cardiomyocytes. *Eur J Pharmacol* 609:105-112.
- Murbartian J, Arias JM, Perez-Reyes E (2004) Functional impact of alternative splicing of human T-type Ca_v3.3 calcium channels. *J Neurophysiol* 92:3399-3407.
- Murbartian J, Arias JM, Lee JH, Gomora JC, Perez-Reyes E (2002) Alternative splicing of the rat Ca_v3.3 T-type calcium channel gene produces variants with distinct functional properties(1). *FEBS Lett* 528:272-278.
- Nakagawa Y, Kuwahara K, Harada M, Takahashi N, Yasuno S, Adachi Y, Kawakami R, Nakanishi M, Tanimoto K, Usami S, Kinoshita H, Saito Y, Nakao K (2006) Class II HDACs mediate CaMK-dependent signaling to NRSF in ventricular myocytes. *J Mol Cell Cardiol* 41:1010-1022.
- Nakayama H, Bodi I, Correll RN, Chen X, Lorenz J, Houser SR, Robbins J, Schwartz A, Molkenin JD (2009) α 1G-dependent T-type Ca²⁺ current antagonizes cardiac hypertrophy through a NOS3-dependent mechanism in mice. *The Journal of Clinical Investigation* 119:3787-3796.
- Nelson MT, Woo J, Kang HW, Vitko I, Barrett PQ, Perez-Reyes E, Lee JH, Shin HS, Todorovic SM (2007a) Reducing agents sensitize C-type nociceptors by relieving high-affinity zinc inhibition of T-type calcium channels. *J Neurosci* 27:8250-8260.
- Nelson MT, Joksovic PM, Su P, Kang HW, Van Deusen A, Baumgart JP, David LS, Snutch TP, Barrett PQ, Lee JH, Zorumski CF, Perez-Reyes E, Todorovic SM (2007b) Molecular mechanisms of subtype-specific inhibition of neuronal T-type calcium channels by ascorbate. *J Neurosci* 27:12577-12583.
- Newcomb R, Szoke B, Palma A, Wang G, Chen X, Hopkins W, Cong R, Miller J, Urge L, Tarczy-Hornoch K, Loo JA, Dooley DJ, Nadasdi L, Tsien RW, Lemos J, Miljanich G (1998) Selective peptide antagonist of the class E calcium channel from the venom of the tarantula *Hysteroecrates gigas*. *Biochemistry* 37:15353-15362.
- Nilius B (1986) Possible functional significance of a novel type of cardiac Ca channel. *Biomed Biochim Acta* 45:K37-45.
- Niwa N, Yasui K, Opthof T, Takemura H, Shimizu A, Horiba M, Lee JK, Honjo H, Kamiya K, Kodama I (2004) Ca_v3.2 subunit underlies the functional T-type Ca²⁺ channel in murine hearts during the embryonic period. *Am J Physiol Heart Circ Physiol* 286:H2257-H2263.
- Nuss HB, Houser SR (1993) T-type Ca²⁺ current is expressed in hypertrophied adult feline left ventricular myocytes. *Circ Res* 73:777-782.
- Nuss HB, Marban E (1994) Electrophysiological properties of neonatal mouse cardiac myocytes in primary culture. *J Physiol* 479 (Pt 2):265-279.

- Ohkubo T, Yamazaki J, Kitamura K (2010) Tarantula toxin ProTx-I differentiates between human T-type voltage-gated Ca²⁺ Channels Ca_v3.1 and Ca_v3.2. *J Pharmacol Sci* 112:452-458.
- Ohkubo T, Inoue Y, Kawarabayashi T, Kitamura K (2005) Identification and electrophysiological characteristics of isoforms of T-type calcium channel Ca_v3.2 expressed in pregnant human uterus. *Cell Physiol Biochem* 16:245-254.
- Okoshi MP, Yan X, Okoshi K, Nakayama M, Schuldt AJ, O'Connell TD, Simpson PC, Lorell BH (2004) Aldosterone directly stimulates cardiac myocyte hypertrophy. *J Card Fail* 10:511-518.
- Ono K, Iijima T (2005) Pathophysiological significance of T-type Ca²⁺ channels: properties and functional roles of T-type Ca²⁺ channels in cardiac pacemaking. *J Pharmacol Sci* 99:197-204.
- Ono K, Iijima T (2010) Cardiac T-type Ca²⁺ channels in the heart. *J Mol Cell Cardiol* 48:65-70.
- Opler LA, Feinberg SS (1991) The role of pimozide in clinical psychiatry: a review. *J Clin Psychiatry* 52:221-233.
- Parsey RV, Matteson DR (1993) Ascorbic acid modulation of calcium channels in pancreatic beta cells. *J Gen Physiol* 102:503-523.
- Patil PG, de Leon M, Reed RR, Dubel S, Snutch TP, Yue DT (1996) Elementary events underlying voltage-dependent G-protein inhibition of N-type calcium channels. *Biophys J* 71:2509-2521.
- Pereverzev A, Mikhna M, Vajna R, Gissel C, Henry M, Weiergraber M, Hescheler J, Smyth N, Schneider T (2002) Disturbances in glucose-tolerance, insulin-release, and stress-induced hyperglycemia upon disruption of the Ca_v2.3 (alpha 1E) subunit of voltage-gated Ca_v(2+) channels. *Mol Endocrinol* 16:884-895.
- Perez-Reyes E (2003) Molecular physiology of low-voltage-activated t-type calcium channels. *Physiol Rev* 83:117-161.
- Perez-Reyes E (2006) Molecular characterization of T-type calcium channels. *Cell Calcium* 40:89-96.
- Perez-Reyes E, Cribbs LL, Daud A, Lacerda AE, Barclay J, Williamson MP, Fox M, Rees M, Lee JH (1998) Molecular characterization of a neuronal low-voltage-activated T-type calcium channel. *Nature* 391:896-900.
- Pietrobon D, Hess P (1990) Novel mechanism of voltage-dependent gating in L-type calcium channels. *Nature* 346:651-655.
- Pluteanu F, Cribbs LL (2009) T-type calcium channels are regulated by hypoxia/reoxygenation in ventricular myocytes. *Am J Physiol Heart Circ Physiol* 297:H1304-H1313.
- Powell KL, Cain SM, Ng C, Sirdesai S, David LS, Kyi M, Garcia E, Tyson JR, Reid CA, Bahlo M, Foote SJ, Snutch TP, O'Brien TJ (2009) A Ca_v3.2 T-type calcium channel point mutation has splice-variant-specific effects on function and segregates with seizure expression in a polygenic rat model of absence epilepsy. *J Neurosci* 29:371-380.
- Pragnell M, De Waard M, Mori Y, Tanabe T, Snutch TP, Campbell KP (1994) Calcium channel beta-subunit binds to a conserved motif in the I-II cytoplasmic linker of the alpha 1-subunit. *Nature* 368:67-70.
- Protas L, Robinson RB (2000) Mibefradil, an I(Ca,T) blocker, effectively blocks I(Ca,L) in rabbit sinus node cells. *Eur J Pharmacol* 401:27-30.
- Publicover SJ, Preston MR, El Haj AJ (1995) Voltage-dependent potentiation of low-voltage-activated Ca²⁺ channel currents in cultured rat bone marrow cells. *J Physiol* 489 (Pt 3):649-661.

- Qu Y, Boutjdir M (2001) Gene expression of SERCA2a and L- and T-type Ca channels during human heart development. *Pediatr Res* 50:569-574.
- Quignard JF, Frapier JM, Harricane MC, Albat B, Nargeot J, Richard S (1997) Voltage-gated calcium channel currents in human coronary myocytes. Regulation by cyclic GMP and nitric oxide. *J Clin Invest* 99:185-193.
- Raino J, Castiglioni AJ, Lipscombe D (2007) Alternative splicing controls G protein-dependent inhibition of N-type calcium channels in nociceptors. *Nat Neurosci* 10:285-292.
- Randall A, Tsien RW (1995) Pharmacological dissection of multiple types of Ca²⁺ channel currents in rat cerebellar granule neurons. *The Journal of Neuroscience* 15:2995-3012.
- Randall AD, Tsien RW (1997) Contrasting biophysical and pharmacological properties of T-type and R-type calcium channels. *Neuropharmacology* 36:879-893.
- Rangel A, Sanchez-Armass S, Meza U (2010) Protein kinase C-mediated inhibition of recombinant T-type Cav3.2 channels by neurokinin 1 receptors. *Mol Pharmacol* 77:202-210.
- Regan MR, Emerick MC, Agnew WS (2000) Full-length single-gene cDNA libraries: applications in splice variant analysis. *Anal Biochem* 286:265-276.
- Reuter H, Porzig H, Kokubun S, Prod'hom B (1988) Calcium channels in the heart. Properties and modulation by dihydropyridine enantiomers. *Ann N Y Acad Sci* 522:16-24.
- Rios E, Brum G (1987) Involvement of dihydropyridine receptors in excitation-contraction coupling in skeletal muscle. *Nature* 325:717-720.
- Rosati B, Dun W, Hirose M, Boyden PA, McKinnon D (2007) Molecular basis of the T- and L-type Ca²⁺ currents in canine Purkinje fibres. *J Physiol* 579:465-471.
- Rossier MF, Python M, Maturana AD (2010) Contribution of mineralocorticoid and glucocorticoid receptors to the chronotropic and hypertrophic actions of aldosterone in neonatal rat ventricular myocytes. *Endocrinology* 151:2777-2787.
- Rossier MF, Lenglet S, Vetterli L, Python M, Maturana A (2008) Corticosteroids and redox potential modulate spontaneous contractions in isolated rat ventricular cardiomyocytes. *Hypertension* 52:721-728.
- Rossier MF, Lesouhaitier O, Perrier E, Bockhorn L, Chiappe A, Lalevee N (2003) Aldosterone regulation of T-type calcium channels. *J Steroid Biochem Mol Biol* 85:383-388.
- Ruth P, Rohrkasten A, Biel M, Bosse E, Regulla S, Meyer HE, Flockerzi V, Hofmann F (1989) Primary structure of the beta subunit of the DHP-sensitive calcium channel from skeletal muscle. *Science* 245:1115-1118.
- Saegusa H, Kurihara T, Zong S, Minowa O, Kazuno A, Han W, Matsuda Y, Yamanaka H, Osanai M, Noda T, Tanabe T (2000) Altered pain responses in mice lacking alpha 1E subunit of the voltage-dependent Ca²⁺ channel. *Proc Natl Acad Sci U S A* 97:6132-6137.
- Sala S, Matteson DR (1990) Single-channel recordings of two types of calcium channels in rat pancreatic beta-cells. *Biophys J* 58:567-571.
- Salazar NC, Chen J, Rockman HA (2007) Cardiac GPCRs: GPCR signaling in healthy and failing hearts. *Biochim Biophys Acta* 1768:1006-1018.
- Santi CM, Cayabyab FS, Sutton KG, McRory JE, Mezeyova J, Hamming KS, Parker D, Stea A, Snutch TP (2002) Differential inhibition of T-type calcium channels by neuroleptics. *J Neurosci* 22:396-403.
- Sato M, Ishikawa Y (2010) Accessory proteins for heterotrimeric G-protein: Implication in the cardiovascular system. *Pathophysiology* 17:89-99.
- Schrier AD, Wang H, Talley EM, Perez-Reyes E, Barrett PQ (2001) alpha1H T-type Ca²⁺ channel is the predominant subtype expressed in bovine and rat zona glomerulosa. *Am J Physiol Cell Physiol* 280:C265-272.

- Schultz Jel J, Glascock BJ, Witt SA, Nieman ML, Nattamai KJ, Liu LH, Lorenz JN, Shull GE, Kimball TR, Periasamy M (2004) Accelerated onset of heart failure in mice during pressure overload with chronically decreased SERCA2 calcium pump activity. *Am J Physiol Heart Circ Physiol* 286:H1146-H1153.
- Sculptoreanu A, Scheuer T, Catterall WA (1993a) Voltage-dependent potentiation of L-type Ca^{2+} channels due to phosphorylation by cAMP-dependent protein kinase. *Nature* 364:240-243.
- Sculptoreanu A, Figourov A, De Groat WC (1995) Voltage-dependent potentiation of neuronal L-type calcium channels due to state-dependent phosphorylation. *Am J Physiol* 269:C725-C732.
- Sculptoreanu A, Rotman E, Takahashi M, Scheuer T, Catterall WA (1993b) Voltage-dependent potentiation of the activity of cardiac L-type calcium channel alpha 1 subunits due to phosphorylation by cAMP-dependent protein kinase. *Proc Natl Acad Sci U S A* 90:10135-10139.
- Sen L, Smith TW (1994) T-type Ca^{2+} channels are abnormal in genetically determined cardiomyopathic hamster hearts. *Circ Res* 75:149-155.
- Serrano JR, Perez-Reyes E, Jones SW (1999) State-dependent inactivation of the alpha1G T-type calcium channel. *J Gen Physiol* 114:185-201.
- Shang LL, Pfahnl AE, Sanyal S, Jiao Z, Allen J, Banach K, Fahrenbach J, Weiss D, Taylor WR, Zafari AM, Dudley SC, Jr. (2007) Human heart failure is associated with abnormal C-terminal splicing variants in the cardiac sodium channel. *Circ Res* 101:1146-1154.
- Shorofsky SR, January CT (1992) L- and T-type Ca^{2+} channels in canine cardiac Purkinje cells. Single-channel demonstration of L-type Ca^{2+} window current. *Circ Res* 70:456-464.
- Sidach SS, Mintz IM (2002) Kurtoxin, a gating modifier of neuronal high- and low-threshold calcium channels. *J Neurosci* 22:2023-2034.
- Sipido KR, Carmeliet E, Van de Werf F (1998) T-type Ca^{2+} current as a trigger for Ca^{2+} release from the sarcoplasmic reticulum in guinea-pig ventricular myocytes. *J Physiol* 508 (Pt 2):439-451.
- Smith RD, Goldin AL (1996) Phosphorylation of brain sodium channels in the I--II linker modulates channel function in *Xenopus* oocytes. *J Neurosci* 16:1965-1974.
- Snutch TP, David LS (2006) T-type calcium channels: An emerging therapeutic target for the treatment of pain. *Drug Dev Res* 67:404-415.
- Snutch TP, Tomlinson WJ, Leonard JP, Gilbert MM (1991) Distinct calcium channels are generated by alternative splicing and are differentially expressed in the mammalian CNS. *Neuron* 7:45-57.
- Snutch TP, Peloquin J, Matthews E, McRory JE (2005) Molecular properties of voltage-gated calcium channels. In: *Voltage-gated calcium channels* (Zamponi GW, ed), pp 61-94. New York: Landes Bioscience.
- Soldatov NM, Bouron A, Reuter H (1995) Different voltage-dependent inhibition by dihydropyridines of human Ca^{2+} channel splice variants. *J Biol Chem* 270:10540-10543.
- Son WY, Han CT, Lee JH, Jung KY, Lee HM, Choo YK (2002) Developmental expression patterns of alpha1H T-type Ca^{2+} channels during spermatogenesis and organogenesis in mice. *Dev Growth Differ* 44:181-190.
- Soong TW, DeMaria CD, Alvania RS, Zweifel LS, Liang MC, Mittman S, Agnew WS, Yue DT (2002) Systematic identification of splice variants in human P/Q-type channel alpha1(2.1) subunits: implications for current density and Ca^{2+} -dependent inactivation. *J Neurosci* 22:10142-10152.

- Splawski I, Timothy KW, Decher N, Kumar P, Sachse FB, Beggs AH, Sanguinetti MC, Keating MT (2005) Severe arrhythmia disorder caused by cardiac L-type calcium channel mutations. *Proc Natl Acad Sci U S A* 102:8089-8096; discussion 8086-8088.
- Splawski I, Timothy KW, Sharpe LM, Decher N, Kumar P, Bloise R, Napolitano C, Schwartz PJ, Joseph RM, Condouris K, Tager-Flusberg H, Priori SG, Sanguinetti MC, Keating MT (2004) Ca(V)1.2 calcium channel dysfunction causes a multisystem disorder including arrhythmia and autism. *Cell* 119:19-31.
- Stamm S, Ben-Ari S, Rafalska I, Tang Y, Zhang Z, Toiber D, Thanaraj TA, Soreq H (2005) Function of alternative splicing. *Gene* 344:1-20.
- Starr TV, Prystay W, Snutch TP (1991) Primary structure of a calcium channel that is highly expressed in the rat cerebellum. *Proc Natl Acad Sci U S A* 88:5621-5625.
- Stetefeld J, Ruegg MA (2005) Structural and functional diversity generated by alternative mRNA splicing. *Trends Biochem Sci* 30:515-521.
- Striessnig J, Knaus HG, Grabner M, Moosburger K, Seitz W, Lietz H, Glossmann H (1987) Photoaffinity labelling of the phenylalkylamine receptor of the skeletal muscle transverse-tubule calcium channel. *FEBS Lett* 212:247-253.
- Suzuki S, Kawakami K, Nishimura S, Watanabe Y, Yagi K, Seino M, Miyamoto K (1992) Zonisamide blocks T-type calcium channel in cultured neurons of rat cerebral cortex. *Epilepsy Res* 12:21-27.
- Swayne LA, Bourinet E (2008) Voltage-gated calcium channels in chronic pain: emerging role of alternative splicing. *Pflugers Arch* 456:459-466.
- Takahashi M, Seagar MJ, Jones JF, Reber BF, Catterall WA (1987) Subunit structure of dihydropyridine-sensitive calcium channels from skeletal muscle. *Proc Natl Acad Sci U S A* 84:5478-5482.
- Takebayashi S, Li Y, Kaku T, Inagaki S, Hashimoto Y, Kimura K, Miyamoto S, Hadama T, Ono K (2006) Remodeling excitation-contraction coupling of hypertrophied ventricular myocytes is dependent on T-type calcium channels expression. *Biochem Biophys Res Commun* 345:766-773.
- Talavera K, Nilius B (2006) Biophysics and structure-function relationship of T-type Ca²⁺ channels. *Cell Calcium* 40:97-114.
- Talley EM, Cribbs LL, Lee JH, Daud A, Perez-Reyes E, Bayliss DA (1999) Differential distribution of three members of a gene family encoding low voltage-activated (T-type) calcium channels. *J Neurosci* 19:1895-1911.
- Tanabe T, Beam KG, Powell JA, Numa S (1988) Restoration of excitation-contraction coupling and slow calcium current in dysgenic muscle by dihydropyridine receptor complementary DNA. *Nature* 336:134-139.
- Tanabe T, Mikami A, Numa S, Beam KG (1990) Cardiac-type excitation-contraction coupling in dysgenic skeletal muscle injected with cardiac dihydropyridine receptor cDNA. *Nature* 344:451-453.
- Tanabe T, Takeshima H, Mikami A, Flockerzi V, Takahashi H, Kangawa K, Kojima M, Matsuo H, Hirose T, Numa S (1987) Primary structure of the receptor for calcium channel blockers from skeletal muscle. *Nature* 328:313-318.
- Tanaka H, Komikado C, Shimada H, Takeda K, Namekata I, Kawanishi T, Shigenobu K (2004) The R(-)-enantiomer of efonidipine blocks T-type but not L-type calcium current in guinea pig ventricular myocardium. *J Pharmacol Sci* 96:499-501.
- Tanaka H, Komikado C, Namekata I, Nakamura H, Suzuki M, Tsuneoka Y, Shigenobu K, Takahara A (2008) Species difference in the contribution of T-type calcium current to cardiac pacemaking as revealed by r(-)-efonidipine. *J Pharmacol Sci* 107:99-102.

- Tang ZZ, Hong X, Wang J, Soong TW (2007) Signature combinatorial splicing profiles of rat cardiac- and smooth-muscle Ca_v1.2 channels with distinct biophysical properties. *Cell Calcium* 41:417-428.
- Tang ZZ, Zheng S, Nikolic J, Black DL (2009) Developmental control of Ca_v1.2 L-type calcium channel splicing by Fox proteins. *Mol Cell Biol* 29:4757-4765.
- Tang ZZ, Liang MC, Lu S, Yu D, Yu CY, Yue DT, Soong TW (2004) Transcript scanning reveals novel and extensive splice variations in human l-type voltage-gated calcium channel, Ca_v1.2 alpha1 subunit. *J Biol Chem* 279:44335-44343.
- Tang ZZ, Liao P, Li G, Jiang FL, Yu D, Hong X, Yong TF, Tan G, Lu S, Wang J, Soong TW (2008) Differential splicing patterns of L-type calcium channel Cav1.2 subunit in hearts of Spontaneously Hypertensive Rats and Wistar Kyoto Rats. *Biochim Biophys Acta* 1783:118-130.
- Tao J, Hildebrand ME, Liao P, Liang MC, Tan G, Li S, Snutch TP, Soong TW (2008) Activation of corticotropin-releasing factor receptor 1 selectively inhibits Ca_v3.2 T-type calcium channels. *Mol Pharmacol* 73:1596-1609.
- Thaler C, Gray AC, Lipscombe D (2004) Cumulative inactivation of N-type Ca_v2.2 calcium channels modified by alternative splicing. *Proc Natl Acad Sci U S A* 101:5675-5679.
- Thibault G, Amiri F, Garcia R (1999) Regulation of natriuretic peptide secretion by the heart. *Annu Rev Physiol* 61:193-217.
- Tiwari S, Zhang Y, Heller J, Abernethy DR, Soldatov NM (2006) Atherosclerosis-related molecular alteration of the human Ca_v1.2 calcium channel alpha1C subunit. *Proc Natl Acad Sci U S A* 103:17024-17029.
- Todorovic SM, Lingle CJ (1998) Pharmacological properties of T-type Ca²⁺ current in adult rat sensory neurons: effects of anticonvulsant and anesthetic agents. *J Neurophysiol* 79:240-252.
- Todorovic SM, Perez-Reyes E, Lingle CJ (2000) Anticonvulsants but not general anesthetics have differential blocking effects on different T-type current variants. *Mol Pharmacol* 58:98-108.
- Todorovic SM, Jevtovic-Todorovic V, Mennerick S, Perez-Reyes E, Zorumski CF (2001a) Ca(v)3.2 channel is a molecular substrate for inhibition of T-type calcium currents in rat sensory neurons by nitrous oxide. *Mol Pharmacol* 60:603-610.
- Todorovic SM, Jevtovic-Todorovic V, Meyenburg A, Mennerick S, Perez-Reyes E, Romano C, Olney JW, Zorumski CF (2001b) Redox modulation of T-type calcium channels in rat peripheral nociceptors. *Neuron* 31:75-85.
- Tohse N, Seki S, Kobayashi T, Tsutsuura M, Nagashima M, Yamada Y (2004) Development of excitation-contraction coupling in cardiomyocytes. *Jpn J Physiol* 54:1-6.
- Tseng GN, Boyden PA (1989) Multiple types of Ca²⁺ currents in single canine Purkinje cells. *Circ Res* 65:1735-1750.
- Tseng GN, Boyden PA (1991) Different effects of intracellular Ca and protein kinase C on cardiac T and L Ca currents. *Am J Physiol* 261:H364-379.
- Tsien RW, Ellinor PT, Horne WA (1991) Molecular diversity of voltage-dependent Ca²⁺ channels. *Trends Pharmacol Sci* 12:349-354.
- Tytgat J, Nilius B, Vereecke J, Carmeliet E (1988) The T-type Ca²⁺ channel in guinea-pig ventricular myocytes is insensitive to isoproterenol. *Pflugers Arch* 411:704-706.
- Uchino T, Lee TS, Kaku T, Yamashita N, Noguchi T, Ono K (2005) Voltage-dependent and frequency-independent inhibition of recombinant Cav3.2 T-type Ca²⁺ channel by bepridil. *Pharmacology* 74:174-181.

- Uebele VN et al. (2009) Positive allosteric interaction of structurally diverse T-type calcium channel antagonists. *Cell Biochem Biophys* 55:81-93.
- Underwood JG, Boutz PL, Dougherty JD, Stoilov P, Black DL (2005) Homologues of the *Caenorhabditis elegans* Fox-1 protein are neuronal splicing regulators in mammals. *Mol Cell Biol* 25:10005-10016.
- Vassort G, Alvarez J (1994) Cardiac T-type calcium current: pharmacology and roles in cardiac tissues. *J Cardiovasc Electrophysiol* 5:376-393.
- Vassort G, Talavera K, Alvarez JL (2006) Role of T-type Ca^{2+} channels in the heart. *Cell Calcium* 40:205-220.
- Vitko I, Bidaud I, Arias JM, Mezghrani A, Lory P, Perez-Reyes E (2007) The I-II loop controls plasma membrane expression and gating of $\text{Ca}_v3.2$ T-type Ca^{2+} channels: a paradigm for childhood absence epilepsy mutations. *J Neurosci* 27:322-330.
- Wahler GM, Dollinger SJ, Smith JM, Flemal KL (1994) Time course of postnatal changes in rat heart action potential and in transient outward current is different. *Am J Physiol* 267:H1157-1166.
- Wakamori M, Imoto K (2009) Voltage-gated calcium channels. In: *Handbook of Neurochemistry and Molecular Neurobiology Neural Signaling Mechanisms* (Lajtha A, Mikoshiba K, eds), p 632. New York: Springer Science+Business Media, LLC.
- Wang D, Papp AC, Binkley PF, Johnson JA, Sadee W (2006) Highly variable mRNA expression and splicing of L-type voltage-dependent calcium channel alpha subunit 1C in human heart tissues. *Pharmacogenet Genomics* 16:735-745.
- Wang R, Karpinski E, Pang PK (1991) Two types of voltage-dependent calcium channel currents and their modulation by parathyroid hormone in neonatal rat ventricular cells. *J Cardiovasc Pharmacol* 17:990-998.
- Warnecke C, Surder D, Curth R, Fleck E, Regitz-Zagrosek V (1999) Analysis and functional characterization of alternatively spliced angiotensin II type 1 and 2 receptor transcripts in the human heart. *J Mol Med* 77:718-727.
- Wekstein DR (1965) Heart Rate of the Preweanling Rat and Its Autonomic Control. *Am J Physiol* 208:1259-1262.
- Welling A, Ludwig A, Zimmer S, Klugbauer N, Flockerzi V, Hofmann F (1997) Alternatively spliced IS6 segments of the alpha 1C gene determine the tissue-specific dihydropyridine sensitivity of cardiac and vascular smooth muscle L-type Ca^{2+} channels. *Circ Res* 81:526-532.
- Welsby PJ, Wang H, Wolfe JT, Colbran RJ, Johnson ML, Barrett PQ (2003) A mechanism for the direct regulation of T-type calcium channels by Ca^{2+} /calmodulin-dependent kinase II. *J Neurosci* 23:10116-10121.
- Wen JF, Cui X, Ahn JS, Kim SH, Seul KH, Kim SZ, Park YK, Lee HS, Cho KW (2000) Distinct roles for L- and T-type Ca^{2+} channels in regulation of atrial ANP release. *Am J Physiol Heart Circ Physiol* 279:H2879-2888.
- Westenbroek RE, Babcock DF (1999) Discrete regional distributions suggest diverse functional roles of calcium channel alpha 1 subunits in sperm. *Dev Biol* 207:457-469.
- Wetzel GT, Klitzner TS (1996) Developmental cardiac electrophysiology recent advances in cellular physiology. *Cardiovasc Res* 31 Spec No:E52-60.
- White G, Lovinger DM, Weight FF (1989) Transient low-threshold Ca^{2+} current triggers burst firing through an afterdepolarizing potential in an adult mammalian neuron. *Proc Natl Acad Sci U S A* 86:6802-6806.
- Wielowieyski PA, Wigle JT, Salih M, Hum P, Tuana BS (2001) Alternative splicing in intracellular loop connecting domains II and III of the alpha 1 subunit of $\text{Ca}_v1.2$ Ca^{2+}

- channels predicts two-domain polypeptides with unique C-terminal tails. *J Biol Chem* 276:1398-1406.
- Williams ME, Washburn MS, Hans M, Urrutia A, Brust PF, Prodanovich P, Harpold MM, Stauderman KA (1999) Structure and functional characterization of a novel human low-voltage activated calcium channel. *J Neurochem* 72:791-799.
- Witcher DR, De Waard M, Liu H, Pragnell M, Campbell KP (1995) Association of native Ca²⁺ channel beta subunits with the alpha 1 subunit interaction domain. *J Biol Chem* 270:18088-18093.
- Wolfe JT, Wang H, Perez-Reyes E, Barrett PQ (2002) Stimulation of recombinant Ca_v3.2, T-type, Ca²⁺ channel currents by CaMKIIgamma(C). *J Physiol* 538:343-355.
- Wolfe JT, Wang H, Howard J, Garrison JC, Barrett PQ (2003) T-type calcium channel regulation by specific G-protein betagamma subunits. *Nature* 424:209-213.
- Wu X, Eder P, Chang B, Molkenstin JD (2010) TRPC channels are necessary mediators of pathologic cardiac hypertrophy. *Proc Natl Acad Sci U S A* 107:7000-7005.
- Xiao RP, Cheng H, Lederer WJ, Suzuki T, Lakatta EG (1994) Dual regulation of Ca²⁺/calmodulin-dependent kinase II activity by membrane voltage and by calcium influx. *Proc Natl Acad Sci U S A* 91:9659-9663.
- Xu X, Best PM (1992) Postnatal changes in T-type calcium current density in rat atrial myocytes. *J Physiol* 454:657-672.
- Xu X, Yang D, Ding JH, Wang W, Chu PH, Dalton ND, Wang HY, Bermingham JR, Jr., Ye Z, Liu F, Rosenfeld MG, Manley JL, Ross J, Jr., Chen J, Xiao RP, Cheng H, Fu XD (2005) ASF/SF2-regulated CaMKIIdelta alternative splicing temporally reprograms excitation-contraction coupling in cardiac muscle. *Cell* 120:59-72.
- Yamakage M, Chen X, Tsujiguchi N, Kamada Y, Namiki A (2001) Different inhibitory effects of volatile anesthetics on T- and L-type voltage-dependent Ca²⁺ channels in porcine tracheal and bronchial smooth muscles. *Anesthesiology* 94:683-693.
- Yang Y, Chen X, Margulies K, Jeevanandam V, Pollack P, Bailey BA, Houser SR (2000) L-type Ca²⁺ channel alpha 1c subunit isoform switching in failing human ventricular myocardium. *J Mol Cell Cardiol* 32:973-984.
- Yang ZQ et al. (2008) Discovery of 1,4-substituted piperidines as potent and selective inhibitors of T-type calcium channels. *J Med Chem* 51:6471-6477.
- Yao J, Davies LA, Howard JD, Adney SK, Welsby PJ, Howell N, Carey RM, Colbran RJ, Barrett PQ (2006) Molecular basis for the modulation of native T-type Ca²⁺ channels in vivo by Ca²⁺/calmodulin-dependent protein kinase II. *J Clin Invest* 116:2403-2412.
- Yasui K, Niwa N, Takemura H, Ophof T, Muto T, Horiba M, Shimizu A, Lee JK, Honjo H, Kamiya K, Kodama I (2005) Pathophysiological significance of T-type Ca²⁺ channels: expression of T-type Ca²⁺ channels in fetal and diseased heart. *J Pharmacol Sci* 99:205-210.
- Yeo GW, Coufal NG, Liang TY, Peng GE, Fu XD, Gage FH (2009) An RNA code for the FOX2 splicing regulator revealed by mapping RNA-protein interactions in stem cells. *Nat Struct Mol Biol* 16:130-137.
- Yunker AM (2003) Modulation and pharmacology of low voltage-activated ("T-Type") calcium channels. *J Bioenerg Biomembr* 35:577-598.
- Yunker AM, McEnery MW (2003) Low-voltage-activated ("T-Type") calcium channels in review. *J Bioenerg Biomembr* 35:533-575.
- Zamponi GW, Snutch TP (1998) Decay of prepulse facilitation of N type calcium channels during G protein inhibition is consistent with binding of a single Gbeta subunit. *Proc Natl Acad Sci U S A* 95:4035-4039.

- Zamponi GW, Bourinet E, Nelson D, Nargeot J, Snutch TP (1997) Crosstalk between G proteins and protein kinase C mediated by the calcium channel α_1 subunit. *Nature* 385:442-446.
- Zamponi GW, Lewis RJ, Todorovic SM, Arneric SP, Snutch TP (2009) Role of voltage-gated calcium channels in ascending pain pathways. *Brain Res Rev* 60:84-89.
- Zhang C, Zhang Z, Castle J, Sun S, Johnson J, Krainer AR, Zhang MQ (2008) Defining the regulatory network of the tissue-specific splicing factors Fox-1 and Fox-2. *Genes Dev* 22:2550-2563.
- Zhang JF, Ellinor PT, Aldrich RW, Tsien RW (1996) Multiple structural elements in voltage-dependent Ca^{2+} channels support their inhibition by G proteins. *Neuron* 17:991-1003.
- Zhang Z, Xu Y, Song H, Rodriguez J, Tuteja D, Namkung Y, Shin HS, Chiamvimonvat N (2002) Functional Roles of $\text{Ca}_v1.3$ (α_1D) calcium channel in sinoatrial nodes: insight gained using gene-targeted null mutant mice. *Circ Res* 90:981-987.
- Zhao M, Chow A, Powers J, Fajardo G, Bernstein D (2004) Microarray analysis of gene expression after transverse aortic constriction in mice. *Physiol Genomics* 19:93-105.
- Zhong X, Liu JR, Kyle JW, Hanck DA, Agnew WS (2006) A profile of alternative RNA splicing and transcript variation of CACNA1H, a human T-channel gene candidate for idiopathic generalized epilepsies. *Hum Mol Genet* 15:1497-1512.
- Zhou HL, Lou H (2008) Repression of prespliceosome complex formation at two distinct steps by Fox-1/Fox-2 proteins. *Mol Cell Biol* 28:5507-5516.
- Zhou Z, Lipsius SL (1994) T-type calcium current in latent pacemaker cells isolated from cat right atrium. *J Mol Cell Cardiol* 26:1211-1219.
- Zhou Z, January CT (1998) Both T- and L-type Ca^{2+} channels can contribute to excitation-contraction coupling in cardiac Purkinje cells. *Biophys J* 74:1830-1839.
- Ziman AP, Gomez-Viquez NL, Bloch RJ, Lederer WJ (2010) Excitation-contraction coupling changes during postnatal cardiac development. *J Mol Cell Cardiol* 48:379-386.
- Zoumakis E, Rice KC, Gold PW, Chrousos GP (2006) Potential uses of corticotropin-releasing hormone antagonists. *Ann N Y Acad Sci* 1083:239-251.
- Zuhlke RD, Bouron A, Soldatov NM, Reuter H (1998) Ca^{2+} channel sensitivity towards the blocker isradipine is affected by alternative splicing of the human α_1C subunit gene. *FEBS Lett* 427:220-224.

APPENDIX 1: T-TYPE CALCIUM CHANNELS: AN EMERGING THERAPEUTIC TARGET FOR THE TREATMENT OF PAIN



DRUG DEVELOPMENT RESEARCH 67:404–415 (2006)

Research Overview

T-Type Calcium Channels: An Emerging Therapeutic Target for the Treatment of Pain

Terrance P. Snutch* and Laurence S. David

Michael Smith Laboratories, University of British Columbia, Vancouver, British Columbia, Canada

Strategy, Management and Health Policy				
Enabling Technology, Genomics, Proteomics	Preclinical Research	Preclinical Development Toxicology, Formulation Drug Delivery, Pharmacokinetics	Clinical Development Phases I-III Regulatory, Quality, Manufacturing	Postmarketing Phase IV

ABSTRACT It has become generally accepted that presynaptic high voltage-activated N-type calcium channels located in the spinal dorsal horn are a validated clinical target for therapeutic interventions associated with severe intractable pain. Low voltage-activated (T-type) calcium channels play a number of critical roles in nervous system function, including controlling thalamocortical bursting behaviours and the generation of spike wave discharges associated with slow wave sleep patterns. There is a growing body of evidence that T-type calcium channels also contribute in several ways to both acute and neuropathic nociceptive behaviours. In the one instance, the Cav3.1 T-type channel isoform likely contributes an anti-nociceptive function in thalamocortical central signalling, possibly through the activation of inhibitory nRT neurons. In another instance, the Cav3.2 T-type calcium channel subtype acts at the level of primary afferents in a strongly pro-nociceptive manner in both acute and neuropathic models. While a number of classes of existing clinical agents non-selectively block T-type calcium channels, there are no subtype-specific drugs yet available. The development of agents selectively targeting peripheral Cav3.2 T-type calcium channels may represent an attractive new avenue for therapeutic intervention. *Drug Dev. Res.* 67:404–415, 2006. © 2006 Wiley-Liss, Inc.

Key words: calcium channel; T-type; Cav3.2; nociception; mibefradil; ethosuximide

INTRODUCTION

Twenty-five years ago, Llinas and Yarom [1981a,b] first described low-threshold calcium-dependent spikes in the mammalian inferior olive, a phenomenon that has since been demonstrated in many brain nuclei including those found in the hippocampus, hypothalamus, thalamus, habenula, cortex, and globus pallidus [reviewed in Perez-Reyes, 2003]. Low-threshold calcium spikes generally act as pacemakers, helping to trigger bursts of sodium-dependent action potentials after neuronal membrane hyperpolarization [Huguenard and Prince, 1992; McCormick and Huguenard, 1992]. They also contribute to oscillatory and rebound burst firing behaviors relevant to both normal physiological functions (e.g., thalamocortical processes such as deep sleep) and to

pathophysiological states (e.g., spike-wave discharges associated with absence epilepsy [reviewed in Huguenard, 1996, 2002]). Underlying low-threshold calcium-dependent spiking activity is a physiologically and pharmacologically unique class of voltage-gated calcium channel called low-voltage-activated (LVA) or T-type calcium channels [Carbone and Lux, 1984; Nowycky et al., 1985].

Grant sponsor: Canadian Institutes for Health Research.

*Correspondence to: Dr. T.P. Snutch, Rm 219–2185 East Mall, Michael Smith Laboratories, University of British Columbia, Vancouver, B.C., Canada V6T 1Z4. E-mail: snutch@msl.ubc.ca

Published online in Wiley InterScience (www.interscience.wiley.com). DOI: 10.1002/ddr.20103

© 2006 Wiley-Liss, Inc.



*A version of this appendix has been published. Snutch, T.P. and David, L.S. (2006). T-type calcium channels: An emerging therapeutic target for the treatment of pain. *Drug Discovery Research*. 67:404–415. Reprinted with kind permission of John Wiley and Sons. All rights reserved.

T-type calcium channels are generally distinct from high voltage-activated (HVA) calcium channels (the L-, N-, P/Q, and R-types) in their both negative and overlapping activation (initial activation ~ -70 to -60 mV) and inactivation ($V_{50_{\text{inact}}} \sim -55$ to -85 mV) ranges, fast kinetics of inactivation ($\tau_{\text{inact}} \sim 10$ to 20 ms), rapid recovery from inactivation, slow deactivation (closing), and small single-channel conductance (~ 5 to 10 pS). The low-threshold calcium spikes first observed by Llinas can largely be attributed to the unique properties of T-type calcium channels, which become deactivated after inhibitory synaptic inputs and subsequently trigger calcium-dependent bursting as a result of their negative activation properties.

T-type calcium channels are expressed in many central and peripheral neurons, as well as in other tissues including the heart, smooth muscle, kidney, embryonic skeletal muscle, pituitary, pancreas, adrenal, retina, and testes [reviewed in Perez-Reyes, 2003]. In addition to their pacemaker roles in neurons, these

channels also contribute to secretory processes such as hormone release, the regulation of muscle contraction, olfaction, and cellular differentiation and proliferation. The complete description of the physiological contributions of native T-type calcium channels has been complicated by several factors including (1) the co-expression in many cells of multiple types of HVA and LVA calcium currents with overlapping voltage-dependent and kinetic properties, and (2) a lack of specific, high-affinity T-type channel pharmacological tools. Additionally, even amongst native T-type currents there exists considerable heterogeneity in their activation, inactivation, permeation, and pharmacological properties. While historically referred to as a single class of ion channel, native T-type calcium channels are now known to be encoded by at least three distinct α_1 subunit genes ($\alpha_{1C}/\text{Cav}3.1$, $\alpha_{1H}/\text{Cav}3.2$, and $\alpha_{1I}/\text{Cav}3.3$) and that considerable alternative splicing exists to generate further diversity (Fig. 1) [Cribbs et al., 1998; Lee et al., 1999; McRory et al., 2001; Mittman

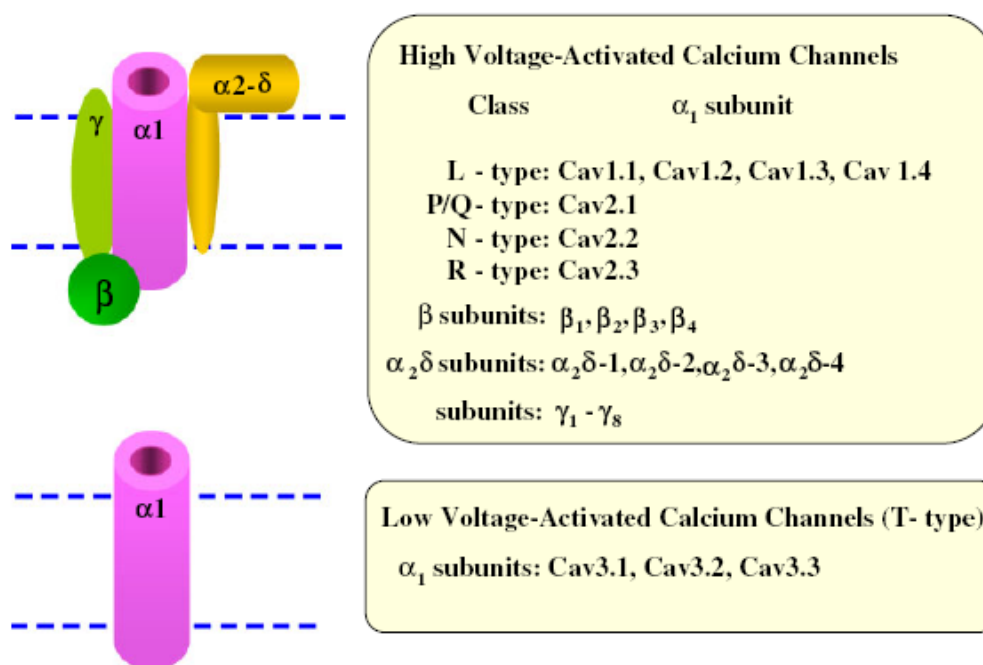


Fig. 1. Composition of neuronal voltage-gated calcium channels. High voltage-activated (HVA) calcium channels are a heteromeric complex consisting of a large (~ 200 – 260 kDa) pore-forming α_1 subunit that contains the voltage-sensor and pore region and is the target of known pharmacological agents. There are ten identified α_1 subunit genes in the mammalian genome. Neuronal HVA channels also contain an ancillary β subunit (four genes) and $\alpha_2\delta$ subunit (four genes) that contribute to modulating a number of channel functions including activation, inactivation and kinetic properties, second-messenger regulation, and channel complex intracellular processing. Biochemical purification of the skeletal muscle HVA L-type calcium channel (Cav1.1) shows that it contains a fourth subunit, γ , although reconstitution of neuronal HVA channel properties does not require a γ subunit and it remains to be determined whether native neuronal HVA calcium channel complexes contain this protein. Low voltage-activated (LVA or T-type) calcium channels have not yet been biochemically purified although known biophysical, pharmacological, and regulatory characteristics can be fully reconstituted with a Cav3 α_1 subunit alone.

et al., 1999; Monteil et al., 2000a,b; Perez-Reyes et al., 1998].

Pathophysiologically, both Cav3.1 and Cav3.2 T-type calcium channels may contribute to the genesis of absence seizures: (1) the genetic absence epilepsy inbred strain of rat (GAERS) exhibits spontaneous spike-wave discharges and absence seizures that are associated with an increased basal level of thalamic reticular T-type currents [Tsakiridou et al., 1995]; (2) gene knock-out of the Cav3.1 T-type channel gene in mice results in animals insensitive to GABA_B receptor agonist-induced spike wave discharges [D. Kim et al., 2001]; and (3) a number of point mutations have been recently identified in the Cav3.2 T-type channel gene in patients with childhood absence epilepsy and generalized idiopathic epilepsy [Chen et al., 2003b; Heron et al., 2004]. Introduction of some of the epilepsy mutations into the wildtype Cav3.2 channel results in biophysical changes consistent with gain-of-function alterations to channel activity and are consistent with the notion that some clinical antiepileptics act mechanistically to inhibit T-type calcium channel activity [Coulter et al., 1989; 1990; Khosravani et al., 2004, 2005; Peloquin et al., 2006; Vitko et al., 2005].

CALCIUM CHANNELS AND PAIN

Nociceptive processes are known to be highly sensitive to intracellular calcium levels and to date there have been two distinct classes of pain therapeutics developed to target components of HVA calcium channels. In one instance, the N-type calcium channel blocking peptide, ziconitide, is a 25 amino acid synthetic peptide (ω -conotoxin MVIIA) derived from the marine hunting cone snail *Conus magus*, which has recently been approved (PrialtTM) both in the United States and in Europe for the treatment of intractable pain [Snutch, 2005]. N-type calcium channels are highly concentrated in the cell bodies and synaptic terminals of a subset of primary afferents that terminate in the dorsal horn of the spinal cord (mainly C-fibers and A- δ fibers). In animals, block of N-type channels by the intrathecal administration of ziconitide inhibits the release of the nociceptive transmitters, substance P and CGRP, consistent mechanistically with the role of N-type channels in triggering neurotransmission at dorsal horn primary afferent terminals [Evans et al., 1996]. The activation μ -opioid receptors attenuates N-type channel activity through the direct binding of a single G_{p γ} dimer to the N-type channel α_1 subunit consistent with the notion that opioids in part mediate their analgesic effects through inhibiting presynaptic calcium channel activity [Bourinet et al., 1996; Soldo and Moises, 1998; Zamponi et al., 1997; Zamponi and

Snutch, 1998]. Knock-out of the N-type channel genetically in mice results in animals largely resistant to the induction of neuropathic and inflammatory pain although otherwise exhibiting normal sensory and motor functions [Ino et al., 2001; C. Kim et al., 2001; Saegusa et al., 2001]. Clinically, intrathecal ziconitide (PrialtTM) is highly efficacious in the treatment of morphine-refractory neuropathic and malignant pain conditions, although it exhibits a narrow therapeutic index (ratio of relative toxicity to relative efficacy) and must be titrated carefully in each patient. Interestingly, while the N-type channel is downstream in the opioid receptor pathway, the direct N-type channel blockade by ziconitide does not result in opioid-type side effects such as tolerance and addiction [Brose et al., 1997; McGuire et al., 1997; Ridgeway et al., 2000; Staats et al., 2004].

In the second instance of approved pain therapeutics targeting HVA calcium channels, the orally administered small organic molecules gabapentin and pregabalin bind to the $\alpha_2\delta$ subunit associated with HVA calcium channel complexes. Gabapentin and pregabalin are clinically effective anticonvulsants that while synthetic analogs of the neurotransmitter γ -aminobutyric acid (GABA), do not exert their effects via interacting with GABA receptors or transporters but rather bind with high affinity to the HVA calcium channel ancillary $\alpha_2\delta$ -1 and $\alpha_2\delta$ -2 subunits [Gee et al., 1996; Marais et al., 2001]. Peripheral nerve injury upregulates $\alpha_2\delta$ expression in both the DRG and spinal dorsal horn, leading to the proposal that the $\alpha_2\delta$ subunit contributes to central sensitization [Li et al., 2004; Luo et al., 2002]. Numerous open label and double-blinded clinical trials show that gabapentin is efficacious in the treatment of neuropathic pain conditions including diabetic neuropathy, postherpetic neuralgia, trigeminal neuralgia, migraine, and pain associated with cancer and multiple sclerosis [Backonja et al., 1998; Caraceni et al., 1999; Di Trapani et al., 2000; Houtchens et al., 1997; Laird and Gidal, 2000; Rowbotham et al., 1998]. Interestingly, while the $\alpha_2\delta$ subunit is associated with all known HVA calcium channel α_1 subunits, including the L-type channels found in skeletal, smooth, and cardiac muscles, gabapentin and pregabalin exhibit relatively few motor or cardiovascular adverse effects even at high therapeutic doses. Along these lines, determination of the exact mechanism of action of gabapentin has proven elusive with reports both supporting and refuting direct inhibitory actions on HVA calcium channels [Bayer et al., 2004; Brown and Randall, 2005; Sutton and Snutch, 2002].

Is there a role for T-type calcium channels in pain processing? A significant component of neuropathic

pain related to peripheral nerve injury is thought to result from hypersensitivity and/or abnormal spontaneous firing along the primary afferent pathway. Wind-up is a frequency-dependent facilitation of spinal cord excitability mediated via afferent C-fibers and has been suggested to be linked to the central sensitization observed after peripheral nerve damage [for review see Herrero et al., 2000]. As T-type calcium channels activate at sub-threshold membrane potentials, one physiological route to altering the ectopic discharge of primary afferents may involve either the altered expression and/or modulation of T-type calcium channels. Of particular relevance, reducing agents such as L-cysteine modulate both thermal and mechanical nociception when injected into peripheral receptive fields [Todorovic et al., 2001]. Redox modulation appears to occur through a mechanism involving the selective up-regulation of T-type whole cell currents in a subset of DRGs [Nelson et al., 2005; Todorovic et al., 2001, 2004]. Interestingly, both in the higher CNS and spinal cord there also exists a number of similarities between the proposed physiological functions of T-type calcium channels in processes such as long-term potentiation and kindling, and those for the central sensitization associated with neuropathic pain wherein postsynaptic responses progressively increase [Ikeda et al., 2003].

Which of the three functionally distinct T-type calcium channel isoforms might be involved in nociceptive behaviors? In the periphery, a subset of small- and medium-size DRG neurons are known to express large whole cell T-type calcium currents [Schroeder et al., 1990; Scroggs and Fox, 1992]. In situ hybridization and reverse-transcription PCR studies show that of the three known T-type channel subtypes, Cav3.2 (α_{1H}) is most highly expressed in DRGs while these same cells express relatively low levels of Cav3.3 (α_{1I}) and little to none of Cav3.1 (α_{1G}). In D-hair cell mechanoreceptors (a subset of medium sized DRGs), the Cav3.2 T-type channel has also been shown to contribute to a slow after depolarizing potential that lowers the voltage-threshold for action potential generation. Pharmacological block of Cav3.2 in D-hair cells suggests that this T-type channel subtype is required for the normal transduction of slow-moving mechanical stimuli [Dubreuil et al., 2004; Shin et al., 2003].

Utilizing intrathecal injection of antisense oligonucleotides, Bourinet et al. [2005] found that selective Cav3.2 T-type channel knock-down affects both acute and neuropathic pain behaviors in rat. An approximate 50% reduction in Cav3.2 mRNA expression resulted in a 75 to 90% decrease in whole cell T-type current density in small- and medium-size DRGs, and a

concomitant increase in both the vocalization threshold and tail withdrawal latency in response to noxious acute mechanical and thermal stimuli. Similarly, a complete reversal of mechanical allodynia in the Bennett neuropathic model was noted in Cav3.2 knock-down animals. In agreement with the low levels of detectable Cav3.1 and Cav3.3 in the DRG, the intrathecal injection of antisense oligonucleotides against Cav3.1 and Cav3.3 did not significantly affect nociceptive behavior in rats. Taken together, these data are strongly suggestive for the Cav3.2 T-type calcium channel selectively contributing both to normal acute nociception and to chronic pain hyperexcitable states.

While the low expression of the Cav3.1 T-type in DRG neurons suggests a minimal role for this calcium channel related to peripheral pain mechanisms, the Cav3.1 channel is highly expressed in the thalamus and appears to play a significant role in central pain processing at least as it relates to visceral pain. Kim and co-workers found that either knock-out of the Cav3.1 gene in mice or infusion of mibefradil directly into the ventroposterolateral (VPL) thalamus (to block Cav3.1 channels) act to enhance the pain response elicited by intraperitoneal administration of acetic acid or magnesium sulphate [Kim et al., 2003]. In response to visceral pain stimuli, wild type VPL neurons generate both increased single spikes and clustered bursts of action potentials. In Cav3.1 knockout mice, VPL neurons exhibit normal single spike activity but an almost total absence of burst spikes suggesting that Cav3.1-dependent bursting activity mediates a downstream inhibitory process likely involving nRT neurons. In contrast to that for the Cav3.2 channel, it therefore appears that central native Cav3.1 T-type channels act in an anti-nociceptive capacity. It remains to be determined whether the selective pharmacological blockade of this low-threshold calcium channel might have the unwanted effect of enhancing the central perception of noxious stimuli.

CLINICAL AGENTS WITH T-TYPE CALCIUM CHANNEL BLOCKING ACTIVITY

There appears a strong connection both mechanistically and pharmacologically between epilepsy, neuropathic pain, and migraine headache; thus targeting the T-type calcium channels that contribute to these pathophysiological processes is quite attractive. Although selectively targeting T-type calcium channels for therapeutic purposes has been of significant interest, to date there are no "pure" T-type channel blockers presently in clinical usage. In spite of this critical pharmacological limitation, there are a number of structurally distinct classes of drugs that more broadly interact with multiple ionic conductances

including T-type calcium channels. These agents may provide important clues concerning the validation of the T-type channel targets, and perhaps also suggest chemical backbones relevant towards future compound-based structure-activity development.

Antiepileptics

Zonisamide (Fig. 2) is a widely utilized broad-spectrum antiepileptic. Mechanistically, zonisamide is known to variously inhibit nitric oxide formation, to increase serotonergic transmission and basal acetylcholine and gamma-aminobutyric acid (GABA) release, and to block both voltage-gated sodium channels (Kd ~1 μ M) and T-type calcium channels [Mimaki et al., 1990; Schauf, 1987; Zhu et al., 2002]. Zonisamide blocks T-type calcium currents in a concentration-dependent manner without altering either the voltage-dependence of activation or inactivation kinetics. In

cultured neurons of rat cerebral cortex, the mean percentage reduction in T-type current is approximately 60% at 500 μ M with no observed block of L-type currents [Suzuki et al., 1992]. In addition, 50 μ M zonisamide also reduces T-type currents (by ~40%) in cultured neuroblastoma cells [Kito et al., 1996]. In the Bennett chronic constriction rat model, zonisamide relieves thermal hyperalgesia in a dose-dependent manner although it has little effect on mechanical allodynia [Hord et al., 2003]. Clinically, in a number of open-label case studies, zonisamide has been shown to be effective in a variety of treatment-refractory neuropathic pain conditions [Guay, 2003; Takahashi et al., 2004]. Additionally, in several open-label analyses of treatment-refractory migraine patients, zonisamide is also highly effective as a prophylactic agent [Drake et al., 2004]. Zonisamide is contraindicated in patients with sulfonamide allergies

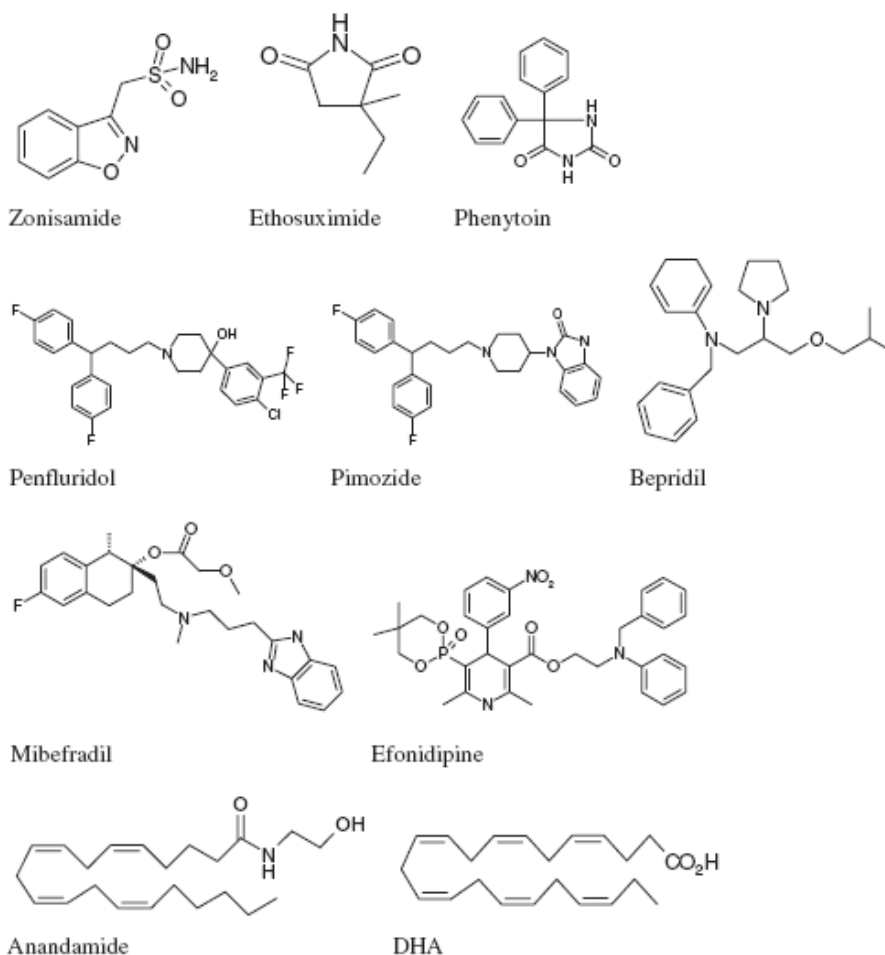


Fig. 2. Structures of compounds mentioned in the text.

and any future structure-activity relation (SAR) studies targeted at improving T-type affinity and/or selectivity might also address this limitation.

Ethosuximide

The succinimides methyl-phenyl-succinimide (MPS) and ethosuximide (Fig. 2) are widely utilized antiepileptics thought to in part act therapeutically via the inhibition of cortical-thalamic T-type calcium channels involved in mediating 3 Hz spike-wave discharges. MPS and ethosuximide inhibit cloned T-type calcium channels in a state-dependent manner and at concentrations considered to be clinically relevant (IC_{50} s; ~ 0.3 to 1 mM for Cav3.1, Cav3.2, and Cav3.3 subtypes vs. therapeutic plasma levels ~ 0.1 mM for MPS and ~ 0.3 to 0.7 mM for ethosuximide [Gomora et al., 2001]). In both nerve-injured and sham-operated animals, in vivo recordings show that ethosuximide applied directly to the spinal cord inhibits both mechanical and thermal-evoked responses in a dose-dependent manner [Matthews and Dickenson, 2001]. Direct spinal application of ethosuximide produces the greatest maximal inhibition on C-fibers and A δ -fibers compared to A β -fibers, consistent with the notion both that T-type channels are differentially expressed amongst DRG neurons and are preferentially localized to C-fibers and A δ -fibers that convey thermal and nociceptive information and not to A β -fibers that subserve proprioception and responses to tactile stimuli.

Examining L5/L6 nerve-injured animals, Dogrul and colleagues found that i.p. administration of ethosuximide produces a dose-dependent inhibition of both thermal hyperalgesia ($A_{50} = 126$ mg/kg) and mechanical allodynia ($A_{50} = 174$ mg/kg) [Dogrul et al., 2003]. Direct intrathecal (i.t.) administration of ethosuximide is without effect, perhaps suggesting a peripheral target site of action, although the direct injection of ethosuximide into the injured paw (intraplantar) is also without effect. Ethosuximide administered i.p. also completely reverses capsaicin-induced mechanical allodynia ($ED_{50} = 108$ mg/kg) and is antinociceptive in both the early and late phases of the formalin response as well as the acute tail flick assay [Barton et al., 2005]. Finally, i.p.-administered ethosuximide is highly efficacious in reversing paclitaxil- and vincristine-induced peripheral neuropathy [Flatters and Bennett, 2004]. In spite of these promising animal data, in the over 40 years that ethosuximide has been utilized clinically there are few if any reports of it being efficacious towards human neuropathies.

Phenytoin

Phenytoin (Fig. 2) is clinically utilized as both an anticonvulsant as well as an analgesic for neuropathic

pain [McCleane, 1999]. The antinociceptive properties of phenytoin have been attributed to its ability to block both voltage-dependent sodium and calcium channels. Phenytoin blocks sodium channels from rat cortical synaptosomes ($IC_{50} > 800$ μ M) and cloned sodium channels expressed in *Xenopus* oocytes [Anderson et al., 2003; Lingamaneni and Hemmings, 1999; Twombly et al., 1988]. In N1E-115 neuroblastoma cells, phenytoin at concentrations of between 3 and 100 μ M inhibits T-type calcium currents without altering channel activation or kinetic properties. However, the steady-state inactivation profile is shifted more hyperpolarized. Phenytoin blocks cloned α_{1C} (Cav3.1) and α_{1H} (Cav3.2) T-type channels expressed in HEK 293 cells at IC_{50} s of 140 and 8.3 μ M, respectively [Todorovic et al., 2000]. In addition, in cultured dorsal root ganglia neurons (DRGs) phenytoin blocks whole cell T-type calcium currents in a concentration-dependent manner ($IC_{50} \sim 8.3$ μ M). In a bradykinin-induced pain model in rats, phenytoin produces dose-dependent analgesic effects at an ED_{50} of 3 mg/kg applied subcutaneously [Foong et al., 1982]. In a mouse acute pain model using plantar and tail pressure to evaluate acute thermal and mechanical nociception, phenytoin preferentially relieves thermal pain at dose between 2.5 to 25 mg/kg applied intraperitoneally [Sakaue et al., 2004]. Clinically, in a randomized, double-blinded, placebo-controlled, crossover study, phenytoin relieves flare-ups of chronic neuropathic pain and has also been shown to significantly enhance buprenorphine analgesia in cancer patients [McCleane, 1999; Yajnik et al., 1992].

Antipsychotics

The neuroleptics comprise a chemically diverse set of molecules that largely act clinically to inhibit dopamine D2 receptors although, interestingly, a subset of these agents also exhibit potent calcium channel blocking activity. In particular, the diphenylbutylpiperidines, pimozide and penfluridol (Fig. 2), block T-type channels in a variety of cell types including from adrenal, heart, neural crest, and spermatogenic tissues [Enyeart et al., 1990a,b, 1992]. Examination of pimozide and penfluridol on cloned T-type channels showed that they block all three mammalian T-type channel isoforms (Cav3.1, Cav3.2, and Cav3.3) with a higher affinity than either ethosuximide or mibefradil (K_{d} s ranging from ~ 40 to 100 nM) [Santi et al., 2002]. Block is state dependent, shifting T-type channel steady-state inactivation profiles to more negative potentials, but does not affect T-type channel activation or kinetic parameters. Interestingly, from a structure-activity perspective, the highly structurally related diphenyldipiperazine,

flunarizine, and the butyrophenone antipsychotic, haloperidol, show both significantly less potent T-type channel-blocking activities (K_d s ranging from ~500 to 3,500 nM for Cav3.1, Cav3.2, and Cav3.3) and also exhibit distinct clinical pharmacologies in patients [Opler and Feinberg, 1991].

In one study examining a mouse formalin model of inflammatory pain, relatively low doses of pimozide (0.05–0.25 mg/kg i.p.) were not shown to be highly efficacious [Saddi and Abbott, 2000]. Interestingly, however, although pimozide has been widely used clinically as a neuroleptic to treat conditions such as schizophrenia, Tourette's, and obsessive compulsive disorder, it has also proven efficacious in several neuropathic pain conditions. In particular, and while the pathophysiological mechanism underlying its therapeutic effects are unknown, pimozide appears to provide significant relief in the management of trigeminal neuralgia, a relatively uncommon but severe facial pain syndrome associated with repetitive action potentials [Green and Selman, 1991; Lechin et al., 1989].

Antiarrhythmics and Antihypertensives

A number of cardiovascular agents are thought to act in part mechanistically via inhibiting T-type calcium channels, either solely or as mixed T-type and L-type calcium channel blockers. None of these agents has yet to be shown efficacious in the clinical setting for pain management although given their pharmacological characteristics, there is compelling reason to examine some of these drugs in various neuropathies.

Bepidil (Fig. 2) is a widely utilized clinical antiarrhythmic agent with antianginal properties known to non-specifically inhibit a variety of ionic conductances including various sodium (IC_{50} ~30 μ M) and potassium channels (IC_{50} from 1 to 30 μ M) as well as the L-type calcium channel (IC_{50} from 0.5 to 30 μ M) [Hollingshead et al., 1992; Li et al., 1999; Wang et al., 1999; Yatani et al., 1986]. More recently, bepridil has been shown to inhibit the Cav3.2 ($\alpha 1$ H) T-type calcium channel with an IC_{50} ~400 nM. Block is not affected by pulse frequency but is strongly dependent upon holding potential and also shifts steady-state inactivation and activation profiles to more hyperpolarized potentials [Uchino et al., 2005].

Mibefradil

Next to ethosuximide, mibefradil (Fig. 2) is probably the most widely recognized agent generally described as a selective T-type calcium channel blocker. In fact, while this tetralol derivative was originally developed by Roche and briefly brought onto the market as an effective antihypertensive and chronic stable angina pectoris agent targeting T-type

channels, mibefradil has been shown to be a somewhat non-selective blocker of both HVA calcium channels (IC_{50} values in barium recording saline; P/Q-type ~0.3 μ M, R-type ~0.4 μ M, L-type ~10 to 20 μ M) and T-type channels (IC_{50} values; ~1 μ M for Cav3.1, Cav3.2, and Cav3.3) [Jimenez et al., 2000]. There are conflicting reports concerning the mechanism of mibefradil mediated T-type channel blockade with resting-, inactivated-, and open-state block all being suggested, and with some evidence that reducing channel availability can increase affinity by up to tenfold [Martin et al., 2000].

In L5/L6 nerve-injured rats, i.p.-administered mibefradil effectively inhibits both tactile allodynia (A_{50} = 7.4 mg/kg) and thermal hyperalgesia (A_{50} = 12 mg/kg) [Dogrul et al., 2003]. Interestingly, while the direct injection of mibefradil into the injured limb also produces a dose-dependent reversal of tactile allodynia (A_{50} = 92 μ g) suggestive of a peripheral mechanism of action, a similar direct administration of ethosuximide (up to 500 μ g) is without effect. Barton and colleagues report that while i.p.-administered mibefradil has no effect on capsaicin-induced allodynia, i.t.-administered mibefradil both potently reverses mechanical allodynia in a dose range similar to that for intrathecal morphine (ED_{50} = 9.2 and 4.1 μ g for mibefradil and morphine, respectively) and is also antinociceptive in both the early and late phases of the formalin response [Barton et al., 2005]. In contrast to that for ethosuximide, mibefradil (up to 30 μ g/rat i.t.) is without effect in the acute tail flick reflex. Dogrul and coworkers also observed no effect of i.t.-administered mibefradil in the rat acute tail-flick assay but found that mibefradil significantly potentiates the ability of low-dose i.t. morphine to prolong response latency (a 5-fold increase in ED_{50} for morphine) and that the response is specific for the μ -opioid receptor subtype (a 30-fold increase in the ED_{50} for DAMGO) [Dogrul et al., 2001]. While mibefradil was removed from the market for issues related to drug-drug interactions, it may yet represent an attractive chemical backbone for the further development of selective T-type calcium channel antagonists.

Efonidipine

Efonidipine (Fig. 2) is an orally active antihypertensive with inhibitory effects on both L- and T-type calcium channels [Masumiya et al., 2000]. In baby hamster kidney (BHK) cells and *Xenopus* oocytes, efonidipine (mixture of R(-) and S(+)-isomers) inhibits exogenously expressed HVA α_{1C} (L-type) calcium currents with IC_{50} values ranging from 0.5 to 2 μ M (BHK cells) to 8 to 20 μ M (oocytes). It also blocks the cloned Cav3.1 T-type calcium channel with similar affinities in both cell types [Furukawa et al.,

2004]. Interestingly, the R(-)-efonidipine isomer selectively blocks Cav3.1 T-type channels. Inhibition is frequency-dependent, with an increasing potency at higher stimulation frequencies. In fact, in myocardial cells, efonidipine was shown to inhibit native T-type calcium currents in a frequency-dependent manner with IC_{50} values of 13 nM, 2 μ M, and 6.3 μ M with stimulation frequencies of 1, 0.2, and 0.05 Hz, respectively [Masumiya et al., 2000]. Clinically, efonidipine decreases heart rate and has favourable effects on the nervous system supporting its significance in improving the prognosis in patients with hypertension and its protective influence on the heart and other organs [Harada et al., 2003].

ω -3 fatty acids

The cis-polyunsaturated ω -3 fatty acids are essential dietary agents that exhibit a range of physiological effects including possessing both cardioprotective and neuroprotective activities. At least in part, their protective effects may result from their blockade of voltage-gated sodium channels and HVA L-type calcium channels resulting in reduced electrical excitability in cardiac muscle and neurons [for review, see van der Stelt and Di Marzo, 2005]. More recently, Enyeart and colleagues found that the ω -3 fatty acids docosahexaenoic acid (DHA; Fig 2), eicosapentaenoic acid, and α -linolenic acid also inhibit native T-type calcium channels at potencies significantly higher than that for the clinically utilized succinimides [Danthi et al., 2005]. Block of whole cell T-type currents by the ω -3 fatty acids in bovine adrenal zona fasciculata cells occurs with IC_{50} s ranging from 2.5 to 14 μ M and is accompanied by changes in T-type channel voltage-dependent and kinetic parameters. DHA in particular shows significant use-dependent inhibition, suggestive of a preferential interaction with T-type channel open or inactivated states, and a characteristic of most clinical ion channel blocking agents that exhibit good therapeutic ratios. The major T-type channel isoform expressed in zona glomerulosa cells is reported to be Cav3.2 [Schrier et al., 2001], the same subtype implicated in primary afferent nociceptive behaviour and it will, therefore, be interesting to examine the effects of DHA on both acute and neuropathic pain states. A significant number of ω -3 fatty acid derivatives have already been synthesized around this backbone and, given the abundance of DHA in the human diet, both DHA and its metabolites should prove relatively safe [Itoh et al., 2006].

Anandamide

Endocannabinoids are highly lipophilic molecules thought to act as retrograde messengers and to protect,

in part, against excitotoxicity by modulating neuronal excitability. Anandamide (N-arachidonyl-ethanolamine; Fig. 2) is an endogenous CB1 cannabinoid receptor ligand that mimics many of the psychoactive effects of δ^9 -tetrahydrocannabinol, the most widely recognized active component of marijuana [Lambert and Fowler, 2005]. Anandamide has also been shown to activate TRPV1 vanilloid and $\alpha 7$ -nicotinic acetylcholine receptors, to inhibit Kv1.2 and TASK-1 potassium channels, and to bind to the 1,4-dihydropyridine site of L-type calcium channels, although the exact physiological consequences of these interactions remain unknown.

Independent of CB1 receptors, at sub-micromolar concentrations anandamide has also been shown to block the Cav3.2 T-type calcium channel (IC_{50} \sim 300 nM for Cav3.2) and at micromolar concentrations to inhibit Cav3.1 and Cav3.3 T-type channels (IC_{50} \sim 4 μ M for Cav3.1 and 1 μ M for Cav3.3) [Chemin et al., 2001]. Anandamide does not affect T-type activation properties but blockade is strongly dependent upon the channel inactivation state and would therefore result in a significant decrease in the available window current. In the case of Cav3.3 channels, the potency of a block by anandamide could be increased \sim tenfold (IC_{50} \sim 100 nM) under depolarizing waveforms that mimic thalamocortical firing activity. Of particular relevance, unlike that for the effects of cannabinoids on the high threshold N-type and P/Q-type calcium channels [Mackie and Hille, 1992], anandamide blockade of the T-type channels appears to be a result of direct binding to the channel and is independent of G-proteins, phospholipases, and protein kinases. Similar to that for DHA, it will be interesting to examine the effects of both peripherally and centrally administered anandamide on acute and neuropathic pain states. While the psychoactive effects of anandamide likely precluded the use of this agent for the treatment of pain (at least centrally), there exists considerable room for the development of structurally related derivatives.

POTENTIAL ADVERSE EFFECTS OF CAV3.2 T-TYPE CHANNEL BLOCKADE?

Implication of the Cav3.2 T-type calcium channel in pain mechanisms raises a whole new series of clinically relevant issues that may require addressing. For example, gene knockout of the Cav3.2 T-type channel gene in mice has been shown to result in abnormal cardiovascular function including constitutively constricted coronary arterioles and focal myocardial fibrosis [Chen et al., 2003a]. T-type calcium channels are known to be critically involved in early development and neuritogenesis; thus, there also may be developmentally related issues of concern [Chemin

et al., 2002; McCobb et al., 1989]. T-type calcium channels are also implicated in the calcium-dependent secretion of a variety of hormones from endocrine tissues and the Cav3.2 channel appears selectively expressed in the adrenal cortex and implicated in aldosterone secretion [Schrier et al., 2001]. What might be the physiological consequences of long-term blockade of this channel aimed at treating chronic/neuropathic pain conditions? In isolation, these issues may seem to raise a significant barrier to targeting the Cav3.2 T-type calcium channel. In fact, as described above a number of clinical agents that non-selectively target T-type calcium channels have been long used clinically, many with few apparent serious adverse effects. Additionally, as per the reality of many other clinical agents targeting voltage-gated ion channels (e.g., L-type calcium, sodium, and potassium channels), while many of the apparent physiological barriers in isolation might suggest the potential for serious clinical obstacles, these can often be overcome by the development of selective, state-dependent drugs that block a subset of pathophysiologically relevant target molecules.

ACKNOWLEDGMENTS

We thank Ms. Cynthia Chow and Dr. Hassan Pajouhesh for help with the figures and Dr. Emmanuel Bourinet for comments on the manuscript. The authors' work at the Michael Smith Laboratories is supported by an operating grant from the Canadian Institutes for Health Research and by a Canadian Research Tier 1 Chair in Neurobiology-Genomics. L.S.D. is supported by a fellowship from the Heart and Stroke Foundation of Canada.

REFERENCES

- Anderson JD, Hansen TP, Lenkowski PW, Walls AM, Choudhury IM, Schenck HA, Friehling M, Holl GM, Patel MK, Sikes RA, et al. 2003. Voltage-gated sodium channel blockers as cytostatic inhibitors of the androgen-independent prostate cancer cell line PC-3. *Mol Cancer Ther* 2:1149–1154.
- Backonja M, Beydoun A, Edwards KR, Schwartz SL, Fonseca V, Hes M, LaMoreaux L, Garofalo E. 1998. Gabapentin for the symptomatic treatment of painful neuropathy in patients with diabetes mellitus: a randomized controlled trial. *JAMA* 280: 1831–1836.
- Barton ME, Eberle EL, Shannon HE. 2005. The antihyperalgesic effects of the T-type calcium channel blockers ethosuximide, trimethadione, and mibefradil. *Eur J Pharmacol* 521:79–85.
- Bayer K, Ahmadi S, Zeilhofer HU. 2004. Gabapentin may inhibit synaptic transmission in the mouse spinal cord dorsal horn through a preferential block of P/Q-type Ca²⁺ channels. *Neuropharmacology* 46:743–749.
- Bourinet E, Soong TW, Stea A, Snutch TP. 1996. Determinants of the G protein-dependent opioid modulation of neuronal calcium channels. *Proc Natl Acad Sci USA* 93:1486–1491.
- Bourinet E, Alloui A, Monteil A, Barrere C, Couette B, Poirot O, Pages A, McRory J, Snutch TP, Eschalier A, et al. 2005. Silencing of the Cav3.2 T-type calcium channel gene in sensory neurons demonstrates its major role in nociception. *Embo J* 24:315–324.
- Brose WG, Gutlove DP, Luther RR, Bowersox SS, McGuire D. 1997. Use of intrathecal SNX-111, a novel, N-type, voltage-sensitive, calcium channel blocker, in the management of intractable brachial plexus avulsion pain. *Clin J Pain* 13:256–259.
- Brown JT, Randall A. 2005. Gabapentin fails to alter P/Q-type Ca²⁺ channel-mediated synaptic transmission in the hippocampus in vitro. *Synapse* 55:262–269.
- Caraceni A, Zecca E, Martini C, De Conno F. 1999. Gabapentin as an adjuvant to opioid analgesia for neuropathic cancer pain. *J Pain Symptom Manage* 17:441–445.
- Carbone E, Lux HD. 1984. A low voltage-activated, fully inactivating Ca channel in vertebrate sensory neurones. *Nature* 310: 501–502.
- Chemin J, Monteil A, Perez-Reyes E, Nargeot J, Lory P. 2001. Direct inhibition of T-type calcium channels by the endogenous cannabinoid anandamide. *Embo J* 20:7033–7040.
- Chemin J, Nargeot J, Lory P. 2002. Neuronal T-type alpha 1H calcium channels induce neuritegenesis and expression of high-voltage-activated calcium channels in the NG108-15 cell line. *J Neurosci* 22:6856–6862.
- Chen CC, Lamping KG, Nuno DW, Barresi R, Prouty SJ, Lavoie JL, Cribbs LL, England SK, Sigmund CD, Weiss RM, et al. 2003a. Abnormal coronary function in mice deficient in alpha1H T-type Ca²⁺ channels. *Science* 302:1416–1418.
- Chen Y, Lu J, Pan H, Zhang Y, Wu H, Xu K, Liu X, Jiang Y, Bao X, Yao Z, et al. 2003b. Association between genetic variation of CACNA1H and childhood absence epilepsy. *Ann Neurol* 54: 239–243.
- Coulter DA, Huguenard JR, Prince DA. 1989. Characterization of ethosuximide reduction of low-threshold calcium current in thalamic neurons. *Ann Neurol* 25:582–593.
- Coulter DA, Huguenard JR, Prince DA. 1990. Differential effects of petit mal anticonvulsants and convulsants on thalamic neurones: calcium current reduction. *Br J Pharmacol* 100:800–806.
- Cribbs LL, Lee JH, Yang J, Satin J, Zhang Y, Daud A, Barclay J, Williamson MP, Fox M, Rees M, and others. 1998. Cloning and characterization of alpha1H from human heart, a member of the T-type Ca²⁺ channel gene family. *Circ Res* 83:103–109.
- Danthi SJ, Enyeart JA, Enyeart JJ. 2005. Modulation of native T-type calcium channels by omega-3 fatty acids. *Biochem Biophys Res Commun* 327:485–493.
- Di Trapani G, Mei D, Marra C, Mazza S, Capuano A. 2000. Gabapentin in the prophylaxis of migraine: a double-blind randomized placebo-controlled study. *Clin Ter* 151:145–148.
- Dogrul A, Yesilyurt O, Isimer A, Guzeldemir ME. 2001. L-type and T-type calcium channel blockade potentiate the analgesic effects of morphine and selective mu opioid agonist, but not to selective delta and kappa agonist at the level of the spinal cord in mice. *Pain* 93:61–68.
- Dogrul A, Gardell LR, Ossipov MH, Tulumay FC, Lai J, Porreca F. 2003. Reversal of experimental neuropathic pain by T-type calcium channel blockers. *Pain* 105:159–168.
- Drake ME Jr, Greathouse NI, Renner JB, Armentbright AD. 2004. Open-label zonisamide for refractory migraine. *Clin Neuropharmacol* 27:278–280.

- Dubreuil AS, Boukhaddaoui H, Desmadryl G, Martinez-Salgado C, Moshourab R, Lewin GR, Carroll P, Valmier J, Scamps F. 2004. Role of T-type calcium current in identified D-hair mechanoreceptor neurons studied in vitro. *J Neurosci* 24:8480–8484.
- Enyeart JJ, Biagi BA, Day RN, Sheu SS, Maurer RA. 1990a. Blockade of low and high threshold Ca²⁺ channels by diphenylbutylpiperidine antipsychotics linked to inhibition of prolactin gene expression. *J Biol Chem* 265:16373–16379.
- Enyeart JJ, Dirksen RT, Sharma VK, Williford DJ, Sheu SS. 1990b. Antipsychotic pimozide is a potent Ca²⁺ channel blocker in heart. *Mol Pharmacol* 37:752–757.
- Enyeart JJ, Biagi BA, Mlinar B. 1992. Preferential block of T-type calcium channels by neuroleptics in neural crest-derived rat and human C cell lines. *Mol Pharmacol* 42:364–372.
- Evans AR, Nicol GD, Vasko MR. 1996. Differential regulation of evoked peptide release by voltage-sensitive calcium channels in rat sensory neurons. *Brain Res* 712:265–273.
- Flatters SJ, Bennett GJ. 2004. Ethosuximide reverses paclitaxel- and vincristine-induced painful peripheral neuropathy. *Pain* 109:150–161.
- Foong FW, Satoh M, Takagi H. 1982. A newly devised reliable method for evaluating analgesic potencies of drugs on trigeminal pain. *J Pharmacol Methods* 7:271–278.
- Furukawa T, Miura R, Honda M, Kamiya N, Mori Y, Takeshita S, Isshiki T, Nukada T. 2004. Identification of R(-)-isomer of efonidipine as a selective blocker of T-type Ca²⁺ channels. *Br J Pharmacol* 143:1050–1057.
- Gee NS, Brown JP, Dissanayake VU, Offord J, Thurlow R, Woodruff GN. 1996. The novel anticonvulsant drug, gabapentin (Neurontin), binds to the alpha2delta subunit of a calcium channel. *J Biol Chem* 271:5768–5776.
- Gomora JC, Daud AN, Weiergraber M, Perez-Reyes E. 2001. Block of cloned human T-type calcium channels by succinimide antiepileptic drugs. *Mol Pharmacol* 60:1121–1132.
- Green MW, Selman JE. 1991. Review article: the medical management of trigeminal neuralgia. *Headache* 31:588–592.
- Guay DR. 2003. Oxcarbazepine, topiramate, zonisamide, and levetiracetam: potential use in neuropathic pain. *Am J Geriatr Pharmacother* 1:18–37.
- Harada K, Nomura M, Nishikado A, Uehara K, Nakaya Y, Ito S. 2003. Clinical efficacy of efonidipine hydrochloride, a T-type calcium channel inhibitor, on sympathetic activities. *Circ J* 67:139–145.
- Heron SE, Phillips HA, Mulley JC, Mazarib A, Neufeld MY, Berkovic SF, Scheffer IE. 2004. Genetic variation of CACNA1H in idiopathic generalized epilepsy. *Ann Neurol* 55:595–596.
- Herrero JF, Laird JM, Lopez-Garcia JA. 2000. Wind-up of spinal cord neurones and pain sensation: much ado about something? *Prog Neurobiol* 61:169–203.
- Hollingshead LM, Faulds D, Fitton A. 1992. Bepridil. A review of its pharmacological properties and therapeutic use in stable angina pectoris. *Drugs* 44:835–857.
- Hord AH, Denson DD, Chalfoun AG, Azevedo MI. 2003. The effect of systemic zonisamide (Zonegran) on thermal hyperalgesia and mechanical allodynia in rats with an experimental mononeuropathy. *Anesth Analg* 96:1700–1706.
- Houtchens MK, Richert JR, Sami A, Rose JW. 1997. Open label gabapentin treatment for pain in multiple sclerosis. *Mult Scler* 3:250–253.
- Huguenard JR. 1996. Low-threshold calcium currents in central nervous system neurons. *Annu Rev Physiol* 58:329–348.
- Huguenard JR. 2002. Block of T-Type Ca(2+) Channels is an important action of succinimide antiepileptic drugs. *Epilepsy Curr* 2:49–52.
- Huguenard JR, Prince DA. 1992. A novel T-type current underlies prolonged Ca(2+)-dependent burst firing in GABAergic neurons of rat thalamic reticular nucleus. *J Neurosci* 12:3804–3817.
- Ikeda H, Heinke B, Ruscheweyh R, Sandkuhler J. 2003. Synaptic plasticity in spinal lamina I projection neurons that mediate hyperalgesia. *Science* 299:1237–1240.
- Ino M, Yoshinaga T, Wakamori M, Miyamoto N, Takahashi E, Sonoda J, Kagaya T, Oki T, Nagasu T, Nishizawa Y, and others. 2001. Functional disorders of the sympathetic nervous system in mice lacking the alpha 1B subunit (Cav 2.2) of N-type calcium channels. *Proc Natl Acad Sci USA* 98:5323–5328.
- Itoh T, Murota I, Yoshikai K, Yamada S, Yamamoto K. 2006. Synthesis of docosahexaenoic acid derivatives designed as novel PPARgamma agonists and antidiabetic agents. *Bioorg Med Chem* 14:98–108.
- Jimenez C, Bourinet E, Leuranguer V, Richard S, Snutch TP, Nargeot J. 2000. Determinants of voltage-dependent inactivation affect Mibefradil block of calcium channels. *Neuropharmacology* 39:1–10.
- Khosravani H, Altier C, Simms B, Hamming KS, Snutch TP, Mezeyova J, McRory JE, Zamponi GW. 2004. Gating effects of mutations in the Cav3.2 T-type calcium channel associated with childhood absence epilepsy. *J Biol Chem* 279:9681–9684.
- Khosravani H, Bladen C, Parker DB, Snutch TP, McRory JE, Zamponi GW. 2005. Effects of Cav3.2 channel mutations linked to idiopathic generalized epilepsy. *Ann Neurol* 57:745–749.
- Kim C, Jun K, Lee T, Kim SS, McEnery MW, Chin H, Kim HL, Park JM, Kim DK, Jung SJ, et al. 2001. Altered nociceptive response in mice deficient in the alpha(1B) subunit of the voltage-dependent calcium channel. *Mol Cell Neurosci* 18:235–245.
- Kim D, Song I, Keum S, Lee T, Jeong MJ, Kim SS, McEnery MW, Shin HS. 2001. Lack of the burst firing of thalamocortical relay neurons and resistance to absence seizures in mice lacking alpha(1G) T-type Ca(2+) channels. *Neuron* 31:35–45.
- Kim D, Park D, Choi S, Lee S, Sun M, Kim C, Shin HS. 2003. Thalamic control of visceral nociception mediated by T-type Ca²⁺ channels. *Science* 302:117–119.
- Kito M, Maehara, Watanabe K. 1996. Mechanisms of T-type calcium channel blockade by zonisamide. *Seizure* 5:115–119.
- Laird MA, Gidal BE. 2000. Use of gabapentin in the treatment of neuropathic pain. *Ann Pharmacother* 34:802–807.
- Lambert DM, Fowler CJ. 2005. The endocannabinoid system: drug targets, lead compounds, and potential therapeutic applications. *J Med Chem* 48:5059–5087.
- Lechin F, van der Dijs B, Lechin ME, Amat J, Lechin AE, Cabrera A, Gomez F, Acosta E, Arocha L, Villa S, et al. 1989. Pimozide therapy for trigeminal neuralgia. *Arch Neurol* 46:960–963.
- Lee JH, Daud AN, Cribbs LL, Lacerda AE, Pereverzev A, Klockner U, Schneider T, Perez-Reyes E. 1999. Cloning and expression of a novel member of the low voltage-activated T-type calcium channel family. *J Neurosci* 19:1912–1921.
- Li CY, Song YH, Higuera ES, Luo ZD. 2004. Spinal dorsal horn calcium channel alpha2delta-1 subunit upregulation contributes

- to peripheral nerve injury-induced tactile allodynia. *J Neurosci* 24:8494–8499.
- Li Y, Sato T, Arita M. 1999. Bepridil blunts the shortening of action potential duration caused by metabolic inhibition via blockade of ATP-sensitive K(+) channels and Na(+)-activated K(+) channels. *J Pharmacol Exp Ther* 291:562–568.
- Lingamaneni R, Hemmings HC Jr. 1999. Effects of anticonvulsants on veratridine- and KCl-evoked glutamate release from rat cortical synaptosomes. *Neurosci Lett* 276:127–130.
- Llinas R, Yarom Y. 1981a. Electrophysiology of mammalian inferior olivary neurones in vitro. Different types of voltage-dependent ionic conductances. *J Physiol* 315:549–567.
- Llinas R, Yarom Y. 1981b. Properties and distribution of ionic conductances generating electroresponsiveness of mammalian inferior olivary neurones in vitro. *J Physiol* 315:569–584.
- Luo ZD, Calcutt NA, Higuera ES, Valder CR, Song YH, Svensson CI, Myers RR. 2002. Injury type-specific calcium channel alpha 2 delta-1 subunit up-regulation in rat neuropathic pain models correlates with antiallodynic effects of gabapentin. *J Pharmacol Exp Ther* 303:1199–1205.
- Mackie K, Hille B. 1992. Cannabinoids inhibit N-type calcium channels in neuroblastoma-glioma cells. *Proc Natl Acad Sci USA* 89:3825–3829.
- Marais E, Klugbauer N, Hofmann F. 2001. Calcium channel alpha(2)delta subunits-structure and Gabapentin binding. *Mol Pharmacol* 59:1243–1248.
- Martin RL, Lee JH, Cribbs LL, Perez-Reyes E, Hanck DA. 2000. Mibefradil block of cloned T-type calcium channels. *J Pharmacol Exp Ther* 295:302–308.
- Masumiya H, Kase J, Tanaka Y, Tanaka H, Shigenobu K. 2000. Frequency-dependent blockade of T-type Ca²⁺ current by efonidipine in cardiomyocytes. *Life Sci* 68:345–351.
- Matthews EA, Dickenson AH. 2001. Effects of ethosuximide, a T-type Ca(2+) channel blocker, on dorsal horn neuronal responses in rats. *Eur J Pharmacol* 415:141–149.
- McCleane GJ. 1999. Intravenous infusion of phenytoin relieves neuropathic pain: a randomized, double-blinded, placebo-controlled, crossover study. *Anesth Analg* 89:985–988.
- McCobb DP, Best PM, Beam KG. 1989. Development alters the expression of calcium currents in chick limb motoneurons. *Neuron* 2:1633–1643.
- McCormick DA, Huguenard JR. 1992. A model of the electrophysiological properties of thalamocortical relay neurons. *J Neurophysiol* 68:1384–1400.
- McGuire D, Bowersox S, Fellmann JD, Luther RR. 1997. Sympatholysis after neuron-specific, N-type, voltage-sensitive calcium channel blockade: first demonstration of N-channel function in humans. *J Cardiovasc Pharmacol* 30:400–403.
- McRory JE, Santi CM, Hamming KS, Mezeyova J, Sutton KG, Baillie DL, Stea A, Snutch TP. 2001. Molecular and functional characterization of a family of rat brain T-type calcium channels. *J Biol Chem* 276:3999–4011.
- Mimaki T, Suzuki Y, Tagawa T, Karasawa T, Yabuuchi H. 1990. Interaction of zonisamide with benzodiazepine and GABA receptors in rat brain. *Med J Osaka Univ* 39:13–17.
- Mittman S, Guo J, Emerick MC, Agnew WS. 1999. Structure and alternative splicing of the gene encoding alphaII, a human brain T calcium channel alpha subunit. *Neurosci Lett* 269:121–124.
- Monteil A, Chemin J, Bourinet E, Mennessier G, Lory P, Nargeot J. 2000a. Molecular and functional properties of the human alpha(1G) subunit that forms T-type calcium channels. *J Biol Chem* 275:6090–6100.
- Monteil A, Chemin J, Leuranguer V, Altier C, Mennessier G, Bourinet E, Lory P, Nargeot J. 2000b. Specific properties of T-type calcium channels generated by the human alpha II subunit. *J Biol Chem* 275:16530–16535.
- Nelson MT, Joksovic PM, Perez-Reyes E, Todorovic SM. 2005. The endogenous redox agent L-cysteine induces T-type Ca²⁺ channel-dependent sensitization of a novel subpopulation of rat peripheral nociceptors. *J Neurosci* 25:8766–8775.
- Nowicky MC, Fox AP, Tsien RW. 1985. Three types of neuronal calcium channel with different calcium agonist sensitivity. *Nature* 316:440–443.
- Opler LA, Feinberg SS. 1991. The role of pimozide in clinical psychiatry: a review. *J Clin Psychiatry* 52:221–233.
- Peloquin JB, Khosravani H, Barr W, Bladen C, Evans R, Mezeyova J, Parker DB, Snutch TP, McRory JE, Zamponi GW. 2006. Functional analysis of Cav3.2 T-type calcium channel mutations linked to childhood absence epilepsy. *Epilepsia* 47:655–658.
- Perez-Reyes E. 2003. Molecular physiology of low-voltage-activated t-type calcium channels. *Physiol Rev* 83:117–161.
- Perez-Reyes E, Cribbs LL, Daud A, Lacerda AE, Barclay J, Williamson MP, Fox M, Rees M, Lee JH. 1998. Molecular characterization of a neuronal low-voltage-activated T-type calcium channel. *Nature* 391:896–900.
- Ridgeway B, Wallace M, Gerayli A. 2000. Ziconotide for the treatment of severe spasticity after spinal cord injury. *Pain* 85:287–289.
- Rowbotham M, Harden N, Stacey B, Bernstein P, Magnus-Miller L. 1998. Gabapentin for the treatment of postherpetic neuralgia: a randomized controlled trial. *JAMA* 280:1837–1842.
- Saddi G, Abbott FV. 2000. The formalin test in the mouse: a parametric analysis of scoring properties. *Pain* 89:53–63.
- Saegusa H, Kurihara T, Zong S, Kazuno A, Matsuda Y, Nonaka T, Han W, Toriyama H, Tanabe T. 2001. Suppression of inflammatory and neuropathic pain symptoms in mice lacking the N-type Ca²⁺ channel. *Embo J* 20:2349–2356.
- Sakaue A, Honda M, Tanabe M, Ono H. 2004. Antinociceptive effects of sodium channel-blocking agents on acute pain in mice. *J Pharmacol Sci* 95:181–188.
- Santi CM, Cayabyab FS, Sutton KG, McRory JE, Mezeyova J, Hamming KS, Parker D, Schauf CL. 1987. Zonisamide enhances slow sodium inactivation in *Myxicola*. *Brain Res* 413:185–188.
- Schrier AD, Wang H, Talley EM, Perez-Reyes E, Barrett PQ. 2001. alpha H T-type Ca²⁺ channel is the predominant subtype expressed in bovine and rat zona glomerulosa. *Am J Physiol Cell Physiol* 280:C265–C272.
- Schroeder JE, Fischbach PS, McCleskey EW. 1990. T-type calcium channels: heterogeneous expression in rat sensory neurons and selective modulation by phorbol esters. *J Neurosci* 10:947–951.
- Scroggs RS, Fox AP. 1992. Calcium current variation between acutely isolated adult rat dorsal root ganglion neurons of different size. *J Physiol* 445:639–658.
- Shin JB, Martinez-Salgado C, Heppenstall PA, Lewin GR. 2003. A T-type calcium channel required for normal function of a mammalian mechanoreceptor. *Nat Neurosci* 6:724–730.

- Snutch TP. 2005. Targeting chronic and neuropathic pain: the N-type calcium channel comes of age. *NeuroRx* 2:662–670.
- Soldo BL, Moises HC. 1998. μ -opioid receptor activation inhibits N- and P-type Ca^{2+} channel currents in magnocellular neurones of the rat supraoptic nucleus. *J Physiol* 513:787–804.
- Staats PS, Yearwood T, Charapata SG, Presley RW, Wallace MS, Byas-Smith M, Fisher R, Bryce DA, Mangieri EA, Luther RR, et al. 2004. Intrathecal ziconotide in the treatment of refractory pain in patients with cancer or AIDS: a randomized controlled trial. *JAMA* 291:63–70.
- Stea A, Snutch TP. 2002. Differential inhibition of T-type calcium channels by neuroleptics. *J Neurosci* 22:396–403.
- Sutton KG, Snutch TP. 2002. Gabapentin: A novel analgesic targeting voltage-gated Ca channels. *Drug Dev Res* 54:167–172.
- Suzuki S, Kawakami K, Nishimura S, Watanabe Y, Yagi K, Seino M, Miyamoto K. 1992. Zonisamide blocks T-type calcium channels in cultured neurons of cerebral cortex. *Epilepsy Res* 12:21–27.
- Takahashi Y, Hashimoto K, Tsuji S. 2004. Successful use of zonisamide for central poststroke pain. *J Pain* 5:192–194.
- Todorovic SM, Perez-Reyes E, Lingle CJ. 2000. Anticonvulsants but not general anesthetics have differential blocking effects on different T-type current variants. *Mol Pharmacol* 58:98–108.
- Todorovic SM, Jevtovic-Todorovic V, Meyenburg A, Mennerick S, Perez-Reyes E, Romano C, Olney JW, Zorumski CF. 2001. Redox modulation of T-type calcium channels in rat peripheral nociceptors. *Neuron* 31:75–85.
- Todorovic SM, Meyenburg A, Jevtovic-Todorovic V. 2004. Redox modulation of peripheral T-type Ca^{2+} channels in vivo: alteration of nerve injury-induced thermal hyperalgesia. *Pain* 109:328–339.
- Tsakiridou E, Bertollini L, de Curtis M, Avanzini G, Pape HC. 1995. Selective increase in T-type calcium conductance of reticular thalamic neurons in a rat model of absence epilepsy. *J Neurosci* 15:3110–3117.
- Twombly DA, Yoshii M, Narahashi T. 1988. Mechanisms of calcium channel block by phenytoin. *J Pharmacol Exp Ther* 246:189–195.
- Uchino T, Lee TS, Kaku T, Yamashita N, Noguchi T, Ono K. 2005. Voltage-dependent and frequency-independent inhibition of recombinant Cav3.2 T-type Ca^{2+} channel by bepridil. *Pharmacology* 74:174–181.
- van der Stelt M, Di Marzo V. 2005. Anandamide as an intracellular messenger regulating ion channel activity. *Prostaglandin Other Lipid Mediat* 77:111–122.
- Vitko I, Chen Y, Arias JM, Shen Y, Wu XR, Perez-Reyes E. 2005. Functional characterization and neuronal modeling of the effects of childhood absence epilepsy variants of CACNA1H, a T-type calcium channel. *J Neurosci* 25:4844–4855.
- Wang JC, Kiyosue T, Kiriya M, Arita M. 1999. Bepridil differentially inhibits two delayed rectifier $\text{K}^{(+)}$ currents, $\text{I}(\text{Kr})$ and $\text{I}(\text{Ks})$, in guinea-pig ventricular myocytes. *Br J Pharmacol* 128:1733–1738.
- Yajnik S, Singh GP, Singh G, Kumar M. 1992. Phenytoin as a coanalgesic in cancer pain. *J Pain Symptom Manage* 7:209–213.
- Yatani A, Brown AM, Schwartz A. 1986. Bepridil block of cardiac calcium and sodium channels. *J Pharmacol Exp Ther* 237:9–17.
- Zamponi GW, Snutch TP. 1998. Decay of prepulse facilitation of N type calcium channels during G protein inhibition is consistent with binding of a single G β subunit. *Proc Natl Acad Sci USA* 95:4035–4039.
- Zamponi GW, Bourinet E, Nelson D, Nargeot J, Snutch TP. 1997. Crosstalk between G proteins and protein kinase C mediated by the calcium channel α_1 subunit. *Nature* 385:442–446.
- Zhu G, Okada M, Murakami T, Kawata Y, Kamata A, Kaneko S. 2002. Interaction between carbamazepine, zonisamide and voltage-sensitive Ca^{2+} channel on acetylcholine release in rat frontal cortex. *Epilepsy Res* 49:49–60.

APPENDIX 2: SELECTIVE INHIBITION OF Ca_v3.3 T-TYPE CALCIUM CHANNELS BY G_{αq/11}-COUPLED MUSCARINIC ACETYLCHOLINE RECEPTORS

THE JOURNAL OF BIOLOGICAL CHEMISTRY VOL. 282, NO. 29, PP. 21043–21055, JULY 20, 2007
© 2007 by The American Society for Biochemistry and Molecular Biology, Inc. Printed in the U.S.A.

Selective Inhibition of Cav3.3 T-type Calcium Channels by G_{αq/11}-coupled Muscarinic Acetylcholine Receptors*

Received for publication, December 26, 2006, and in revised form, April 19, 2007. Published, JBC Papers in Press, May 29, 2007, DOI 10.1074/jbc.M611809200

Michael E. Hildebrand[‡], Laurence S. David[‡], Jawed Hamid[‡], Kirk Mulatz[‡], Esperanza Garcia[‡], Gerald W. Zamponi[§], and Terrance P. Snutch^{‡1}

From the [‡]Michael Smith Laboratories, University of British Columbia, Vancouver, British Columbia V6T 1Z4 and the [§]Hotchkiss Brain Institute, University of Calgary, Calgary, Alberta T2N 4N1, Canada

T-type calcium channels play critical roles in controlling neuronal excitability, including the generation of complex spiking patterns and the modulation of synaptic plasticity, although the mechanisms and extent to which T-type Ca²⁺ channels are modulated by G-protein-coupled receptors (GPCRs) remain largely unexplored. To examine specific interactions between T-type Ca²⁺ channel subtypes and muscarinic acetylcholine receptors (mAChRs), the Cav3.1 (α_{1G}), Cav3.2 (α_{1H}), and Cav3.3 (α_{1I}) T-type Ca²⁺ channels were co-expressed with the M1 G_{αq/11}-coupled mAChR. Perforated patch recordings demonstrate that activation of M1 receptors has a strong inhibitory effect on Cav3.3 T-type Ca²⁺ currents but either no effect or a moderate stimulating effect on Cav3.1 and Cav3.2 peak current amplitudes. This differential modulation was observed for both rat and human T-type Ca²⁺ channel variants. The inhibition of Cav3.3 channels by M1 receptors is reversible, use-independent, and associated with a concomitant increase in inactivation kinetics. Loss-of-function experiments with genetically encoded antagonists of G_α and G_{βγ} proteins and gain-of-function experiments with genetically encoded G_α subtypes indicate that M1 receptor-mediated inhibition of Cav3.3 occurs through G_{αq/11}. This is supported by experiments showing that activation of the M3 and M5 G_{αq/11}-coupled mAChRs also causes inhibition of Cav3.3 currents, although G_{α_i}-coupled mAChRs (M2 and M4) have no effect. Examining Cav3.1-Cav3.3 chimeric channels demonstrates that two distinct regions of the Cav3.3 channel are necessary and sufficient for complete M1 receptor-mediated channel inhibition and represent novel sites not previously implicated in T-type channel modulation.

T-type calcium channels play critical roles in shaping the electrical, chemical, and plastic properties of neurons through-

out the central and peripheral nervous systems. In thalamic reticular and relay neurons, T-type channels are involved in rhythmic rebound burst firing and spindle waves associated with slow-wave sleep (1–5). Studies on knock-out mice and a rat model of absence epilepsy indicate that altering T-type activity within thalamic cells can contribute to pathological conditions such as sleep disorders and epilepsy (1–5). Certain human epilepsies appear to be associated with T-type Ca²⁺ channel point mutations conferring channel gain-of-function phenotype (6–9). T-type channels also play crucial roles in dendritic integration and Ca²⁺ spiking in hippocampal pyramidal cells (10, 11). Within the olfactory bulb, T-type channels are implicated in modulating Ca²⁺ transients and synaptic release at dendrodendritic synapses (12, 13). In the periphery, antisense oligonucleotides and pharmacological approaches have implicated T-type channels in contributing to both acute and chronic nociceptive behaviors (14, 15).

Previous studies have identified three main subtypes of T-type Ca²⁺ channel α₁ subunits (Cav3.1/α_{1G}, Cav3.2/α_{1H} and Cav3.3/α_{1I}) and characterized their voltage-dependent, kinetic, and pharmacological properties (16–21). Cav3.1 and Cav3.2 channels display “typical” T-type properties, including relatively small conductance, fast activation and inactivation kinetics, and slow deactivation kinetics, whereas Cav3.3 channels uniquely display a larger conductance, much slower activation and inactivation kinetics, as well as faster deactivation kinetics (17, 19). Some of the distinct biophysical properties associated with Cav3.3 T-type currents have been observed in certain populations of native T-type currents (4, 17, 19, 22). The biophysical differences between the T-type channels likely enable them to differentially shape and modulate firing patterns, with the more slowly inactivating Cav3.3 currents able to produce longer bursts of spikes and tonic firing patterns (17, 23, 24).

Although the basic properties of both cloned and native T-type channels have now been largely characterized, there remains relatively little information concerning their modulation by GPCR²-linked pathways. Neurotransmitters such as acetylcholine have been shown to either attenuate or stimulate low threshold Ca²⁺ currents depending on the type of native cells examined, and sometimes multiple forms of modulation

* This work was supported in part by operating grants from the Canadian Institutes for Health Research and Canada Research Tier 1 Chairs (to T. P. S. and G. W. Z.), a fellowship from the Heart and Stroke Foundation of Canada, and trainee fellowships from the Natural Sciences and Engineering Research Council of Canada and Michael Smith Foundation for Health Research (to M. E. H.). The costs of publication of this article were defrayed in part by the payment of page charges. This article must therefore be hereby marked “advertisement” in accordance with 18 U.S.C. Section 1734 solely to indicate this fact.

¹ To whom correspondence should be addressed: Michael Smith Laboratories, University of British Columbia, 2185 East Mall, Vancouver, British Columbia V6T 1Z4, Canada. Tel: 604-822-6968; Fax: 604-822-6470; E-mail: snutch@mssl.ubc.ca.

² The abbreviations used are: GPCR, G-protein coupled receptor; mAChR, muscarinic acetylcholine receptor; pEGFP, enhanced green fluorescent protein; WT, wild type; PI(4,5)P₂, phosphatidylinositol 4,5-bisphosphate; CCh, carbachol; PLC, phospholipase C; PKC, protein kinase C; BAPTA-AM, 1,2-bis(2-aminophenoxy)ethane-N,N,N',N'-tetraacetic acid-acetoxymethyl ester.

JULY 20, 2007 • VOLUME 282 • NUMBER 29



JOURNAL OF BIOLOGICAL CHEMISTRY 21043



The Journal of Biological Chemistry



Downloaded from www.jbc.org at University of British Columbia on July 30, 2007

*A version of this appendix has been originally published in The Journal of Biological Chemistry. Hildebrand, M.E., David, L.S., Hamid, J., Mulatz, K., Garcia, E., Zamponi, G.W. and Snutch, T.P. (2007). Selective inhibition of Ca_v3.3 T-type calcium channels by G_{αq/11}-coupled muscarinic acetylcholine receptors. Journal of Biological Chemistry. 282(29), 21043–21055. © The American Society for Biochemistry and Molecular Biology.

Inhibition of Cav3.3 T-type Ca^{2+} Channels by mAChRs

can be observed within the same cell type (25–29). Multiple T-type Ca^{2+} channel subtypes are expressed in most native cells (30, 31), although pharmacological tools with the specificity needed to separate these currents have not been generated. In this regard, the description of the modulation of specific T-type Ca^{2+} channels in heterologous systems will provide insights crucial toward further investigations within native systems. This approach is also well suited for GPCR studies as most neurotransmitters activate multiple receptor subtypes in neurons.

Within thalamic reticular, hippocampal pyramidal, and olfactory granule cells, there is evidence for the expression of both T-type Ca^{2+} channels and $G\alpha_{q/11}$ -coupled muscarinic acetylcholine receptors (mAChRs) (25, 30–36). As both T-type Ca^{2+} currents and mAChRs have been independently shown to play important physiological roles within these cell types, their functional coupling could be relevant to a number of neuronal processes. Here we studied the modulatory effects of mAChRs on the three main subtypes of low threshold T-type Ca^{2+} channels expressed in the mammalian nervous system. We found the selective modulation of Cav3.3 Ca^{2+} channels by $G\alpha_{q/11}$ -coupled mAChRs and combined pharmacological, genetic, and chimeric channel approaches to examine the G-protein-mediated pathway and structural regions responsible for the distinct Cav3.3 signaling characteristics.

EXPERIMENTAL PROCEDURES

Molecular Biology—Human Cav3.1–Cav3.3 T-type Ca^{2+} channel α_1 subunit chimeras were constructed as described in detail by Hamid *et al.* (37).

Cell Culture and Transfection—Human embryonic kidney cells (HEK 293H, Invitrogen) were grown in standard Dulbecco's modified Eagle's medium (10% fetal bovine serum and 50 units/ml penicillin/streptomycin) to ~80% confluence and maintained at 37 °C in a humidified incubator with 95% atmosphere and 5% CO_2 . The generation of stable T-type cell lines (in HEK 293, tsa-201) expressing rat brain Cav3.1, Cav3.2, or Cav3.3 α_1 subunits has been described previously (16). Stable cell lines were transiently transfected with human muscarinic M1, M2, M3, M4, or M5 cDNAs (all in pcDNA3.1) using Lipofectamine (Invitrogen). As a reporter for transfection, all transient transfections included co-transfection with either CD8 or pEGFP marker plasmids at a 1:0.25 molar ratio compared with receptor and/or channel plasmid DNA, unless otherwise indicated. Lipofectamine-mediated transfections used 1–1.25 μ g of DNA/35-mm dish and 5 μ l of Lipofectamine/dish. In G-protein experiments, stable Cav3.3 cells were co-transfected with M1 receptors and equal amounts of either MAS-GRK3ct (in pcDNA3.1), $G\alpha_i$ (in pcDNA3.1), or RGS2 (in pEGFP) using Lipofectamine. Only MAS-GRK3ct and $G\alpha_i$ transfections required co-transfection with marker plasmids as RGS2 expression could be directly detected with fluorescence. In $G\alpha$ transfection experiments, stable Cav3.3 cells were transfected with constitutively active mutants of $G\alpha_q$, $G\alpha_{11}$, or $G\alpha_{13}$ ($G\alpha_{q-Q209L}$, $G\alpha_{11-Q209L}$, and $G\alpha_{13-Q226L}$, respectively, all in pcDNA3.1) using Lipofectamine. Twelve to 18 h after transfection, the medium was changed from Opti-MEM I to regular Dulbecco's modified Eagle's medium, and cells were transferred to a

28 °C incubator. The M1 to M5, $G\alpha_{q-Q209L}$, $G\alpha_{11-Q209L}$, and $G\alpha_{13-Q226L}$ cDNAs were all obtained from the UMR cDNA Resource Center (Rolla, MO), and the RGS2 and MAS-GRK3ct constructs were a generous gift from Dr. Brett Adams.

In separate experiments, HEK 293H cells were co-transfected with M1 and wild type (WT) or chimeric human Cav3.1 or Cav3.3 channels using standard Ca^{2+} phosphate transfection with 2 μ g of total cDNA/dish, 0.15 to 0.4 μ g of channel cDNA/dish, and 0.2 μ g of M1 cDNA/dish. In a subset of these experiments involving co-transfection of WT Cav3.3 and M1, either 200 μ M di-C8 PI(4,5) P_2 (Echelon Biosciences Inc., Salt Lake City, UT) or 50 μ g/ml PI(4,5) P_2 IgG $_{2b}$ antibody (~1:30 dilution) (Assay Designs, Ann Arbor, MI) was included in the internal solution to explore the role of PI(4,5) P_2 signaling. As the PI(4,5) P_2 antibody was supplied in a phosphate-buffered saline solution containing 10% calf serum and 0.05% sodium azide, the control Cav3.3 + M1 cells were recorded in an internal solution containing a 1:30 dilution of phosphate-buffered saline with 10% fetal bovine serum and 0.05% sodium azide. Electrophysiological recordings for all experiments were performed 24–48 h after transfection. Transiently transfected cells were selected for CD8 or pEGFP expression using either adherence of Dynabeads (Dyna, Great Neck, NY) or fluorescence of EGFP under UV light.

Electrophysiological Recordings and Analysis—Macroscopic currents were recorded using the perforated patch clamp technique to reduce current rundown and to preserve cytoplasmic signaling pathways. The external recording solution contained (in mM) 2 $CaCl_2$, 1 $MgCl_2$, 10 HEPES, 40 tetraethylammonium chloride, 92 CsCl, 10 glucose, pH 7.4, and the internal pipette solution contained (in mM) 120 Cs^+ methanesulfonate, 11 EGTA, 10 HEPES, 2 $MgCl_2$, 75–100 μ M β -escin, pH 7.2. For these perforated patch recordings, experimental recording did not begin until the series resistance was below 20 megohms and constant, as measured by amplifier compensation. Whole-cell recordings were used for the transiently transfected WT or chimeric human Cav3.1 and Cav3.3 channel experiments as well as the $G\alpha$ transfection experiments. The internal solution for these recordings contained (in mM) 120 Cs^+ methanesulfonate, 11 EGTA, 10 HEPES, 2 $MgCl_2$, 4 Mg-ATP, 0.3 sodium GTP. Macroscopic currents were recorded using Axopatch 200A and 200B amplifiers (Axon Instruments, Foster City, CA), controlled and monitored with Pentium 4 personal computers running pClamp software version 9 (Axon Instruments). Patch pipettes (borosilicate glass BF150-86-10; Sutter Instruments, Novato, CA) were pulled using a Sutter P-87 puller and polished with a Narishige (Tokyo, Japan) microforge, with typical resistances of 3–6 megohms when filled with internal solution. The bath was connected to the ground via a 3 M KCl agar bridge.

Data were low-pass filtered at 2 kHz using the built-in Bessel filter of the amplifier, with sampling at 10 kHz. The amplifier was also used for capacitance and series resistance compensation between 70 and 85% on every cell. Leak subtraction of capacitance and leakage current was performed on-line using a P/5 protocol or else performed with Clampfit (Axon Instruments) during off-line analysis. Figures and fittings utilized the software program Microcal Origin (version

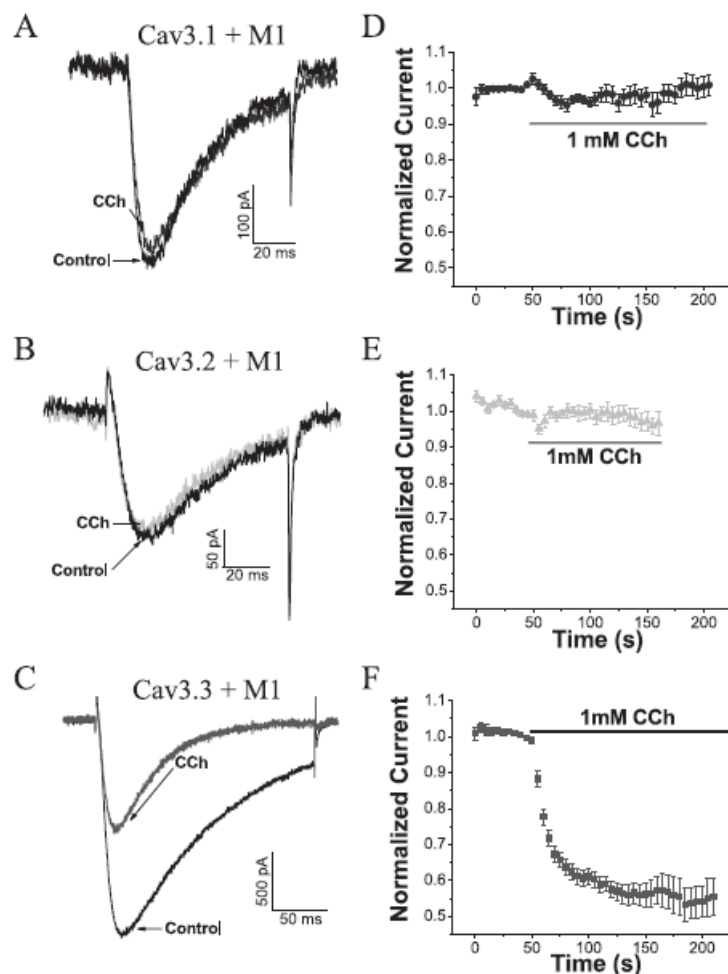
Inhibition of Cav3.3 T-type Ca^{2+} Channels by mAChRs

FIGURE 1. T-type Ca^{2+} channels are differentially modulated by M1 receptors. *A* and *B*, representative perforated patch current traces during depolarizing pulses from -110 to -30 mV demonstrating no effect on Cav3.1 currents (*A*) and Cav3.2 currents (*B*) when M1 is activated with 1 mM CCh. *D* and *E*, normalized peak current levels during perfusion of control recording solution (2 mM Ca^{2+}) followed by 1 mM CCh for Cav3.1 (+M1) currents (*D*) and Cav3.2 (+M1) currents (*E*). Perfusion of CCh usually had no effect on Cav3.1 peak current amplitudes ($-2.1 \pm 2.0\%$, $n = 18$) and Cav3.2 peak current amplitudes ($-0.1 \pm 2.3\%$, $n = 17$). *C*, representative perforated patch current traces during depolarizing pulses from -110 to -40 mV showing inhibition of Cav3.3 currents by M1. *F*, normalized peak current levels during perfusion of control recording solution (2 mM Ca^{2+}) followed by 1 mM CCh for Cav3.3 (+M1) currents. Perfusion of CCh caused a 45% ($\pm 2\%$, $n = 34$) decrease in Cav3.3 currents. All data points correspond to mean \pm S.E.

7.5, Northampton, MA). All recordings were performed at room temperature (20–22 °C).

The voltage dependence of activation for Cav3.1, Cav3.2, and Cav3.3 currents was measured by a series of 100–220-ms depolarizing pulses applied from a holding potential of -110 mV to membrane potentials from -80 to $+10$ mV, increasing at 5-mV increments, with 2 s between pulses. The potential that elicited peak currents ("peak potential" ranging from -45 to -25 mV) was obtained from this protocol and used in subsequent protocols. Series resistance was also monitored with a 5-ms depolarizing pulse to -105 mV immediately before the test pulse to

ensure that this variable was relatively constant, and any changes in peak current levels were not because of significant changes in series resistance. Effects of saturating concentrations of mAChR agonist (1 mM CCh) on stable T-type currents were then investigated using steps to peak potential every 5 s (0.2 Hz) from a holding potential of -110 mV. These depolarizing steps were 80 ms in duration for Cav3.1 and Cav3.2 and 200 ms in duration for Cav3.3. The -140 -mV prepulse protocol for Cav3.3 included a 1-s prepulse to -140 mV to remove any accumulated channel inactivation. To quantify the percent of channel inhibition, stimulation, or washout during CCh or control solution perfusion, the peak current magnitude at equilibrium was averaged (2–5 values). When distinct effects were observed (*i.e.* stimulation *versus* no effect of M1 on Cav3.1 currents), all cells displaying a $>10\%$ modulating effect with a clear exponential time course were grouped into one group, while the rest of the cells were grouped into the "no effect" group.

Current-voltage relationships were fitted with the modified Boltzmann equation, $I = (G_{\text{max}} \times (V_m - E_{\text{rev}})) / (1 + \exp((V_m - V_{0.5a})/k_a))$, where V_m is the test potential; $V_{0.5a}$ is the half-activation potential; E_{rev} is the extrapolated reversal potential; G_{max} is the maximum slope conductance, and k_a reflects the slope of the activation curve. Data from CCh concentration-response studies were fitted with the equation, $y = ((A_1 - A_2) / (1 + (x/x_0)^P)) + A_2$, where A_1 is initial amplitude ($=0$) and A_2 is final block value; x_0 is IC_{50} (concentration causing 50%

inhibition of currents), and P gives a measure of the steepness of the curve. The activation and inactivation rates during steps to peak potential were well described by single exponential curves to give τ_{act} and τ_{inact} values, respectively. Statistical significance was tested with Student's *t* tests with significance being determined at a confidence interval of $p < 0.02$.

Solutions, Drugs, and Perfusion—A 25 mM stock of β -escin (in distilled H_2O) was prepared fresh, with dilution to working stocks in intracellular solution. Carbachol (CCh) was added directly to the extracellular recording solution. Wortmannin, okadaic acid, genistein, and H9 were all obtained from Tocris

Inhibition of Cav3.3 T-type Ca^{2+} Channels by mAChRs

TABLE 1
Effects of receptor activation on T-type channel kinetic and voltage-dependent properties

	2 mM Ca^{2+} control			1 mM carbachol		
	τ_{act} ms	τ_{inact} ms	V_{50act} mV	τ_{act} ms	τ_{inact} ms	V_{50act} mV
Cav3.3 + M1(inhibition)	6.0 ± 0.4, n = 27	86 ± 6, n = 27	-51 ± 2, n = 13	4.1 ± 0.3, n = 27 ^a	31 ± 2, n = 27 ^a	-49 ± 1, n = 13
Human Cav3.3 + M1(whole-cell; inhibition)	9.7 ± 0.8, n = 10	117 ± 6, n = 10	-44 ± 1, n = 4	5.4 ± 0.6, n = 10 ^a	41 ± 5, n = 10 ^a	-47 ± 1, n = 4
Cav3.3 + M2(no effect)	6.1 ± 0.7, n = 10	81 ± 9, n = 10	-53 ± 3, n = 4	5.5 ± 0.7, n = 10	76 ± 9, n = 10	-52 ± 3, n = 4
Cav3.3 + M3(inhibition)	9.5 ± 0.9, n = 9	104 ± 13, n = 9	-53 ± 4, n = 4	6.2 ± 0.6, n = 9 ^b	56 ± 6, n = 8 ^b	-50 ± 4, n = 4
Cav3.3 + M4(no effect)	6.7 ± 0.9, n = 6	110 ± 18, n = 6	-50 ± 1, n = 5	6.0 ± 0.9, n = 6	101 ± 16, n = 6	-51 ± 2, n = 5
Cav3.3 + M5(inhibition)	8.6 ± 0.9, n = 6	127 ± 23, n = 7	-48 ± 1, n = 5	5.6 ± 0.6, n = 6	49 ± 6, n = 7 ^b	-45 ± 1, n = 5
Cav3.3 + Control Plasmid	6.0 ± 0.4, n = 5	78 ± 13, n = 5		5.2 ± 0.2, n = 5	71 ± 12, n = 5	
Cav3.1 + M1(no effect)	2.3 ± 0.2, n = 17	19 ± 2, n = 17	-36 ± 2, n = 17	2.1 ± 0.2, n = 17	17 ± 1, n = 17	-39 ± 3, n = 11
Human Cav3.1 + M1(whole-cell; no effect)	2.0 ± 0.4, n = 9	14 ± 1, n = 9	-42 ± 2, n = 6	1.2 ± 0.1, n = 9	13 ± 1, n = 9	-51 ± 3, n = 4
Cav3.2 + M1(no effect)	4.7 ± 0.2, n = 16	36 ± 2, n = 15	-42 ± 1, n = 7	4.3 ± 0.2, n = 16	34 ± 2, n = 15	-40 ± 2, n = 7

^a $p < 0.001$.

^b $p < 0.02$.

Cookson (Ellisville, MO). (R_p)-cAMP was obtained from BioMol International (Plymouth Meeting, PA). BAPTA-AM was obtained from Molecular Probes (Eugene, OR). Unless otherwise stated, all other drugs were obtained from Sigma. Drugs were dissolved in either distilled H_2O or Me_2SO , according to manufacturer's solubility data. The highest concentration of Me_2SO in the recording solution did not exceed 0.1%, a concentration that did not detectably affect T-type properties (data not shown). Gravity-driven perfusion occurred at a rate of $\sim 400 \mu\text{l}/\text{min}$, and the outputs of the manifold were placed within close proximity of the cell, resulting in the cell being bathed in new solutions with minimal delay (within 1 s).

RESULTS

Muscarinic M1 Receptors Selectively Inhibit Cav3.3 T-type Ca^{2+} Channels—To investigate the potential for T-type Ca^{2+} channel modulation by mAChRs, we transiently transfected HEK cell lines stably expressing individual subtypes of recombinant rat brain T-type channels with the human muscarinic M1 receptor. Perforated patch recordings with β -escin demonstrated that activation of M1 with 1 mM CCh caused a rapid (< 30 s) and robust inhibition of exogenously expressed rat brain Cav3.3 T-type channel peak currents ($-45 \pm 2\%$, $n = 34$) (Fig. 1, C and F). Only a small subpopulation of stable Cav3.3 cells ($< 10\%$) was not affected by CCh application (likely representing cells untransfected with the M1 receptor).

Activation of M1 with 1 mM CCh had no significant effect ($p > 0.05$) on the voltage dependence of Cav3.3 currents but significantly increased both the rates of activation and inactivation ($p < 0.001$; Table 1). In contrast to the clear inhibition of Cav3.3 T-type currents, activation of M1 receptors with 1 mM CCh largely had no effect on the peak current amplitude of either rat brain Cav3.1 ($-2.1 \pm 2.0\%$, $n = 18$) or Cav3.2 channels ($-0.1 \pm 2.3\%$, $n = 17$) (Fig. 1, A, B, D, and E). In a small subset of both Cav3.1 and Cav3.2 currents we noted a stimulation induced by M1 activation (Cav3.1 = $35 \pm 12\%$, $n = 4$; Cav3.2 = $36 \pm 12\%$, $n = 5$), with a slower time course to equilibrium of greater than 1 min ($n = 3$ and $n = 4$, respectively). For the prevalent null effect on Cav3.1 and Cav3.2 currents, 1 mM CCh application had no significant effect on channel activation and inactivation kinetics or the voltage dependence of activation ($p > 0.05$; Table 1).

Different Cav3.3 T-type channel isoforms with distinct carboxyl termini have been identified from both the rat and human

brain (17, 19, 21, 38). To test whether inhibition of the Cav3.3 channel by M1 receptors was restricted to the rat brain short carboxyl-terminal isoform (17), we also examined the longer human Cav3.3 isoform (21) transiently co-transfected into HEK cells with the M1 receptor. Similar to that for the shorter rat brain isoform, application of 1 mM CCh resulted in significant inhibition of the human Cav3.3 peak current amplitude ($-28 \pm 2\%$, $n = 15$) and also significantly increased activation and inactivation kinetics ($p < 0.001$; Fig. 5A; Table 1). Additionally, similar to that for the rat Cav3.1 T-type channel, application of 1 mM CCh to HEK cells co-transfected with the human Cav3.1 channel and M1 receptor had no significant effect on peak current amplitude ($-0.3 \pm 2.0\%$, $n = 9$) or channel kinetics (for 100% cells tested; $p > 0.05$; Fig. 7B; Table 1). Overall, the differential modulation of T-type Ca^{2+} channel subtypes mediated by M1 receptors was consistent across both rat and human recombinant T-type channels.

Muscarinic M1 Receptors Dose-dependently Modulate Cav3.3 Biophysical Properties—Perforated patch recordings on stable rat Cav3.3 cells transiently transfected with M1 receptors revealed that the CCh-induced inhibition of peak current levels was reversible over a time course of about 2 min ($n = 13$; Fig. 2, A and B). As previously mentioned, activation of M1 receptors with 1 mM CCh caused a significant ($p < 0.001$) increase in inactivation kinetics (control, $\tau_{inact} = 86 \pm 6$, $n = 27$; 1 mM CCh, $\tau_{inact} = 31 \pm 2$, $n = 27$). Along with peak current inhibition, the CCh-induced increase in Cav3.3 inactivation kinetics was reversible (Fig. 2, A and C). Both the M1 receptor-induced inhibition of Cav3.3 peak currents and the increased inactivation rate would be predicted to reduce the total amount of Ca^{2+} flowing through Cav3.3 T-type channels during a cellular depolarization. The effect of M1 receptor activation on total Ca^{2+} influx was determined by integrating the area over Cav3.3 current traces during 200-ms depolarizing pulses to peak potential before and after 1 mM CCh application. Normalizing these Ca^{2+} influx values to control levels showed a $77 \pm 2\%$ ($n = 20$) reduction in Ca^{2+} influx mediated by M1 receptor activation (Fig. 2D).

As activation of M1 receptors increases the kinetics of Cav3.3 activation and inactivation, it is possible that this signaling pathway modulates Cav3.3 function via acting upon the open and/or inactivated states. A protocol that involved perfusion of 1 mM CCh for 50 s (time to reach normal inhibition equilib-

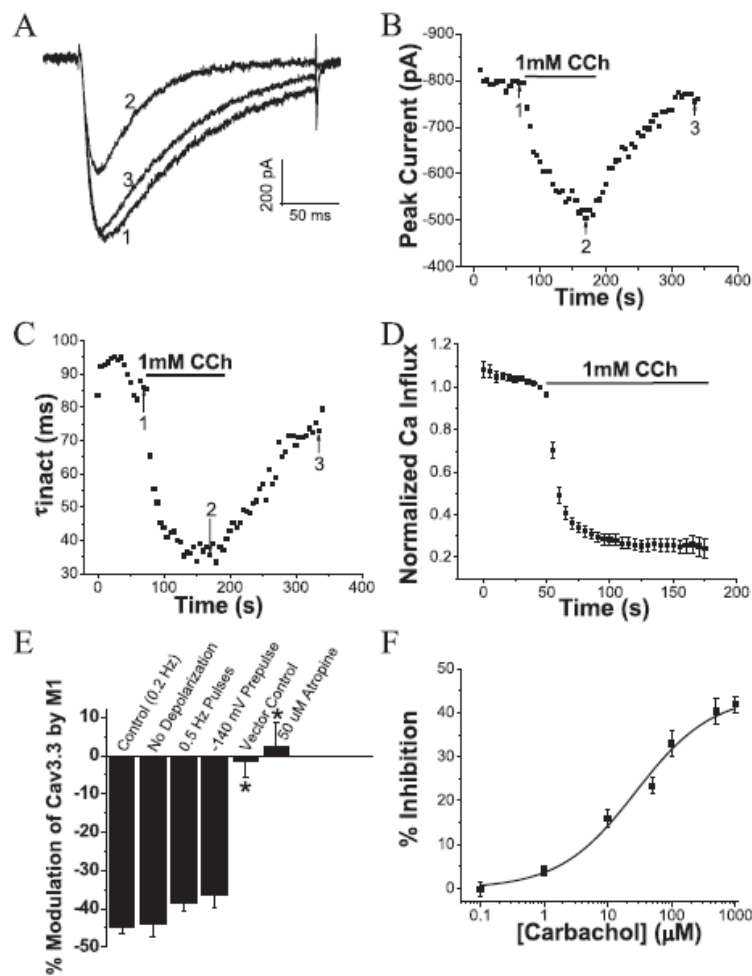
Inhibition of Cav3.3 T-type Ca^{2+} Channels by mAChRs

FIGURE 2. Mechanistic properties of inhibition of Cav3.3 currents by M1 receptors. A, Inhibition of Cav3.3 channels by M1 is reversible. Representative Cav3.3 perforated patch current traces during depolarizing pulses from -110 to -40 mV before (trace 1), during (trace 2), and after (trace 3) perfusion of 1 mM CCh. Note the increase in inactivation kinetics when CCh is applied (Table 1). B, Plot of peak current amplitude for same cell as in A showing the rate of inhibition by 1 mM CCh perfusion and the rate of washout, with the selected traces from A (traces 1–3) labeled. C, Application of 1 mM CCh increases Cav3.3 inactivation kinetics in a reversible manner. The inactivating component of every trace from B was fit with an exponential equation to give τ_{inact} . D, Application of 1 mM CCh dramatically reduces the amount of Ca^{2+} influx through Cav3.3 channels. The effects of M1 activation on normalized Ca^{2+} influx is shown for all Cav3.3 cells. Perfusion of 1 mM CCh caused a 77% ($\pm 2\%$, $n = 20$) decrease in Ca^{2+} influx. E, Inhibition of Cav3.3 currents by 1 mM CCh occurs through M1 receptors. Control experiments show elimination of the inhibition because of 1 mM CCh when a muscarinic antagonist (50 μM atropine) is co-applied or when a control vector (pBluescript) is transfected instead of M1. A lack of depolarizing test pulses during initial CCh perfusion, increase in test pulse frequency to 0.5 Hz, or a hyperpolarizing prepulse to -140 mV for 1 s had no significant ($p > 0.02$) effect on the magnitude of Cav3.3 inhibition by M1. * Indicates significance at $p < 0.001$ compared with control (0.2 Hz). F, CCh inhibited Cav3.3 currents in a dose-dependent manner. CCh concentration versus percentage block data were fit with a Hill equation, and the IC_{50} for CCh inhibition of Cav3.3 currents was 27 μM . All data points correspond to mean \pm S.E.

rium) in the absence of test pulses, followed by regular 0.2-Hz test pulses to peak potential, examined whether the M1 receptor-mediated inhibitory effect is use-dependent. Fig. 2E shows that this “no depolarization” protocol displayed the same level of inhibition of Cav3.3 currents observed in the regular 0.2-Hz

experiments, indicating that M1 effects on Cav3.3 are use-independent. Increasing the test pulse frequency to 0.5 Hz also caused no significant ($p > 0.05$) change in the level of Cav3.3 inhibition, indicating that the M1 effects on Cav3.3 are also frequency-independent (Fig. 2E). Another possibility is that M1 receptor activation inhibits Cav3.3 currents by shifting steady-state inactivation to more hyperpolarized potentials, reducing the proportion of channels available (in the closed state) to open at the holding potential of -110 mV. A protocol with a 1-s prepulse to -140 mV to remove accumulated channel inactivation demonstrated no significant ($p > 0.05$) difference in inhibition compared with the control protocol, suggesting that the inhibitory effect is not because of changes in the steady-state inactivation of Cav3.3 channels (Fig. 2E).

Control experiments with mock transfections of an empty control vector or with a preincubated mAChR antagonist (atropine) demonstrated that the CCh-induced inhibition of Cav3.3 currents is mediated specifically via the transfected M1 receptor (Fig. 2E). Testing the effects of varying concentrations of CCh on stable Cav3.3 cells with transfected M1 receptors revealed that the inhibitory effect is dose-dependent (Fig. 2F). The IC_{50} for inhibition of Cav3.3 currents by CCh = 27 μM , consistent with that reported for phosphatidylinositol hydrolysis triggered by M1 receptor activation in both HEK 293 and Chinese hamster ovary cells (39, 40).

Inhibition of Cav3.3 Channels by M1 Receptors Requires $\text{G}\alpha_{q/11}$ —The inhibitory effect of M1 receptor activation on Cav3.3 currents could occur either through $\text{G}\beta\gamma$ - or $\text{G}\alpha$ -mediated processes. To test for the involvement of $\text{G}\beta\gamma$, a membrane-targeted version of the carboxyl terminus of β -arrestin kinase, MAS-GRK3ct (41), was co-transfected with M1 receptors into the stable Cav3.3 HEK cell line. Control experiments showed that the MAS-GRK3ct construct was able to completely abolish the well described $\text{G}\beta\gamma$ -dependent inhibition of N-type Ca^{2+} channels (data not shown). MAS-GRK3ct only partially

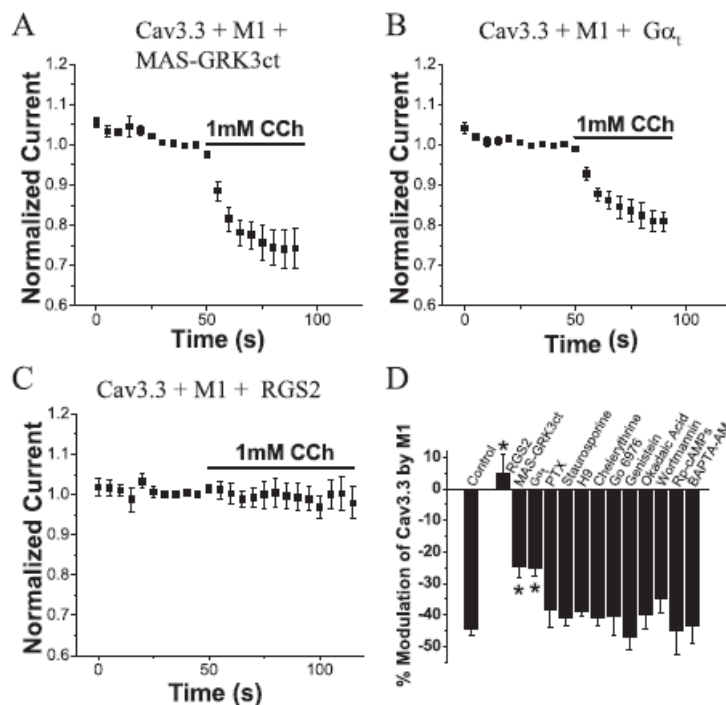
Inhibition of Cav3.3 T-type Ca^{2+} Channels by mAChRs

FIGURE 3. Inhibition of Cav3.3 channels by M1 requires $G\alpha_{q/11}$ signaling. *A*, In perforated patch recordings of Cav3.3 stable cells co-transfected with M1 and a membrane targeted form of the carboxyl terminus of β -arrestin kinase that sequesters active $G\beta\gamma$ subunits (MAS-GRK3ct), application of 1 mM CCh caused inhibition of Cav3.3 currents ($-24.8 \pm 3.4\%$, $n = 10$). *B*, Similarly, inhibition by perfusion of 1 mM CCh was observed for Cav3.3 cells co-transfected with the $G\beta\gamma$ buffer $G\alpha_{transducin}$ ($G\alpha_i$) and M1 ($-25.1 \pm 2.5\%$, $n = 10$). *C*, In perforated patch recordings of Cav3.3 cells co-transfected with M1 and RGS2 (antagonist of active $G\alpha_{q/11}$ subunits), application of 1 mM CCh predominantly had no effect ($1 \pm 5\%$, $n = 7$) on Cav3.3 currents. *D*, Bar graph comparing various genetic and pharmacological manipulations to control conditions where stable Cav3.3 cells are transfected with M1 and inhibited by 1 mM CCh. Inhibitors of serine/threonine kinases (500 nM staurosporine, $n = 7$; 50 μ M H9, $n = 6$), PKC (10 μ M chelerythrine, $n = 5$; 500 nM Go 6976, $n = 6$), tyrosine kinases (10 μ M genistein, $n = 7$), phosphatases (100 nM okadaic acid, $n = 6$), phosphoinositide 3-kinases (200 nM wortmannin, $n = 7$), PTX-sensitive $G\alpha$ proteins (0.5 μ g/ml PTX, $n = 6$), cAMP (10 μ M R_p -cAMP, $n = 5$), and internal Ca^{2+} (10 μ M BAPTA-AM, $n = 5$) had no significant effect ($p > 0.02$) on the inhibition of Cav3.3 currents by M1. RGS2, MAS-GRK3ct, and $G\alpha_i$ ($p < 0.001$) caused a significant elimination or reduction in the inhibition of Cav3.3 currents by M1. All data points correspond to mean \pm S.E. * Indicates significance at $p < 0.001$ compared with control.

reduced M1-mediated Cav3.3 current inhibition ($-24.8 \pm 3.4\%$, $n = 10$) in most cells, suggesting that inhibition is distinct from the previously reported pure $G\beta\gamma$ -mediated inhibition of N- and P/Q-type and Cav3.2 Ca^{2+} channels (42, 43) (Fig. 3, *A* and *D*). A smaller subset of MAS-GRK3ct co-transfected cells displayed no exponential inhibitory effect ($-9.3 \pm 3.0\%$, $n = 7$). Co-expression of transducin ($G\alpha_i$), which also buffers $G\beta\gamma$ signaling (41), caused the same reduction in M1-mediated inhibition of Cav3.3 currents ($-25.1 \pm 2.5\%$, $n = 10$), with a small number of cells not being inhibited at all ($7.0 \pm 10.1\%$, $n = 3$) (Fig. 3, *B* and *D*).

In contrast to the partial effect of $G\beta\gamma$ signaling antagonists, co-expression of the regulator of G-protein signaling 2 (RGS2), an effector antagonist for $G\alpha_{q/11}$ (44), completely prevented the M1 receptor-induced inhibition of Cav3.3 currents for all cells examined. In perforated patch recordings of Cav3.3 cells co-transfected with M1 and RGS2, application of 1 mM CCh either

had no effect (Fig. 3, *C* and *D*; $1\% \pm 5\%$, $n = 7$) or caused a stimulation of Cav3.3 currents ($30\% \pm 9\%$, $n = 5$). RGS2 has been thoroughly characterized and shown to be a selective GTPase-activating protein for $G\alpha_q/G\alpha_{11}$, but not for other $G\alpha$ proteins (44), and is an effector antagonist that does not block the $G\beta\gamma$ -mediated inhibition of R-type Ca^{2+} channels (45).

Constitutively Active $G\alpha_{q/11}$ Proteins Modulate Cav3.3 T-type Ca^{2+} Channels—To further test whether active $G\alpha_{q/11}$ G-proteins are sufficient to produce inhibition of Cav3.3 currents, stable Cav3.3 cells were transiently transfected with various constitutively active $G\alpha$ subunit constructs. These constructs contain missense mutations that confer constitutive activity by reducing GTPase activity. If $G\alpha_{q/11}$ is the downstream signal of M1 receptor activation mediating the effects on Cav3.3 currents, then it is hypothesized that activation of the co-expressed $G\alpha_q$ or $G\alpha_{11}$ mutants by dialysis of GTP would cause a reduction in current amplitude and an increase in inactivation kinetics. Similar to a study that analyzed inhibition of KCNQ2/KCNQ3 channels by $G\alpha_{q/11}$ (46), we used constitutively active $G\alpha_q$ ($G\alpha_{q-Q209L}$) and $G\alpha_{11}$ ($G\alpha_{11-Q209L}$) mutants to test for the hypothesized effect and a constitutively active $G\alpha$ protein ($G\alpha_{13-Q226L}$) that does not couple to the same

downstream effectors (PLC) as a negative control. We also performed controls wherein empty vectors were transfected. By comparing traces 30 s after forming the whole-cell configuration with traces 2 min after whole-cell in Fig. 4, *A–D*, we found that dialysis of the cell with the GTP-containing pipette internal solution caused both a significant reduction in peak current levels and an increase in inactivation kinetics only for the $G\alpha_{q-Q209L}$ and $G\alpha_{11-Q209L}$ transfections. The ratio of peak current levels at 2 min divided by the peak current levels at 30 s was significantly reduced ($p < 0.001$) for $G\alpha_{q-Q209L}$ ($n = 16$) and $G\alpha_{11-Q209L}$ ($n = 15$) compared with the control transfection ($n = 18$), whereas the $G\alpha_{13-Q226L}$ ($n = 17$) transfection current ratio was not significantly altered ($p > 0.05$, Fig. 4*E*). The rates of inactivation (τ_{inact}) were determined during depolarizing steps from -110 to -30 mV for all transfection types. The τ_{inact} was significantly faster ($p < 0.001$) for $G\alpha_{q-Q209L}$ and $G\alpha_{11-Q209L}$

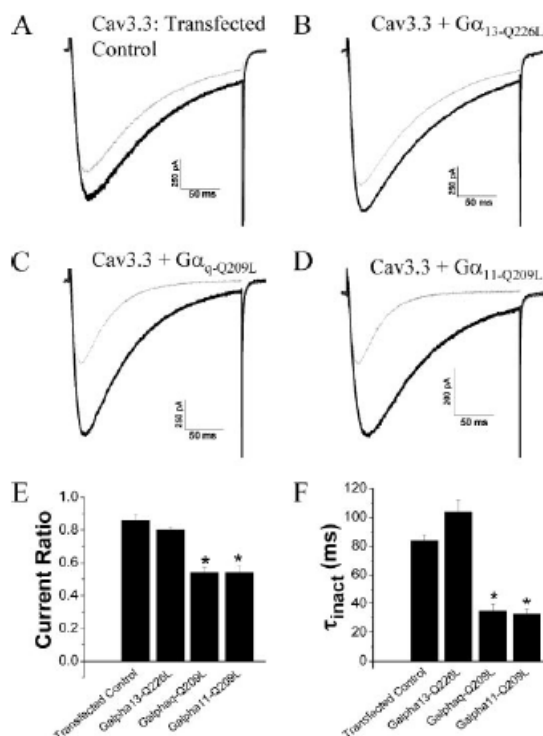


FIGURE 4. The $G\alpha_{q/11}$ subtypes of $G\alpha$ proteins specifically cause inhibition of Cav3.3 currents. A–D, representative whole-cell current traces of stable Cav3.3 cells transfected with various control or $G\alpha$ plasmids during depolarizing steps from -110 to -30 mV. Traces were obtained 30 s (black) and 2 min (gray) after the whole-cell conformation was formed, using an internal solution that contained 4 mM ATP and 0.3 mM GTP. The stable Cav3.3 cells were mock-transfected with empty plasmid (A) or transfected with the constitutively active forms (lack of GTPase activity) of $G\alpha$ proteins as follows: $G\alpha_{13-Q226L}$ (B), $G\alpha_{q-Q209L}$ (C), $G\alpha_{11-Q209L}$ (D). E, $G\alpha_{q-Q209L}$ and $G\alpha_{11-Q209L}$ cause a time-dependent reduction in Cav3.3 current magnitude. The peak current levels at 2 min were divided by the peak current levels at 30 s to determine the level of inhibition because of internal solution dialysis for the various types of transfected Cav3.3 cells, as described above. The Cav3.3 currents co-transfected with $G\alpha_{q-Q209L}$ and $G\alpha_{11-Q209L}$ had a significant ($p < 0.001$) reduction in current ratio compared with the control transfection, whereas the $G\alpha_{13-Q226L}$ transfection caused no significant change ($p > 0.05$). F, rate of inactivation (τ_{inact}) was determined during depolarizing steps from -110 to -30 mV for all transfection types. The τ_{inact} was significantly ($p < 0.001$) faster for $G\alpha_{q-Q209L}$ and $G\alpha_{11-Q209L}$ compared with control transfections, whereas the τ_{inact} was not significantly ($p > 0.02$) different for $G\alpha_{13-Q226L}$. All data points correspond to mean \pm S.E. * Indicates significance at $p < 0.001$ compared with transfected control.

compared with control transfections, whereas the τ_{inact} was not significantly different for $G\alpha_{13-Q226L}$ ($p > 0.02$; Fig. 4F).

$G\alpha_{q/11}$ Inhibits Cav3.3 Channels through an Unidentified Nonclassical Pathway—The active GTP-bound form of $G\alpha_{q/11}$ causes the activation of PLC, which then produces inositol 1,4,5-trisphosphate- and diacylglycerol/PKC-mediated signals. Various pharmacological antagonists were used to investigate the role of potential cellular signals downstream of $G\alpha_{q/11}$. Specific inhibitors of PKC, including 10 μ M chelerythrine ($n = 5$) and 500 nM Go 6976 ($n = 6$), had no significant ($p > 0.05$) effect on the M1-mediated inhibition of Cav3.3 currents (Fig. 3D). To

Inhibition of Cav3.3 T-type Ca^{2+} Channels by mAChRs

ensure pharmacological activity of these antagonists, the PKC-mediated stimulation of Cav3.2 channels by 300 nM phorbol 12-myristate 13-acetate ($65 \pm 17\%$, $n = 7$; see Ref 47) was shown to be significantly ($p < 0.02$) abolished by both 10 μ M chelerythrine ($-15 \pm 6\%$, $n = 5$) and 500 nM Go 6976 ($3 \pm 5\%$, $n = 5$) (data not shown). Inhibitors of serine/threonine kinases (500 nM staurosporine, $n = 7$; 50 μ M H9, $n = 6$), tyrosine kinases (10 μ M genistein, $n = 7$), phosphatases (100 nM okadaic acid, $n = 6$), phosphoinositide 3-kinases (200 nM wortmannin, $n = 7$), pertussis toxin-sensitive $G\alpha$ proteins (0.5 μ g/ml pertussis toxin, $n = 6$), cAMP (10 μ M $(R_p)_2$ -cAMP, $n = 5$), and internal Ca^{2+} (10 μ M BAPTA-AM, $n = 5$) also had no significant effect ($p > 0.02$) on the inhibition of Cav3.3 currents by M1 receptors (Fig. 3D). In this regard, classical $G\alpha_{q/11}$ downstream effectors such as PKC, cAMP-dependent protein kinase, and increased cytosolic Ca^{2+} concentration appear not to be directly involved in the M1 receptor-mediated inhibition of Cav3.3 T-type Ca^{2+} currents. Phospholipase C activity has been shown recently to directly inhibit voltage-gated ion channels through the depletion of membrane PI(4,5) P_2 levels, which are thought to stabilize active channels in the membrane (48). Dialyzing cells with a PI(4,5) P_2 antibody (50 μ g/ml) to reduce available PI(4,5) P_2 levels had no significant effect ($p > 0.05$) on the M1 receptor-mediated inhibition of Cav3.3 currents (Fig. 5, B and D). Similarly, dialyzing cells with synthetic PI(4,5) P_2 (200 μ M di-C8 PI(4,5) P_2) to saturate membrane PI(4,5) P_2 levels also had no significant effect ($p > 0.05$) on M1 receptor-mediated inhibition of Cav3.3 currents (Fig. 5, C and D). As a positive control for di-C8 PI(4,5) P_2 activity and as previously shown (49), dialysis of 200 μ M di-C8 PI(4,5) P_2 into HEK 293 cells stably expressing HERG K^+ channels caused a significant ($p < 0.02$) stimulation of K^+ channel currents ($n = 8$) compared with control recordings ($n = 5$; data not shown). Taken together, these results indicate that inhibition of Cav3.3 by M1 receptors occurs either directly through $G\alpha_{q/11}$ or a downstream pathway that is independent of PI(4,5) P_2 metabolism and other classical effectors.

$G\alpha_{q/11}$ -coupled Muscarinic Receptors Selectively Inhibit Cav3.3 Channels—If inhibition of Cav3.3 T-type Ca^{2+} channels by M1 receptors is primarily dependent on $G\alpha_{q/11}$ signaling, then all $G\alpha_q/G\alpha_{11}$ -coupled mAChRs should similarly inhibit Cav3.3 currents, whereas $G\alpha_i$ -coupled mAChRs should have no effect. Indeed, activation of co-expressed $G\alpha_i$ -coupled M2 and M4 receptors with 1 mM CCh had no effect on Cav3.3 current amplitude (M2 = $-4 \pm 2\%$, $n = 11$; M4 = $-4 \pm 3\%$, $n = 8$) or kinetics (Fig. 6, A, C, E, and G; Table 1). In contrast, upon transfection of either the $G\alpha_q/G\alpha_{11}$ -coupled M3 or M5 receptor subtypes into stable Cav3.3 cells, perforated patch recordings revealed a significant CCh-mediated inhibition (M3 = $-25 \pm 3\%$, $n = 10$; M5 = $-31 \pm 3\%$, $n = 10$) as well as a concomitant increase in both activation and inactivation kinetics (Fig. 6, B, D, F, and H; Table 1). Overall, experiments with genetically encoded antagonists of $G\alpha_{q/11}$ (RGS2) and $G\beta\gamma$ (MAS-GRK3ct) and genetically encoded $G\alpha$ subtypes, as well as inhibition experiments with various mAChRs, all support the assertion that inhibition of Cav3.3 channels by mAChRs specifically occurs through $G\alpha_{q/11}$.

Inhibition of Cav3.3 T-type Ca^{2+} Channels by mAChRs

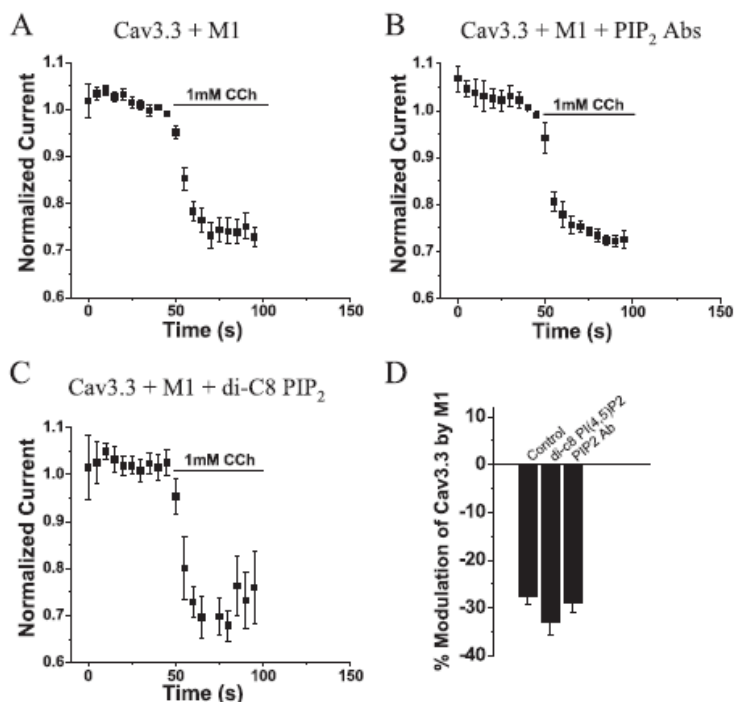


FIGURE 5. Inhibition of Cav3.3 channels by M1 does not require PI(4,5)P₂ signaling. **A**, In whole-cell recordings of HEK 293 cells co-transfected with human Cav3.3 and M1, application of 1 mM CCh caused inhibition of Cav3.3 currents ($-27.7 \pm 1.5\%$, $n = 15$). **B**, dialyzing cells with 50 μ g/ml PI(4,5)P₂ antibody for 10+ min had no effect on the inhibition of human Cav3.3 currents by M1 receptor activation ($-30.8 \pm 3.9\%$, $n = 7$). **C**, dialyzing cells with 200 μ M di-C8 PI(4,5)P₂ for 5+ min had no effect on the inhibition of human Cav3.3 currents by M1 receptor activation ($-29.0 \pm 1.8\%$, $n = 6$). **D**, bar graph showing that attenuating PI(4,5)P₂ signaling with either PI(4,5)P₂ antibodies or di-C8 PI(4,5)P₂ had no significant effect ($p > 0.05$) on M1-mediated inhibition compared with whole-cell recordings from control human Cav3.3 + M1 cells.

Two Distinct Cav3.3 Channel Regions Are Involved in M1-mediated Inhibition—Most modulation of Ca^{2+} channels by intracellular signaling pathways involves physical interactions between various effectors and cytoplasmic channel domains (42, 50). Chimeric T-type Ca^{2+} channels between human Cav3.1 and human Cav3.3 were generated to determine the molecular regions of the Cav3.3 channel involved in the M1 receptor-mediated inhibition (Fig. 7). The Cav3.1 and Cav3.3 full-length channels were initially divided into four approximately equal portions, and chimeric channels were constructed using restriction enzyme digestion and religation (see Ref. 37). The four channel portions were named as follows: region 1 = amino terminus + domain I; region 2 = domain I–II linker, domain II + the first 39–63 amino acids of the domain II–III linker; region 3 = remainder of the domain II–III linker + domain III; and region 4 = the domain III–IV linker, domain IV + the carboxyl terminus. Chimeric channel names were assigned based on whether the chimera contained Cav3.1 (G) or Cav3.3 (I) sequence in each of the four regions described (e.g. the chimeric Cav3.3 channel that contained region 2 from Cav3.1 is called IGII).

Co-expression of M1 receptors with chimeric GIII and IIGI T-type channels both showed a similar degree of M1 receptor-

mediated peak current inhibition compared with that of the inhibition of the WT Cav3.3 channel (III) (Fig. 7, A and E). In contrast, when the IGII chimera was co-transfected with M1 receptors, application of 1 mM CCh resulted in a significantly attenuated degree of inhibition ($-5.6 \pm 2.1\%$, $n = 11$, ($p < 0.001$)) compared with the wild type III channel ($-26.9 \pm 2.3\%$, $n = 9$; Fig. 7E). Interestingly, although the chimeric IGII channels exhibited lowered M1 receptor-mediated inhibition, they still possessed significantly increased inactivation kinetics ($p < 0.001$; Table 2). Finally, although the IIG chimeric channels showed similar degree of M1 receptor-mediated peak current inhibition compared with the wild type III, the rate of inhibition was notably slower (not shown). The changes in the rate of inhibition for IIG and the significant decrease in the amount of inhibition for IGII suggested that both regions 2 and 4 might be involved in the M1-induced inhibition of Cav3.3 channels. To explore this, a double chimera (IGIG) was co-transfected into HEK cells with M1 receptors. Fig. 7, C and E, shows that the inhibiting effect of 1 mM CCh application on peak current amplitude was completely abolished for the IGIG chimera ($0.9 \pm 2.5\%$, $n = 8$). Activation of M1 with 1 mM CCh still caused a significant increase ($p < 0.001$) in the inactivation kinetics of IGIG, but the τ_{inact} decreased by less than 25% for IGIG, and it decreased by 40–65% for all the single chimeric and wild type Cav3.3 channels (Table 2).

The chimeric channel loss-of-function experiments indicate that both regions 2 and 4 are involved in the M1-mediated inhibition of current amplitude and increase in inactivation kinetics of Cav3.3 currents. In gain-of-function experiments, substitution of either region 2 (GIGG) or region 4 (GGGI) into the Cav3.1 channel resulted in 1 mM CCh-induced inhibition (GIGG = $-14.3 \pm 0.8\%$, $n = 7$; GGGI = $-9.1 \pm 2.6\%$, $n = 9$) that was significantly different ($p < 0.001$ and $p < 0.02$, respectively) when compared with GGGG ($-0.3 \pm 2.2\%$, $n = 9$; Fig. 7, B and E; Table 2). In contrast, inclusion of either region 1 or region 3 of Cav3.3 into Cav3.1 resulted in no significant change ($p > 0.05$) in M1-mediated inhibition when compared with GGGG (Fig. 7E). Although both GIGG and GGGI were inhibited by M1, the level of inhibition was significantly lower ($p < 0.001$) than the inhibition of III by M1 (Fig. 7E). When the effect of 1 mM CCh application on GIGI current amplitude was tested, M1 activation was found to produce a significant level of

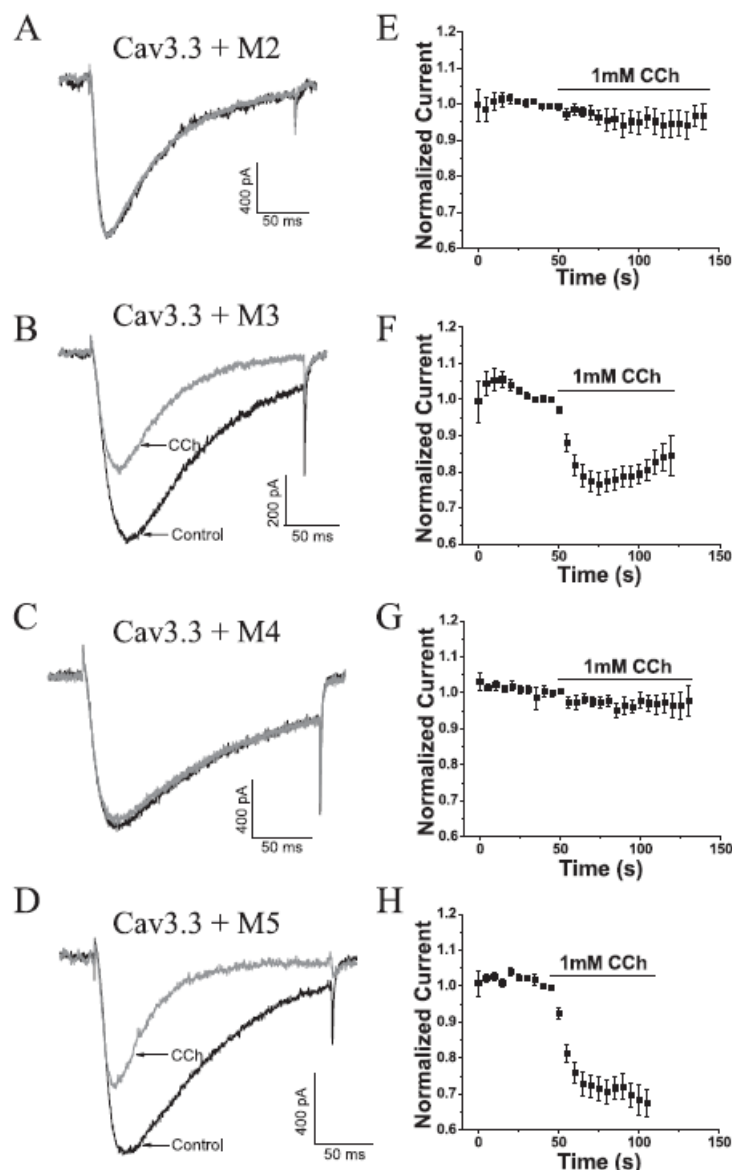


FIGURE 6. Inhibition of Cav3.3 currents occurs specifically through $G\alpha_{q11}$ -coupled muscarinic receptors. A and C, representative perforated patch current traces during depolarizing pulses from -110 to -40 mV showing no effect on Cav3.3 currents by the $G\alpha_q$ -coupled M2 and M4 receptors, respectively. Traces during control perfusion and perfusion of 1 mM CCh are indistinguishable, and CCh application had no significant effect on channel kinetics (Table 1). E and G, averaged time course of normalized peak current levels during perfusion of control recording solution (2 mM Ca^{2+}) followed by 1 mM CCh for Cav3.3 (+M2/M4) currents. Perfusion of CCh had no effect on Cav3.3 currents for M2 (E; $-4 \pm 2\%$, $n = 11$) and M4 (G; $-4 \pm 3\%$, $n = 8$) receptors. B and D, representative perforated patch current traces during depolarizing pulses from -110 to -40 mV showing inhibition of Cav3.3 currents by the $G\alpha_{q11}$ -coupled M3 and M5 receptors, respectively. Activating the receptors with 1 mM CCh also significantly ($p < 0.02$) increased channel kinetics (Table 1). F and H, averaged time course of normalized peak current levels during perfusion of control recording solution (2 mM Ca^{2+}) followed by 1 mM CCh for Cav3.3 plus either M3 or M5 receptors. Perfusion of CCh caused a $25 \pm 3\%$ decrease ($n = 10$) of Cav3.3 currents with co-transfected M3 receptors (F) and a $31 \pm 3\%$ decrease ($n = 10$) of Cav3.3 currents with co-transfected M5 receptors. Only a small number of cells ($n = 2$ for both M3 and M5) were not inhibited by CCh. All data points correspond to mean \pm S.E.

GIGI inhibition ($-25.1 \pm 2.4\%$, $n = 11$; $p < 0.001$) compared with GGGG that was not significantly ($p > 0.05$) different from the inhibition of IIII (Fig. 7, A, B, D, and E). Application of 1 mM CCh also significantly increased ($p < 0.001$) the rate of inactivation for the GIGI Cav3.1 chimera but not for GIGG, GGGI, or the other Cav3.1 single chimeras (Table 2). Overall, the combined substitution of regions 2 and 4 from the Cav3.3 channel into the Cav3.1 channel completely restores M1-induced inhibition together with the associated increase in channel inactivation kinetics.

DISCUSSION

In this study we systematically explored the effects of activated muscarinic GPCRs on the three main T-type Ca^{2+} channel isoforms expressed in the mammalian nervous system, and we report for the first time the differential modulation between a G-protein signaling pathway and Cav3.3 T-type Ca^{2+} channels. Most studies on T-type Ca^{2+} channel modulation have involved the Cav3.2 (α_{1H}) subtype, revealing specific modulatory responses to $G\beta_2\gamma$, CAMKII, and redox modulation that are not observed for the Cav3.1 and Cav3.3 T-type Ca^{2+} channel isoforms (42, 51, 52). The exclusive inhibition of Cav3.3 channels by $G\alpha_{q11}$ -coupled mAChRs is the first example of specific GPCR-mediated modulation of a T-type Ca^{2+} channel subtype other than for Cav3.2.

Differential Effects of mAChRs on T-type Ca^{2+} Channel Isoforms—Examination of the literature shows that activation of mAChRs can result in multiple effects on native T-type Ca^{2+} currents, including causing stimulation (26, 27, 53), inhibition (28), or having no effect (54). Given the heterogeneous nature of native low threshold Ca^{2+} currents, without investigating interactions between specific mAChR gene products and specific T-type Ca^{2+} channel isoforms, the published differences in modulation

TABLE 2
Effects of M1 receptor activation on chimeric T-type channel inactivation kinetics

	III	IGH	IIG	IGIG	GGGG	GIGG	GGGI	GIGI
Control - τ_{inact} (ms)	117 \pm 6, n = 10	86 \pm 7, n = 11	103 \pm 11, n = 10	62 \pm 2, n = 8	14 \pm 1, n = 9	20 \pm 1, n = 9	38 \pm 3, n = 8	58 \pm 2, n = 10
1 mM CCh - τ_{inact} (ms)	41 \pm 5, n = 10 ^a	43 \pm 3, n = 11 ^a	58 \pm 4, n = 10 ^b	47 \pm 3, n = 8 ^b	13 \pm 1, n = 9	17 \pm 2, n = 7	32 \pm 2, n = 8	38 \pm 1, n = 10 ^a

^a $p < 0.001$.

^b $p < 0.02$.

are nearly impossible to interpret. Our results using exogenous expression of cloned T-type Ca^{2+} channels indicates that M1 receptor activation has a robust inhibitory effect on Cav3.3 currents and has either no effect or a small stimulation on both Cav3.1 and Cav3.2 currents. Similarly, experiments examining native Cav3.2 Ca^{2+} channels in NIH3T3 cells transiently transfected with mAChRs demonstrated that M1 receptor activation had either no effect or a stimulatory effect if a PKC inhibitor was applied (27). Active $\text{G}\beta\gamma$ subunits have been shown to specifically inhibit Cav3.2 currents (42, 55), and the lack of inhibition of Cav3.3 currents, whereas $\text{G}\alpha_i$ -coupled M2 and M4 receptors had no effect on Cav3.3 currents. Thus it is likely that any stimulation of T-type Ca^{2+} currents by mAChRs in native systems does not involve Cav3.3 channels. Experiments testing the effects of recombinant M2–M5 receptors on the Cav3.2 and Cav3.1 Ca^{2+} channel isoforms in a heterologous system are required to further facilitate the possibility of interactions between these T-type channels and mAChRs.

Functional Effects of M1 Receptor Activation on Cav3.3 Currents—Activation of M1 receptors dramatically altered Cav3.3 currents by both reversibly attenuating peak current levels and increasing the rate of inactivation, resulting in a significant reduction in the influx of Ca^{2+} . The relationship between these effects was explored using both structural channel chimeras and classical gating property studies. In chimeric studies (see below), the activation of M1 receptors primarily caused an increase in inactivation kinetics of the IGH chimera and, conversely, primarily a decrease in peak current levels for the GIGG chimera. Both this isolation of the two specific M1 receptor-mediated effects and the gating results discussed below suggest that the effects of M1 on current amplitude and inactivation kinetics are complementary but distinct phenomena. For gating studies, reduction of Cav3.3 current magnitude by M1 receptor activation was equally robust when the Cav3.3 channels were held in various states including: 1) during a prolonged hyperpolarization with no test depolarizations (chan-

nels mostly in closed state); 2) after a strong hyperpolarizing prepulse to -140 mV; and 3) during 200-ms test depolarizations to peak potential at 0.2 and 0.5 Hz. Combining this lack of use dependence with the observed reduction in peak current amplitude and the increase in activation and inactivation kinetics indicates that all states of the Cav3.3 channel are subject to modulation by M1 receptor activation. The acceleration of Cav3.3 channel kinetics by M1 receptor activation also supports the hypothesis that modulation affects channel biophysical properties and not channel density via internalization, which has recently been shown to occur for the voltage-independent, GPCR-mediated inhibition of N-type Ca^{2+} channels on a relatively fast time scale (57). Physiologically, the combined decrease in Cav3.3 peak currents and the increased activation and inactivation kinetics would be predicted to alter neuronal firing patterns and perhaps eliminate rhythmic oscillations (23, 58). In support of this notion, the concomitant reduction in peak current and increase in inactivation kinetics of Cav3.3 currents triggered by anandamide have been shown to completely eliminate the sustained, rhythmic Cav3.3 current during an action potential voltage clamp experiment with an oscillating thalamic waveform (59).

Signal Transduction Pathway of M1 Receptor-mediated Cav3.3 Inhibition—Use of genetically encoded antagonists of $\text{G}\beta\gamma$ (MAS-GRK3ct and $\text{G}\alpha_i$) and $\text{G}\alpha_{q/11}$ (RGS2) demonstrated that $\text{G}\beta\gamma$ may partially contribute to the M1-mediated inhibition of Cav3.3 currents, whereas $\text{G}\alpha_{q/11}$ is absolutely required for complete inhibition. The potential involvement of both $\text{G}\alpha_{q/11}$ and $\text{G}\beta\gamma$ in a nonclassical, voltage-independent mechanism of Ca^{2+} channel inhibition by mAChRs has been described previously for HVA Ca^{2+} channels. In rat superior cervical ganglion sympathetic neurons, application of a muscarinic agonist causes the voltage-independent inhibition of endogenous N-type Ca^{2+} channels that is abolished by co-expression of RGS2, $\text{G}\alpha_i$, or MAS-GRK3ct and exhibits a time course similar to the Cav3.3 inhibition reported here (41). As $\text{G}\beta\gamma$ is a cofactor for PLC β activity, a possible explanation is that sequestering $\text{G}\beta\gamma$ reduces PLC β activity (60). Although $\text{G}\beta\gamma$ may potentiate the inhibitory effect of M1 receptor activation, transfection of constitutively active $\text{G}\alpha_{q/11}$ mutants into

FIGURE 7. Regions II and IV of human Cav3.3 channels are required and appear sufficient for M1-mediated inhibition. A–D, *left*, schematic diagrams of the various chimeric channels that were co-transfected into HEK cells with M1. The lighter transmembrane domains and intra/extracellular regions correspond to Cav3.3 (labeled I) sequences, whereas the darker transmembrane domains and intra/extracellular regions correspond to Cav3.1 (labeled G) sequences. *Middle*, effect of activating M1 receptors with 1 mM CCh on the normalized peak current levels of chimeric channel types shown to the *left*. Inclusion of Cav3.1 sequence at regions II and IV (C) eliminated M1-mediated inhibition and attenuated the effect on inactivation kinetics, whereas inclusion of Cav3.3 sequence at regions II and IV (D) restored M1-mediated inhibition to a level that was not significantly ($p > 0.05$) different from IIII inhibition levels (see Table 1). *Right*, insets include chimeric whole-cell current traces during depolarizing pulses from -110 mV to peak potential before (line arrow) and after (block arrow) application of 1 mM CCh. Traces are representative of the various chimeras in terms of activation and inactivation kinetics as well as magnitude of inhibition. For inset scale bars, $x = 50$ ms and $y = 100$ pA. E, histogram where GIII, IGII, IIG, IIGG, and IGIG inhibition values were statistically compared with the IIII control, and IGGG, GIGG, GGI, and GGGI values were compared with the GGGG control, and the GIGI value was compared with both the IIII and GGGG controls. * Indicates significant difference (< 0.02) compared with IIII inhibition, and ** indicates a significant difference ($p < 0.02$) compared with GGGG modulation levels. All data points correspond to mean \pm S.E.

Inhibition of Cav3.3 T-type Ca^{2+} Channels by mAChRs

stable Cav3.3 cells demonstrated that active $\text{G}\alpha_{q/11}$ alone is sufficient to induce the inhibition of Cav3.3 currents. In support of this notion, only $\text{G}\alpha_{q/11}$ -coupled mAChRs (M1, M3, and M5) inhibited Cav3.3 currents, whereas $\text{G}\alpha_i$ -coupled M2 and M4 receptors that activate $\text{G}\beta\gamma$ signaling have no effect on Cav3.3 currents. Unlike that reported for the attenuation of Cav3.2 channels by $\text{G}\beta_2\gamma$, this novel form of T-type Ca^{2+} channel inhibition involves the $\text{G}\alpha_{q/11}$ subunit and also affects channel kinetics. This inhibitory mechanism for the Cav3.3 T-type isoform may be applicable to all $\text{G}\alpha_{q/11}$ -coupled receptors as we have also found a similar inhibition of Cav3.3 channels by mGluR_{1a} receptors (61).

Pharmacological antagonists eliminated the potential involvement of various intracellular signals downstream of $\text{G}\alpha_{q/11}$ activation that may be involved in the inhibition of Cav3.3 by M1 receptor activation. Abolishing the activity of PKC, serine/threonine kinases (including cAMP-dependent protein kinase), tyrosine kinases, phosphatases, phosphoinositide 3-kinases, and intracellular Ca^{2+} signaling all had no effect on inhibition. This profile of M1/ $\text{G}\alpha_{q/11}$ -mediated Ca^{2+} channel inhibition resistant to common antagonists of cytoplasmic signaling is not unique and has been reported for the inhibition of L-type channels by $\text{G}\alpha_q$ -coupled M1/3/5 receptors in HEK cells (62). Like the inhibition of Cav3.3 via M1 receptors, this inhibition is voltage-independent, relatively slow kinetically ($\tau_{\text{on}} = 13$ s), and insensitive to antagonists of protein kinases and protein phosphatases (62).

A more recent explanation for the $\text{G}\alpha_{q/11}$ -mediated inhibition of ion channels, including voltage-gated K^+ channels and HVA Ca^{2+} channels, has emerged wherein channel activity is suppressed through the depletion of membrane $\text{PI}(4,5)\text{P}_2$ levels via PLC activity (46, 63, 64). In these studies, $\text{G}\alpha_{q/11}$ -mediated inhibition was shown to be inhibited via dialysis of synthetic $\text{PI}(4,5)\text{P}_2$ or a $\text{PI}(4,5)\text{P}_2$ -specific antibody into the cytoplasm. In our experiments, adding di-C8 $\text{PI}(4,5)\text{P}_2$ or the $\text{PI}(4,5)\text{P}_2$ antibody into the internal pipette solution and dialyzing cells for up to 25 min had no significant effect on M1-mediated inhibition of Cav3.3 channels, suggestive of another to-be-defined mechanism whereby $\text{G}\alpha_{q/11}$ signaling causes the inhibition of voltage-gated ion channels. Further biophysical and biochemical experiments are required to clarify the nature of the intracellular messengers and/or scaffolding proteins that can modulate Cav3.3 T-type Ca^{2+} channels and also whether $\text{G}\alpha_{q/11}$ can interact directly with the channel through a novel mechanism.

$\text{G}\alpha_{q/11}$ -mediated Inhibition of Cav3.3 Involves Two Discrete Channel Regions—Replacing both regions 2 and 4 in the Cav3.3 channel with the corresponding Cav3.1 T-type Ca^{2+} channel sequences abrogated both the M1 receptor-mediated peak current inhibition and concomitant increase in inactivation kinetics. Conversely, substituting regions 2 and 4 from Cav3.3 into Cav3.1 conferred M1 receptor-mediated inhibition and increased inactivation kinetics. These data suggest that regions 2 and 4 of the Cav3.3 channel are both necessary and sufficient to recapitulate M1 receptor-mediated channel modulation. Region 2 of the Cav3.1 and Cav3.3 sequence contains the highly divergent domain I–II linker, the highly conserved domain II, and 39–63 amino acids of the domain II–III linker, and region 4 contains most of the III–IV linker, the highly conserved

domain IV, and the highly divergent carboxyl terminus. Based on their putatively intracellular regions and their high divergence between the two T-type isoforms, the I–II linker, proximal region of the II–III linker, the III–IV linker, and the carboxyl terminus are all candidates for modulation sites within regions 2 and 4. Interestingly, the only identified sites of alternative splicing within the rat and human Cav3.3 channel occur both in the I–II linker and the carboxyl-terminal regions (38, 65). The effects of these splicing variations on the biophysical properties (activation kinetics) of the human Cav3.3 channel are interdependent rather than additive, suggesting a possible direct interaction between the I–II linker and carboxyl terminus that affects channel kinetics (24). Both the human and rat Cav3.3 channels inhibited by M1 receptor activation in our study lack exon 9 located in the I–II linker, whereas both the rat and human Cav3.1 channels have a 10-amino acid insertion in this region in a manner similar to that for the +exon 9 Cav3.3 splice variant. Thus, several observations suggest that the I–II linker may be a target region in the inhibition of Cav3.3 by M1, and some evidence points to a possible role for the carboxyl terminus. However, as multiple structural determinants contribute to the slow inactivation kinetics of Cav3.3 compared with Cav3.1 in a nearly additive manner (37), and M1 activation dramatically speeds up Cav3.3 inactivation kinetics, it is also possible that multiple intracellular loci within regions 2 and 4 of the Cav3.3 channel may be involved in the M1-mediated effect.

In summary, we find that activation of known $\text{G}\alpha_{q/11}$ -coupled mAChRs results in the selective inhibition of Cav3.3 T-type Ca^{2+} currents with a concomitant increase in inactivation kinetics. The $\text{G}\alpha_{q/11}$ -mediated signaling pathway appears to be mediated via two disparate regions of the Cav3.3 channel. Functional interactions between mAChRs and Cav3.3 Ca^{2+} channels could potentially impact firing patterns of various cell types, including thalamic nRT cells. Biophysical and pharmacological evidence suggests that primarily Cav3.3 channels compose dendritic T-type currents in nRT cells (22), whereas immunostaining suggests the presence of M3 receptors in these cells (33). This raises the possibility that the inhibition of Cav3.3 T-type Ca^{2+} channels by M3 receptors in the dendrites of nRT cells could be involved in cholinergic modulation of thalamic firing patterns.

Acknowledgments—We thank Dr. Brett Adams for the kind gifts of MAS-GRK3ct and EGFP-RGS2 and Drs. Aaron Beedle, Arnaud Monteil, and Philippe Lory for the human Cav3.1 and Cav3.3 channels used in the chimeric channel experiments. We also thank Dr. Colin Thacker, Tracy Evans, Paul Adams, and Dr. John Tyson for molecular biology support, Diana Janke and Dr. David Parker for providing stable cell lines, and to Dr. Philippe Isope for comments on the manuscript.

REFERENCES

1. Anderson, M. P., Mochizuki, T., Xie, J., Fischler, W., Manger, J. P., Talley, E. M., Scammell, T. E., and Tonegawa, S. (2005) *Proc. Natl. Acad. Sci. U. S. A.* 102, 1743–1748
2. Kim, D., Song, I., Keum, S., Lee, T., Jeong, M. J., Kim, S. S., McEnery, M. W., and Shin, H. S. (2001) *Neuron* 31, 35–45
3. Destexhe, A., and Sejnowski, T. J. (2003) *Physiol. Rev.* 83, 1401–1453

4. Huguenard, J. R., and Prince, D. A. (1992) *J. Neurosci.* 12, 3804–3817
5. Tsakiridou, E., Bertollini, L., de Curtis, M., Avanzini, G., and Pape, H. C. (1995) *J. Neurosci.* 15, 3110–3117
6. Peloquin, J. B., Khosravani, H., Barr, W., Bladen, C., Evans, R., Mezeyova, J., Parker, D., Snutch, T. P., McRory, J. E., and Zamponi, G. W. (2006) *Epilepsia* 47, 655–658
7. Khosravani, H., Bladen, C., Parker, D. B., Snutch, T. P., McRory, J. E., and Zamponi, G. W. (2005) *Ann. Neurol.* 57, 745–749
8. Khosravani, H., Altier, C., Simms, B., Hamming, K. S., Snutch, T. P., Mezeyova, J., McRory, J. E., and Zamponi, G. W. (2004) *J. Biol. Chem.* 279, 9681–9684
9. Vitko, L., Chen, Y., Arias, J. M., Shen, Y., Wu, X. R., and Perez-Reyes, E. (2005) *J. Neurosci.* 25, 4844–4855
10. Thompson, S. M., and Wong, R. K. (1991) *J. Physiol. (Lond.)* 439, 671–689
11. Christie, B. R., Eliot, L. S., Ito, K., Miyakawa, H., and Johnston, D. (1995) *J. Neurophysiol.* 73, 2553–2557
12. Egger, V., Svoboda, K., and Mainen, Z. F. (2005) *J. Neurosci.* 25, 3521–3530
13. Egger, V., Svoboda, K., and Mainen, Z. F. (2003) *J. Neurosci.* 23, 7551–7558
14. Hildebrand, M. E., and Snutch, T. P. (2006) *Drug Discov. Today* 3, 335–341
15. Bourinet, E., Alloui, A., Monteil, A., Barrere, C., Couette, B., Poirrot, O., Pages, A., McRory, J., Snutch, T. P., Eschaliere, A., and Nargeot, J. (2005) *EMBO J.* 24, 315–324
16. Santi, C. M., Cayabyab, F. S., Sutton, K. G., McRory, J. E., Mezeyova, J., Hamming, K. S., Parker, D., Stea, A., and Snutch, T. P. (2002) *J. Neurosci.* 22, 396–403
17. McRory, J. E., Santi, C. M., Hamming, K. S., Mezeyova, J., Sutton, K. G., Baillie, D. L., Stea, A., and Snutch, T. P. (2001) *J. Biol. Chem.* 276, 3999–4011
18. Cribbs, L. L., Lee, J. H., Yang, J., Satin, J., Zhang, Y., Daud, A., Barclay, J., Williamson, M. P., Fox, M., Rees, M., and Perez-Reyes, E. (1998) *Circ. Res.* 83, 103–109
19. Lee, J. H., Daud, A. N., Cribbs, L. L., Lacerda, A. E., Pereverzev, A., Klockner, U., Schneider, T., and Perez-Reyes, E. (1999) *J. Neurosci.* 19, 1912–1921
20. Perez-Reyes, E., Cribbs, L. L., Daud, A., Lacerda, A. E., Barclay, J., Williamson, M. P., Fox, M., Rees, M., and Lee, J. H. (1998) *Nature* 391, 896–900
21. Monteil, A., Chemin, J., Leuranguer, V., Altier, C., Mennessier, G., Bourinet, E., Lory, P., and Nargeot, J. (2000) *J. Biol. Chem.* 275, 16530–16535
22. Joksovic, P. M., Bayliss, D. A., and Todorovic, S. M. (2005) *J. Physiol. (Lond.)* 566, 125–142
23. Chevalier, M., Lory, P., Mironneau, C., Macrez, N., and Quignard, J. F. (2006) *Eur. J. Neurosci.* 23, 2321–2329
24. Murbartian, J., Arias, J. M., and Perez-Reyes, E. (2004) *J. Neurophysiol.* 92, 3399–3407
25. Castillo, P. E., Carleton, A., Vincent, J. D., and Lledo, P. M. (1999) *J. Neurosci.* 19, 9180–9191
26. Fraser, D. D., and MacVicar, B. A. (1991) *J. Neurosci.* 11, 2812–2820
27. Pemberton, K. E., Hill-Eubanks, L. J., and Jones, S. V. (2000) *Dfluegers Arch.* 440, 452–461
28. Wan, X., Desilets, M., Soboloff, J., Morris, C., and Tsang, B. K. (1996) *Endocrinology* 137, 2514–2521
29. Chemin, J., Traboulsie, A., and Lory, P. (2006) *Cell Calcium* 40, 121–134
30. Talley, E. M., Cribbs, L. L., Lee, J. H., Daud, A., Perez-Reyes, E., and Bayliss, D. A. (1999) *J. Neurosci.* 19, 1895–1911
31. Yunker, A. M., Sharp, A. H., Sundarraj, S., Ranganathan, V., Copeland, T. D., and McEnery, M. W. (2003) *Neuroscience* 117, 321–335
32. Plummer, K. L., Manning, K. A., Levey, A. I., Rees, H. D., and Uhrich, D. J. (1999) *J. Comp. Neurol.* 404, 408–425
33. Levey, A. I., Edmunds, S. M., Heilman, C. J., Desmond, T. J., and Frey, K. A. (1994) *Neuroscience* 63, 207–221
34. Wei, J., Walton, E. A., Milici, A., and Buccafusco, J. J. (1994) *J. Neurochem.* 63, 815–821
35. Levey, A. I., Edmunds, S. M., Koliatsos, V., Wiley, R. G., and Heilman, C. J. (1995) *J. Neurosci.* 15, 4077–4092
36. McKay, B. E., McRory, J. E., Molineux, M. L., Hamid, J., Snutch, T. P., Zamponi, G. W., and Turner, R. W. (2006) *Eur. J. Neurosci.* 24, 2581–2594
37. Hamid, J., Peloquin, J. B., Monteil, A., and Zamponi, G. W. (2006) *Neuroscience* 143, 717–728
38. Murbartian, J., Arias, J. M., Lee, J. H., Gomora, J. C., and Perez-Reyes, E. (2002) *FEBS Lett.* 528, 272–278
39. Hogger, P., Shockley, M. S., Lameh, J., and Sadee, W. (1995) *J. Biol. Chem.* 270, 7405–7410
40. Schwarz, R. D., Davis, R. E., Jaen, J. C., Spencer, C. J., Teclé, H., and Thomas, A. J. (1993) *Life Sci.* 52, 465–472
41. Kammermeier, P. J., Ruiz-Velasco, V., and Ikeda, S. R. (2000) *J. Neurosci.* 20, 5623–5629
42. Wolfe, J. T., Wang, H., Howard, J., Garrison, J. C., and Barrett, P. Q. (2003) *Nature* 424, 209–213
43. Dolphin, A. C. (2003) *Pharmacol. Rev.* 55, 607–627
44. Heximer, S. P., Watson, N., Linder, M. E., Blumer, K. J., and Hepler, J. R. (1997) *Proc. Natl. Acad. Sci. U. S. A.* 94, 14389–14393
45. Melliti, K., Meza, U., and Adams, B. (2000) *J. Neurosci.* 20, 7167–7173
46. Suh, B. C., Horowitz, L. F., Hirdes, W., Mackie, K., and Hille, B. (2004) *J. Gen. Physiol.* 123, 663–683
47. Park, J. Y., Kang, H. W., Moon, H. J., Huh, S. U., Jeong, S. W., Soldatov, N. M., and Lee, J. H. (2006) *J. Physiol. (Lond.)* 577, 513–523
48. Suh, B. C., and Hille, B. (2005) *Curr. Opin. Neurobiol.* 15, 370–378
49. Bian, J., Cui, J., and McDonald, T. V. (2001) *Circ. Res.* 89, 1168–1176
50. Zamponi, G. W., and Snutch, T. P. (2002) *Mol. Interv.* 2, 476–478
51. Joksovic, P., Nelson, M., Jevtic-Todorovic, V., Patel, M., Perez-Reyes, E., Campbell, K., Chen, C. C., and Todorovic, S. (2006) *J. Physiol. (Lond.)* 574, 415–430
52. Welsby, P. J., Wang, H., Wolfe, J. T., Colbran, R. J., Johnson, M. L., and Barrett, P. Q. (2003) *J. Neurosci.* 23, 10116–10121
53. Fisher, R., and Johnston, D. (1990) *J. Neurophysiol.* 64, 1291–1302
54. Allen, T. G., and Brown, D. A. (1993) *J. Physiol. (Lond.)* 466, 173–189
55. Dupuy, S. D., Yao, J., Hu, C., McIntire, W., Bidaud, I., Lory, P., Rastinejad, F., Gonzalez, C., Garrison, J. C., and Barrett, P. Q. (2006) *Proc. Natl. Acad. Sci. U. S. A.* 103, 14590–14595
56. Dippel, E., Kalkbrenner, F., Wittig, B., and Schultz, G. (1996) *Proc. Natl. Acad. Sci. U. S. A.* 93, 1391–1396
57. Tomblar, E., Cabanilla, N. J., Carman, P., Permaul, N., Hall, J. J., Richman, R. W., Lee, J., Rodriguez, J., Felsenfeld, D. P., Hennigan, R. F., and Diverse-Pierluissi, M. A. (2006) *J. Biol. Chem.* 281, 1827–1839
58. Chemin, J., Monteil, A., Perez-Reyes, E., Bourinet, E., Nargeot, J., and Lory, P. (2002) *J. Physiol. (Lond.)* 540, 3–14
59. Chemin, J., Monteil, A., Perez-Reyes, E., Nargeot, J., and Lory, P. (2001) *EMBO J.* 20, 7033–7040
60. Rhee, S. G., and Bae, Y. S. (1997) *J. Biol. Chem.* 272, 15045–15048
61. Hildebrand, M. E., David, L. S., and Snutch, T. P. (2005) *Biophysical Society 49th Annual Meeting, Long Beach, CA, February 12–16, 2005*, abstr. 1346-Pos, Biophysical Society, Bethesda
62. Bannister, R. A., Melliti, K., and Adams, B. A. (2002) *Biophys. J.* 83, 3256–3267
63. Wu, L., Bauer, C. S., Zhen, X. G., Xie, C., and Yang, J. (2002) *Nature* 419, 947–952
64. Gamper, N., Reznikov, V., Yamada, Y., Yang, J., and Shapiro, M. S. (2004) *J. Neurosci.* 24, 10980–10992
65. Mittman, S., Guo, J., Emerick, M. C., and Agnew, W. S. (1999) *Neurosci. Lett.* 269, 121–124

APPENDIX 3: MOLECULAR MECHANISMS OF SUBTYPE-SPECIFIC INHIBITION OF NEURONAL T-TYPE CALCIUM CHANNELS BY ASCORBATE

The Journal of Neuroscience, November 14, 2007 • 27(46):12577–12583 • 12577

Cellular/Molecular

Molecular Mechanisms of Subtype-Specific Inhibition of Neuronal T-Type Calcium Channels by Ascorbate

Michael T. Nelson,^{1,4} Pavle M. Joksovic,¹ Peihan Su,^{1,4} Ho-Won Kang,^{6,7} Amy Van Deusen,² Joel P. Baumgart,^{2,4} Laurence S. David,⁵ Terrance P. Snutch,⁵ Paula Q. Barrett,² Jung-Ha Lee,^{6,7} Charles F. Zorumski,⁸ Edward Perez-Reyes,^{2,4} and Slobodan M. Todorovic^{1,5,4}

Departments of ¹Anesthesiology, ²Pharmacology, ³Neuroscience, and ⁴Neuroscience Graduate Program, University of Virginia Health System, Charlottesville, Virginia 22908, ⁵Michael Smith Laboratories, University of British Columbia, Vancouver British Columbia, Canada V6T 1Z4, ⁶Department of Life Science and ⁷Interdisciplinary Program of Biotechnology, Sogang University, Shinsu-Dong, Seoul 121-742, Korea, and ⁸Department of Psychiatry, Washington University School of Medicine, St. Louis, Missouri 63130

T-type Ca^{2+} channels (T-channels) are involved in the control of neuronal excitability and their gating can be modulated by a variety of redox agents. Ascorbate is an endogenous redox agent that can function as both an anti- and pro-oxidant. Here, we show that ascorbate selectively inhibits native $\text{Ca}_v3.2$ T-channels in peripheral and central neurons, as well as recombinant $\text{Ca}_v3.2$ channels heterologously expressed in human embryonic kidney 293 cells, by initiating the metal-catalyzed oxidation of a specific, metal-binding histidine residue in domain 1 of the channel. Our biophysical experiments indicate that ascorbate reduces the availability of $\text{Ca}_v3.2$ channels over a wide range of membrane potentials, and inhibits $\text{Ca}_v3.2$ -dependent low-threshold- Ca^{2+} spikes as well as burst-firing in reticular thalamic neurons at physiologically relevant concentrations. This study represents the first mechanistic demonstration of ion channel modulation by ascorbate, and suggests that ascorbate may function as an endogenous modulator of neuronal excitability.

Key words: ascorbic; calcium current; dorsal root ganglion; DRG; low-threshold calcium channel; oxidation; thalamus

Introduction

Ascorbate (ascorbic acid, vitamin C) is a ubiquitous redox agent present at particularly high concentrations in neurons (Rice, 2000), but its interaction with the ion channels that control neuronal excitability is poorly understood. We have shown previously that T-type Ca^{2+} channels (T-channels) can be modulated by a variety of redox agents (Todorovic et al., 2001; Nelson et al., 2005; Joksovic et al., 2006); thus, we reasoned that ascorbate might also affect the gating of these channels. Ascorbate often functions as an antioxidant, readily scavenging reactive oxygen and nitrogen species. However, ascorbate can also function as a pro-oxidant by catalyzing the formation of several reactive oxygen species (ROS). Ascorbate generates ROS by reducing transition metals by a one-electron transfer mechanism, and oxygen by a two-electron transfer mechanism; the products of these reactions can subsequently interact to create several powerful ROS including hydroxyl radicals ($\cdot\text{OH}$) (Stadtman, 1991). Collectively, this process is termed metal-catalyzed oxidation (MCO) (Stadtman, 1991; Stadtman, 1993). A unique feature of proteinaceous MCO is that only one or at most a select number of amino

acids are modified. This site specificity has been attributed to the formation of ROS directly at metal binding sites, where they attack the functional groups of nearby residues. Histidine residues are particularly prone to MCO, in part because they are often structural components of metal binding sites (Stadtman, 1993). Here we present evidence that ascorbate inhibits $\text{Ca}_v3.2$, but not $\text{Ca}_v3.1$ or $\text{Ca}_v3.3$ T-channels by initiating the MCO of a unique, metal-binding histidine residue in domain 1 of the channel. Because $\text{Ca}_v3.2$ channels play an important role in tuning the excitability of several neuronal populations (White et al., 1989; Nelson et al., 2005; Vitko et al., 2005; Joksovic et al., 2006), ascorbate may function as an endogenous modulator of neuronal firing under physiological or pathological conditions.

Materials and Methods

DRG and thalamic neurons. Acutely dissociated dorsal root ganglion (DRG) cells were prepared from adolescent rats as described previously (Nelson et al., 2005). For recording, cells were plated onto uncoated glass coverslips, placed in a culture dish, and perfused with external solution. Thalamic slices were prepared from adolescent rats as previously described (Joksovic et al., 2006). For recording, slices were placed in a recording chamber and perfused with external solution. All experiments were performed at room temperature.

HEK293 cells. Human embryonic kidney 293 (HEK293) cells were grown in DMEM/F12 media (Invitrogen, Grand Island, NY) supplemented with fetal calf serum (10%), penicillin G (100 U/ml), and streptomycin (0.1 mg/ml). $\text{Ca}_v3.1$ (Perez-Reyes et al., 1998), human $\text{Ca}_v3.2$ (Vitko et al., 2005), $\text{Ca}_v3.3$ (Lee et al., 1999b), and GGHG (Welsby et al., 2003) plasmids were as described previously. HHGG, GHGG, HGGG, $\text{Ca}_v3.2$ (H191Q), and $\text{Ca}_v3.1$ (Q172H) plasmids were constructed as de-

Received May 14, 2007; revised Oct. 1, 2007; accepted Oct. 4, 2007.

This work was supported by National Institutes of Health Grants NS054521 (M.T.N.), HL36977 (P.D.R.), MH07791 and NS057105 (C.F.Z.), NS38091 (E.P.-R.), and GM075299 (S.M.T.), the Canadian Institutes of Health Research (T.P.S.), and the Heart and Stroke Foundation of Canada (S.M.T.). We thank Le-Ban of the University of Virginia for helpful comments on this manuscript.

Correspondence should be addressed to Slobodan M. Todorovic, Department of Anesthesiology, University of Virginia Health System, Box 900710, Charlottesville, VA 22908. E-mail: st5d@virginia.edu.

DOI:10.1523/JNEUROSCI.2206-07.2007

Copyright © 2007 Society for Neuroscience 0270-6474/07/2712577-07\$15.00/0

*A version of this appendix has been published. Nelson, M.T., Joksovic, P.M., Su, P., Kang, H-W., Van Deusen, A., Baumgart, J.P., David, L.S., Snutch, T.P., Barrett, P.Q., Lee, J.-H., Zorumski, C.F., Perez-Reyes, E., and Todorovic, S.M. (2007). Molecular mechanisms of subtype-specific inhibition of neuronal T-type calcium channels by ascorbate. *The Journal of Neuroscience*, 27(46), 12577–12583. Reprinted with kind permission of The Society for Neuroscience. All rights reserved.

scribed previously (Kang et al., 2006) and subcloned into pcDNA3 (Invitrogen). To construct the $Ca_v3.2(H191C)$ plasmid, a human $Ca_v3.2$ cDNA (GenBank accession number AF051946) contained in pcDNA3 was mutated using oligonucleotide primers and a QuickChange site-directed mutagenesis kit (Stratagene, La Jolla, CA). The primers were obtained from Operon (Alameda, CA) and used without purification. The full-length cDNA was reassembled using a fragment of the mutated clone. The sequence corresponding to this fragment, as well as the flanking regions, was verified by automated sequencing. The full-length rat $Ca_v3.2$ cDNA was generated by full-length RT-PCR using total RNA isolated from adult rat thalamic tissue and oligonucleotides 5'-GATAAGCTTATGACCGAGGGCAGC-3' and 5'-CGCTCTAGACTACACAGGCTCATC-3'. The resulting ~7 kb PCR products were subcloned into pGEM T-Easy vector and then into pCNA 3.1 zeo(+) (Invitrogen). The full-length thalamic cDNA was confirmed by DNA sequencing and compared with the reported PubMed sequences for $Ca_v3.2$ cDNAs from multiple organisms as well as the rat $Ca_v3.2$ genomic DNA sequence. The His191 residue examined in the present study is conserved across the $Ca_v3.2$ T-type channels in all species in the database including chicken, dog, mouse, rat and human. Cells were transiently cotransfected using Lipofectamine 2000 (Invitrogen) at a 10:1 molar ratio with a plasmid encoding CD8 antigen and incubated with polystyrene microbeads coated with antiCD8 antibody (Invitrogen). After 48 h, cells with bound microbeads were selected for recording.

Electrophysiology. Recording electrodes were pulled from borosilicate glass microcapillary tubes (Drummond Scientific, Broomall, PA), and had resistances from 1 to 4 M Ω when filled with internal solution. Recordings were made using an Axopatch 200B patch-clamp amplifier (Molecular Devices, Foster City, CA). Digitization of membrane voltages and currents were controlled using a Digidata 1322A interfaced with Clampex 8.2 (Molecular Devices). We analyzed data using Clampfit 8.2 (Molecular Devices) and Origin 7.0 (Microcal Software, Northampton, MA). Currents were low-pass filtered at 2–5 kHz. Series resistance and capacitance values were taken directly from readings of the amplifier after electronic subtraction of the capacitive transients. Series resistance was compensated to the maximum extent possible (usually 50–80%). Multiple independently controlled glass syringes served as reservoirs for a gravity-driven perfusion system. The external solution for DRG and HEK293 cell experiments contained (in mM) 152 tetraethylammonium (TEA)-Cl, 10 BaCl₂, and 10 HEPES, adjusted to pH 7.4 with TEA-OH. The external solution for thalamic slice experiments contained (in mM) 130 NaCl, 26 NaHCO₃, 10 glucose, 2.5 MgCl₂, 2 CaCl₂, 1.25 NaH₂PO₄, and 0.001 TTX, equilibrated with a mixture of 95% O₂ and 5% CO₂. In some experiments, TTX was omitted to study burst firing of nucleus reticularis thalami (nRT) neurons. The internal solution for voltage-clamp experiments with DRG neurons and thalamic slices contained (in mM) 135 tetramethylammonium-OH, 40 HEPES, 10 EGTA, and 2 MgCl₂, adjusted to pH 7.2 with hydrofluoric acid. The internal solution for voltage-clamp experiments with HEK293 cells contained (in mM) 110 Cs-MeSO₄, 14 Cr-PO₄, 10 HEPES, 9 EGTA, 5 Mg-ATP, and 0.3 Tris-GTP, adjusted to pH 7.3 with CsOH. The internal solution for current-clamp experiments with thalamic slices contained (in mM) 130 KCl, 40 HEPES, 5 MgCl₂, 2 Mg-ATP, 1 EGTA, 0.1 Na₃GTP, adjusted to pH 7.3 with KOH.

Analysis. Statistical comparisons were made using paired or unpaired *t* tests or Mann-Whitney *U* tests where appropriate. All data are expressed as mean \pm SEM and *p* values are reported only when statistically significant (<0.05). The percentage reductions in peak current at various ascorbate and Cu²⁺ concentrations were used to generate concentration–response curves. Mean values were fit to the following Hill–Langmuir function:

$$PB([\text{drug}]) = PB_{\text{max}} / (1 + (IC_{50} / [\text{drug}])^h), \quad (1)$$

where PB_{max} is the maximal percentage inhibition of peak current, IC_{50} is the concentration that produces 50% inhibition, and *h* is the apparent Hill–Langmuir coefficient for inhibition. The fitted values are reported with >95% linear confidence limits. The voltage dependencies of activation and steady-state inactivation were described with single Boltzmann distributions of the following forms:

$$\text{Activation: } I(V) = I_{\text{max}} / (1 + \exp[-(V - V_{50})/k]), \quad (2)$$

$$\text{Inactivation: } I(V) = I_{\text{max}} / (1 + \exp[(V - V_{50})/k]), \quad (3)$$

where I_{max} is the maximal activatable current, V_{50} is the voltage where half the current is activated or inactivated, and *k* is the voltage dependence (slope) of the distribution.

Results

We used whole-cell patch-clamp recordings to determine the effects of ascorbate on voltage-gated Ca^{2+} currents present in acutely dissociated DRG neurons. Ascorbate rapidly inhibited

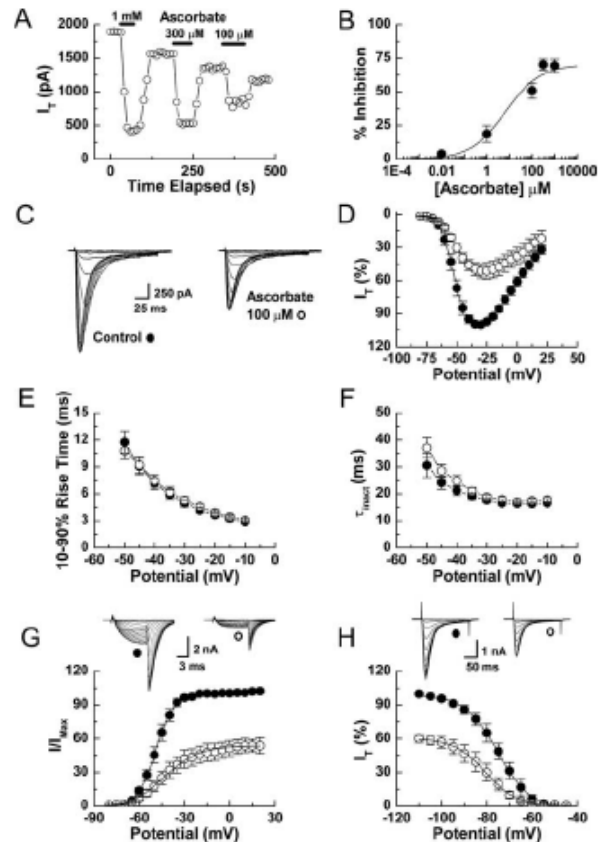


Figure 1. Ascorbate inhibition of rat DRG T-currents. *A*, Time course showing the effects of various ascorbate concentrations on T-currents from an acutely dissociated DRG neuron. T-currents were evoked by 175 ms steps from -90 to -40 mV every 10 s. *B*, Concentration–response curve for inhibition of DRG T-currents by ascorbate. Average data were fit with Equation 1 to generate the curve: $IC_{50} = 6.5 \pm 3.9 \mu\text{M}$; $h = 0.56 \pm 0.12$; maximal inhibition, $70.2 \pm 2.1\%$; ($n = 4-9$). *C*, T-currents evoked from a DRG neuron by steps from -90 to -80 through -20 mV ($\Delta 5$ mV), before and during exposure to ascorbate. *D*, Averaged effects of ascorbate on DRG T-currents evoked by steps from -90 mV to the indicated test potentials ($n = 8$). *E*, Averaged effects of ascorbate on the kinetics of DRG T-current activation calculated as 10–90% rise time from IV data ($n = 8$). *F*, Averaged effects of ascorbate on the kinetics of DRG T-current inactivation calculated from single exponential fits of IV data ($n = 8$). *G*, Raw traces and average effects of ascorbate on voltage-dependent activation of DRG T-currents: control, $V_{50} = -49.0 \pm 0.3$; $k = 6.2 \pm 0.2$; ascorbate, $V_{50} = -44.1 \pm 0.9$; $k = 11.9 \pm 0.8$ ($n = 6$). Data were calculated from isochronal tail currents evoked by 10 ms steps from -90 to -80 through 20 mV ($\Delta 5$ mV), where the amplitude of the tail current is a measure of the conductance activated during the preceding pulse. Average data were fit with Equation 2 to generate curves. *H*, Raw traces and average effects of ascorbate on steady-state inactivation of DRG T-currents: control, $V_{50} = -75.0 \pm 0.3$; $k = 7.3 \pm 0.3$; ascorbate, $V_{50} = -80.4 \pm 0.4$; $k = 7.1 \pm 0.4$ ($n = 6$). Currents were recorded at -30 mV after prepulses lasting 3.5 s to potentials from -110 to -45 mV. Average data were fit with Equation 3 to generate curves.

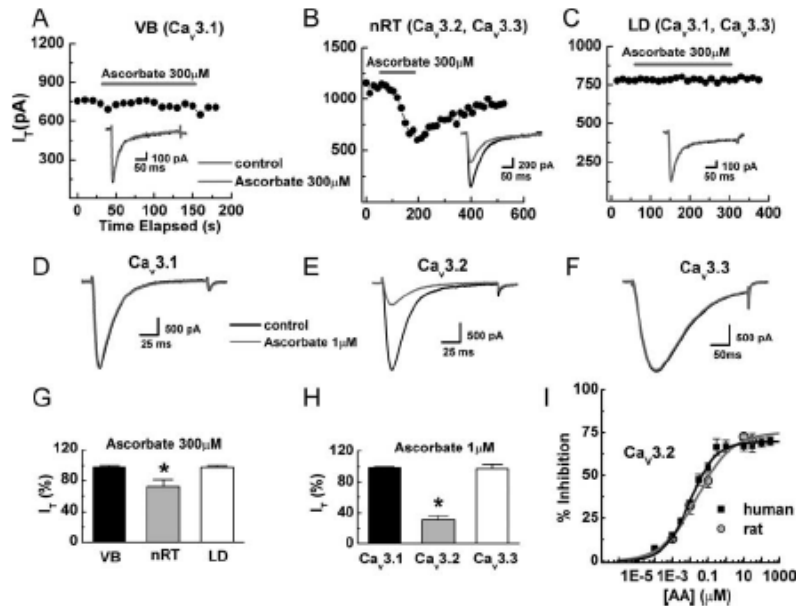


Figure 2. Ascorbate inhibits $Ca_v3.2$, but not $Ca_v3.1$ or $Ca_v3.3$ T-currents in both native thalamic and recombinant HEK293 cells. *A–C*, Time courses and raw traces showing the differential effects of ascorbate on T-currents from representative nRT, LD, and VB thalamic neurons. *D–F*, Raw traces showing the differential effects of ascorbate on T-currents from recombinant $Ca_v3.1$, $Ca_v3.2$, and $Ca_v3.3$ channels expressed in HEK293 cells. *G*, Averaged effects of ascorbate on T-currents in thalamic nuclei expressed as a percentage of control: nRT, $72.6 \pm 2.9\%$; $p < 0.01$; LD, $97.8 \pm 1.4\%$; VB, $98.0 \pm 1.6\%$ ($n = 3–9$). *H*, Averaged effects of ascorbate on recombinant T-currents expressed as a percentage of control: $Ca_v3.1$, $98.8 \pm 1.1\%$; $Ca_v3.2$, $30.7 \pm 5.5\%$; $p < 0.01$; $Ca_v3.3$, $97.4 \pm 5.6\%$ ($n = 5–8$). *I*, Concentration–response curve for inhibition of recombinant $Ca_v3.2$ currents by ascorbate. Average data were fit with Equation 1 to generate the curve: IC_{50} , 9.75 ± 0.01 nM; h , 0.60 ± 0.05 ; maximal inhibition, $69.9 \pm 1.2\%$ ($n = 4–7$) for the human clone and IC_{50} , 25.10 ± 0.01 nM; h , 0.45 ± 0.08 ; maximal inhibition, $75.1 \pm 4.0\%$ ($n = 4–7$) for the rat clone. * $p < 0.01$.

T-currents (Fig. 1A), but had no effect on high-voltage-activated Ca^{2+} currents even at 50-fold higher concentrations (data not shown). T-current inhibition was dose-dependent and partial with an effective concentration (IC_{50}) of 6.5μ M and a maximal reduction in peak current of 70% (Fig. 1B). The inhibition induced by brief exposure to ascorbate was partially reversible after washout, with $\sim 75–90\%$ recovery occurring after exposures of less than a minute; the effects of prolonged exposures were significantly less reversible (data not shown).

To assess the effects of ascorbate on the biophysical properties of DRG T-currents, we measured current–voltage ($I–V$) relationships in the presence and absence of ascorbate (Fig. 1C,D). Ascorbate significantly reduced T-currents at all potentials between -70 and 20 mV, but had no significant effect on the kinetics of current activation or inactivation (Fig. 1E,F). Ascorbate did induce a 5 mV rightward shift in half-maximal activation (V_{50}) with a decrease in voltage dependence, as well as a 5 mV leftward shift in the V_{50} of inactivation, but without an effect on voltage dependence (Fig. 1G,H).

$Ca_v3.2$ is overwhelmingly the predominant T-channel isoform expressed in DRG neurons (Talley et al., 1999; Chen et al., 2003). Therefore we also examined the effects of ascorbate on intact neurons in brain slices of thalamic nuclei known to express diverse T-channels (Talley et al., 1999; Joksovic et al., 2006). Ascorbate significantly inhibited T-currents from reticular (nRT, $Ca_v3.2$ and $Ca_v3.3$), but not ventrobasal (VB, $Ca_v3.1$) or laterodorsal (LD, $Ca_v3.1$ and $Ca_v3.3$) thalamic neurons, suggesting selective inhibition of $Ca_v3.2$ (Fig. 2A–C,G). We confirmed this

using both recombinant human and rat T-channels heterologously expressed in HEK293 cells. Ascorbate significantly inhibited $Ca_v3.2$ currents, but had no effect on either $Ca_v3.1$ or $Ca_v3.3$ currents even at a 1000-fold higher concentration (Fig. 2D–F,H,I). Additionally, ascorbate induced gating shifts in recombinant human $Ca_v3.2$ currents (Fig. 3) that were nearly identical to those observed in native rat DRG neurons (Fig. 1).

To determine the molecular substrate for ascorbate inhibition of $Ca_v3.2$, we constructed chimeras between $Ca_v3.1$ ($\alpha 1G$, insensitive) and $Ca_v3.2$ ($\alpha 1H$, sensitive) and screened for sensitivity to ascorbate. The chimeras were named using letters to represent the α -subunit donor for each of the four channel domains (Fig. 4). GGHH currents were insensitive to ascorbate, whereas HHGG currents were sensitive, indicating that critical residues are located within domains 1 or 2 of $Ca_v3.2$ (Fig. 4A,B,E). We then constructed two single-domain chimeras, exchanging either domain 1 or 2. GHGG currents were insensitive to ascorbate whereas HGGG currents were sensitive. Thus, domain 1 of $Ca_v3.2$ is required for ascorbate inhibition (Fig. 4C–E).

Notably, ascorbate inhibition of the chimeras mirrors their reported inhibition by Ni^{2+} (Kang et al., 2006). This is of interest because similar to ascorbate, Ni^{2+} is one of the few agents capable of discriminating among T-channel isoforms, as $Ca_v3.2$ is ~ 20 -fold more sensitive than $Ca_v3.1$ or $Ca_v3.3$ (Lee et al., 1999a; Jeong et al., 2003; Kang et al., 2006). Furthermore, mutation of a single extracellular histidine (H) residue to glutamine (Q) at position 191 (H191Q) greatly reduces the Ni^{2+} sensitivity of $Ca_v3.2$, indicating that H191 is part of a high-affinity Ni^{2+} binding site (Kang et al., 2006). Based on these observations and studies demonstrating that ascorbate-induced MCO can selectively modify histidine residues at metal-binding sites (Uchida and Kawakishi, 1990; Stadtman, 1993; Zhao et al., 1997; Hovorka et al., 2002), we hypothesized that H191 is also important for ascorbate inhibition of $Ca_v3.2$. Consistent with this, the effects of ascorbate were completely abolished in $Ca_v3.2$ (H191Q) (Fig. 4F). The biophysical parameters of $Ca_v3.2$ (H191Q) currents were similar to $Ca_v3.2$, but were unaffected by ascorbate, indicating the mutation disrupted ascorbate sensitivity, but not basic channel gating (data not shown). We next attempted to confer ascorbate sensitivity to $Ca_v3.1$ by performing the analogous reverse mutation (Q172H). Figure 4F shows that $Ca_v3.1$ (Q172H) currents were significantly inhibited by ascorbate, confirming the requirement of H191 for sensitivity.

Similar to Ni^{2+} , $Ca_v3.2$ is significantly more sensitive to inhibition by other divalent transition metals such as Cu^{2+} and Zn^{2+} than $Ca_v3.1$ or $Ca_v3.3$ (Jeong et al., 2003; Traboulsie et al., 2007). Hence, H191 may not be a Ni^{2+} -exclusive binding site, and may also be critical for high-affinity Cu^{2+} and Zn^{2+} binding. Because highly redox reactive metals such as Cu^{2+} and Fe^{3+} are much more likely to play a role in MCO than relatively redox inactive

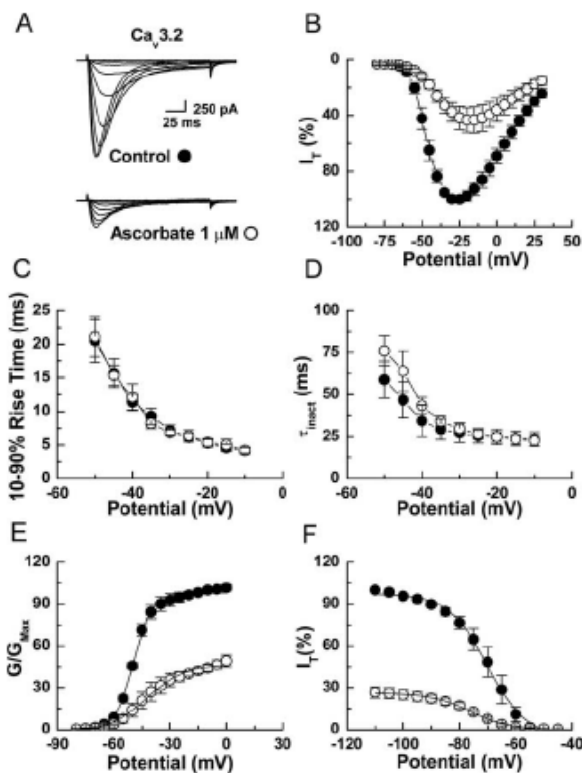


Figure 3. Ascorbate inhibition of recombinant $Ca_v3.2$ T-currents in HEK293 cells. *A*, Currents evoked from an HEK293 cell expressing human $Ca_v3.2$ by steps from -90 to -80 through -25 mV ($\Delta 5$ mV), before and during exposure to ascorbate. *B*, Averaged effects of ascorbate on $Ca_v3.2$ currents evoked by steps from -90 to -80 through 25 mV ($n = 8$). *C*, Averaged effects of ascorbate on the kinetics of $Ca_v3.2$ current activation calculated as 10–90% rise time from IV data ($n = 8$). *D*, Averaged effects of ascorbate on the kinetics of $Ca_v3.2$ current inactivation calculated from single exponential fits of IV data ($n = 8$). *E*, Average effects of ascorbate on voltage-dependent activation of $Ca_v3.2$ current: control, $V_{50} = -49.3 \pm 0.3$; $k = 5.0 \pm 0.3$; ascorbate, $V_{50} = -42.5 \pm 1.2$; $k = 10.6 \pm 1.3$ ($n = 4$). Data were calculated from isochronal tail currents evoked by 10 ms steps from -90 to -80 through 0 mV ($\Delta 5$ mV), where the amplitude of the tail current is a measure of the conductance activated during the preceding pulse. Average data were fit with Equation 2 to generate curves. *F*, Average effects of ascorbate on steady-state inactivation of $Ca_v3.2$ current: control, $V_{50} = -70.0 \pm 0.4$; $k = 6.9 \pm 0.4$; ascorbate, $V_{50} = -76.0 \pm 0.4$; $k = 7.2 \pm 1.6$ ($n = 5$). Currents were recorded at -30 mV after prepulses lasting 3.5 s to potentials from -110 to -45 mV. Average data were fit with Equation 3 to generate curves.

metals such as Ni^{2+} or Zn^{2+} (Stadtman, 1991, 1993), we examined whether the Cu^{2+} sensitivity of $Ca_v3.2$ is also disrupted by the H191Q mutation. As shown in Figure 4G, $Ca_v3.2(H191Q)$ was >40 -fold less sensitive to Cu^{2+} than $Ca_v3.2$, supporting the hypothesis that H191 is part of a general high-affinity metal binding site located on the external surface of $Ca_v3.2$.

Ascorbate generates ROS through reactions that depend on transition metals. A point that has been repeatedly demonstrated by the use of metal chelators; in particular, ascorbate inhibition of T-currents in pancreatic β cells is completely abolished by previous application of the chelator diethylenetriaminepentaacetic acid (DTPA) (Parsey and Matteson, 1993). Of note, DTPA results in a large increase in baseline T-currents, indicating that channels are subject to tonic inhibition by trace metals (Parsey and Matteson, 1993). Similarly, we found that DTPA significantly enhanced T-currents in DRG neurons, and completely occluded the effects of subsequently applied ascorbate (Fig. 5A, E). In addition

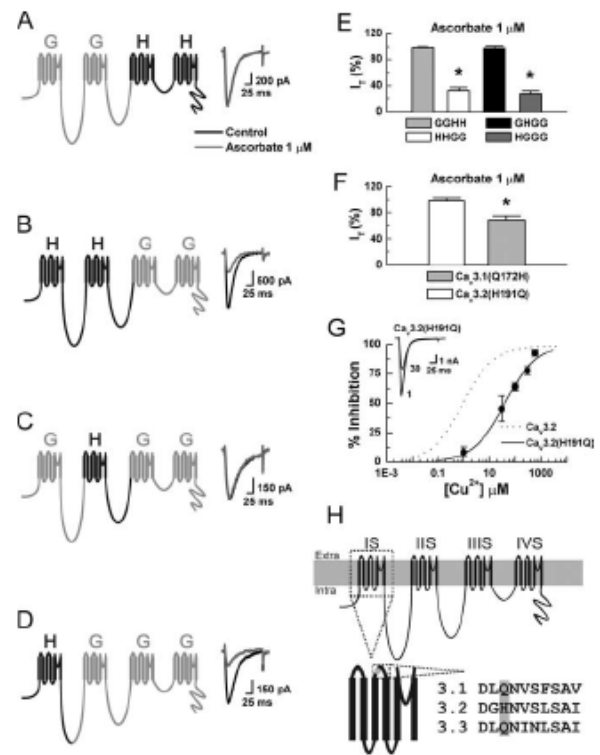


Figure 4. H191 is required for the ascorbate sensitivity of $Ca_v3.2$. *A–D*, Currents were evoked from HEK293 cells expressing the indicated constructs by steps from -90 to -30 mV, before and during exposure to ascorbate. *E*, Average effects of ascorbate on the indicated constructs expressed as a percentage of control: GGHH, $99.1 \pm 1.1\%$; HHGG, $32.7 \pm 4.7\%$, $p < 0.01$; GHGG, $97.9 \pm 3.1\%$; HGGG, $28.2 \pm 4.1\%$, $p < 0.01$ ($n = 5–9$). *F*, Average effects of ascorbate on the indicated constructs expressed as % of control: $Ca_v3.2(H191Q)$, $98.7 \pm 4.1\%$; $Ca_v3.1(Q172H)$, $72.6 \pm 6.1\%$, $p < 0.01$ ($n = 6–8$). *G*, Raw traces and concentration–response curve for inhibition of human $Ca_v3.2(H191Q)$ by Cu^{2+} . Average data were fit with Equation 1 to generate the curve: $IC_{50} = 39.7 \pm 6.4 \mu M$; $h = 0.70 \pm 0.08$ ($n = 4–6$). The dotted line represents $Ca_v3.2$ data recorded under nearly identical conditions (HEK293 cells, 10 mM Ba^{2+}) (Jeong et al., 2003). *H*, Schematic diagram of $Ca_v3.2$ showing the position of H191 in the extracellular loop between transmembrane segments 3 and 4 of domain 1, as well as the amino acid sequence of the loop across T-channels. * $p < 0.01$.

to chelators, previous studies in other systems have implicated MCO as a mechanism for the effects of ascorbate by showing that catalase, which decomposes hydrogen peroxide (H_2O_2) and thus prevents formation of ROS via MCO, protects against ascorbate (Uchida and Kawakishi, 1990; Zhao et al., 1997; Hovorka et al., 2002). We found that catalase completely prevented the inhibition of DRG T-currents by ascorbate (Fig. 5B, E), as did high concentrations of the ROS scavenger 2-(4-carboxyphenyl)-4,4,5,5-tetramethylimidazole-1-oxyl-3-oxide (c-PTIO) (Fig. 5C, E). These results, in combination with our mutational studies, suggest that ascorbate likely modulates $Ca_v3.2$ via MCO.

In general, electrophysiological solutions contain several trace metal contaminants, with Zn^{2+} predominating (Li et al., 1996; Paoletti et al., 1997; Thio and Zhang, 2006). This implies that the observed increase in $Ca_v3.2$ currents after the addition of DTPA largely results from relief of tonic Zn^{2+} inhibition. This is interesting because Zn^{2+} is relatively redox inactive and does not readily participate in MCO; in fact, total replacement of Cu^{2+} with Zn^{2+} can protect against MCO in some systems (Chevion, 1988). However, histidine residues have significantly higher af-

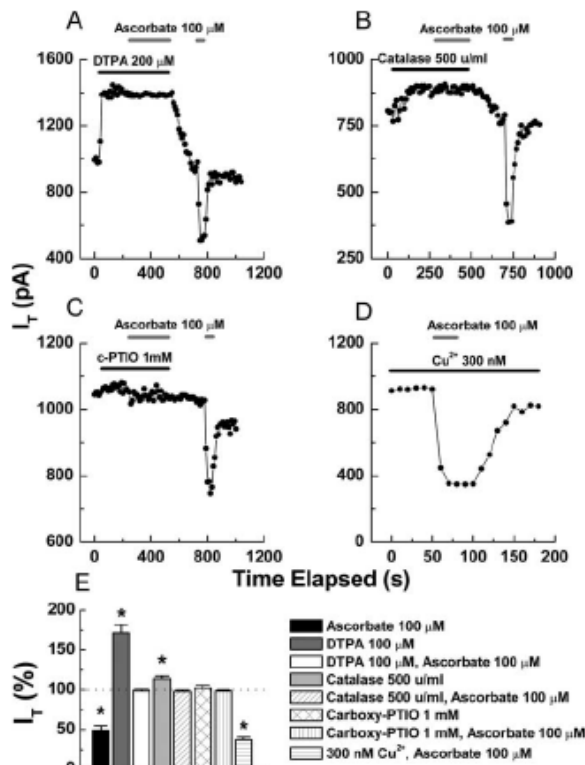


Figure 5. MCO underlies the effects of ascorbate on $Ca_v3.2$. *A–C*, Application of DTPA (*A*), catalase (*B*), and c-PTIO (*C*) occludes inhibition of T-currents by ascorbate in 3 representative DRG neurons. *D*, Representative time course from a DRG neuron showing that the inhibition by ascorbate is increased by the addition of 300 nM Cu^{2+} to the external solution. *E*, Averaged effects of the indicated agents on DRG T-currents expressed as a percentage of control: ascorbate, 49.2 ± 5.8 , $p < 0.01$ (from Fig. 1*B*); DTPA, 17.4 ± 10.6 , $p < 0.01$; DTPA and ascorbate, 98.4 ± 2.3 ; catalase, 113.8 ± 3.7 , $p < 0.01$; catalase and ascorbate, 97.7 ± 2.1 ; c-PTIO, 102.6 ± 3.2 ; c-PTIO and ascorbate, 98.3 ± 1.6 ; 300 nM Cu^{2+} and ascorbate, 37.3 ± 4.2 , $p < 0.01$ ($n = 5–12$). For these experiments, the steady-state effect of the first agent was considered a new baseline to calculate the subsequent inhibition by ascorbate. * $p < 0.01$.

finitly for Cu^{2+} than Zn^{2+} (Sundberg and Martin, 1974), thus many Zn^{2+} -binding proteins are nonetheless susceptible to modification by MCO in the presence of even trace amounts of Cu^{2+} . This was specifically demonstrated by Hovorka et al. (2002), who showed that Zn^{2+} -insulin was less susceptible to MCO as the Cu^{2+}/Zn^{2+} ratio was decreased from 1:1 to 1:10, but that even a 1:1000 ratio was unable to protect against ascorbate completely. Along these lines, we found that increasing the Cu^{2+}/Zn^{2+} ratio in our extracellular solution by adding 300 nM Cu^{2+} , resulted in a significant increase (12%) in the inhibition produced by ascorbate (Fig. 5*D,E*).

Collectively, our data indicate that H191 is a critical component of a high-affinity metal binding site located on the external surface of $Ca_v3.2$, and that ascorbate inhibits $Ca_v3.2$ via interaction with trace metal contaminants bound at this site, likely resulting in MCO. It is less clear which specific amino acid(s) are modified. H191 may be the residue modified by ROS, but because the affinity of metals for any single amino acid is relatively low, H191 is more likely only one part of a multiresidue binding site. Thus, it is possible that the ascorbate insensitivity of $Ca_v3.2$ (H191Q) results solely from the disruption of metal binding, which prevents subsequent MCO of a neighboring residue in

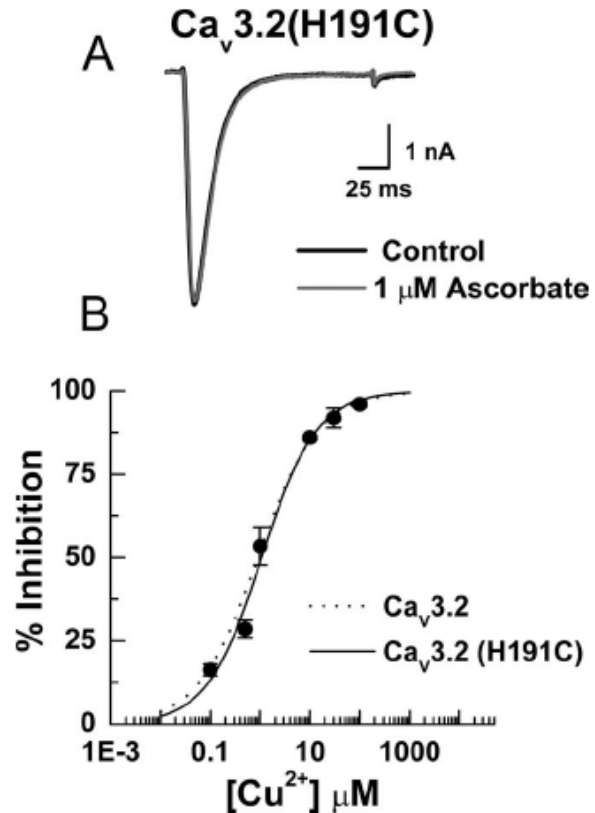


Figure 6. $Ca_v3.2$ (H191C) is ascorbate-insensitive, but Cu^{2+} -sensitive. *A*, Raw traces showing the lack of ascorbate effect on $Ca_v3.2$ (H191C) currents in an HEK293 cell. Similar results were obtained in experiments from five additional cells (peak current in the presence of ascorbate was $96.2 \pm 1.2\%$ of control). *B*, Concentration–response curve for inhibition of $Ca_v3.2$ (H191C) by Cu^{2+} . Average data were fit with Equation 1 to generate the curve: IC_{50} , 1.07 ± 0.16 μ M; h , 0.79 ± 0.09 ($n = 4–7$). The dotted line represents $Ca_v3.2$ data recorded under nearly identical conditions (HEK293 cells, 10 mM Ba^{2+}) (Jeong et al., 2003).

the binding site. To investigate this, we made another point mutation, $Ca_v3.2$ (H191C), because cysteine residues have metal binding abilities comparable to histidines, but are less sensitive to MCO. Figure 6 shows that $Ca_v3.2$ (H191C) channels were ascorbate-insensitive, but highly Cu^{2+} -sensitive, strongly suggesting that the effects of ascorbate on $Ca_v3.2$ are the result of the MCO of H191 and not a neighboring residue.

Last, we examined the ability of ascorbate to modulate $Ca_v3.2$ -dependent neuronal excitability in nRT neurons in intact brain slices. The ability of thalamic neurons to fire low-threshold Ca^{2+} spikes (LTSs) is dependent on T-currents and contributes to the ability of these neurons to fire bursts of action potentials (APs) in response to small membrane depolarizations such as those caused by excitatory postsynaptic potentials (Perez-Reyes, 2003). As shown in Figure 7, application of ascorbate at physiologically relevant concentrations (Rice, 2000) reversibly inhibited both the isolated LTSs as well as burst-firing in current-clamp recordings from nRT neurons, suggesting that ascorbate may function as an endogenous modulator of nRT excitability.

Discussion

Our results demonstrate the remarkably specific inhibition of $Ca_v3.2$ channels by ascorbate. Indeed, ascorbate is the most

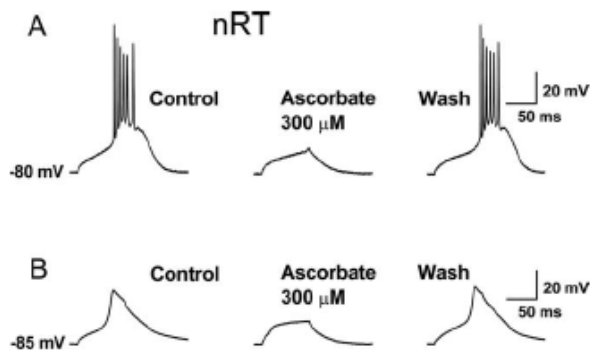


Figure 7. Ascorbate inhibition of LTSs and burst firing in nRT neurons. *A*, Representative current-clamp trace from an nRT neuron (the LTS was evoked by a 250 ms, 100 pA current injection at the indicated membrane potential). Application of ascorbate reversibly reduced the amplitude of the LTS and abolished the resulting burst of APs. In similar experiments from five cells, ascorbate reduced the average number of APs crowning the LTS from 4.6 ± 0.7 to 2.4 ± 1.1 ($p < 0.01$). *B*, Ascorbate reversibly inhibited the isolated LTS in another nRT neuron. The protocol was similar to that in *A*, but with the addition of $1 \mu\text{M}$ TTX to block APs. In similar experiments from six cells, ascorbate reduced the amplitude of the LTS by $44.6 \pm 11.4\%$ ($p < 0.01$).

selective agent capable of discriminating among T-channel isoforms yet described. Thus, ascorbate may be a useful pharmacological tool for identifying the contribution of $\text{Ca}_v3.2$ current to total Ca^{2+} current, as well as to cellular excitability.

Additionally, our findings suggest that MCO is the likely molecular mechanism for inhibition of $\text{Ca}_v3.2$ channels by ascorbate. Several reaction products can result from the MCO of histidine, but the most common is 2-oxo-histidine, which is created by oxidation at the C-2 position of histidine's imidazole ring (Uchida and Kawakishi, 1990; Stadtman, 1993; Schoneich, 2006). The formation of 2-oxo-histidine has been demonstrated in small peptides *in vitro* and *in vivo* using high-resolution mass spectrometry (Schoneich, 2006). However, current technology is limited to small peptides and is unable to detect such small covalent modifications in larger proteins such as Ca^{2+} channels. Despite being unable to demonstrate the precise reaction product, our data collectively implicate MCO as the mechanism underlying the effects of ascorbate on $\text{Ca}_v3.2$.

One particularly interesting observation of this study was the significantly increased inhibitory potency of ascorbate against both recombinant human and rat $\text{Ca}_v3.2$ channels compared with native rat $\text{Ca}_v3.2$ channels. This discrepancy may be attributable to the interaction of native $\text{Ca}_v3.2$ channels with accessory subunits or other regulatory proteins, or the presence of endogenous redox buffers that are absent or altered in heterologous systems.

Another intriguing aspect of our findings concerns the observation that the effects of brief applications of ascorbate are at least partially reversible, which is interesting given the fact that MCO is a covalent modification. However, there are numerous biological examples of reversible covalent modification serving as a mechanism for the regulation of protein function (Rakitzis, 1990; Veal et al., 2007), including modulation of ion channel gating, as exemplified by the activation of TRPA1 channels by natural isothiocyanate-containing compounds (Hinman et al., 2006). Additionally, there are several reactions involving reversible covalent modifications of histidine residues in other systems (in-

cluding several mediated by ascorbate), despite the fact that the reversibility is predicted to be energetically unfavorable (Farver et al., 1998; Njus et al., 2001). It is possible that endogenous enzymes with the ability to reverse the effects of MCO exist within neurons; however, additional experiments will be necessary to evaluate this possibility.

Ascorbate can function as a neuromodulator, is concentrated in both extra ($100\text{--}500 \mu\text{M}$) and intracellular (up to 10 mM) brain spaces, and can undergo dynamic changes in a variety of physiological and pathophysiological conditions (Rice, 2000). Thus, it is interesting to speculate on the functional significance of $\text{Ca}_v3.2$ modulation by ascorbate, especially considering $\text{Ca}_v3.2$ -dependent LTSs are crucial to the synchronization of low-amplitude oscillations in the loop of mutually interconnected nRT, thalamic relay, and cortical neurons (Perez-Reyes, 2003). Additionally, modulation of $\text{Ca}_v3.2$ by genetic or pharmacological means has been shown to modulate LTSs and burst firing in nRT neurons as evidenced by altered excitability in both current-clamp recordings (Jokovic et al., 2006) and *in silico* simulations (Vitko et al., 2005). Thus, modulation of these channels by ascorbate under conditions that favor MCO may have important consequences for a variety of physiological processes and pathological conditions. Such conditions may include those associated with neuronal injury, epilepsy, Alzheimer's disease, Menke's disease, and Wilson's disease, where there are documented increases in extracellular (free) redox-reactive transition metals such as Cu^{2+} and Fe^{3+} (Strausak et al., 2001; Bush, 2003; Mathie et al., 2006). High levels of Cu^{2+} ($200\text{--}400 \mu\text{M}$) can also be released from synaptic terminals onto postsynaptic cells known to contain $\text{Ca}_v3.2$ channels in such brain areas as the hippocampus and olfactory bulb (Mathie et al., 2006). Future studies are necessary to investigate these possibilities, as well as to determine whether other ion channels such as $\text{NR}_1/\text{NR}_2\text{A}$ NMDA receptors that are known to contain high-affinity metal binding sites (Herin and Aizenman, 2004), show inhibition by ascorbate (Majewska and Bell, 1990; Majewska et al., 1990), and undergo covalent modification by free radicals (Aizenman et al., 1990) are subject to similar regulation.

References

- Aizenman E, Hartnett KA, Reynolds IJ (1990) Oxygen free radicals regulate NMDA receptor function via a redox modulatory site. *Neuron* 5:841–846.
- Bush AI (2003) The metallobiology of Alzheimer's disease. *Trends Neurosci* 26:207–214.
- Chen CC, Lamping KG, Nuno DW, Barresi R, Prouty SJ, Lavoie JL, Cribbs LL, England SK, Sigmund CD, Weiss RM, Williamson RA, Hill JA, Campbell KP (2003) Abnormal coronary function in mice deficient in alpha1H T-type Ca^{2+} channels. *Science* 302:1416–1418.
- Chevion M (1988) A site-specific mechanism for free radical induced biological damage: The essential role of redox-active transition metals. *Free Radic Biol Med* 5:27–37.
- Farver O, Eady RR, Abraham ZH, Pecht I (1998) The intramolecular electron transfer between copper sites of nitrite reductase: A comparison with ascorbate oxidase. *FEBS Lett* 436:239–242.
- Herin GA, Aizenman E (2004) Amino terminal domain regulation of NMDA receptor function. *Eur J Pharmacol* 500:101–111.
- Hinman A, Chuang HH, Bautista DM, Julius D (2006) TRP channel activation by reversible covalent modification. *Proc Natl Acad Sci USA* 103:19564–19568.
- Hovorka SW, Biesiada H, Williams TD, Huhmer A, Schoneich C (2002) High sensitivity of Zn^{2+} insulin to metal-catalyzed oxidation: Detection of 2-oxo-histidine by tandem mass spectrometry. *Pharm Res* 19:530–537.
- Jeong SW, Park BG, Park JY, Lee JW, Lee JH (2003) Divalent metals differentially block cloned T-type calcium channels. *NeuroReport* 14:1537–1540.

- Joksovic PM, Nelson MT, Jevtovic-Todorovic V, Patel MK, Perez-Reyes E, Campbell KP, Chen CC, Todorovic SM (2006) CaV3.2 is the major molecular substrate for redox regulation of T-type Ca²⁺ channels in the rat and mouse thalamus. *J Physiol (Lond)* 574:415–430.
- Kang HW, Park JY, Jeong SW, Kim JA, Moon HJ, Perez-Reyes E, Lee JH (2006) A molecular determinant of nickel inhibition in Cav3.2 T-type calcium channels. *J Biol Chem* 281:4823–4830.
- Lee JH, Gomora JC, Cribbs LL, Perez-Reyes E (1999a) Nickel block of three cloned T-type calcium channels: Low concentrations selectively block $\alpha 1H$. *Biophys J* 77:3034–3042.
- Lee JH, Daud AN, Cribbs LL, Lacerda AE, Pereverzev A, Klockner U, Schneider T, Perez-Reyes E (1999b) Cloning and expression of a novel member of the low voltage-activated T-type calcium channel family. *J Neurosci* 19:1912–1921.
- Li C, Peoples RW, Weight FF (1996) Proton potentiation of ATP-gated ion channel responses to ATP and Zn²⁺ in rat nodose ganglion neurons. *J Neurophysiol* 76:3048–3058.
- Majewska MD, Bell JA (1990) Ascorbic acid protects neurons from injury induced by glutamate and NMDA. *NeuroReport* 1:194–196.
- Majewska MD, Bell JA, London ED (1990) Regulation of the NMDA receptor by redox phenomena: Inhibitory role of ascorbate. *Brain Res* 537:328–332.
- Mathie A, Sutton GL, Clarke CE, Veale EL (2006) Zinc and copper: Pharmacological probes and endogenous modulators of neuronal excitability. *Pharmacol Ther* 111:567–583.
- Nelson MT, Joksovic PM, Perez-Reyes E, Todorovic SM (2005) The endogenous redox agent L-cysteine induces T-type Ca²⁺ channel-dependent sensitization of a novel subpopulation of rat peripheral nociceptors. *J Neurosci* 25:8766–8775.
- Njus D, Wagle M, Kelley PM, Kipp BH, Schlegel HB (2001) Mechanism of ascorbic acid oxidation by cytochrome b(561). *Biochemistry* 40:11905–11911.
- Paoletti P, Ascher P, Neyton J (1997) High-affinity zinc inhibition of NMDA NR1-NR2A receptors. *J Neurosci* 17:5711–5725.
- Parsey RV, Matteson DR (1993) Ascorbic acid modulation of calcium channels in pancreatic beta cells. *J Gen Physiol* 102:503–523.
- Perez-Reyes E (2003) Molecular physiology of low-voltage-activated t-type calcium channels. *Physiol Rev* 83:117–161.
- Perez-Reyes E, Cribbs LL, Daud A, Lacerda AE, Barclay J, Williamson MP, Fox M, Rees M, Lee JH (1998) Molecular characterization of a neuronal low-voltage-activated T-type calcium channel. *Nature* 391:896–900.
- Rakitzis ET (1990) Utilization of the free energy of the reversible binding of protein and modifying agent towards the rate-enhancement of protein covalent modification. *Biochem J* 269:835–838.
- Rice ME (2000) Ascorbate regulation and its neuroprotective role in the brain. *Trends Neurosci* 23:209–216.
- Schoneich C (2006) Protein modification in aging: an update. *Exp Gerontol* 41:807–812.
- Stadtman ER (1991) Ascorbic acid and oxidative inactivation of proteins. *Am J Clin Nutr* 54:1125S–1128S.
- Stadtman ER (1993) Oxidation of free amino acids and amino acid residues in proteins by radiolysis and by metal-catalyzed reactions. *Annu Rev Biochem* 62:797–821.
- Strausak D, Mercer JF, Dieter HH, Stremmel W, Multhaup G (2001) Copper in disorders with neurological symptoms: Alzheimer's, Menkes, and Wilson diseases. *Brain Res Bull* 55:175–185.
- Sundberg RJ, Martin BR (1974) Interactions of histidine and other imidazole derivatives with transition metal ions in chemical and biological systems. *Chem Rev* 74:471–517.
- Talley EM, Cribbs LL, Lee JH, Daud A, Perez-Reyes E, Bayliss DA (1999) Differential distribution of three members of a gene family encoding low voltage-activated (T-type) calcium channels. *J Neurosci* 19:1895–1911.
- Thio LL, Zhang HX (2006) Modulation of inhibitory glycine receptors in cultured embryonic mouse hippocampal neurons by zinc, thiol containing redox agents and carnosine. *Neuroscience* 139:1315–1327.
- Todorovic SM, Jevtovic-Todorovic V, Meyenburg A, Mennerick S, Perez-Reyes E, Romano C, Olney JW, Zorumski CF (2001) Redox modulation of T-type calcium channels in rat peripheral nociceptors. *Neuron* 31:75–85.
- Traboulsie A, Chemin J, Chevalier M, Quignard JF, Nargeot J, Lory P (2007) Subunit-specific modulation of T-type calcium channels by zinc. *J Physiol (Lond)* 578:159–171.
- Uchida K, Kawakishi S (1990) Site-specific oxidation of angiotensin I by copper(II) and L-ascorbate: conversion of histidine residues to 2-imidazolones. *Arch Biochem Biophys* 283:20–26.
- Veal EA, Day AM, Morgan BA (2007) Hydrogen peroxide sensing and signaling. *Mol Cell* 26:1–14.
- Vitko I, Chen Y, Arias JM, Shen Y, Wu XR, Perez-Reyes E (2005) Functional characterization and neuronal modeling of the effects of childhood absence epilepsy variants of CACNA1H, a T-type calcium channel. *J Neurosci* 25:4844–4855.
- Welsby PJ, Wang H, Wolfe JT, Colbran RJ, Johnson ML, Barrett PQ (2003) A mechanism for the direct regulation of T-type calcium channels by Ca²⁺/calmodulin-dependent kinase II. *J Neurosci* 23:10116–10121.
- White G, Lovinger DM, Weight FF (1989) Transient low-threshold Ca²⁺ current triggers burst firing through an afterdepolarizing potential in an adult mammalian neuron. *Proc Natl Acad Sci USA* 86:6802–6806.
- Zhao F, Ghezzi-Schoneich E, Aced GI, Hong J, Milby T, Schoneich C (1997) Metal-catalyzed oxidation of histidine in human growth hormone. mechanism, isotope effects, and inhibition by a mild denaturing alcohol. *J Biol Chem* 272:9019–9029.

APPENDIX 4: Ca_v2.1 P/Q-TYPE CALCIUM CHANNEL ALTERNATIVE SPLICING AFFECTS THE FUNCTIONAL IMPACT OF FAMILIAL HEMIPLEGIC MIGRAINE MUTATIONS: IMPLICATIONS FOR CALCIUM CHANNELOPATHIES

Research Paper

Ca_v2.1 P/Q-type calcium channel alternative splicing affects the functional impact of familial hemiplegic migraine mutations

Implications for calcium channelopathies

Paul J. Adams,¹ Esperanza Garcia,¹ Laurence S. David,¹ Kirk J. Mulatz,¹ Sian D. Spacey^{1,2} and Terrance P. Snutch^{1,*}

¹Michael Smith Laboratories; and ²Division of Neurology; University of British Columbia; Vancouver, BC CA

Key words: calcium channel, P/Q-type, familial hemiplegic migraine, alternative splicing

Alternative splicing is known to generate multiple functionally distinct calcium channel variants that exhibit unique spatial and temporal expression patterns. In humans, naturally occurring mutations in genes encoding calcium channel pore forming α_1 -subunits are associated with several severe hereditary disorders although it remains to be described whether there exists any relationship between the physiological effects of these mutations and calcium channel splice variation. In the present study, we systematically compare the biophysical effects of three type-1 familial hemiplegic migraine (FHM-1) mutations in two predominant splice variants of the neuronal Ca_v2.1 P/Q-type channel. All three FHM-1 mutations cause a greater hyperpolarizing shift in voltage-dependent properties when expressed in the short carboxyl terminus variant (Ca_v2.1 $\Delta 47$) compared to the long variant (Ca_v2.1 +47). Furthermore, the FHM-1 mutations also exhibit differential splice variant-specific effects on recovery from inactivation and accumulation of inactivation during tonic and burst firing. Our findings provide important insight concerning the role of calcium channel alternatively spliced variants and the molecular pathophysiology of FHM-1 and potentially of other calcium channelopathies.

Introduction

Voltage-gated calcium channels are important in many normal physiological processes including muscle contraction, neurotransmitter release, regulation of calcium-dependent enzymes and gene expression (reviewed in ref. 1). It is therefore perhaps not surprising that naturally occurring mutations in calcium channel genes have been implicated in a number of severe human diseases. Since the first mutation in a calcium channel was identified,²⁻³ over 150 individual mutations have now been reported in five of the ten

genes encoding calcium channel pore forming α_1 -subunits (Ca_v) and are associated with nine distinguishable disorders ("calcium channelopathies"). Over the past decade studies using recombinant channels in various expression systems have shown that many of these mutations have significant positive or negative effects on channel gating and/or expression levels, while others result in non-functional channels or have dominant negative effects (reviewed in ref. 4). It is noteworthy that the effects of mutations on channel function have thus far only been tested in a small subset of known calcium channel variants and a direct comparison of how mutations affect channel alternative splice variants has been largely unexplored.

It has been predicted that the ten genes encoding Ca_v subunits have the potential to generate thousands of functionally distinct splice variants.^{5,6} Indeed, isolation and characterization of some variants has shown that alternative splicing can be a means to obtain specialized calcium channel function and to optimize calcium signalling regionally, temporally and under altered environmental conditions (reviewed in refs. 6-8). It is evident that mutations directly at a splice-site or in an alternate exon can have effects on pre-mRNA splicing and/or affect a subset of splice variants expressing alternate exons.⁹⁻¹² However, the majority of identified mutations associated with calcium channelopathies are missense mutations in coding sequences other than splice-sites and alternate exons (reviewed in ref. 4). Whether channel splice variants have different functional responses to disease-causing missense mutations has not been directly explored. We hypothesized that point mutations associated with calcium channelopathies might have splice-variant specific effects with important implications for both understanding disease pathophysiology and also towards interpreting results obtained from heterologous studies using recombinant channels.

Familial Hemiplegic Migraine (FHM) is an autosomal dominant subtype of migraine characterized by an aura of hemiplegia that is associated with at least one other aura symptom such as hemianopsia, hemisensory deficit or aphasia.^{13,14} Approximately 20 missense mutations associated with FHM have been identified in the CACNA1A gene¹⁵ (called FHM-1) which encodes the

*Correspondence to: Terrance P. Snutch; Michael Smith Laboratories; University of British Columbia; Rm 219-2185 East Mall; Vancouver, BC V6T 1Z4 CA; Tel.: 604.822.6968; Fax: 604.822.6470; Email: snutch@mssl.ubc.ca

Submitted: 01/23/09; Accepted: 01/23/09

Previously published online as a Channels Epublication:
<http://www.landesbioscience.com/journals/channels/article/7932>

*A version of this appendix has been published. Adams, P.J., Garcia, E., David, L.S., Mulatz, K.J., Spacey, S.D., Snutch, T.P. (2009). Ca_v2.1 P/Q-type calcium channel alternative splicing affects the functional impact of familial hemiplegic migraine mutations: Implications for calcium channelopathies. Channels (Austin). 3(2):110-121. Reprinted with kind permission of Landes Biosciences. All rights reserved.

α_1 subunit ($\text{Ca}_v2.1$; α_{1A}) of the P/Q-type voltage-gated calcium channel. P/Q-type calcium channels are abundantly expressed throughout mammalian brain and spinal cord where they mediate calcium influx essential for neurotransmitter release, calcium-mediated second messenger signalling and calcium-dependent gene transcription.¹⁶⁻²⁰ The functional consequences of FHM-1 mutations on $\text{Ca}_v2.1$ P/Q-type channel properties have been investigated in heterologous *Xenopus* oocyte and mammalian expression systems, and more recently in neurons and whole brains of FHM-1 mutant R192Q and S218L knock-in mice.²¹⁻²⁸ While there have been some noted discrepancies reported, in both heterologous and knock-in mice systems there is a general demonstrated trend for FHM-1 mutations to exhibit gain-of-function properties: increased channel availability and increased calcium influx at lower membrane potentials resulting in a greater susceptibility to the cortical spreading depression (CSD) thought to be the underlying mechanism of aura.^{21,22,27,29-31}

There are seven identified alternatively spliced sites within the $\text{Ca}_v2.1$ subunit gene and the various splice variants exhibit distinct biophysical characteristics, calcium-dependent properties, pharmacological sensitivities and subtype-specific temporal and regional localizations in human brain.^{16,32-35} However, it is not known whether the functional impact of FHM-1 mutations is similar amongst the different $\text{Ca}_v2.1$ splice variants or whether alternative splicing contributes to the spatial and temporal nature of the FHM-1 phenotype. The carboxyl terminus of $\text{Ca}_v2.1$ channels is known to affect several physiological processes and alternative splicing in this region confers functional changes in channel properties.^{16,32,35-38} The most substantial changes induced by alternative splicing in the C-terminus of $\text{Ca}_v2.1$ channels results from the use of an alternative three prime acceptor site in the intron upstream of the last exon, exon 47.^{32,36,39,40} Alternative splicing at exon 47 introduces a frame-shift resulting in a stop codon at the beginning of exon 47. As a result, P/Q-type channels can be of either the short form (isoform 1; $\text{Ca}_v2.1$ ($\Delta 47$)) or the long form (isoform 2; $\text{Ca}_v2.1$ (+47)). The voltage-dependent and kinetic properties of the $\text{Ca}_v2.1$ (+47) and $\text{Ca}_v2.1$ ($\Delta 47$) splice variants and their relative contributions concerning FHM-1 mutations has not been explored.

In the present study we compared the biophysical properties of wild-type (WT) $\text{Ca}_v2.1$ (+47) and $\text{Ca}_v2.1$ ($\Delta 47$) P/Q-type channel splice variants and also explored the effects of three FHM-1 mutations introduced into the two variants. We investigated two mutations, K1336E and R192Q, that are associated with an FHM-1 phenotype of pure hemiplegia and migraine without any other neurological symptoms.^{14,15} We further investigated the S218L FHM-1 mutation which is associated with a severe clinical phenotype wherein typical FHM-1 attacks induced by minor head trauma are often followed by a delayed cerebral edema, fever, stupor and sometimes coma (fatal in one reported instance).⁴¹⁻⁴³ We find that the two P/Q-type channel carboxyl tail splice variants exhibit functionally distinct properties and also that the three FHM-1 mutations have differential splice-dependent effects on voltage-dependent and kinetic properties. We discuss the potential importance of the splice-variant differential effects in the

context of FHM-1 pathophysiology as well as the implications for other calcium channelopathies.

Results

$\text{Ca}_v2.1$ (+47) and $\text{Ca}_v2.1$ ($\Delta 47$) variants are expressed in human cortex. Mutations in the P/Q-type channel $\text{Ca}_v2.1$ subunit underlie FHM-1 and the current consensus is that initiation of migraine attacks is in the cortex, however the expression of splice variants has not yet been described in the human cortex. In order to determine whether the $\text{Ca}_v2.1$ (+47) and $\text{Ca}_v2.1$ ($\Delta 47$) variants are expressed in human cortex we utilized RT-PCR to amplify a ~1.1 Kb carboxyl terminal fragment of $\text{Ca}_v2.1$ from adult human cortex RNA using oligonucleotide primers that recognize both carboxyl alternatively spliced variants in a non-biased manner. The PCR products were subsequently re-amplified using splice-variant specific primers. Figure 1 shows that the $\text{Ca}_v2.1$ (+47) and $\text{Ca}_v2.1$ ($\Delta 47$) splice variants are both expressed in human cortex. To determine their relative proportions, the human cortical $\text{Ca}_v2.1$ carboxyl terminal PCR products were sub-cloned and individual cDNAs analyzed using splice-variant specific primers and direct DNA sequencing. From the 53 cDNA clones analyzed we determined that the $\text{Ca}_v2.1$ (+47) and $\text{Ca}_v2.1$ ($\Delta 47$) splice variants were present in whole cortex in relative proportions of 79% and 21%, respectively.

All subsequent biophysical analyses were performed using human long $\text{Ca}_v2.1$ (+47) and short $\text{Ca}_v2.1$ ($\Delta 47$) splice-variant cDNA clones with either WT or FHM-1 mutant K1336E, R192Q or S218L changes introduced (see Fig. 1A for the location of the FHM-1 mutations).

FHM-1 mutations exhibit differential effects on the voltage-dependent properties of $\text{Ca}_v2.1$ splice variants. Whole cell current analysis of transiently transfected cells showed that the WT $\text{Ca}_v2.1$ ($\Delta 47$) and WT $\text{Ca}_v2.1$ (+47) variants possess similar membrane potentials at which half the channels are activated ($V_{50\text{act}} = -14.02 \pm 1.49$, and -15.08 ± 1.20 , respectively) and similar membrane potentials at which half of the channels are inactivated ($V_{50\text{inact}} = -58.20 \pm 2.04$, and -62.07 ± 1.87 , respectively; see Table 1 and Fig. 2). The K1336E, R192Q and S218L mutations have been previously reported to cause a hyperpolarizing shift in the current-voltage relationship relative to WT $\text{Ca}_v2.1$ channels.^{24,26,27,29,46} Examining the FHM-1 mutations in the P/Q-type +47 and $\Delta 47$ carboxyl tail splice variants we found differential effects. The K1336E $\text{Ca}_v2.1$ (+47) and R192Q $\text{Ca}_v2.1$ (+47) channels both exhibited a small but significant shift in $V_{50\text{act}}$ relative to WT $\text{Ca}_v2.1$ (+47) channels (-21.53 ± 1.35 and -19.11 ± 1.11 vs. -15.08 ± 1.20 , respectively; $p < 0.05$; ANOVA), while the S218L mutation had no significant effect on $\text{Ca}_v2.1$ (+47) channels relative to WT (Table 1 and Fig. 2). In contrast, all three FHM-1 mutations caused large significant hyperpolarizing shifts in $V_{50\text{act}}$ when expressed in $\text{Ca}_v2.1$ ($\Delta 47$) variant channels ($p < 0.001$; ANOVA; Table 1 and Fig. 2). Similar differential splice-dependent effects of the FHM-1 mutations were apparent in examining $V_{50\text{inact}}$. Figure 2 shows that the R192Q and S218L mutations resulted in large (-15 – 17 mV) hyperpolarizing shifts in $V_{50\text{inact}}$ in the $\text{Ca}_v2.1$ ($\Delta 47$) variant relative to WT $\text{Ca}_v2.1$ ($\Delta 47$) channels ($p < 0.001$; ANOVA), while

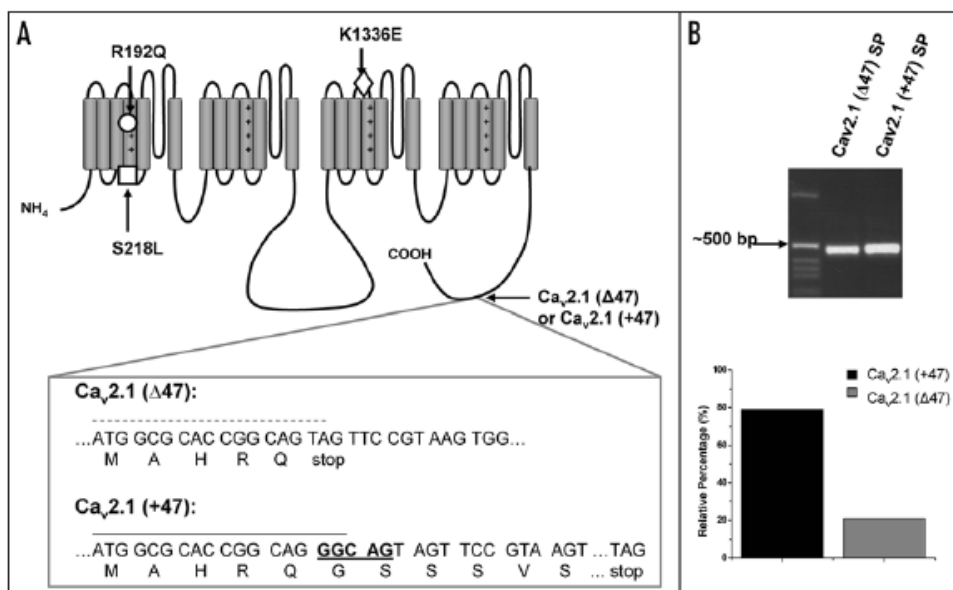


Figure 1. Human P/Q-type calcium channel topology and splice-variant expression in human cortex. (A) schematic showing the location of the three FHM-1 mutations and the carboxyl terminal splice site in the human Ca_v2.1 channel. In the box below the channel diagram are partial sequences of the Ca_v2.1 (+47) and Ca_v2.1 (Δ47) variants at the exon 46/exon 47 boundary. The pentanucleotide insertion is shown in bold for the Ca_v2.1 (+47) variant. (B) the last ~1 Kb of the Ca_v2.1 carboxyl terminus was amplified from human cortical RNA and purified. Subsequently, splice-variant specific forward primers (SP) designed to exclusively bind either Ca_v2.1 (Δ47) or Ca_v2.1 (+47) transcripts were used in PCR reactions to generate an ~500 bp fragment from the purified carboxyl fragments; Ca_v2.1 (Δ47)-SP and Ca_v2.1 (+47)-SP, respectively (dotted line is above the sequence that Ca_v2.1 (Δ47)-SP binds and the solid line is above the sequence that Ca_v2.1 (+47)-SP binds in (A)). Both splice-variant specific primers generated the expected product from the carboxyl PCR fragment of the Ca_v2.1 cDNA obtained from human cortex, verifying both Ca_v2.1 (Δ47) or Ca_v2.1 (+47) are present in human cortex. Products were verified by direct DNA sequencing and determined to be in relative proportions of 79% Ca_v2.1 (+47) and 21% Ca_v2.1 (Δ47) (bar graph); for protocol details see Materials and Methods.

these same two FHM-1 mutations had a smaller effects on Ca_v2.1 (+47) variant channels ($p < 0.05$; ANOVA; Table 1). Interestingly, the K1336E mutation did not cause a significant change in $V_{50inact}$ in either splice variant. Overall, these data indicate that the impact of individual FHM-1 mutations on P/Q-type channel gating properties is differentially affected by the nature of the splice-variant background in which the mutation is expressed.

FHM-1 mutations exhibit differential effects on recovery from inactivation of Ca_v2.1 splice variants. Analysis of WT Ca_v2.1 (Δ47) and Ca_v2.1 (+47) variants showed different rates of recovery from inactivation for these P/Q-type channel splice variants. WT Ca_v2.1 (Δ47) channels exhibit faster rates of recovery ($\tau_1 = 0.67 \pm 0.11$ and $\tau_2 = 3.08 \pm 0.61$) than the Ca_v2.1 (+47) variant channels ($\tau_1 = 0.76 \pm 0.21$ and $\tau_2 = 3.39 \pm 0.84$). As a result, Ca_v2.1 (Δ47) channels show a significantly higher percentage of channels recovered at 7.5 seconds after inactivation relative to Ca_v2.1 (+47) channels (89.0 ± 1.8 vs. 77.3 ± 3.8 %, respectively; $p < 0.05$; ANOVA) (Fig. 3 and Table 2).

Examining the effects of FHM-1 mutations in the Ca_v2.1 (Δ47) background, Figure 3 shows that the K1336E Ca_v2.1 (Δ47) and R192Q Ca_v2.1 (Δ47) variants exhibit a significant decrease in current recovered at 7.5 seconds relative to WT Ca_v2.1 (Δ47)

channels ($70.4 \pm 3.7\%$ and $83.3 \pm 2.3\%$ vs. 89.0 ± 1.8 %, respectively; $p < 0.05$; ANOVA). Contrastingly, K1336E Ca_v2.1 (+47) and R192Q Ca_v2.1 (+47) channels showed increases in recovery relative to WT Ca_v2.1 (+47) channels (86.8 ± 1.7 and 87.0 ± 2.0 vs. 77.3 ± 3.8 %, respectively; $p < 0.05$; ANOVA) (Fig. 3 and Table 2). The S218L mutation was found to increase the recovery in both splice variants, however, only the S218L Ca_v2.1 (+47) channels showed a significant increase in recovery relative to WT Ca_v2.1 (+47) channels at 7.5 seconds (94.7 ± 1.5 vs. 77.3 ± 3.8 %, respectively; $p < 0.001$; ANOVA) (Fig. 3 and Table 2).

Overall, in agreement with previous reports,^{24,27} we observed that both the K1336E and S218L mutations can cause significant changes to recovery from inactivation and show for the first time that the R192Q mutation also changes recovery from inactivation. Importantly, we also show that the quantitative effects of the FHM-1 mutations on channel function are dependant upon the nature of the Ca_v2.1 splice variant. We also note that the differential effects of the mutations resulted in significant changes to the functional distinction observed between the two WT channel variants; that is, while the WT Ca_v2.1 (Δ47) channel variant recovered significantly faster than the WT Ca_v2.1 (+47) channel variant, the K1336E Ca_v2.1 (Δ47) channels recovered significantly slower

Table 1 Mean values for voltage-dependent activation and inactivation parameters

	V_{50} Activation (mV)	k Activation	τ_{act} (msec)	V_{50} Inactivation (mV)	k Inactivation
Ca _v 2.1 (Δ 47) Wild-type	-14.02 \pm 1.49 (n = 16)	4.82 \pm 0.27	1.42 \pm 0.09	-58.20 \pm 2.04 (n = 21)	7.03 \pm 0.29
Ca _v 2.1 (Δ 47) K1336E	-24.12 \pm 1.33 [#] (n = 10)	2.80 \pm 0.20 [#]	1.16 \pm 0.21	-62.27 \pm 1.81 (n = 7)	7.23 \pm 0.45
Ca _v 2.1 (Δ 47) R192Q	-20.84 \pm 0.94 [#] (n = 16)	4.30 \pm 0.19	1.31 \pm 0.07	-73.41 \pm 3.15 [#] (n = 11)	7.58 \pm 0.57
Ca _v 2.1 (Δ 47) S218L	-24.10 \pm 1.15 [#] (n = 9)	5.53 \pm 0.39	0.97 \pm 0.11*	-75.07 \pm 3.96 [#] (n = 10)	6.34 \pm 0.62
Ca _v 2.1 (+47) Wild-type	-15.08 \pm 1.20 (n = 16)	4.33 \pm 0.24	1.28 \pm 0.07	-62.07 \pm 1.87 (n = 16)	6.85 \pm 0.38
Ca _v 2.1 (+47) K1336E	-21.53 \pm 1.35* (n = 9)	3.10 \pm 0.18*	1.33 \pm 0.10	-65.02 \pm 1.87 (n = 8)	8.39 \pm 0.78
Ca _v 2.1 (+47) R192Q	-19.11 \pm 1.11* (n = 16)	4.79 \pm 0.26	1.43 \pm 0.10	-70.27 \pm 2.36* (n = 16)	7.19 \pm 0.47
Ca _v 2.1 (+47) S218L	-18.08 \pm 1.28 (n = 11)	6.26 \pm 0.31 [#]	1.06 \pm 0.08*	-72.54 \pm 1.70* (n = 9)	5.92 \pm 0.37

The voltage at which half of the channels are in the activated state (V_{50act}) and inactivated state ($V_{50inact}$), and the steepness of the curves for activation (k_{act}) and inactivation (k_{inact}) were obtained by fitting the data with the Boltzmann equation for the indicated number of cells in parentheses. The kinetics of activation (τ_{act}) were obtained by fitting the maximum current trace from the IV curves with a single exponential. Asterisks (*) and number signs (#) indicate significant difference relative to wild-type with p-values less than either 0.05 or 0.001 (one-way ANOVA), respectively.

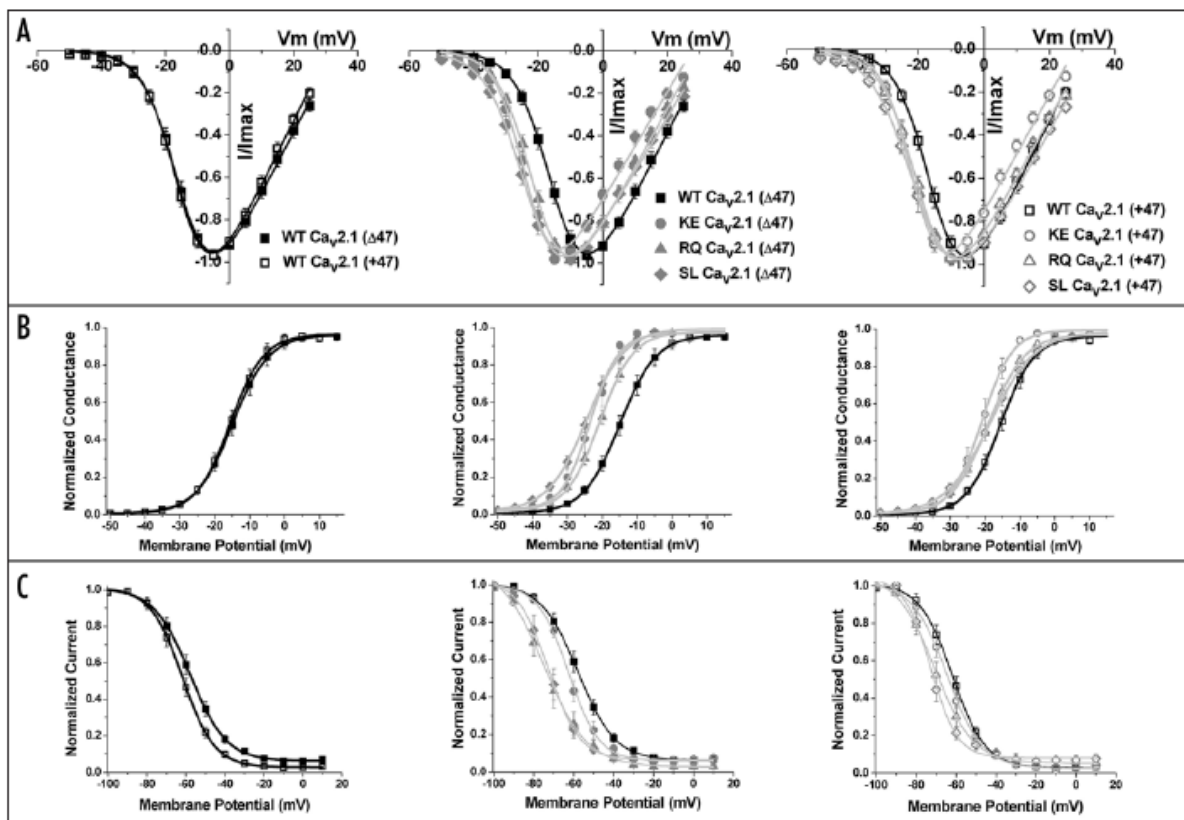


Figure 2. FHM-1 mutations differentially affect voltage-dependent properties of Ca_v2.1 (Δ 47) and Ca_v2.1 (+47) P/Q-type variants. (A) shows the comparison between current-voltage relationships (IV-curves) for wild-type (WT; black squares), FHM-1 mutant K1336E (KE; grey circles), R192Q (RQ; grey triangles) and S218L (SL; grey diamond) in both the short Ca_v2.1 (Δ 47) (filled symbols) and long Ca_v2.1 (+47) (open symbols) C-terminus splice variants. IV curves for all constructs were determined from currents evoked during 90 ms square pulse depolarizations shown between -50 mV and +20 mV from a holding potential of -90 mV. (B) conductance values were calculated from IV curves to obtain activation curves. (C) steady-state inactivation curves were generated using a standard protocol in which 5 s prepulse holdings of -100 to +10 mV were elicited prior to the 80 ms, 0 mV test pulse from a holding of -120 mV. Normalized current evoked during the test pulse is plotted vs. prepulse membrane potential. For complete statistics see Table 1 and for details of protocols see Methods.

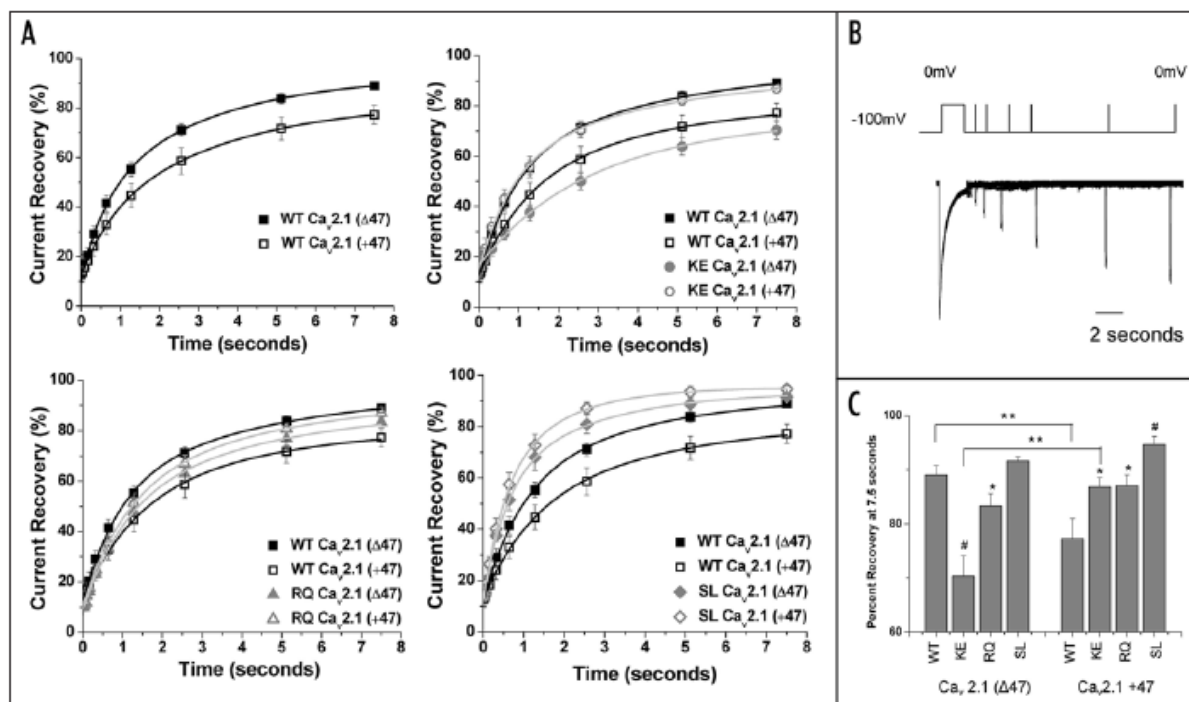


Figure 3. Wild-type and FHM-1 mutant $Ca_v2.1$ ($\Delta47$) and $Ca_v2.1$ (+47) variants exhibit different rates of recovery from inactivation. (A) graphs show percentage of the current recovered vs. time given to recover for all WT and FHM-1 mutated constructs. Recovery from inactivation was examined for wildtype (WT; black squares), FHM-1 mutant K1336E (KE; grey circles), R192Q (RQ; grey triangles) and S218L (SL; grey diamond) in both the short $Ca_v2.1$ ($\Delta47$) (filled symbols) and long $Ca_v2.1$ (+47) (open symbols) C-terminus splice variants. (B) shows a representative (WT) trace (transient currents removed for clarity) and the two pulse protocol used. The protocol consists of a 2 second, 0 mV prepulse followed by a 50 ms, 0 mV test pulse elicited after inter-pulse intervals between 10 ms and 7.5 seconds. Time constants were determined by fitting the average values for percent recovery with a single exponential or double exponential (values shown in Table 2). (C) bar graph shows percent recovery at 7.5 seconds for all WT and FHM-1 mutant clones studied. Single asterisks and number signs indicate significant difference between mutant and wild-type of the same variant with p -values less than either 0.05 or 0.001 (one-way ANOVA), respectively. Double asterisks indicate significant difference between the $\Delta47$ and +47 variants containing the same sequence (i.e., WT or mutant) with p -value less than 0.05 (one-way ANOVA).

than K1336E $Ca_v2.1$ (+47) channels. In addition, the R192Q and S218L mutations altered recovery such that the R192Q $Ca_v2.1$ ($\Delta47$) and R192Q $Ca_v2.1$ (+47) channels and S218L $Ca_v2.1$ ($\Delta47$) and S218L $Ca_v2.1$ (+47) channels were not functionally distinct in this parameter (Fig. 3 and Table 2).

FHM-1 mutations exhibit differential effects on inactivation of $Ca_v2.1$ splice variants during tonic depolarization. WT $Ca_v2.1$ (+47) and $Ca_v2.1$ ($\Delta47$) variants exhibit functional differences with regard to accumulation of inactivation during short (3.5 msec) 25 Hz repetitive stimulations (Fig. 4). While $Ca_v2.1$ ($\Delta47$) variant channels showed $95.0 \pm 1.4\%$ of current remaining at the end of 25 pulses, $Ca_v2.1$ (+47) variant channels had $90.0 \pm 0.9\%$ ($p < 0.05$; ANOVA) (Fig. 4C).

All three FHM-1 mutations examined significantly altered accumulation of inactivation (Fig. 4A); however, again the effects were contingent on the nature of the $Ca_v2.1$ variant in which mutations were expressed. The K1336E $Ca_v2.1$ ($\Delta47$) and K1336E $Ca_v2.1$ (+47) channels had a significant increase in accumulation

of inactivation and thus a lower percent of current remaining at the end of 25 pulses relative to WT $Ca_v2.1$ ($\Delta47$) and WT $Ca_v2.1$ (+47) ($88.0 \pm 2.2\%$ and $84.0 \pm 1.7\%$ vs. 95.0 ± 1.4 and $90.0 \pm 0.9\%$, respectively; $p < 0.05$; ANOVA) (Fig. 4C). The changes were such that the K1336E $Ca_v2.1$ (+47) and K1336E $Ca_v2.1$ ($\Delta47$) variants had similar current remaining at the end of the repetitive stimulation and thus lacked the clear functional distinction observed between the WT channel variants.

In the context of the $Ca_v2.1$ ($\Delta47$) variant background the R192Q mutation caused a significant increase in accumulation of inactivation relative to WT $Ca_v2.1$ ($\Delta47$) (current remaining at end of the 25 pulses = $90.0 \pm 1.6\%$ vs. $95.0 \pm 1.4\%$; $p < 0.05$; ANOVA). In contrast, R192Q $Ca_v2.1$ (+47) channels were similar to WT $Ca_v2.1$ (+47) channels ($92 \pm 1.3\%$ vs. $90 \pm 0.9\%$) (Fig. 4C). Similar to K1336E channels, the R192Q $Ca_v2.1$ ($\Delta47$) and R192Q $Ca_v2.1$ (+47) channel variants lacked the clear functional distinction observed between the WT variants for this property.

The S218L mutation showed a large and significant increase in accumulation of inactivation and thus a lower percent of current remaining at the end of 25 pulses relative to both the WT $Ca_v2.1$ ($\Delta 47$) and $Ca_v2.1$ (+47) channel variants ($81 \pm 2.5\%$ and $77 \pm 1.7\%$ vs. 95 ± 1.4 and $90 \pm 0.9\%$, respectively; $p < 0.05$; ANOVA). Similar to that for R192Q and K1336E, a further overall effect of the S218L mutation is to decrease the relative difference in current remaining observed between WT $Ca_v2.1$ ($\Delta 47$) and $Ca_v2.1$ (+47) variant channels.

FHM-1 mutations exhibit differential effects on inactivation of $Ca_v2.1$ splice variants during bursts of depolarization. In addition to tonic depolarizations, neurons experience various frequencies of burst firing in which brief periods of tonic firing are interspersed with silent periods as the membrane potential drops below threshold.⁴⁷⁻⁵¹ During the tonic firing periods P/Q-type channels will inactivate and during silent periods they will have the opportunity to recover from inactivation. Based upon the above noted splice-variant changes in accumulation of inactivation and recovery from inactivation, we predicted that bursts of depolarization would also differentially affect WT and FHM-1 mutated $Ca_v2.1$ (+47) and $Ca_v2.1$ ($\Delta 47$) variant channels.

Figure 5 shows that WT $Ca_v2.1$ (+47) and $Ca_v2.1$ ($\Delta 47$) variants exhibit significant differences in the amount of current remaining at the end of five 25 Hz bursts given at 3.5 Hz. Current through the WT $Ca_v2.1$ (+47) variant decayed to $73 \pm 3.4\%$ by the end of the fifth burst while current through the WT $Ca_v2.1$ ($\Delta 47$) variant decayed to $88 \pm 3.6\%$ ($p < 0.05$; ANOVA) (Fig. 5C). The increased inactivation during the depolarizations and the reduced recovery from inactivation of WT $Ca_v2.1$ (+47) variants discussed above likely contributed to the overall 15% decrease in current relative to the WT $Ca_v2.1$ ($\Delta 47$) variant.

Figure 5 shows that during burst firing the K1336E mutation in the $Ca_v2.1$ ($\Delta 47$) variant background results in an overall lower percentage of current remaining at the end of five bursts ($70 \pm 4.9\%$ vs. $88 \pm 3.6\%$, respectively; $p < 0.05$; ANOVA) (Fig. 5C), likely resulting from the increased accumulation of inactivation and slowed recovery from inactivation of K1336E $Ca_v2.1$ ($\Delta 47$) channels relative to WT $Ca_v2.1$ ($\Delta 47$) (see Figs. 3 and 4). Contrastingly, the K1336E mutation in the $Ca_v2.1$ (+47) variant background did not show significant current decay relative to WT, likely due to the fact that although the K1336E $Ca_v2.1$ (+47) variant channels exhibit a small increase in accumulation of inactivation during tonic stimulation (Fig. 4), they also possess an increased rate of recovery from inactivation (Fig. 3A). We note that unlike WT channel variants, the K1336E $Ca_v2.1$ (+47) and K1336E $Ca_v2.1$ ($\Delta 47$) variants did not differ significantly relative to one another.

Similar to that for the K1336E mutation in the $\Delta 47$ background, examination of burst firing effects on the R192Q mutation showed an increase in current decay during burst firing relative to WT $Ca_v2.1$ ($\Delta 47$) channels ($70 \pm 3.6\%$ vs. $88 \pm 3.6\%$ current remaining, respectively; $p < 0.05$; ANOVA) (Fig. 5C). In contrast, the R192Q mutation in the +47 background resulted in a higher degree of current remaining compared to WT $Ca_v2.1$ (+47) channels ($83 \pm 2.7\%$ vs. $73 \pm 3.4\%$ current remaining, respectively;

Table 2 Time constant values and recovery from inactivation

	τ_1 (Fast) (msec)	τ_2 (Slow) (msec)	% Recovery at 7.5 seconds
$Ca_v2.1$ ($\Delta 47$) Wild-type	0.67 ± 0.11	3.08 ± 0.61	89.0 ± 1.8 (n = 5)
$Ca_v2.1$ ($\Delta 47$) K1336E	2.89 ± 0.12	N.A.	$70.4 \pm 3.7^{\#}$ (n = 8)
$Ca_v2.1$ ($\Delta 47$) R192Q	0.91 ± 0.19	4.97 ± 2.65	$83.3 \pm 2.3^*$ (n = 7)
$Ca_v2.1$ ($\Delta 47$) S218L	0.617 ± 0.10	2.71 ± 1.18	91.6 ± 0.8 (n = 5)
$Ca_v2.1$ (+47) Wild-type	0.76 ± 0.21	3.39 ± 0.84	$77.3 \pm 3.8^{**}$ (n = 7)
$Ca_v2.1$ (+47) K1336E	0.54 ± 0.13	2.67 ± 0.53	$86.8 \pm 1.7^*$ (n = 5)
$Ca_v2.1$ (+47) R192Q	1.08 ± 0.20	5.78 ± 4.96	$87.0 \pm 2.0^*$ (n = 6)
$Ca_v2.1$ (+47) S218L	0.50 ± 0.12	1.71 ± 0.59	$94.7 \pm 1.5^{\#}$ (n = 5)

Time constants were determined by fitting the average percent recovery with a double exponential for all constructs except the $Ca_v2.1$ ($\Delta 47$) K1336E which was best fit with a single exponential. Percent recovery is a measure of the percentage of current evoked during the test pulse, given at 7.5 seconds after the prepulse, relative to the maximum current evoked during the prepulse. Asterisks and number signs indicate significant difference between mutant and wild-type of the same variant with p-values less than either 0.05 or 0.001 (one-way ANOVA), respectively. Double asterisks indicate significant difference between the $Ca_v2.1$ $\Delta 47$ and +47 variants containing the same sequence (i.e. WT or mutant) with p-value less than 0.05 (one-way ANOVA). Number of cells recorded for each clone is indicated in parenthesis. N.A. = not applicable.

$p < 0.05$; ANOVA). This may reflect the fact that R192Q $Ca_v2.1$ (+47) channels exhibit increased recovery from inactivation (see Fig. 3). We note that an overall effect concerning current decay during burst firing is for R192Q $Ca_v2.1$ (+47) channels to behave more similar to that for the WT $\Delta 47$ channels and for R192Q $Ca_v2.1$ ($\Delta 47$) channels to behave more similar to those of the WT +47 variant.

Similar to that for the K1336E mutation, the S218L mutation only caused a significant current decay during the burst firing in the $Ca_v2.1$ ($\Delta 47$) variant background ($73.0 \pm 4.0\%$ vs. $88.0 \pm 3.6\%$ current remaining at the end of five bursts, respectively; $p < 0.05$; ANOVA). Presumably, although the S218L mutation increased accumulation of inactivation substantially in both splice variants (see Fig. 4), S218L $Ca_v2.1$ (+47) channels had a larger increase in the rate of recovery from inactivation (Fig. 3) which likely slowed overall accumulation of inactivation during the burst firing. The S218L $Ca_v2.1$ (+47) and S218L $Ca_v2.1$ ($\Delta 47$) variants did not differ significantly relative to one another.

Discussion

We report here that FHM-1 missense mutations confer differential effects on the biophysical properties of the $Ca_v2.1$ (+47) and $Ca_v2.1$ ($\Delta 47$) P/Q-type channel splice variants. Although the current-voltage relationships and steady-state properties of the two WT P/Q-type splice variants are similar, all three

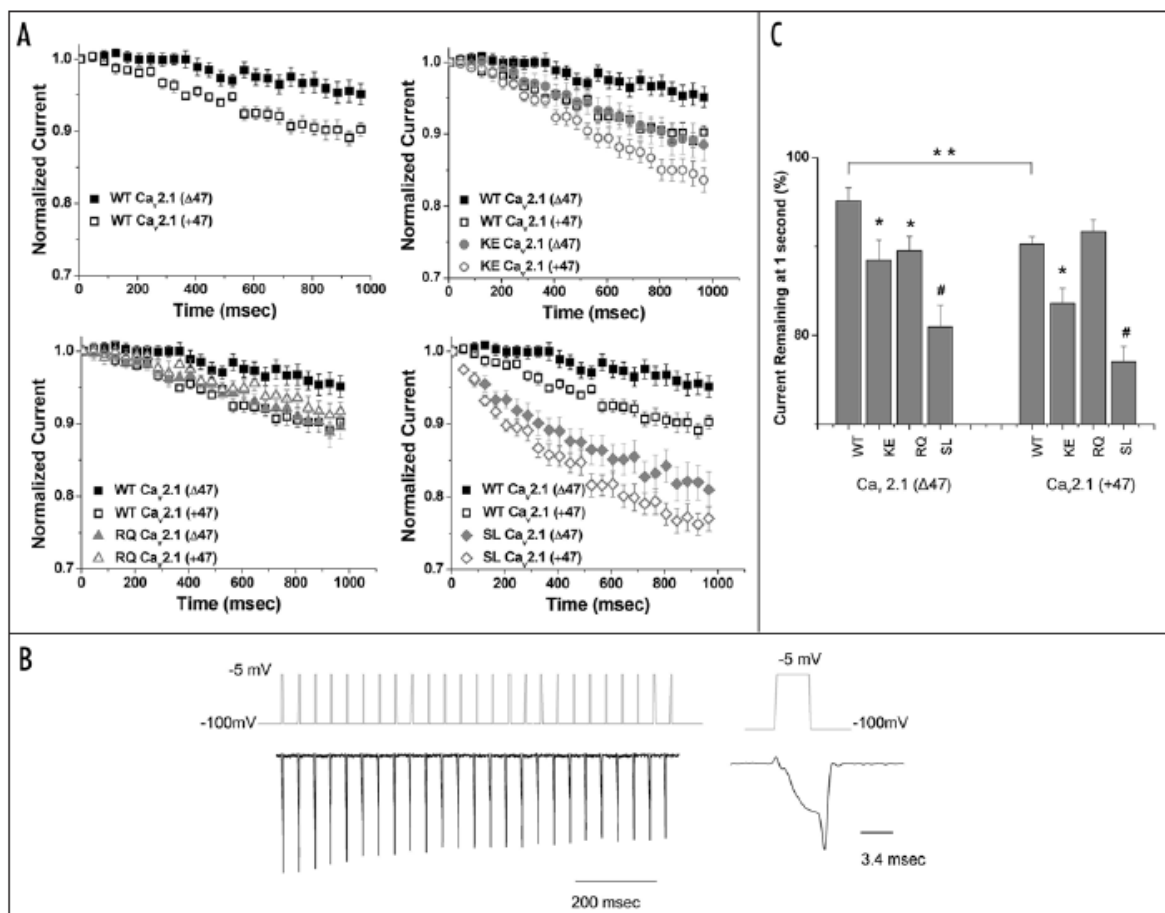


Figure 4. Wild-type and FHM-1 mutant $Ca_v2.1$ ($\Delta47$) and $Ca_v2.1$ (+47) variants exhibit different current decay during 25 Hz tonic depolarizations. (A) graphs show normalized current remaining vs. time after initial onset of depolarizations. Current decay was measured for wild-type (WT; black squares), FHM-1 mutant K1336E (KE; grey circles), R192Q (RQ; grey triangles) and S218L (SL; grey diamond) in both the short $Ca_v2.1$ ($\Delta47$) (filled symbols) and long $Ca_v2.1$ (+47) (open symbols) C-terminus splice variants. (B) to investigate current decay during repetitive stimulations we used 25 square pulses from a holding of -100 mV to a depolarizing potential of -5 mV for a duration of 3.4 ms. The test pulses were given at a rate of 25 Hz. Representative current trace and pulse protocol indicated at bottom (capacitive transients were compensated using a P/4 protocol), with single current response enlarged. (C) bar graph shows the percent of current remaining at the end of 25 pulses for each clone. Single asterisks and number signs indicate significant difference between mutant and wild-type of the same variant with p-values less than either 0.05 or 0.001 (one-way ANOVA), respectively. Double asterisks indicate significant difference between the $\Delta47$ and +47 variants containing the same sequence (i.e., WT or mutant) with p-value less than 0.05 (one-way ANOVA). Number of cells recorded for WT $Ca_v2.1$ ($\Delta47$) (n = 14), WT $Ca_v2.1$ (+47) (n = 13), KE $Ca_v2.1$ ($\Delta47$) (n = 15), KE $Ca_v2.1$ (+47) (n = 18), RQ $Ca_v2.1$ ($\Delta47$) (n = 17), RQ $Ca_v2.1$ (+47) (n = 15), SL $Ca_v2.1$ ($\Delta47$) (n = 15), SL $Ca_v2.1$ (+47) (n = 14).

FHM-1 mutations exhibited a greater hyperpolarizing shift when expressed in the $Ca_v2.1$ ($\Delta47$) variant compared to the $Ca_v2.1$ (+47) variant (Fig. 2). In addition, we show for the first time that WT $Ca_v2.1$ ($\Delta47$) and WT $Ca_v2.1$ (+47) variants have both different kinetics of recovery from inactivation and accumulation of inactivation during tonic depolarization that are likely relevant to the differential response of channel variants during bursts of depolarization (Figs. 3–5). It is known that

$Ca_v2.1$ channels in different states possess alternative modes of gating that are reflected in biophysical properties at the whole cell current level.^{52,53} Furthermore, it has been shown that alternative splicing in the EF-hand region of the $Ca_v2.1$ carboxyl terminus can shift gating modes.⁵⁴ It is therefore possible that WT $Ca_v2.1$ ($\Delta47$) and WT $Ca_v2.1$ (+47) variants also have distinct gating modes that respond differently to FHM-1 mutations which are localized near voltage sensor regions (e.g., R192Q, S218L,

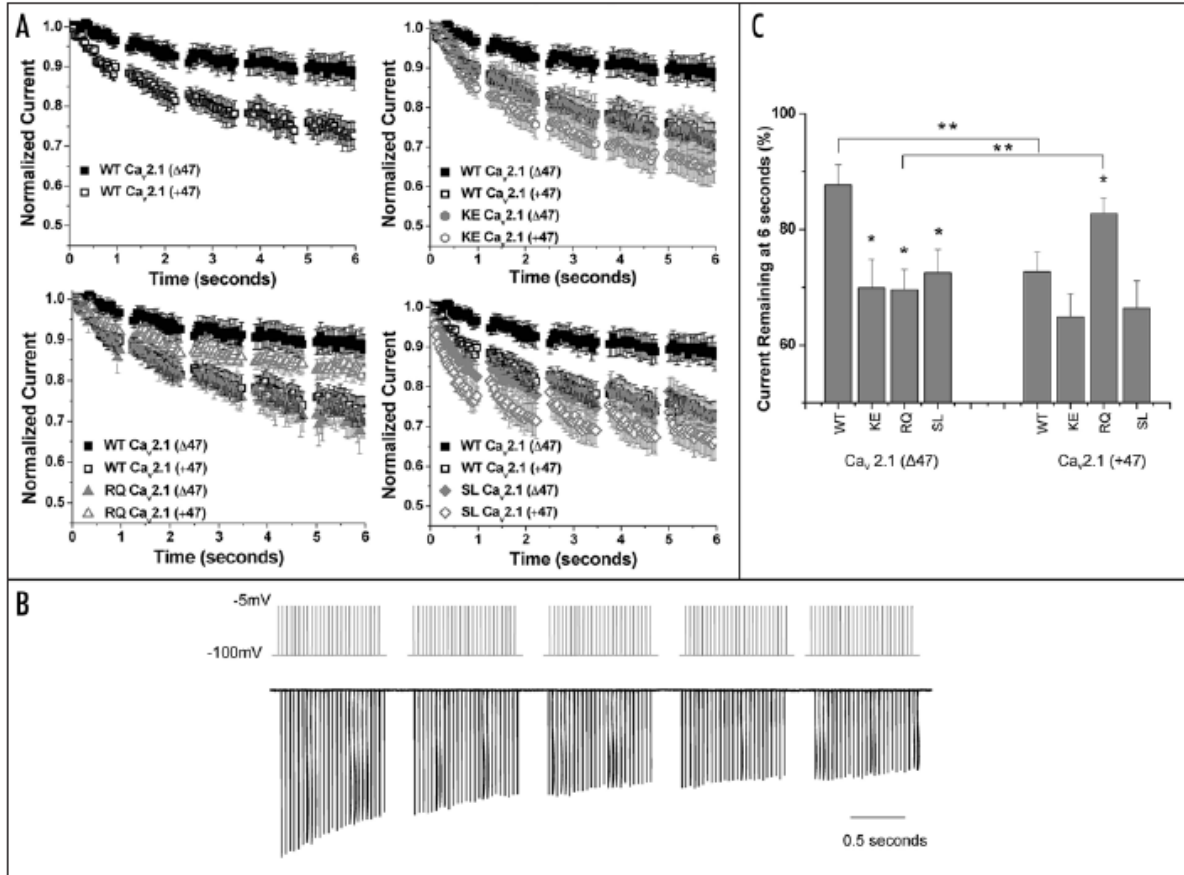


Figure 5. Wild-type and FHM-1 mutant $Ca_v2.1 (\Delta47)$ and $Ca_v2.1 (+47)$ variants exhibit different current decay during bursts of depolarizations. (A) graphs show normalized current remaining vs. time after initial onset of depolarizations. Current decay was measured for wild-type (WT; black squares), FHM-1 mutant K1336E (KE; grey circles), R192Q (RQ; grey triangles) and S218L (SL; grey diamond) in both the short $Ca_v2.1 (\Delta47)$ (filled symbols) and long $Ca_v2.1 (+47)$ (open symbols) C-terminus splice variants. (B) to investigate current decay during bursts of repetitive stimulations we used five bursts of 25 square pulses to -5 mV for 3.4 msec from a holding of -100 mV; bursts given at 290 msec intervals (3.5 Hz burst firing). Each burst contained 25 pulses at a rate of 25 Hz. Representative current trace indicated at bottom (capacitive transients were compensated using a P/4 protocol). (C) bar graph shows the percent of current remaining at the end of 6 seconds for each clone. Single asterisks and number signs indicate significant difference between mutant and wild-type of the same variant with *p*-values less than either 0.05 or 0.001 (one-way ANOVA), respectively. Double asterisks indicate significant difference between the $Ca_v2.1 \Delta47$ and +47 variants containing the same sequence (i.e., WT or mutant) with *p*-value less than 0.05 (one-way ANOVA). Number of cells recorded for WT $Ca_v2.1 (\Delta47)$ (*n* = 8), WT $Ca_v2.1 (+47)$ (*n* = 7), KE $Ca_v2.1 (\Delta47)$ (*n* = 8), KE $Ca_v2.1 (+47)$ (*n* = 10), RQ $Ca_v2.1 (\Delta47)$ (*n* = 9), RQ $Ca_v2.1 (+47)$ (*n* = 7), SL $Ca_v2.1 (\Delta47)$ (*n* = 8), SL $Ca_v2.1 (+47)$ (*n* = 8).

K1336E). Detailed single channel analyses would be required to fully explore this hypothesis.

Our findings provide the first suggestion for a potential role of P/Q-type channel alternative splicing in FHM-1 pathophysiology and raise the notion that even though $Ca_v2.1$ channels are widely expressed in the central and peripheral nervous systems, point mutations can have greater or lesser functional effects on specific splice variants. Although the mechanism of FHM-1 pathophysiology is not completely resolved, the current opinion is that the migraine usually initiates with aura due to CSD, which leads to

headache pain through activation of the trigeminovascular pain pathway.^{55,56} In this regard, specific $Ca_v2.1$ variants within the cortex may have important roles in the onset of migraine attacks.

We show that the $Ca_v2.1 (\Delta47)$ and $Ca_v2.1 (+47)$ variants are both expressed in whole human cortex (Fig. 1B), and that the three FHM-1 mutations all cause a greater hyperpolarizing shift in the voltage-dependence of activation in $Ca_v2.1 (\Delta47)$ channels relative to that for $Ca_v2.1 (+47)$ variant channels. A hyperpolarizing shift in P/Q-type channel activation has been suggested as an underlying mechanism of increased susceptibility to CSD and the initiation

of migraine.^{22,57} CSD begins within small domains of the cortex and propagates outward from a focal point. Our data supports the notion that Ca_v2.1 splice variants with greater sensitivity to hyperpolarizing shifts in the voltage-dependence of activation (e.g., Ca_v2.1 (Δ47), could result in cortical regions with greater susceptibility to CSD and migraine initiation. Conversely, the effects of FHM-1 mutations on other Ca_v2.1 splice variants (e.g., Ca_v2.1 (+47)), expressed elsewhere in the cortex or other brain regions may be below the threshold to initiate CSD and/or other pathological effects. Future exploration of the exact regional and cellular distributions of these and other Ca_v2.1 splice variants within the cortex and throughout the human brain using *in situ* hybridization and/or RT-PCR analyses will be necessary to fully understand the role of Ca_v2.1 splice variants in FHM-1 pathology.

Our results examining tonic and burst firing patterns also suggests the possibility of differential effects of FHM-1 mutations on P/Q-type channel splice variants under different firing conditions. This is most clearly seen with the S218L mutation in the Ca_v2.1 (+47) variant; during tonic depolarization current decay is significantly faster relative to WT, yet during burst firing the S218L Ca_v2.1 (+47) variant has similar current decay to WT channels after five bursts, likely due to rapid recovery from inactivation (see Figs. 4 and 5). On the other hand, in Ca_v2.1 (Δ47) variant channels the S218L mutation has significant effects on current decay under both tonic and burst firing conditions. Interestingly, certain initiating factors of FHM-1 attacks such as emotional stress¹⁴ are known to alter neuronal firing patterns in the brain.^{58,59} Although the exact firing conditions directly associated with precipitating factors of migraine are unknown, the episodic nature of the FHM-1 phenotype may in part be associated with changes in neuronal firing pattern and/or frequency that could be relevant to specific Ca_v2.1 splice variants expressed in localized brain regions.

It is likely that there exists a complex relationship between channel missense mutations and disease mechanism. While we show alternative splicing at a single Ca_v2.1 splice-site can determine the functional impact of FHM-1 mutations, we recognize that across the entire brain many additional factors are likely to be involved in ultimately defining disease pathophysiology. These likely include the expression of multiple splice P/Q-type variants with distinct combinations of alternative splicing as well as the interaction with different auxiliary subunits²⁷ and other structural and regulatory proteins. Nonetheless, our results demonstrate the relevance of alternative splicing as an important factor in considering underlying disease molecular mechanisms and also the need for a comprehensive understanding of the splice-variant profile of Ca_v2.1 channels across brain regions and developmental stages as they might relate to FHM-1 pathology.

While in the present report we show that individual FHM-1 mutations can have differential effects on the biophysical properties of the short and long P/Q-type channel splice variants, we predict this phenomenon is likely relevant to both other FHM-1 mutations and Ca_v2.1 variants and also to other types of Ca_v channels and calcium channelopathies.⁶¹ Understanding the differential effects of channelopathy mutations on ion channel splice variants

is likely to be important for interpreting results obtained in both heterologous and native systems, as well as for making inferences concerning disease mechanisms and phenotypes. Mutations in the Ca_v1.1 L-type channel are associated with hypokalemic periodic paralysis, the Ca_v1.2 L-type with Timothy syndrome, the Ca_v1.4 L-type with incomplete X-linked congenital stationary night blindness and X-linked cone-rod dystrophy, and the Ca_v3.2 T-type with idiopathic generalized epilepsy and autism spectrum disorder (reviewed in ref. 4). Similar to FHM-1, many of these disorders exhibit phenotypes with episodic and/or developmentally specific attributes localized to a subset of regions or tissues that express the respective channels, and like Ca_v2.1, these channels also undergo alternative splicing that generates functionally distinct channel variants (reviewed in refs. 6 and 7). The identification of specific Ca_v splice variants involved in disease pathophysiology may also provide the opportunity for targeted therapeutic approaches. For example, while the Ca_v2.2 N-type channels have a central role in nociceptive signalling, distinct Ca_v2.2 splice variants are involved in the transmission of specific types of pain and has led to new strategies for splice variant-specific targeting in pain therapy.⁶⁰

Methods

Site-directed mutagenesis. Standard PCR-based *in vitro* mutagenesis was performed using the Pfu Turbo DNA Polymerase (Stratagene, La Jolla, CA), 10 mM dNTPs (Invitrogen) and paired forward and reverse mutagenesis primers.⁴⁴ The human Ca_v2.1 long (+47) (isoform 2) (NCBI accession number NM_023035.1) cloned in pcDNA 3.1 Zeo (+) was used as the source for the generation of the WT short human Ca_v2.1 (Δ47) (isoform 1) cDNA (the other known six splice sites are: Δ10A, 16+/17+, -VEA, -NP, EFa, 43+/44+). Paired forward and reverse primers were designed to adhere to the C-terminus of the Ca_v2.1 isoform 2 at the exon 46/47 boundary nucleotide number 6784 and removed the GGCAG pentanucleotide sequence creating the premature stop in exon 47 (Ca_v2.1 (Δ47)). Both Ca_v2.1 splice variant cDNAs were used in site-directed mutagenesis reactions to generate human Ca_v2.1 K1336E, R192Q and S218L mutants in the short and long variants; paired forward and reverse primers were designed to convert codon 1336 from AAA to GAA, codon 192 from CGG to CAG, and codon 218 from TCG to TTA. The integrity of all constructs generated through site-directed mutagenesis were verified by direct DNA sequencing.

Cell culture and transfection. Human embryonic kidney (HEK 293) cells were grown in standard Dulbecco's modified Eagle's medium supplemented with 10% fetal bovine serum (heat inactivated) and 50 U/ml penicillin-50ug/ml streptomycin. Cells were incubated at 37°C in a humidified incubator with 95% atmosphere and 5% CO₂ and grown to 8–15% confluency for transfection. HEK 293 cells were transiently transfected with either WT human Ca_v2.1 (Δ47) or Ca_v2.1 (+47), or mutant K1336E Ca_v2.1 (Δ47), R192Q Ca_v2.1 (Δ47), S218L Ca_v2.1 (Δ47) or K1336E Ca_v2.1 (+47), R192Q Ca_v2.1 (+47), S218L Ca_v2.1 (+47) in combination with calcium channel auxiliary subunits β₄, α₂δ-1, and the CD8 marker plasmid in a 1:1:1:0.25 molar ratio using Lipofectamine (Invitrogen, La Jolla, CA). To ensure accurate

comparisons, transfections were performed at the same time and electrophysiological recordings alternated within the same day for all channel types.

Electrophysiological recordings. On the second day after transfection, macroscopic Ba^{2+} currents were recorded at room temperature using the whole-cell patch-clamp technique.⁴⁵ The internal pipette solution used contained 105 mM CsCl, 25 mM TEACL, 1 mM $CaCl_2$, 11 mM EGTA, 10 mM HEPES and 5 mM ATP (pH 7.2 with CsOH); external: 5 mM $BaCl_2$, 1 mM $MgCl_2$, 10 mM HEPES, 40 mM TEACL, 10 mM glucose and 87.5 mM CsCl (pH 7.4 with TEAOH). Patch pipettes (borosilicate glass BF150-86-10; Sutter Instrument Company, Novato, CA) were made using a horizontal puller (P-87; Sutter Instruments Company) and fire polished using a microforge (Narishige, Tokyo, Japan), with resistances typically of 3 to 5 M Ω when containing internal solution. External solution bath was connected to ground with a 3 M KCl agar bridge. Whole cell currents were recorded and filtered at 2–5 kHz bandwidth using an Axopatch 200A amplifier monitored and stored on a personal computer running pClamp software package version 9. Sampling frequencies were between 2 and 10 kHz. Recordings were analyzed using Clampfit 9 and figures, fittings and statistics (ANOVA) were made using the software program Origin version 7.5 (OriginLab Corp., Northampton, MA). Data are represented as mean \pm standard error (S.E.).

Recording protocols and data analysis. Current-voltage relationships were determined by measured currents obtained using a series of 90 millisecond depolarization pulses applied from a holding potential of -90 mV to membrane potentials from -50 mV to +45 mV, increasing by 5 mV increments. Current-voltage relationships were fitted, and IV curves generated, using a modified Boltzmann equation:

$$I = (G_{max} \cdot (V_m - E_r)) / (1 + \exp((V_m - V_{50})/k))$$

where G_{max} is the maximum slope conductance, V_m is the test potential, E_r is the extrapolated reversal potential, V_{50} is the half-activation potential, and k reflects the slope of the activation curve. Activation curves were constructed by calculating conductance from the IV curves and plotting the normalized conductance as a function of the membrane potential. The data were fit with the Boltzmann equation:

$$G/G_{max} = A2 + (A1 - A2) / (1 + \exp((V_m - V_{50})/k))$$

where $A1$ is minimum normalized conductance, $A2$ is maximum normalized conductance, V_m is the test potential, V_{50} is the half-activation potential, and k reflects the slope of the activation curve (goodness of fit had R^2 values \geq 0.998).

Voltage-dependence of inactivation was analyzed using depolarizations to 0 mV for 80 ms following 5 s prepulses ranging from -100 to +10 mV at 10mV increments (holding potential of -120 mV). Steady state inactivation curves were constructed by plotting the maximum normalized current during the test pulse as a function of the prepulse potential. The data were fit with the

Boltzmann equation:

$$I/I_{max} = A2 + (A1 - A2) / (1 + \exp((V_m - V_{50})/k))$$

where $A1$ is minimum normalized current, $A2$ is the maximum normalized current, V_m is the test potential, V_{50} is the half-inactivation potential, and k reflects the slope of the inactivation curve (goodness of fit had R^2 values \geq 0.998).

The kinetics of activation (τ_{act}) were determined from currents obtained from the IV protocol. Current traces were fit with a standard single exponential equation: $I = A \cdot \exp(-t/\tau)$, where A is the amplitude of the current, and τ is the time constant.

Recovery from inactivation was determined using a double-pulse protocol. The first depolarization was to 0 mV for 2 s (the prepulse), followed by a return to the holding potential of -100 mV for variable lengths between 10 ms and 7.5 s. At the end of the variable repolarization period, a second 0 mV (the test pulse) was given for 50 ms. The time interval between sweeps was a total of 1 minute to ensure maximum recovery between sweeps. All traces were normalized to the maximum current during the prepulse for each sweep. The peak current from the test pulse was plotted as a percentage of maximum prepulse current vs. repolarization time. Average traces were fit with either a single or double exponential equation (goodness of fit had R^2 values \geq 0.998).

Current decay during a tonic depolarization was examined using a 25 Hz train of 25 square pulses from a holding of -100 mV to a depolarizing potential of -5 mV for 3.4 ms. Current decay curves were generated by plotting normalized maximum current during the test pulses as a function of the time of pulse onset. Current decay during bursts of depolarization was examined using square pulses to -5 mV for 3.4 msec from a holding of -100 mV. Five bursts were given with 290 msec intervals (3.5 burst firing). Each burst contained 25 pulses at a rate of 25 Hz. Current decay curves were generated by plotting normalized maximum current during the test pulses as a function of the time of pulse onset.

RT-PCR of $Ca_v2.1$ carboxyl-terminal region from human cortex RNA. Prior to reverse transcription, 1 μ g total RNA from human cortex (Clontech; 636561) was treated with 1X DNase I reaction buffer and 1 unit DNase I (Invitrogen) in a final volume adjusted to 10 μ L using sterile DEPC-treated H_2O . Following a 15-minute incubation period at room temperature, the reaction was inactivated by adding 1 μ L of 25 mM EDTA and heating at 65°C for 10 minutes. cDNA synthesis was performed using Superscript II Reverse Transcriptase (Invitrogen) following manufacturer's instructions with slight modification. A -1.1-Kb nucleotide fragment of the carboxyl end of the $Ca_v2.1$ channel was amplified from the human cortex cDNA using standard PCR. The reaction mixture consisted of 3% DMSO, 1X Phusion enzyme buffer, 0.4 pmol/ μ L of forward and reverse primers, 0.2 mM dNTPs, 1 μ L of cortex cDNA, and 1 unit of Phusion enzyme in a final volume of 25 μ L. The forward primer (5'GGC ACA TGG AGT CCG GAA CA 3') corresponds to nucleotide position 6130 and the reverse primer (5'GGT AGT AGC CAT GGT GCC3') to nucleotide position 7211 of the human $Ca_v2.1 \alpha_1$ subunit (NCBI accession number NM_023035.1). The cycling profile included an initial activation step of 98°C for 30 s

followed by 30 cycles of 98°C for 30 s, 65°C for 30 s, 72°C for 2.5 minutes and a final extension period of 72°C for 10 minutes. As positive controls, the same PCR reaction was performed on human Ca_v2.1 (Δ47) and Ca_v2.1 (+47) cDNA plasmids to demonstrate unbiased amplification. PCR reactions using primers for tubulin were used to verify the success of RT reactions. As negative controls, identical PCR reactions without template and containing no RT were performed. To analyze individual Ca_v2.1 amplified carboxyl terminal transcripts, PCR products were ligated into pGEMT-Easy (Promega) and then transformed into competent XL-1 *E. coli* bacterial cells. Bacteria containing PCR inserts were identified by blue-white screening and collected and subject to Ca_v2.1 (Δ47) and Ca_v2.1 (+47) specific PCR reactions. The reverse primer (5'GGT AGT AGC CAT GGT GCC3') was used for both Ca_v2.1 (Δ47) and Ca_v2.1 (+47) specific PCR reactions. Forward primer (5'ATG GCG CAC CGG CAG TA3') and (5'CAT GGC GCA CCG GCA GGG3') were designed to specifically amplify Ca_v2.1 (Δ47) and Ca_v2.1 (+47), respectively. All PCR products were run on a 1% agarose gel. In determining the percentage of each variant, only colonies positive for Ca_v2.1 (Δ47) and negative for Ca_v2.1 (+47), and visa versa, were included and ambiguous results discarded. Direct DNA sequence determination of several representative clones confirmed both the veracity of the splice-variant specific PCR reactions and the identity of the cloned PCR products.

Acknowledgements

This work was funded by operating grant #10677 from the Canadian Institutes of Health Research (CIHR) and a Tier 1 Canada Research Chair in Biotechnology and Genomics-Neurobiology to Terrance P. Snutch, an operating grant from the National Ataxia Foundation and a salary award from the Vancouver Coastal Health Authority to Sian D. Spacey, graduate fellowships from the Michael Smith Foundation for Health Research to Paul J. Adams and Kirk J. Mulatz, and a doctoral fellowship from the Heart and Stroke Foundation of Canada to Laurence S. David. We thank Dr. David Parker and Luke Materek for providing the wild-type isoform 2 Ca_v2.1 human cDNA and Ms. Alexi Millman for protocol optimization.

References

- Catterall WA. Structure and regulation of voltage-gated Ca²⁺ channels. *Annu Rev Cell Dev Biol* 2000; 16:521-55.
- Praoek LJ, Tawil R, Griggs RC, Engel AG, Layzer RB, Kwiatkowski H, et al. Dihydropyridine receptor mutations cause hypokalemic periodic paralysis. *Cell* 1994; 77:863-8.
- Fontaine B, Vale-Santos J, Judat-Rott K, Reboul J, Plassart E, Rime CS, et al. Mapping of the hypokalemic periodic paralysis (HypoPP) locus to chromosome 1q31-32 in three European families. *Nat Genet* 1994; 6:267-72.
- Adams PJ, Snutch TP. Calcium channelopathies: voltage-gated calcium channels. *Subcell Biochem* 2007; 45:215-51.
- Emerick MC, Stein R, Kunze R, McNulty MM, Regan MR, Hanck DA, Agnew WS. Profiling the array of Ca_v3.1 variants from the human T-type calcium channel gene CACNA1G: alternative structures, developmental expression and biophysical variations. *Proteins* 2006; 64:320-42.
- Lipscombe D, Castiglioni AJ. Alternative Splicing in Voltage Gated Calcium Channels. In: McDonough SI, ed. *Calcium Channel Pharmacology*. Kluwer Academic/Plenum Publishers 2004; 369-409.
- Lipscombe D, Pan JQ, Gray AC. Functional diversity in neuronal voltage-gated calcium channels by alternative splicing of Ca_v3.1. *Mol Neurobiol* 2002; 26:21-44.
- Gray AC, Raingo J, Lipscombe D. Neuronal calcium channels: splicing for optimal performance. *Cell Calcium* 2007; 42:409-17.
- Splawski I, Timothy KW, Sharpe LM, Decher N, Kumar P, Bloise R, et al. Ca_v1.2 calcium channel dysfunction causes a multisystem disorder including arrhythmia and autism. *Cell* 2004; 119:19-31.
- Splawski I, Timothy KW, Decher N, Kumar P, Sachse FB, Beggs AH, et al. Severe arrhythmia disorder caused by cardiac L-type calcium channel mutations. *Proc Natl Acad Sci USA* 2005; 102:8089-96.
- Graves TD, Imbrici B, Koss EE, Terwindt GM, Eunsou LH, Frants RR, et al. Premature stop codons in a facilitating EF-hand splice variant of Ca_v2.1 cause episodic ataxia type 2. *Neurobiol Dis* 2008; 32:10-5.
- Zhuchenko O, Bailey J, Bonnen P, Ashizawa T, Stockton DW, Amos C, et al. Autosomal dominant cerebellar ataxia (SCA6) associated with small polyglutamine expansions in the alpha 1A-voltage-dependent calcium channel. *Nat Genet* 1997; 15:62-9.
- Thomsen LL, Eriksen MK, Roemer SF, Andersen I, Olesen J, Russell MB. A population-based study of familial hemiplegic migraine suggests revised diagnostic criteria. *Bain* 2002; 125:1379-91.
- Ducos A, Denier C, Joutel A, Cecillon M, Lescoat C, Vahedi K, et al. The clinical spectrum of familial hemiplegic migraine associated with mutations in a neuronal calcium channel. *N Engl J Med* 2001; 345:17-24.
- Ophoff RA, Terwindt GM, Vergouwe MN, van Eijk R, Oefner PJ, Hoffman SM, et al. Familial hemiplegic migraine and episodic ataxia type-2 are caused by mutations in the Ca²⁺ channel gene CACNA1A. *Cell* 1996; 87:543-52.
- Bourinot E, Soong TW, Sutton K, Szymaker S, Matthews E, Montell A, et al. Splicing of alpha 1A subunit gene generates phenotypic variants of P- and Q-type calcium channels. *Nat Neurosci* 1999; 2:407-15.
- Starr TV, Prystay W, Snutch TP. Primary structure of a calcium channel that is highly expressed in the rat cerebellum. *Proc Natl Acad Sci USA* 1991; 88:5621-5.
- Westenbroek RE, Sakurai T, Elliott EM, Hell JW, Starr TV, Snutch TP, Catterall WA. Immunohistochemical identification and subcellular distribution of the alpha 1A subunits of brain calcium channels. *J Neurosci* 1995; 15:6403-18.
- Takahashi T, Momiya A. Different types of calcium channels mediate central synaptic transmission. *Nature* 1993; 366:156-8.
- Sutton KG, McRory JE, Guthrie H, Murphy TH, Snutch TP. P/Q-type calcium channels mediate the activity-dependent feedback of syntaxin-1A. *Nature* 1999; 401:800-4.
- Hans M, Luvisetto S, Williams ME, Spagnolo M, Urrutia A, Totene A, et al. Functional consequences of mutations in the human alpha1A calcium channel subunit linked to familial hemiplegic migraine. *J Neurosci* 1999; 19:1610-9.
- van den Maagdenberg AM, Pietrobon D, Pizzorusso T, Kaja S, Broos LA, Cesetti T, et al. A Cacna1a knockin migraine mouse model with increased susceptibility to cortical spreading depression. *Neuron* 2004; 41:701-10.
- Totene A, Fellin T, Pagnutti S, Luvisetto S, Striessnig J, Fletcher C, Pietrobon D. Familial hemiplegic migraine mutations increase Ca²⁺ influx through single human Ca_v2.1 channels and decrease maximal Ca_v2.1 current density in neurons. *Proc Natl Acad Sci USA* 2002; 99:13284-9.
- Totene A, Pivotto F, Fellin T, Cesetti T, van den Maagdenberg AM, Pietrobon D. Specific kinetic alterations of human Ca_v2.1 calcium channels produced by mutation S218L causing familial hemiplegic migraine and delayed cerebral edema and coma after minor head trauma. *J Biol Chem* 2005; 280:17678-86.
- Totene ASM, Frants RR, Ferrari M, van den Maagdenberg AMJ, Pietrobon D. Gain-Of-Function Of Ca_v2.1 Calcium Channels Leads To Increased Excitatory Synaptic Transmission In Microcultures Of Cortical Neurons From Cacna1a Knock-In Mice With The R192Q Familial Hemiplegic Migraine Mutation. *Abstract Viewer/Itinerary Planner* Washington, DC: Society for Neuroscience 2005; Online 2005.
- Cao YQ, Tsien RW. Effects of familial hemiplegic migraine type 1 mutations on neuronal P/Q-type Ca²⁺ channel activity and inhibitory synaptic transmission. *Proc Natl Acad Sci USA* 2005; 102:2590-5.
- Mullner C, Broos LA, van den Maagdenberg AM, Striessnig J. Familial hemiplegic migraine type 1 mutations K1336E, W1684R and V1696I alter Ca_v2.1 Ca²⁺ channel gating: evidence for beta-subunit isoform-specific effects. *J Biol Chem* 2004; 279:51844-50.
- Kraus RL, Sinnegger MJ, Koschak A, Glossmann H, Steniri S, Carrera P, Striessnig J. Three new familial hemiplegic migraine mutants affect P/Q-type Ca²⁺ channel kinetics. *J Biol Chem* 2000; 275:9239-43.
- Melliti K, Grabner M, Seabrook GR. The familial hemiplegic migraine mutation R192Q reduces G-protein-mediated inhibition of P/Q-type (Ca_v2.1) calcium channels expressed in human embryonic kidney cells. *J Physiol* 2003; 546:337-47.
- Gherardini LVDMA, Van De Ven RCG, Ferrari MD, Frants RR, Pietrobon D, Pizzorusso T. Increased susceptibility to cortical spreading depression in knockin mice carrying the S218L mutation of human Ca_v2.1 calcium channels: a new model for in vivo study of familial hemiplegic migraine type 1 (FHMI). *Poster*: Federation of European Neuroscience Societies Forum, Vienna Austria 2006.
- Kraus RL, Sinnegger MJ, Glossmann H, Hering S, Striessnig J. Familial hemiplegic migraine mutations change alpha1A Ca²⁺ channel kinetics. *J Biol Chem* 1998; 273:5586-90.

32. Soong TW, DeMaria CD, Alvania RS, Zweifel LS, Liang MC, Mittman S, et al. Systematic identification of splice variants in human P/Q-type channel $\alpha 1(2.1)$ subunits: implications for current density and Ca^{2+} -dependent inactivation. *J Neurosci* 2002; 22:10142-52.
33. Chang SY, Yong TF, Yu CY, Liang MC, Pletnikova O, Troncoso J, et al. Age and gender-dependent alternative splicing of P/Q-type calcium channel EF-hand. *Neuroscience* 2007; 145:1026-36.
34. Timmermann DB, Westenbroek RE, Schousboe A, Carterall WA. Distribution of high-voltage-activated calcium channels in cultured gamma-aminobutyric acidergic neurons from mouse cerebral cortex. *J Neurosci Res* 2002; 67:48-61.
35. Chaudhuri D, Chang SY, DeMaria CD, Alvania RS, Soong TW, Yue DT. Alternative splicing as a molecular switch for Ca^{2+} /calmodulin-dependent facilitation of P/Q-type Ca^{2+} channels. *J Neurosci* 2004; 24:6334-42.
36. Krovetz HS, Helton TD, Crews AL, Horne WA. C-Terminal alternative splicing changes the gating properties of a human spinal cord calcium channel $\alpha 1A$ subunit. *J Neurosci* 2000; 20:7564-70.
37. Restituito S, Thompson RM, Eliet J, Raife RS, Riedel M, Charner P, Gomez CM. The polyglutamine expansion in spinocerebellar ataxia type 6 causes a β subunit-specific enhanced activation of P/Q-type calcium channels in *Xenopus* oocytes. *J Neurosci* 2000; 20:6394-403.
38. Maximov A, Sudhof TC, Bezprozvanny I. Association of neuronal calcium channels with modular adaptor proteins. *J Biol Chem* 1999; 274:24453-6.
39. Mori Y, Friedrich T, Kim MS, Mikami A, Nakai J, Ruth P, et al. Primary structure and functional expression from complementary DNA of a brain calcium channel. *Nature* 1991; 350:398-402.
40. Hans M, Utruria A, Deal C, Brust PE, Stauderman K, Ellis SB, et al. Structural elements in domain IV that influence biophysical and pharmacological properties of human $\alpha 1A$ -containing high-voltage-activated calcium channels. *Biophys J* 1999; 76:1384-400.
41. Fitzsimons RB, Wolfenden WH. Migraine coma. Meningitic migraine with cerebral oedema associated with a new form of autosomal dominant cerebellar ataxia. *Brain* 1985; 108:555-77.
42. Kors EE, Terwindt GM, Vermeulen FL, Fitzsimons RB, Jardine PE, Heywood P, et al. Delayed cerebral edema and fatal coma after minor head trauma: role of the CACNA1A calcium channel subunit gene and relationship with familial hemiplegic migraine. *Ann Neurol* 2001; 49:753-60.
43. Chan YC, Burgunder JM, Wilder-Smith E, Chew SE, Lam-Mok-Sing KM, Sharma V, Ong BK. Electroencephalographic changes and seizures in familial hemiplegic migraine patients with the CACNA1A gene S218L mutation. *J Clin Neurosci* 2008; 15:891-4.
44. Zoller MJ, Smith M. Oligonucleotide-directed mutagenesis: a simple method using two oligonucleotide primers and a single-stranded DNA template. *DNA* 1984; 3:479-88.
45. Hamill OP, Marty A, Neher E, Sakmann B, Sigworth FJ. Improved patch-clamp techniques for high-resolution current recording from cells and cell-free membrane patches. *Pflügers Arch* 1981; 391:85-100.
46. Weiss N, Sandoval A, Felix R, Van den Maagdenberg A, De Waard M. The S218L familial hemiplegic migraine mutation promotes de/inhibition of $\text{Ca}_v2.1$ calcium channels during direct G-protein regulation. *Pflügers Arch* 2008; 457:315-26.
47. Womack M, Khodakhah K. Active contribution of dendrites to the tonic and trimodal patterns of activity in cerebellar Purkinje neurons. *J Neurosci* 2002; 22:10603-12.
48. Fernandez FR, Engbers JD, Turner RW. Firing dynamics of cerebellar Purkinje cells. *J Neurophysiol* 2007; 98:278-94.
49. Shin SL, Rotter S, Aertsen A, De Schutter E. Stochastic description of complex and simple spike firing in cerebellar Purkinje cells. *Eur J Neurosci* 2007; 25:785-94.
50. McCormick DA, Connors BW, Lighthall JW, Prince DA. Comparative electrophysiology of pyramidal and sparsely spiny stellate neurons of the neocortex. *J Neurophysiol* 1985; 54:782-806.
51. Brumberg JC. Firing pattern modulation by oscillatory input in supragranular pyramidal neurons. *Neuroscience* 2002; 114:239-46.
52. Fellin T, Luvisetto S, Spagnolo M, Pietrobon D. Modal gating of human $\text{Ca}_v2.1$ (P/Q-type) calcium channels. II. The b mode and reversible uncoupling of inactivation. *J Gen Physiol* 2004; 124:463-74.
53. Luvisetto S, Fellin T, Spagnolo M, Hivert B, Brust PE, Harpold MM, et al. Modal gating of human $\text{Ca}_v2.1$ (P/Q-type) calcium channels. I. The slow and the fast gating modes and their modulation by beta subunits. *J Gen Physiol* 2004; 124:445-61.
54. Chaudhuri D, Issa JB, Yue DT. Elementary mechanisms producing facilitation of $\text{Ca}_v2.1$ (P/Q-type) channels. *J Gen Physiol* 2007; 129:385-401.
55. Belay H, Reuter U, Dunn AK, Huang Z, Boas DA, Moskowitz MA. Intrinsic brain activity triggers trigeminal meningeal afferents in a migraine model. *Nat Med* 2002; 8:136-42.
56. Pietrobon D. Migraine: new molecular mechanisms. *Neuroscientist* 2005; 11:373-86.
57. Pietrobon D. Familial hemiplegic migraine. *Neurotherapeutics* 2007; 4:274-84.
58. Weiss JM, Simson PE. Neurochemical and electrophysiological events underlying stress-induced depression in an animal model. *Adv Exp Med Biol* 1988; 245:425-40.
59. McEwen BS. Physiology and neurobiology of stress and adaptation: central role of the brain. *Physiol Rev* 2007; 87:873-904.
60. Altier C, Dale CS, Kisilevsky AE, Chapman K, Castiglioni AJ, Mathews EA, et al. Differential role of N-type calcium channel splice isoforms in pain. *J Neurosci* 2007; 27:6363-73.
61. Powell KL, Cain SM, Ng C, Sirdesai S, David LS, Kyri M, Garcia E, Tyson JR, Reid CA, Bahlo M, Foote SJ, Snutch TP, O'Brien TJ. A $\text{Ca}_v3.2$ T-type calcium channel point mutation has splice-variant-specific effects on function and segregates with seizure expression in a polygenic rat model of absence epilepsy. *J Neurosci* 2009; 29:371-80.

APPENDIX 5: A Ca_v3.2 T-TYPE CALCIUM CHANNEL POINT MUTATION HAS SPLICE-VARIANT SPECIFIC EFFECTS ON FUNCTION AND SEGREGATES WITH SEIZURE EXPRESSION IN POLYGENIC RAT MODEL OF ABSENCE EPILEPSY

The Journal of Neuroscience, January 14, 2009 • 29(2):371–380 • 371

Neurobiology of Disease

A Ca_v3.2 T-Type Calcium Channel Point Mutation Has Splice-Variant-Specific Effects on Function and Segregates with Seizure Expression in a Polygenic Rat Model of Absence Epilepsy

Kim L. Powell,^{1*} Stuart M. Cain,^{2*} Caroline Ng,¹ Shreerang Sirdesai,¹ Laurence S. David,² Mervyn Kyi,¹ Esperanza Garcia,² John R. Tyson,³ Christopher A. Reid,³ Melanie Bahlo,⁴ Simon J. Foote,⁵ Terrance P. Snutch,² and Terence J. O'Brien¹

¹Departments of Medicine, Surgery, and Neurology, The Royal Melbourne Hospital, University of Melbourne, Melbourne, Victoria 3050, Australia, ²Michael Smith Laboratories, University of British Columbia, Vancouver, British Columbia, Canada V6T 1Z4, ³Howard Florey Institute, University of Melbourne, Melbourne, Victoria 3010, Australia, ⁴The Walter and Eliza Hall Institute of Medical Research, Melbourne, Victoria 3050, Australia, and ⁵Menzies Research Institute, University of Tasmania, Hobart, Tasmania 7000, Australia

Low-voltage-activated, or T-type, calcium (Ca²⁺) channels are believed to play an essential role in the generation of absence seizures in the idiopathic generalized epilepsies (IGEs). We describe a homozygous, missense, single nucleotide (G to C) mutation in the Ca_v3.2 T-type Ca²⁺ channel gene (*Cacna1h*) in the genetic absence epilepsy rats from Strasbourg (GAERS) model of IGE. The GAERS Ca_v3.2 mutation (*gcm*) produces an arginine to proline (R1584P) substitution in exon 24 of *Cacna1h*, encoding a portion of the III–IV linker region in Ca_v3.2. *gcm* segregates codominantly with the number of seizures and time in seizure activity in progeny of an F1 intercross. We have further identified two major thalamic *Cacna1h* splice variants, either with or without exon 25. *gcm* introduced into the splice variants acts “epistatically,” requiring the presence of exon 25 to produce significantly faster recovery from channel inactivation and greater charge transference during high-frequency bursts. This gain-of-function mutation, the first reported in the GAERS polygenic animal model, has a novel mechanism of action, being dependent on exonic splicing for its functional consequences to be expressed.

Key words: idiopathic generalized epilepsy; absence seizures; T-type calcium channel; splice variant; point mutation; genetic absence epilepsy rats from Strasbourg; GAERS

Introduction

The idiopathic generalized epilepsies (IGEs) are a common group of diseases with a strong hereditary component. Despite a small number of genes explaining the disease in rare families, the genetic causes of the majority of the IGEs remain undetermined and are generally believed to be polygenic. Absence seizures, which form part of the IGE spectrum, are nonconvulsive generalized seizures resulting in a brief impairment of consciousness (Mattson, 2003). The genetic absence epilepsy rats from Strasbourg (GAERS) are a well validated genetic rat model of absence

epilepsy (Marescaux et al., 1984) that exhibit spontaneous spike-and-wave discharges (SWDs) on a normal electroencephalogram (EEG) background, closely resembling the human condition. Cross-breeding (Marescaux et al., 1992) and qualitative trait linkage analysis (Rudolf et al., 2004) studies indicate that the epilepsy phenotype in GAERS is polygenically determined. However, despite two decades of study, the nature of the genetic determinants underlying the epileptic phenotype of GAERS has not been identified previously.

The thalamocortical network is critically involved in the propagation of SWDs in both human absence epilepsy and many animal models (Crunelli and Leresche, 2002). Extensive investigation has revealed that neuronal low-voltage-activated (T-type) Ca²⁺ channels underlie burst firing and oscillatory behavior in this network as a result of their ability to generate Ca²⁺ spikes near resting membrane potential (Llinas and Yarom, 1981; Carbone and Lux, 1984; Huguenard and Prince, 1992; Perez-Reyes, 2003). Three lines of evidence specifically implicate the T-type Ca²⁺ channel with absence epilepsy. First, Ca_v3.2 mRNA expression (Talley et al., 2000) and T-type Ca²⁺ currents (Tsakiridou et al., 1995) have been found to be elevated in the reticular nucleus of the thalamus (nRT) of GAERS. Second, elevated thalamic

Received Nov. 3, 2008; accepted Nov. 20, 2008.

This work was supported by National Health and Medical Research Council Grants 406640 (T.J.O., S.J.F.) and 454655 (C.A.R.), the Molly McInnes Foundation Scholarship (K.L.P.), and Canadian Institutes of Health Research Grant 10677 (T.P.S.). T.P.S. is a Tier 1 Canada Research Chair in Biotechnology and Genomic–Neurobiology.

*K.L.P. and S.M.C. contributed equally to this work.

Correspondence should be addressed to either of the following: Terence O'Brien, Department of Medicine (Royal Melbourne Hospital/Western Hospital), The University of Melbourne, 4th Floor, Clinical Sciences Building, Royal Melbourne Hospital, Royal Parade, Parkville, Victoria 3050, Australia. E-mail: obiden@unimelb.edu.au; or Terence Snutch, Michael Smith Laboratories, The University of British Columbia, 301-2115 East Mall, Vancouver, British Columbia, Canada V6T 1Z4. E-mail: snutch@msl.ubc.ca.

DOI:10.1523/JNEUROSCI.5295-08.2009

Copyright © 2009 Society for Neuroscience 0270-6474/09/290371-10\$15.00/0

*A version of this appendix has been published. Powell, K.L., Cain, S.M., Ng, C., Sirdesai, S., David, L.S., Kyi, M., Garcia, E., Tyson, J.R., Reid, C.A., Bahlo, M., Foote, S.J., Snutch, T.P., O'Brien, T.J. (2009). A Ca_v3.2 T-type calcium channel point mutation has splice-variant-specific effects on function and segregates with seizure expression in a polygenic rat model of absence epilepsy. The Journal of Neuroscience. 29(2):371–380. Reprinted with kind permission of The Society for Neuroscience. All rights reserved.

T-type currents precede the onset of absence seizures in a SNAP-25-deficient mouse model (Zhang et al., 2004). Third, mutations in the human *CACNA1H* have been found in patients with childhood absence epilepsy and juvenile absence epilepsy (Chen et al., 2003; Liang et al., 2006, 2007; Heron et al., 2007) with exogenous expression of mutant human $Ca_v3.2$ channels revealing a variety of biophysical changes (Khosravani et al., 2004, 2005; Vitko et al., 2005, 2007; Peloquin et al., 2006).

Here we report the first mutation with functional effects in a polygenic animal model of absence epilepsy. The GAERS $Ca_v3.2$ mutation (*gcm*) is situated in exon 24 of *Cacna1h* in a region encoding a portion of the domain III–IV linker. Electrophysiological investigation revealed that *gcm* increases the rate of recovery from channel inactivation, producing a predicted gain-of-function phenotype. The functional effects of *gcm* are dependent on alternative splicing of exon 25, being manifested in the splice variant with this exon [$Ca_v3.2 (+25)$]. These results provide unique insight into the genetic cause of absence seizures in GAERS as well as provide new knowledge regarding the structural–functional relationship for $Ca_v3.2$ T-type Ca^{2+} channels. Of particular importance is the demonstration of the principle that genetic mutations may have functional effects only in certain splice variants of ion channels (Adams et al., 2007).

Materials and Methods

Production of F2 generation. The double cross matings required for this study were produced in two stages. First, GAERS rats (homozygous or $-/-$ for the $Ca_v3.2$ *gcm* mutation) were crossed with nonepileptic control (NEC) rats (null or $+/+$ for the *gcm* mutation) to produce an F1 generation, all of which should be heterozygous for the mutation. Then, two F1 ($+/-$) generation rats were mated to produce an F2 generation. On average, 25% of the F2 progeny would be expected to be homozygous for the mutation, 50% heterozygous for the mutation, and 25% null or not carrying the mutation at all.

Animal surgeries. The study was approved by the Animal Ethics Committee of the Ludwig Institute for Cancer Research/Department of Surgery, The Royal Melbourne Hospital, The University of Melbourne and conformed to National Health and Medical Research Council guidelines for the ethical use of animals in scientific research. All surgeries were performed under deep general anesthetic, with each rat receiving an intraperitoneal injection (5 ml/kg) of anesthetic solution containing ketamine (75 mg/kg; Ketavet 100; Parnell Laboratories) and xylazine (10 mg/kg; Xylazil-20; Troy Laboratories) in 0.9% sodium chloride. Once anesthetized, a single midline incision was made on the scalp, from just posterior to the eyes to between the ears. Six holes were drilled through the skull but not penetrating the dura, one on each side anterior to the bregma and two on each side posterior to the bregma. A recording electrode was screwed into each hole. Each recording electrode comprised a 1.3 mm “male” gold connector (Farnell Components) soldered onto a nickel alloy jeweler screw. The recording electrodes were fixed in position by applying Vertex dental cement around the electrodes and over the skull. The incision was then sutured (Dysilk 3/0). Immediately after surgery, each rat received an intraperitoneal injection of 1 ml/kg analgesic solution containing intraperitoneal carprofen analgesic (5 mg/kg; Rimadyl; Pfizer Australia) in 0.9% sodium chloride. Polyvisc was again applied to the eyes.

EEG recordings and analysis. Seven days after surgery, all rats underwent four 90 min EEG recordings over weeks 17 and 18 (two recordings per week). The rats were connected to an EEG board, and their EEG trace

Table 1. Summary of the genetic alterations in the rat $Ca_v3.2$ T-type calcium channel gene

	Mutation 1	Mutation 2	Mutation 3	Mutation 4
Base pair number	4751	2620	5439	6580
Exon	24	11	31	35
Affected residue number	1584	873	1813	2194
<i>R. norvegicus</i>	G	A	C	T
NEC	G	G	T	G
GAERS	C	G	T	G
Codon change	CGG → CCG ^a	GCA → GCG ^b	TTC → TTT ^b	TCA → GCA ^b
Amino acid change	Arg → Pro	Ala → Ala	Phe → Phe	Ser → Ala
Type of mutation	Nonsynonymous	Synonymous	Synonymous	Nonsynonymous
Structural location	Linker III–IV	IIS3–IIS4	IVS5	COOH
Conservation between species	Conserved region	Conserved region	Conserved region	Nonconserved

In addition to the *gcm* mutation, three more mutations were detected in the Wistar (NEC and GAERS) strains compared with *R. norvegicus*. Two of these mutations are silent and do not cause amino acid changes, whereas the third causes a TCA (serine) to CCA (alanine) change. However, none of these three mutations differed between the NEC and GAERS.

^aCodon and amino acid change between NEC and GAERS.

^bCodon and amino acid change between Wistar rats versus *R. norvegicus*.

was recorded using Compumedics EEG acquisition software. Recordings lasted 90 min after an initial 15 min habituation period. Recordings alternately took place in the morning or afternoon; each rat had two morning and two afternoon recordings. The animals were able to move freely around their cage and were constantly monitored by an investigator to ensure that they did not fall asleep using gentle finger taps on the side of the cage as necessary. Rats were allowed at least 2 d rest between consecutive recordings. All rats were observed during the recording to confirm their seizure status. Seizure expression for the 90 min after injection EEG recording was quantified by visual inspection of the EEG recordings, blinded to the animal's genotype. Standard criteria described for adult GAERS were used to classify the seizures, i.e., an SWD burst of amplitude of more than three times baseline, a frequency of 7–12 Hz, and duration of longer than 0.5 s (Marescaux et al., 1992; Liu et al., 2006). The start and end of each seizure was determined by manually marking the beginning and end of each SWD on the EEG. From this, the total percentage time spent in seizure over the 90 min postinjection EEG recording was determined, the primary endpoint for comparison of the treatment effect on seizure expression.

Genomic DNA extraction and genotyping PCR. Genomic DNA was extracted from tail tips using the Promega Wizard Genomic DNA extraction kit, and genotyping PCR was performed using primers designed to amplify exon 24 (193 bp). Each 20 μ l of PCR reaction contained the following: 1 \times TaqDNA polymerase buffer, 2.5 U of TaqDNA polymerase, 250 μ M dNTPs, 500 nM forward and reverse primers, and 25 ng of genomic DNA (for primer sequences, see supplemental Table 1, available at www.jneurosci.org as supplemental material). To confirm the correct size band, 5 μ l of PCR reactions were run on a 2% agarose gel with molecular weight markers, and gels were stained with GelRed DNA stain (Jomar) and visualized under UV light. PCR reactions were cleaned up using the Promega PCR cleanup kit, and purified PCR products were sent to the Australian Genome Research Facility (Brisbane, Australia) for sequencing (for primer sequences, see supplemental Table 1, available at www.jneurosci.org as supplemental material). Sequence analysis was done using Sequence Scanner version 1.0 (Applied Biosystems).

RNA extraction and cDNA synthesis. Total RNA was extracted from adult Wistar rat thalamus using Trizol reagent (Invitrogen) according to the instructions of the manufacturer. One microgram total RNA was initially treated with DNase to avoid genomic DNA contamination during reverse transcription using the Superscript II reverse transcriptase (Invitrogen) enzyme. A total of 20 μ l of reaction volume was prepared containing DNase-treated total RNA, first strand buffer (1 \times), DTT (10 μ M), oligo-dT (0.5 μ g/L), dNTP mix (500 μ M), RNaseOUT (40 U), and reverse transcriptase (200 U). Reaction mixture was incubated at 42°C for 50 min and inactivated by heating to 70°C for 15 min. Finally, RNase H (2 U) was added to the mixture and incubated at 37°C for 20 min to remove the RNA complementary to the cDNA.

Splice variant screening, cloning, and site-directed mutagenesis. Initially,

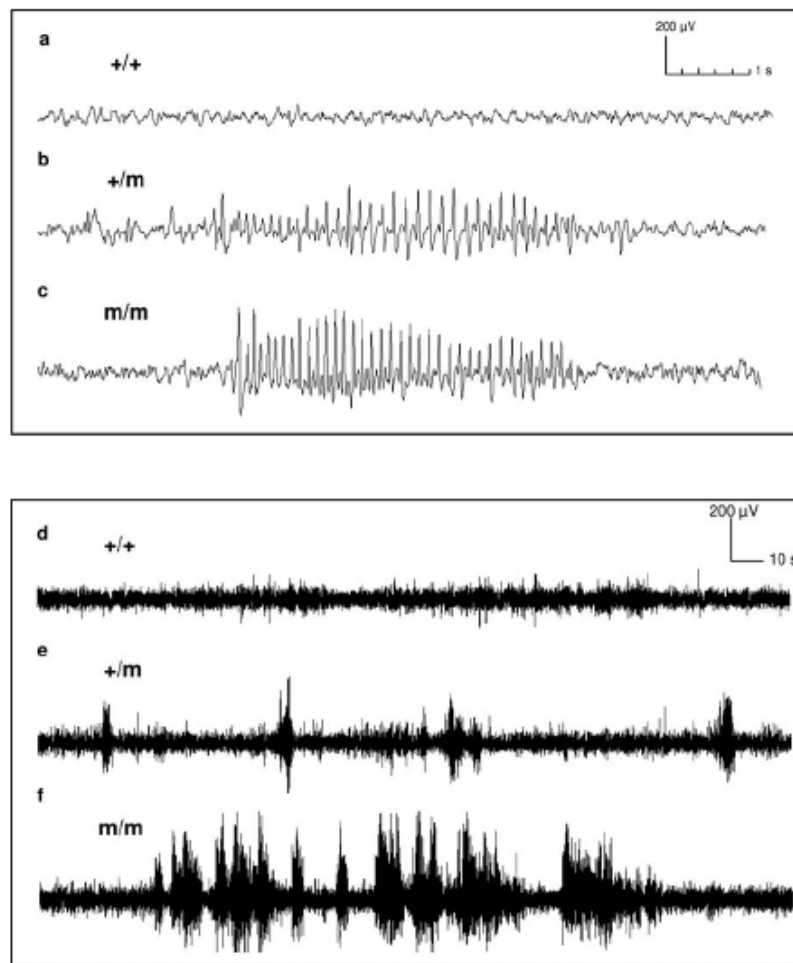


Figure 1. Representative EEG traces from *m/m* (*a, d*), *+/-* (*b, e*), and *+/+* (*c, f*) animals over a 10 s period (*a–c*) and a 5 min period (*d–f*). *+/+* animals are null for the R1584P mutation (*gcm*), *+/-* animals carry one copy of the mutation, and *m/m* animals are homozygous for the *gcm* mutation.

splice variant exon scanning was performed on rat thalamic RNA to identify the existence of expressed $Ca_v3.2$ isoforms. Overlapping primer sets were designed to amplify between two and five exons. PCR products were sequenced and compared with genomic sequence for the presence of splice sites. Subsequently, full-length $Ca_v3.2$ cDNA libraries were made from thalamic total RNA (2 μ g) using $Ca_v3.2$ -specific forward (5'-GATAAGCTTATGACCGAGGGCAGC-3') and reverse (5'-CGCTCTAGACTACACAGGCTCATC-3') primers. The cDNA products were subcloned into the pGEM T-Easy vector (Promega), and a total of 76 full-length $Ca_v3.2$ cDNAs were subject to complete DNA sequencing. Full-length $Ca_v3.2$ with or without exon 25 alternative splice variants were moved from pGEM T-Easy to pCDNA3.1 zeo(+) (Invitrogen) using the restriction enzymes *Hind*III and *Xba*I (introduced at beginning and end, respectively, of the $Ca_v3.2$ cDNAs). The DNA sequence of the full-length $Ca_v3.2$ clones were determined using automated DNA sequencing, and sequences were aligned to available published genomic $Ca_v3.2$ sequences. The *gcm* was introduced into the *+/-* exon 25 $Ca_v3.2$ clones using the Quickchange site-directed mutagenesis (SDM) procedure (Stratagene) with the GAERS-sdm1 (5'-AGGAGGCTCGGCGCCCGGAGGAGAAACGGCT-3') and GAERS-sdm2 (5'-AGCCGTTTCCTCCGGGGCGCGGAGCCTCCT-3') primers. Once generated, the GAERS mutation *+/-* exon 25 was removed as an 872 bp *EcoRV*–*Bst*BI fragment and cloned back into a nonmutagenized $Ca_v3.2$ plasmid background to remove nonspecific mutations introduced during SDM. Fi-

nally, the \pm exon 25 GAERS clones were then fully resequenced to confirm that no other mutation had been introduced.

Tissue collection. Adult chronically epileptic (18–21 weeks) GAERS and age-matched NEC rats were culled by a lethal dose of pentobarbital (Lethobarb) anesthetic (Virbac), followed by rapid extraction of the brain. The thalamic brain region was rapidly dissected and stored in RNALater (Applied Biosystems) and frozen at -80°C .

Quantitative real-time-PCR. RNA was extracted using the RNeasy mini kit (QIAGEN) and treated with DNase I (QIAGEN) to remove any contaminating genomic DNA and stored at -80°C . Spectrophotometric readings were taken with the NanoDrop Spectrophotometer (NanoDrop Technologies) to determine RNA concentration and purity. For each sample, 2 μ g of total RNA was used to synthesize cDNA using the High Capacity cDNA Reverse Transcription kit from Applied Biosystems. Real-time-PCR reaction was performed using Applied Biosystems reagents and TaqMan probes to the respective gene targets on an Applied Biosystems AB 7500 system. Primer mixes used for detection of exon 25 splice variants were as follows: + exon 25 (H- $Ca_v3.2$ -plus25 forward, GCGCAGGAGCACTTTCC; H- $Ca_v3.2$ -plus25 reverse, GAGTGTGTGAATAGTCTGCGTAGTA; H- $Ca_v3.2$ -plus25-Probe, CCAACCCAGAGGCCAG); – exon 25 (H- $Ca_v3.2$ -minus25 forward, CGCCGGGAGGAGAAACG; H- $Ca_v3.2$ -minus25 reverse, GAGTGTGTGAATAGTCTGCGTAGTA; H- $Ca_v3.2$ -minus25-Probe, CTGGGCCTTCTGCGCC). Titration curves to calculate copy number parameters for each of the + and – exon 25 primer sets were produced using splice-variant-specific full-length cDNA plasmid clones. A rat actin B (ActB) primer set (Applied Biosystems AB 4352340E) was run in parallel with the + and – exon 25 probes in all samples as a control for total cDNA input to allow comparison. Copy numbers for each splice variant in each sample were then calculated and scaled, using relative ActB amounts, before being compared. Target and control probe reactions were run in triplicate and averaged for each sample.

Cell culture. Human embryonic kidney (HEK) 293 cells were grown at 37°C in DMEM supplemented with 10% heat-inactivated FBS, 50 U/ml penicillin, and 50 μ g/ml streptomycin. Cells were transiently transfected with $Ca_v3.2$ or $Ca_v3.2$ *gcm* (0.6 μ g of cDNA per 35 mm^2 dish, plus 0.1 μ g per dish of GFP marker) in pcDNA3.1zeo(+) using Lipofectamine (Invitrogen). Cells were incubated at 37°C in a humidified incubator with 5% CO_2 for 24–48 h before recording.

Electrophysiology. Ca^{2+} currents were recorded using the whole-cell patch-clamp technique with the following two solutions (in mM): internal: 120 Cs-methanesulphonate, 11 EGTA, 10 HEPES, 2 MgCl_2 , 5 MgATP, and 0.3 NaGTP, pH 7.2; external: 2 CaCl_2 , 1 MgCl_2 , 10 HEPES, 40 tetraethylammonium-Cl, 92 CsCl, and 10 glucose, pH 7.4. Fire-polished patch pipettes (borosilicate glass) had typical resistances of 3–5 M Ω when containing internal solution. The recording chamber was grounded with an Ag/AgCl pellet. Whole-cell currents were recorded at room temperature using an Axopatch 200B amplifier (Molecular Devices). Data were acquired with pClamp software package version 9 (Molecular Devices). Series resistance (R_s) was compensated by 65–75%, and seals with R_g values >20 M Ω or cells with peak current <100 pA were discarded. Data analysis was performed using Clampfit 9 (Molecular Devices) and software Origin version 7.5 (Microcal Software). Data fol-

lowed a normal distribution, and statistical significance was calculated using one-way ANOVA with Tukey's *post hoc* test considering a *p* value <0.05 as significant. Data were plotted as mean \pm SE values.

The current-voltage (*I-V*) relationship was obtained by depolarizing the membrane with 150 ms pulses from a holding potential of -110 mV (currents sampled at 10 kHz and filtered at 2 kHz). Test pulses from -90 to $+10$ mV were applied at 5 mV steps. Peak amplitude of Ca^{2+} currents was plotted against test pulse potential, and *I-V* curves were fitted using a modified Boltzmann equation: $I = (G_{\text{max}} * (V_m - E_r)) / (1 + \exp((V_m - V_{50})/k))$, where G_{max} is the maximum value of membrane conductance, V_m is the test potential, E_r is the extrapolated reversal potential, V_{50} is the half-activation potential, and k (slope constant: $k = RT/z\delta F$, where r is gas constant, T is absolute temperature, z is valence of conducting ion, δ is electrical distance across the membrane, and F is Faraday's constant) reflects the voltage sensitivity. Activation curves were obtained by calculating conductance from the *I-V* curves and plotting the normalized conductance as a function of the membrane potential. The data were fitted with the following Boltzmann equation: $G/G_{\text{max}} = A_2 + (A_1 - A_2) / (1 + \exp((V_m - V_{50})/k))$, where A_1 is minimum normalized conductance, A_2 is maximum normalized conductance, V_m is the test potential, V_{50} is the half-activation potential, and k value is the slope of the activation curve (slope constant).

Steady-state inactivation was studied using 90 ms test pulses at -30 mV applied after 2 s conditioning prepulses ranging from -120 to -10 mV (currents sampled at 10 kHz and filtered at 2 kHz). The current magnitude obtained during each test pulse was normalized to the maximum at -120 mV and plotted as a function of the prepulse potential. The data were fitted with the following Boltzmann equation: $I/I_{\text{max}} = A_2 + (A_1 - A_2) / (1 + \exp((V_m - V_{50})/k))$, where A_1 is minimum normalized current, A_2 is the maximum normalized current, V_m is the test potential, V_{50} is the half-inactivation potential, and k reflects the slope of the inactivation curve (slope constant). The time course for activation (τ_{act}) and inactivation (τ_{inact}) were analyzed by fitting current recordings obtained from the *I-V* protocol with a single-exponential standard equation: $I = Ae^{-t/\tau}$, where A is the amplitude of the current, and τ is the time constant.

Recovery from inactivation was studied using a double-pulse protocol at a holding potential of -110 mV (currents sampled at 2 kHz and filtered at 2 kHz) to ensure complete deactivation of $\text{Ca}_v3.2$ channels. The cell membrane was depolarized for 400 ms to -30 mV (prepulse) to ensure complete channel inactivation and then to -30 mV (test pulse) after an increasing time period (interpulse interval) between 5 ms and 5 s. The peak current from the test pulse was plotted as a ratio of maximum prepulse current versus interpulse interval. The data were fitted with a double-exponential function: $I/I_{\text{max}} = A_1 * \exp(-t/\tau_1) + A_2 * \exp(-t/\tau_2)$, where A_1 and A_2 are the amplitude for the fast and slow components of the exponential, and τ_1 and τ_2 are the time constants for the fast and slow components, respectively.

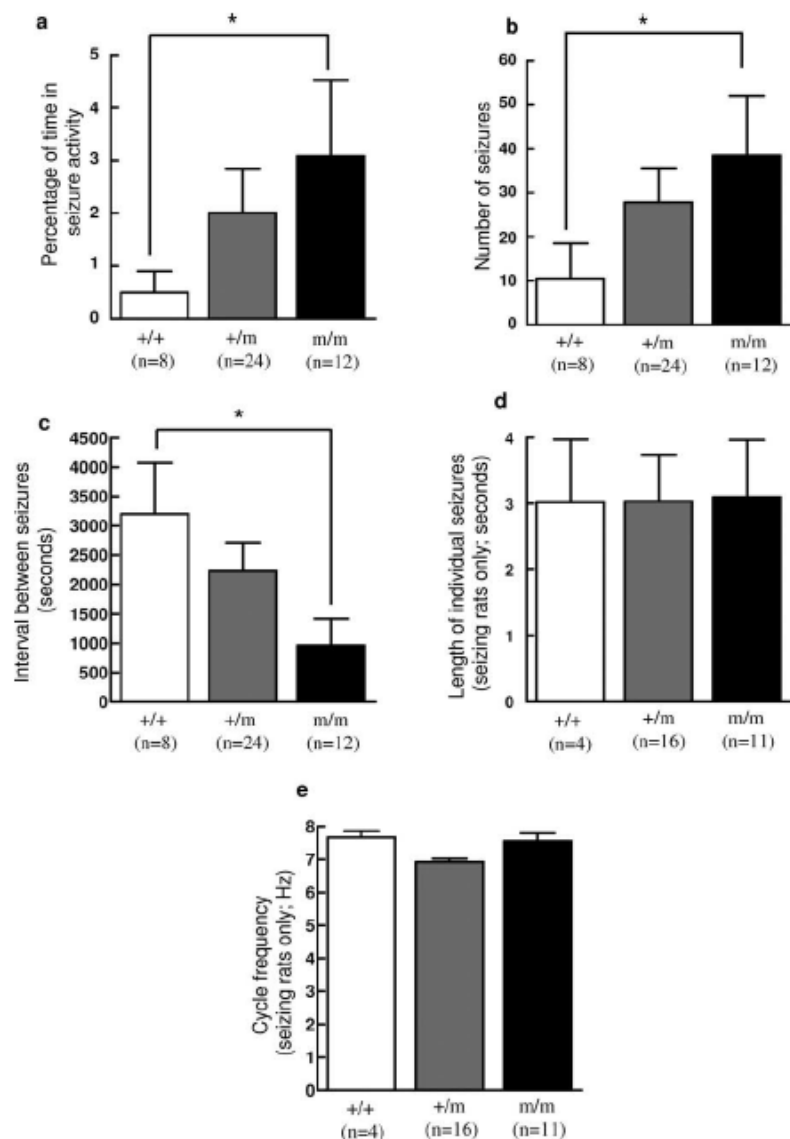


Figure 2. The *gcm* mutation positively correlates with the epileptic phenotype in double-crossed (F2) GAERS versus NEC rats. *a*, Percentage of recording time spent in seizure activity. Animals homozygous for the mutation spend more time in seizure activity than animals null for the *gcm* ($p < 0.05$, Mann-Whitney one-tailed test). *b*, Number of seizures. Animals homozygous for the *gcm* experience more seizures than animals null for the mutation ($p < 0.05$, Mann-Whitney one-tailed test). *c*, The interval between the seizures was significantly shorter for animals homozygous for the mutation compared with animals null for the mutation ($p < 0.05$, Mann-Whitney one-tailed test). *d*, The length of individual seizures did not significantly differ between the genotypes ($p > 0.05$, Mann-Whitney one-tailed test). *e*, The cycle frequency of the spike-and-wave discharges (hertz) did not significantly differ between the genotypes ($p > 0.05$, Mann-Whitney one-tailed test). +/+ animals are null for the *gcm*, +/m animals have one copy of the *gcm*, and m/m animals are homozygous for the *gcm*. Data are expressed as mean \pm SEM. * $p < 0.05$.

$\text{Ca}_v3.2$ activity during high-frequency burst depolarization was studied using a burst square pulse protocol at a holding potential of -70 mV (currents sampled at 10 kHz and filtered at 5 kHz). The membrane was depolarized for 4 ms to -20 mV at a frequency of 125 Hz for 80 ms to produce a high-frequency burst. Burst depolarizations were performed at a frequency of 5 Hz for 1 s. The data were analyzed by taking the integral of each burst individually giving a measurement of charge transference (Q) carried by Ca^{2+} through $\text{Ca}_v3.2$. Charge transference was then divided by the peak current on the first pulse of the first burst to

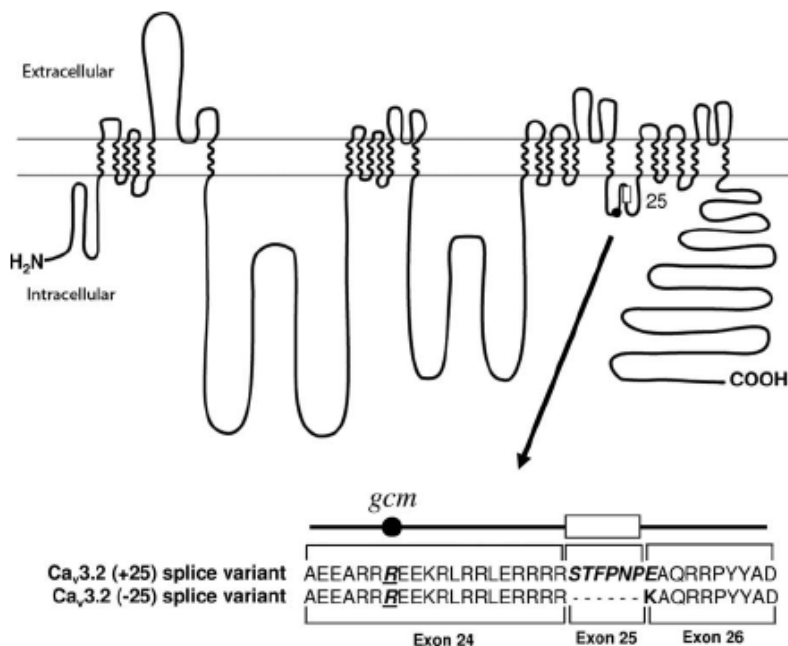


Figure 3. Differential expression of Ca_v3.2 splice variants in NEC and GAERS animals. Exon 25 of the rat *Cacna1h* gene is alternatively spliced to produce Ca_v3.2 (+25) and Cav3.2 (-25) isoforms. The Ca_v3.2 (-25) variant channels have a lysine residue at position 1598. This lysine residue is replaced by the 7 aa sequence (STFPNPE) in the Ca_v3.2 (+25) variant. The R1584P mutation (*gcm*) site is located 13 aa upstream of the beginning of exon 25 region (underlined arginine residue).

account for variation in current magnitude between cells to yield a charge transference factor (Q/pA).

Results

GAERS possess a mutation in the Ca_v3.2 T-type calcium channel gene

The entire coding region (7098 bp) of *Cacna1h* was sequenced in both GAERS ($n = 3$) and NEC ($n = 3$) rats, and we identified a single-nucleotide mutation in GAERS compared with NEC and *Rattus norvegicus* strains (Table 1). At base pair 4751 in exon 24, NEC rats and *R. norvegicus* both possess a guanine (G), whereas GAERS possess a cytosine (C). The base change results in an amino acid change from an arginine (CGG) to a proline (CCG) at position 1584 (R1584P) located within the domain III–IV linker region of the channel. This region of the gene is highly conserved across species and across other T-type Ca²⁺ channels, suggesting a critical functional role. Arginine is a basic amino acid with a long side chain, whereas proline is a cyclic amino acid lacking a hydrogen at the amino end and is unable to form hydrogen bonds and thus can disrupt protein structure. Exon 24, the location of the *gcm*, was then sequenced in another 15 NEC and 22 GAERS, revealing that all NEC rats were null for the *gcm* and all GAERS had two copies of the *gcm*. We screened additional rat strains, i.e., Sprague Dawley, Wistar–Kyoto, spontaneously hypertensive rats, normotensive rats, and WAG/Rij (Wistar Albino Glaxo from Rijswijk; another genetic rat model of absence epilepsy), as well as mouse strains (BALB/c and DBA), and found that none of these carry any copies of the R1584P mutation. NEC rats (which originate from a Wistar strain) and *R. norvegicus* (Brown Norway) also do not carry any copies of the R1584P mutation.

The *gcm* positively correlates with the epileptic phenotype in GAERS

The epileptic phenotype that was attributable to the *gcm* was assessed in the progeny of an F1 cross between GAERS and NEC rats. Homozygous animals carrying either two copies of the *gcm* or null for the *gcm* were compared for the total amount of time spent in seizures during a 90 min EEG recording and also for the number, duration, and frequency of the seizures. Examples of EEG traces from an animal null for the *gcm* are shown in Figure 1, *a* and *d*, from an animal heterozygous for the *gcm* in Figure 1, *b* and *e*, and an animal homozygous for the *gcm* in Figure 1, *c* and *f*. More F2 animals possessing two copies of the *gcm* (92.5%; $n = 12$) express seizures than animals possessing zero (50%; $n = 8$) or one copy (66.7%; $n = 24$) of the *gcm* ($p = 0.058$; m/m vs $+/+$; Fisher's exact test, one tailed). A strong *gcm* dose effect is evident for the time spent in seizure activity, with animals homozygous for the *gcm* spending significantly more time in seizure activity than animals null for the *gcm* ($3.1 \pm 1.5\%$, $n = 12$ vs $0.5 \pm 0.4\%$, $n = 8$; $p < 0.05$) (Fig. 2*a*). A significant association between the presence of the *gcm* and the number of seizures was also seen (Fig. 2*b*). Animals homozygous for the mutation experienced 38.5 ± 13.6 ($n = 12$) seizures compared with 10.5 ± 8.1 ($n = 8$) seizures for animals null for the mutation ($p < 0.05$). Additionally, animals homozygous for the mutation had a significantly shorter interval between the seizures than animals null for the mutation (268.1 ± 5364.8 s, $n = 12$ vs 4048.5 ± 5321.9 s, $n = 8$; $p < 0.05$) (Fig. 2*c*). The length of the individual seizures did not significantly differ between the three genotypes (zero copies, 3.01 ± 0.95 s, $n = 4$; one copy, 3.03 ± 0.7 s, $n = 16$; two copies, 3.1 ± 0.87 s, $n = 11$; $p > 0.05$ null vs homozygous) (Fig. 2*d*). The cycle frequency (hertz) of the spike-and-wave discharges accompanying the seizures was also not affected by the *gcm*. Animals null for the mutation had a seizure frequency of 7.7 ± 0.2 Hz, and animals homozygous for the mutation had a seizure frequency of 7.6 ± 0.2 Hz ($p > 0.05$) (Fig. 2*e*). Only animals that had seizures were included in the seizure duration and cycle frequency analysis.

Although our results provide evidence that the *gcm* plays a significant role in the absence epilepsy phenotype, they also demonstrate that the mutation does not, by itself, account for the entire phenotype. Some of the rats that were null for the *gcm* displayed absence seizures but significantly less often than those with the mutation. Similarly, there were rats that were positive for the *gcm* that either did not experience any (1 of 12) or experienced very few (2 of 12) absence seizures during the recording period. This is consistent with the current hypothesis that the determinants of the absence seizures in patients with IGE are polygenic (Crunelli and Leresche, 2002; Rudolf et al., 2004). A nonparametric Spearman's rank order correlation test was performed to examine the strength of the association between the number of copies of the *gcm* mutation in the F2 animals with their various seizure endpoints. A significant correlation was found for the percentage time in seizures ($r = 0.31$, $p = 0.04$) and the

number of seizures occurring during the recording period ($r = 0.34$, $p = 0.02$). No significant correlation existed for the average length of the individual seizures ($r = -0.17$, $p = 0.35$) or for the cycle frequency (hertz) of the spike-and-wave discharges ($r = 0.12$, $p = 0.52$).

Different splice variants of *Cacna1h* are expressed in the rat thalamus

We identified two major thalamic splice variants of the rat *Cacna1h* that differ with respect to the presence or absence of exon 25. $Ca_v3.2 (+25)$ transcripts include exon 25, whereas $Ca_v3.2 (-25)$ transcripts exclude exon 25 (Fig. 3). We hypothesized that there may be a splice-variant-specific effect of *gcm* in (+25) versus (-25) because the *gcm* mutation is situated in the adjacent exon 24, only 13 aa upstream of the beginning of exon 25 region (Fig. 3a). The inclusion of exon 25 results in an insertion of 18 nt (6 aa) plus the substitution of a lysine to a glutamate at the beginning of exon 26. Examination of adult Wistar full-length thalamic cDNA clones screened for splice variation ($n = 76$) showed approximately equal proportions of both splice variants [$Ca_v3.2 (+25) = 51\%$ and $Ca_v3.2 (-25) = 48\%$ of the total pool of $Ca_v3.2$ channels; data not shown]. Quantitative real-time-PCR analysis of the thalamus from >13-week-old NEC ($n = 7$) and GAERS ($n = 7$) animals revealed that there was no significant difference in the relative copy number of $Ca_v3.2$ mRNA [$Ca_v3.2 (+25) + Ca_v3.2 (-25)$] between NEC and GAERS animals (NEC, 178.2 ± 23.4 , $n = 7$; GAERS, 123.4 ± 19.8 , $n = 7$; $p = 0.09$). However, the ratio of $Ca_v3.2 (+25)$ to $Ca_v3.2 (-25)$ splice variants was ~1.5-fold greater in GAERS animals compared with the NEC strain [NEC, $Ca_v3.2 (+25)/Ca_v3.2 (-25) = 0.91 \pm 0.06$, $n = 7$; GAERS, $Ca_v3.2 (+25)/Ca_v3.2 (-25) = 1.51 \pm 0.11$, $n = 7$; $p < 0.0001$].

The *gcm* results in a splice-variant-specific gain of function effect on $Ca_v3.2 (+25)$ -containing channels

$Ca_v3.2$ channel function was assessed electrophysiologically *in vitro* using HEK293 cells transiently expressing either the $Ca_v3.2 (+25)$ or the $Ca_v3.2 (-25)$ splice variant \pm the *gcm*. The *gcm* had no significant effect on activation and inactivation kinetics, conductance, or steady-state inactivation of $Ca_v3.2$ channels in either splice variant (Fig. 4a,b, Table 2). The *gcm* also had no significant effect on the current density of either variant (Table 2). However, the *gcm* induced a splice-variant-specific gain of function in $Ca_v3.2 (+25)$ biophysical properties that could be highly relevant to neuronal burst firing. $Ca_v3.2 (+25)$ *gcm* channels recovered from an inactivating prepulse at a significantly faster rate (smaller slow

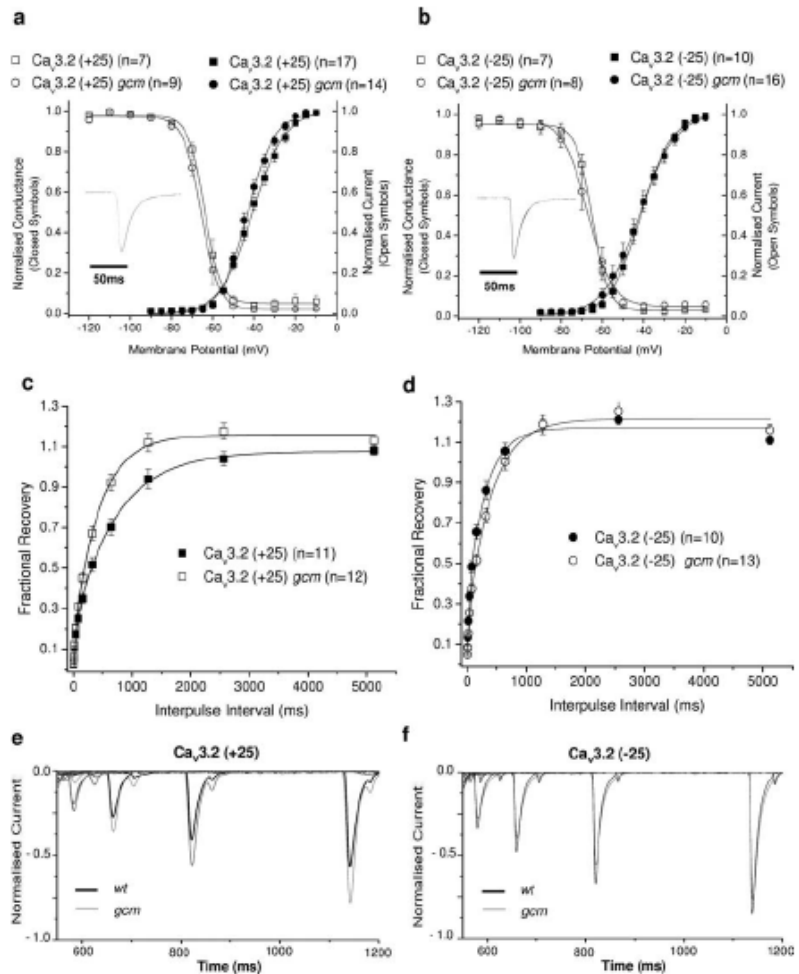


Figure 4. The *gcm* accelerates rate of recovery from inactivation in the $Ca_v3.2 (+25)$ splice variant. *a, b*, The conductance (filled symbols) of $Ca_v3.2 (+25)$ (*a*) and $Ca_v3.2 (-25)$ (*b*) and steady-state inactivation (open symbols) of $Ca_v3.2 (+25)$ (*a*) and $Ca_v3.2 (-25)$ (*b*) were not significantly altered by the *gcm*. Insets (*a, b*) show overlaid *gcm* and wild-type macroscopic currents during a 150 ms depolarizing pulse from a holding potential of -110 to -20 mV. Activation and inactivation kinetics of $Ca_v3.2 (+25)$ (*a*, inset) and $Ca_v3.2 (-25)$ (*b*, inset) splice variant currents are not affected by the *gcm*. $Ca_v3.2$ conductance was calculated from currents recorded during a series of depolarizing steps from a holding potential of -110 mV to various membrane potentials and normalized to maximum conductance. Steady-state inactivation was calculated from $Ca_v3.2$ currents recorded during a test pulse to -30 mV directly after a 2 s inactivating prepulse of varying membrane potentials and normalized to peak current. *c, d*, The effect of the *gcm* on fractional recovery (determined by the ratio of the peak current at the test pulse to the peak current at the prepulse and fitted to a double exponential) is shown for $Ca_v3.2 (+25)$ (*c*) and $Ca_v3.2 (-25)$ (*d*). $Ca_v3.2$ currents were recorded during test voltage pulses from a holding potential of -110 to -30 mV after an inactivating prepulse, with an increasing interpulse interval. *e, f*, Representative traces obtained at test pulses after 160, 320, 640, and 1280 ms interpulse intervals are shown for $Ca_v3.2 (+25)$ (*e*) and $Ca_v3.2 (-25)$ (*f*) currents. Normalized $Ca_v3.2 (+25)$ currents from 80 to 2560 ms interpulse intervals were significantly increased in the *gcm* [80 ms: wild type, 0.25 ± 0.02 ; *gcm*, 0.31 ± 0.02 ($p < 0.05$); 160 ms: wild type, 0.35 ± 0.02 ; *gcm*, 0.45 ± 0.02 ($p < 0.01$); 320 ms: wild type, 0.52 ± 0.03 ; *gcm*, 0.67 ± 0.03 ($p < 0.005$); 640 ms: wild type, 0.70 ± 0.04 ; *gcm*, 0.92 ± 0.04 ($p < 0.005$); 1280 ms: wild type, 0.94 ± 0.05 ; *gcm*, 1.12 ± 0.05 ($p < 0.05$); 2560: wild type, 1.04 ± 0.04 ; *gcm*, 1.16 ± 0.04 ($p < 0.05$); wild type, $n = 11$; *gcm*, $n = 12$].

recovery tau; τ_2) than $Ca_v3.2 (+25)$ channels (Fig. 4c). Conversely, the *gcm*-mediated gain of function was not observed in the $Ca_v3.2 (-25)$ splice variant, in which the $Ca_v3.2 (-25)$ *gcm* channels had a modestly slower rate of recovery (larger τ_2) (Fig. 4d, Table 2). As the *gcm* increases the rate of recovery from inactivation in $Ca_v3.2 (+25)$, more of these channels are available to conduct during subsequent depolarizations, resulting in significantly larger Ca^{2+} currents from 80 to 2560 ms interpulse inter-

Table 2. Whole-cell conductance, steady-state inactivation, and recovery from inactivation properties of Ca_v3.2 (±25) splice variants in the presence and absence of the *gcm*

Biophysical properties	Ca _v 3.2 (+25)	Ca _v 3.2 (+25) <i>gcm</i>	Ca _v 3.2 (−25)	Ca _v 3.2 (−25) <i>gcm</i>
Conductance				
V ₅₀	−41.2 ± 1.2	−43.3 ± 1.0	−41.9 ± 1.2	−42.6 ± 2.2
k	−7.0 ± 0.3	−6.0 ± 0.3	−7.0 ± 0.4	−7.0 ± 0.5
G _{max}	7.7 ± 0.9	8.6 ± 1.0	9.7 ± 2.0	7.0 ± 1.06
Peak / density (pA/pF)	−22.3 ± 3.2	−30.1 ± 4.4	−19.0 ± 3.5	−19.4 ± 3.8
Steady-state inactivation				
V ₅₀	−65.1 ± 1.2	−66.1 ± 1.2	−65.2 ± 1.2	−67.5 ± 2.3
k	3.9 ± 0.4	4.1 ± 0.3	3.9 ± 0.4	4.4 ± 1.0
Recovery from inactivation				
τ ₁	27.5 ± 2.1	24.1 ± 2.5	33.1 ± 3.8	25.3 ± 5.7
τ ₂	745.0 ± 32.2	436.8 ± 37.6*	328.5 ± 35.8	430.5 ± 25.3**

All values were calculated individually for each cell and the mean ± SEM taken to achieve the stated values (ANOVA; **p* < 0.001, ***p* < 0.05 compared with wild-type control).

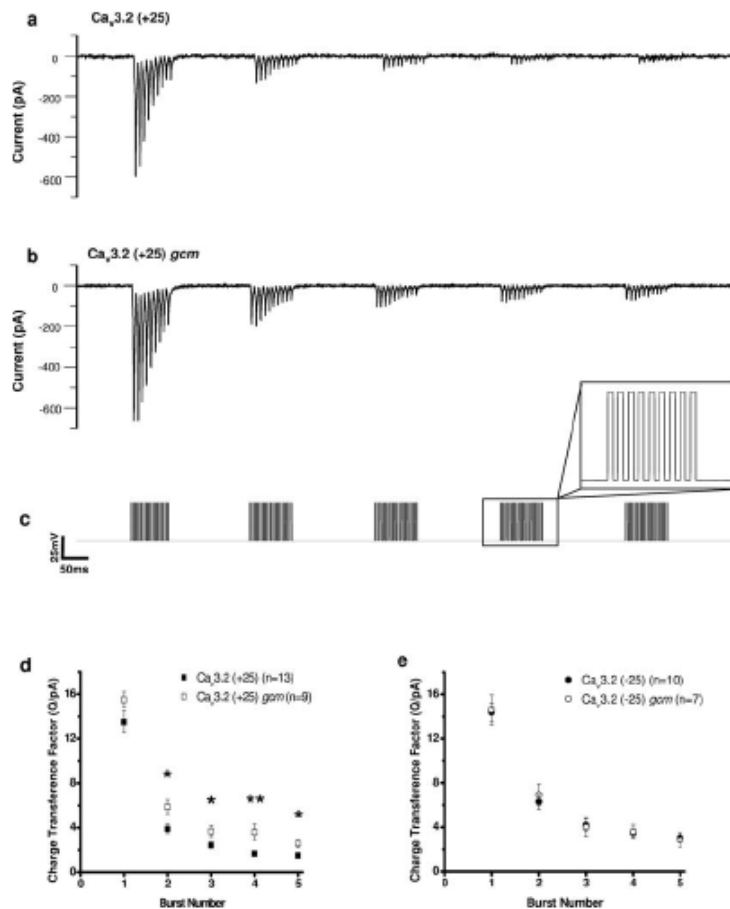


Figure 5. The *gcm* increases the charge transference of Ca_v3.2 (+25) during high-frequency burst depolarizing trains. *a–c*, Representative traces of Ca_v3.2 (+25) wild-type (*a*) and Ca_v3.2 (+25) *gcm* (*b*) currents recorded during high-frequency depolarizing train pulses (125 Hz for 80 ms) from −70 to −20 mV occurring in bursts (5 Hz for 1 s) (*c*). Charge transference of Ca_v3.2 during each burst was divided by the peak current on first pulse of the first burst to account for variations in current magnitude. *d*, In Ca_v3.2 (+25), the *gcm* significantly increased the charge transference factor in all subsequent bursts after one 125 Hz burst. *e*, In Ca_v3.2 (−25), the *gcm* had no significant effect on the charge transference factor. Data are represented as mean ± SEM. **p* < 0.05, ***p* < 0.01, significant difference between charge transference factors (ANOVA).

vals (Fig. 4*e,f*). During multiple depolarizations, this would produce larger Ca²⁺ currents in cells expressing Ca_v3.2 (+25) *gcm* channels, potentially increasing excitability and promoting epileptogenesis (Contreras, 2006).

To assess the potential effect of the *gcm* on the properties of Ca_v3.2 (±25) splice variants during neuronal burst firing conditions, we designed a voltage waveform that used high-frequency burst depolarizing pulses (Fig. 5, Table 3). Ca_v3.2 (+25) *gcm*-containing channels generated a significantly greater value for the charge transference factor in all subsequent bursts after one 125 Hz burst compared with Ca_v3.2 (+25) channels (Fig. 5*d*). Conversely, the *gcm* had no effect on the charge transference factor during high-frequency bursts in Ca_v3.2 (−25) channels (Fig. 5*e*). The increased charge transference factor observed in Ca_v3.2 (+25) *gcm* channels may be directly related to the increased rate of recovery from inactivation, because a faster recovery from inactivation may lead to an increase in the channels available to conduct on subsequent depolarizations.

Discussion

Here we report the first genetic abnormality with a functional effect in any of the spontaneously epileptic rat models of absence epilepsy. We identified a mutation in GAERS (*gcm*) in the rat ortholog of *CACNA1H*, wherein mutations have been identified previously in human absence epilepsy patients (Chen et al., 2003; Liang et al., 2006, 2007; Heron et al., 2007). Examining crosses between NEC and GAERS animals, we found that the presence of the *gcm* mutation segregated with seizure expression in the F1 progeny. These results provide evidence that the *gcm* mutation plays a significant role in the absence epilepsy phenotype, but the mutation does not, by itself, account for the entire phenotype. Some rats that were null for the *gcm* still displayed absence seizures, albeit significantly less often than those possessing the mutation. Correlation analysis indicated that the presence of *gcm* accounted for approximately one-third of the variance for the percentage time in seizures and the number of seizures. These findings are consistent with the current idea that IGE is a polygenic disease (Crunelli and Leresche, 2002; Rudolf et al., 2004; Glasscock et al., 2007). Rudolf et al. (2004) mapped various seizure-related quantitative trait locus (QTL) in GAERS versus Brown Norway rat double crosses to chromosomes 4, 7, and 8. The relevant genes and genetic mutations within the regions represented by these QTLs have not been

identified. Our group has reported an increase in expression of both stargazin mRNA and protein in the cortex and thalamus of GAERS (Powell et al., 2008), the gene for which (*Cacng2*) lies within the QTL on chromosome 7. However, the genetic

Table 3. Mean \pm SEM charge transference values for Ca_v3.2 (\pm 25) splice variants in the presence and absence of the *gcm* during high-frequency bursts

	Charge, Ca _v 3.2 (+25)	Transference, Ca _v 3.2 (+25) <i>gcm</i>	Factor, Ca _v 3.2 (–25)	Q/pA, Ca _v 3.2 (–25) <i>gcm</i>
Burst 1	13.5 \pm 1.0	15.5 \pm 0.7	14.4 \pm 0.8	14.6 \pm 1.3
Burst 2	3.9 \pm 0.4	5.9 \pm 0.6*	6.3 \pm 0.7	6.9 \pm 1.0
Burst 3	2.4 \pm 0.3	3.7 \pm 0.5*	4.2 \pm 0.6	4.0 \pm 0.8
Burst 4	1.67 \pm 0.2	3.6 \pm 0.7**	3.5 \pm 0.4	3.6 \pm 0.6
Burst 5	1.5 \pm 0.2	2.6 \pm 0.4*	3.1 \pm 0.4	2.8 \pm 0.6

ANOVA, * $p < 0.05$, ** $p < 0.01$ compared with wild-type control.

cause for this is still unknown. The Rudolf study failed to identify a QTL on chromosome 10, the location of the Ca_v3.2 gene, but the primary seizure variables associated with the QTLs in this study were the duration, amplitude, and cycle frequency of the spike-and-wave discharges, which we found were not associated with the *gcm* (Fig. 2). The only significant association found with the number of seizures expressed, the variable that we found to be most strongly associated with *gcm*, was with the QTL on chromosome 7 in 6-month-old (but not 3-month-old) rats. The only other genetic abnormality reported in GAERS is an extra alanine residue in a polyalanine tract in the potassium channel, KCNK9 (Holter et al., 2005). However, no functional consequences of this mutation have been identified *in vivo* or *in vitro*.

Our study also identified two major Ca_v3.2 channel splice variants expressed in the rat thalamus, Ca_v3.2 (+25) and Ca_v3.2 (–25), which differ in the presence or absence of the small exon 25. Of particular interest is the finding that the ratio of Ca_v3.2 (+25) mRNA to Ca_v3.2 (–25) mRNA is greater in the thalamus of GAERS animals compared with NECs, suggesting that the relative proportion of Ca_v3.2 (+25) to Ca_v3.2 (–25) is subjected to transcriptional regulation. Whether the increase in relative expression of the +25 variant in GAERS is a direct effect of *gcm* on splicing or an indirect effect on transcription is unknown.

In Ca_v3.2 (+25) channels transiently expressed in HEK293 cells, the *gcm* induces a faster rate of recovery from inactivation, thereby promoting a Ca²⁺ charge transference of greater magnitude during burst firing conditions. Contrastingly, in Ca_v3.2 (–25) channels, the *gcm* modestly slows recovery and has no effect on charge transference during bursts. It would appear that the *gcm* increases the rate of recovery of Ca_v3.2 (+25) channels to a rate similar to that of channels without the 25 exon segment, Ca_v3.2 (–25). It is not known whether this is attributable to the separate mechanisms of *gcm* and exon 25 acting in opposition or whether the *gcm* acts to somehow silence the functional effect of exon 25 inclusion. Whether Ca_v3.2 (+25) and Ca_v3.2 (–25) splice variants are expressed selectively or coexpressed in the same cells is also unknown. If the splice variants are coexpressed within cells, there would be an expected heterologous population of both fast (– exon 25) and slow (+ exon 25) recovering channels in *gcm* +/+ animals. The occurrence of the *gcm* in *m/m* animals would drive all cells expressing Ca_v3.2 channels to a fast recovering type, which may increase synchrony of neuronal firing. Alternatively, if the splice variants are expressed in a mutually exclusive manner, the *gcm* change would be predicted to produce a cell-specific increase in excitability.

T-type Ca²⁺ channels underlie a low-threshold spike that plays an important role in the generation of oscillatory thalamocortical rhythms and in the switch between tonic and burst firing patterns (Destexhe and Sejnowski, 2002; Contreras, 2006; Joksovic et al., 2006). Increased Ca_v3.2 expression and increased T-type currents have been detected in the nRT

of GAERS and WAG/Rij (Tsakiridou et al., 1995; Talley et al., 2000; Kim et al., 2001; Broicher et al., 2008), suggesting that Ca_v3.2 channels may be a strong candidate for contribution to SWD generation in the thalamocortical network. This is supported by computational modeling, demonstrating that increased T-type activity has the ability to promote burst firing (Chorev et al., 2006) and that temporal changes in Ca_v3.2 conductance alone can synchronize oscillations (Huguenard and Prince, 1992). Thus, the larger currents achieved by the *gcm* in Ca_v3.2 (+25) channels during high-frequency bursts alone may be sufficient to induce oscillations. The *gcm* might render neurons of the nRT more susceptible to excitatory corticothalamic and thalamocortical inputs, producing more robust bursting activity. However, the net result of increased Ca²⁺ charge transference during high-frequency bursts is difficult to discern because of the intricacy of the neuronal network involved. In addition, although it may seem logical that the *gcm* would increase the duration of seizure activity attributable to longer-lasting Ca²⁺ conductance during burst firing, there is no direct evidence as yet to confirm that Ca_v3.2 channels are the molecular pacemaker controlling bursting. Aside from any direct biophysical effects of the mutation on excitability, it is also possible that increased Ca²⁺ entry might enhance Ca²⁺ signaling, with the potential to alter gene expression (Rudolf et al., 2004). Ca²⁺ as a signaling molecule has numerous cellular effects and Ca_v3.2 channels, for example, are known to induce increased expression of high-voltage-activated Ca²⁺ channels and to induce neuritegenesis (Chemin et al., 2002).

The expression of different splice variants is now recognized as an important mechanism by which the diversity of cellular effects required for normal functions in different tissues and cell types is achieved. Splice variation in the Ca_v3.1 and Ca_v3.3 T-type Ca²⁺ channels has also been shown to alter electrophysiological properties and provides a general molecular mechanism for the functional diversity of T-type Ca²⁺ channels (Mittman et al., 1999a,b; Monteil et al., 2000; Chemin et al., 2001; Murbartián et al., 2002, 2004). Genetic mutations that have physiological effects only in selected splice variants may be an important mechanism by which some disease-causing mutations exhibit their well defined temporal and spatial phenotypes (Adams et al., 2007). As previously noted, alternative splicing of exon 26 in the human Ca_v3.2 gene (corresponding to the rat exon 25) alters the rate of recovery from inactivation (Ohkubo et al., 2005; Zhong et al., 2006). Our findings show that modification of rat exon 25 by the upstream *gcm* in Ca_v3.2 (\pm 25) splice variants can also alter the rate of recovery from inactivation. Thus, the III–IV linker region of Ca_v3.2 appears to be critically involved in the recovery from inactivation of T-type channels, potentially modulating the stability of the inactivated state. Consistent with our findings, there is also evidence that the III–IV linker region of

Ca_v3.1 channels contributes to T-type channel inactivation (Chemin et al., 2001; Staes et al., 2001).

Overall, the results of our study emphasize that the effects of missense mutations and the effects of alternative splicing on ion channel function must be considered together. Missense mutations that produce little or no direct changes in channel function may nevertheless interfere with regulatory sequences and lead to aberrant splicing, especially if, as found in the human Ca_v3.2 gene, some of the mutations flank splicing junctions (Liu et al., 2001; Zhong et al., 2006). Zhong et al. (2006) have described the splice variations in the human Ca_v3.2 gene and characterized their effects electrophysiologically (Zhong et al., 2006). Importantly, they demonstrated the interdependency of the effect of these variants. Our study extends this further to demonstrate that T-type channel mutations can have measurable functional effects in only certain splice variants. This provides a mechanism by which genetic mutations could produce spatial and temporal cell-type-specific effects dependent on splice variant expression patterns. This concept has potentially important implications for the pathophysiology of the IGEs wherein mild perturbations in the balance of activity between interconnected neuronal networks results in an epileptic phenotype but otherwise retains normal neurological functioning. It may also help explain both why somatic genetic mutations have been observed to result in seizures arising exclusively from topographically restricted focal brain regions (Fukata et al., 2006).

References

- Adams PJ, Garcia E, Snutch TP, Spacey SD (2007) Splice variant composition of P/Q-type calcium channels affects both biophysical properties and sensitivity to an FHM point mutation. *Biophys J* 92:602A.
- Broicher T, Kanyshkova T, Meuth P, Pape HC, Budde T (2008) Correlation of T-channel coding gene expression, IT, and the low threshold Ca²⁺ spike in the thalamus of a rat model of absence epilepsy. *Mol Cell Neurosci* 39:384–399.
- Carbone E, Lux HD (1984) A low voltage-activated, fully inactivating Ca channel in vertebrate sensory neurones. *Nature* 310:501–502.
- Chemin J, Monteil A, Bourinet E, Nargeot J, Lory P (2001) Alternatively spliced α_{1G} (Ca_v3.1) intracellular loops promote specific T-type Ca²⁺ channel gating properties. *Biophys J* 80:1238–1250.
- Chemin J, Nargeot J, Lory P (2002) Neuronal T-type α_{1H} calcium channels induce neurogenesis and expression of high-voltage-activated calcium channels in the NG108–15 cell line. *J Neurosci* 22:6856–6862.
- Chen Y, Lu J, Pan H, Zhang Y, Wu H, Xu K, Liu X, Jiang Y, Bao X, Yao Z, Ding K, Lo WH, Qiang B, Chan P, Shen Y, Wu X (2003) Association between genetic variation of CACNA1H and childhood absence epilepsy. *Ann Neurol* 54:239–243.
- Chorev E, Manor Y, Yarom Y (2006) Density is destiny. On the relation between quantity of T-type Ca²⁺ channels and neuronal electrical behavior. *CNS Neurol Disord Drug Targets* 5:655–662.
- Contreras D (2006) The role of T-channels in the generation of thalamocortical rhythms. *CNS Neurol Disord Drug Targets* 5:571–585.
- Crunelli V, Leresche N (2002) Childhood absence epilepsies: genes, channels, neurons and networks. *Nat Rev Neurosci* 3:371–382.
- Destexhe A, Sejnowski TJ (2002) The initiation of bursts in thalamic neurons and the cortical control of thalamic sensitivity. *Philos Trans R Soc Lond B Biol Sci* 357:1649–1657.
- Fukata Y, Adesnik H, Iwanaga T, Bredt DS, Nicoll RA, Fukata M (2006) Epilepsy-related ligand/receptor complex LGII and ADAM22 regulate synaptic transmission. *Science* 313:1792–1795.
- Glasscock E, Qian J, Yoo JW, Neebels JL (2007) Masking epilepsy by combining two epilepsy genes. *Nat Neurosci* 10:1554–1558.
- Heron SE, Khosravani H, Varela D, Bladen C, Williams TC, Newman MR, Scheffer IE, Berkovic SF, Mulley JC, Zamponi GW (2007) Extended spectrum of idiopathic generalized epilepsies associated with CACNA1H functional variants. *Ann Neurol* 62:560–568.
- Holter J, Carter D, Leresche N, Crunelli V, Vincent P (2005) A TASK3 channel (KCNK9) mutation in a genetic model of absence epilepsy. *J Mol Neurosci* 25:37–51.
- Huguenard JR, Prince DA (1992) A novel T-type current underlies prolonged Ca²⁺-dependent burst firing in GABAergic neurons of rat thalamic reticular nucleus. *J Neurosci* 12:3804–3817.
- Joksovic PM, Nelson MT, Jevtic-Todorovic V, Patel MK, Perez-Reyes E, Campbell KP, Chen CC, Todorovic SM (2006) Cav3.2 is the major substrate for redox regulation of T-type Ca²⁺ channels in the rat heart and mouse thalamus. *J Physiol* 574:415–430.
- Khosravani H, Altier C, Simms B, Hamming KS, Snutch TP, Mezeyova J, McRory JE, Zamponi GW (2004) Gating effects of mutations in the Cav3.2 T-type calcium channel associated with childhood absence epilepsy. *J Biol Chem* 279:9681–9684.
- Khosravani H, Bladen C, Parker DB, Snutch TP, McRory JE, Zamponi GW (2005) Effects of Cav3.2 channel mutations linked to idiopathic generalized epilepsy. *Ann Neurol* 57:745–749.
- Kim D, Song I, Keum S, Lee T, Jeong MJ, Kim SS, McEnery MW, Shin HS (2001) Lack of the burst firing of thalamocortical relay neurons and resistance to absence seizures in mice lacking α_{1G} T-type Ca²⁺ channels. *Neuron* 31:35–45.
- Liang J, Zhang Y, Wang J, Pan H, Wu H, Xu K, Liu X, Jiang Y, Shen Y, Wu X (2006) New variants in the CACNA1H gene identified in childhood absence epilepsy. *Neurosci Lett* 406:27–32.
- Liang J, Zhang Y, Chen Y, Wang J, Pan H, Wu H, Xu K, Liu X, Jiang Y, Shen Y, Wu X (2007) Common polymorphisms in the CACNA1H gene associated with childhood absence epilepsy in Chinese Han population. *Ann Hum Genet* 71:325–335.
- Liu HX, Cartegni L, Zhang MQ, Krainer AR (2001) A mechanism for exon skipping caused by nonsense or missense mutations in BRCA1 and other genes. *Nat Genet* 27:55–58.
- Liu L, Zheng T, Morris MJ, Wallengren C, Clarke AL, Reid CA, Petrou S, O'Brien TJ (2006) The mechanism of carbamazepine aggravation of absence seizures. *J Pharmacol Exp Ther* 319:790–798.
- Llinás R, Yarom Y (1981) Electrophysiology of mammalian inferior olivary neurones in vitro. Different types of voltage-dependent ionic conductances. *J Physiol* 315:549–567.
- Marescaux C, Micheletti G, Vergnes M, Depaulis A, Rumbach L, Warter JM (1984) A model of chronic spontaneous petit mal-like seizures in the rat: comparison with pentylentetrazol-induced seizures. *Epilepsia* 25:326–331.
- Marescaux C, Vergnes M, Depaulis A (1992) Genetic absence epilepsy in rats from Strasbourg: a review. *J Neural Transm Suppl* 35:37–69.
- Mattson RH (2003) Overview: idiopathic generalized epilepsies. *Epilepsia* 44 [Suppl 2]:2–6.
- Mittman S, Guo J, Emerick MC, Agnew WS (1999a) Structure and alternative splicing of the gene encoding alpha1I, a human brain T calcium channel alpha1 subunit. *Neurosci Lett* 269:121–124.
- Mittman S, Guo J, Agnew WS (1999b) Structure and alternative splicing of the gene encoding alpha1G, a human brain T calcium channel alpha1 subunit. *Neurosci Lett* 274:143–146.
- Monteil A, Chemin J, Bourinet E, Mennessier G, Lory P, Nargeot J (2000) Molecular and functional properties of the human α_{1G} subunit that forms T-type calcium channels. *J Biol Chem* 275:6090–6100.
- Murbartian J, Arias JM, Lee JH, Gomora JC, Perez-Reyes E (2002) Alternative splicing of the rat Ca_v3.3 T-type calcium channel gene produces variants with distinct functional properties(1). *FEBS Lett* 528:272–278.
- Murbartian J, Arias JM, Perez-Reyes E (2004) Functional impact of alternative splicing of human T-type Cav3.3 calcium channels. *J Neurophysiol* 92:3399–3407.
- Ohkubo T, Inoue Y, Kawarabayashi T, Kitamura K (2005) Identification and electrophysiological characteristics of isoforms of T-type calcium channel Ca_v3.2 expressed in pregnant human uterus. *Cell Physiol Biochem* 16:245–254.
- Peloquin JB, Khosravani H, Barr W, Bladen C, Evans R, Mezeyova J, Parker D, Snutch TP, McRory JE, Zamponi GW (2006) Functional analysis of Cav3.2 T-type calcium channel mutations linked to childhood absence epilepsy. *Epilepsia* 47:655–658.
- Perez-Reyes E (2003) Molecular physiology of low-voltage-activated t-type calcium channels. *Physiol Rev* 83:117–161.
- Powell KL, Kyi M, Reid CA, Paradiso L, D'Abaco GM, Kaye AH, Foote SJ, O'Brien TJ (2008) Genetic absence epilepsy rats from Strasbourg have

- increased corticothalamic expression of stargazin. *Neurobiol Dis* 31:261–265.
- Rudolf G, Thérèse Bihoreau M, F Godfrey R, P Wilder S, D Cox R, Lathrop M, Marescaux C, Gauguier D (2004) Polygenic control of idiopathic generalized epilepsy phenotypes in the genetic absence rats from Strasbourg (GAERS). *Epilepsia* 45:301–308.
- Staes M, Talavera K, Klugbauer N, Prenen J, Lacinova L, Droogmans G, Hofmann F, Nilius B (2001) The amino side of the C-terminus determines fast inactivation of the T-type calcium channel $\alpha 1G$. *J Physiol* 530:35–45.
- Talley EM, Solórzano G, Depaulis A, Perez-Reyes E, Bayliss DA (2000) Low-voltage-activated calcium channel subunit expression in a genetic model of absence epilepsy in the rat. *Brain Res Mol Brain Res* 75:159–165.
- Tsakiridou E, Bertollini L, de Curtis M, Avanzini G, Pape HC (1995) Selective increase in T-type calcium conductance of reticular thalamic neurons in a rat model of absence epilepsy. *J Neurosci* 15:3110–3117.
- Vitko I, Chen Y, Arias JM, Shen Y, Wu XR, Perez-Reyes E (2005) Functional characterization and neuronal modeling of the effects of childhood absence epilepsy variants of CACNA1H, a T-type calcium channel. *J Neurosci* 25:4844–4855.
- Vitko I, Bidaud I, Arias JM, Mezghrani A, Lory P, Perez-Reyes E (2007) The I-II loop controls plasma membrane expression and gating of $Ca_v3.2$ T-type Ca^{2+} channels: a paradigm for childhood absence epilepsy mutations. *J Neurosci* 27:322–330.
- Zhang Y, Vilaythong AP, Yoshor D, Noebels JL (2004) Elevated thalamic low-voltage-activated currents precede the onset of absence epilepsy in the SNAP25-deficient mouse mutant coloboma. *J Neurosci* 24:5239–5248.
- Zhong X, Liu JR, Kyle JW, Hanck DA, Agnew WS (2006) A profile of alternative RNA splicing and transcript variation of CACNA1H, a human T-channel gene candidate for idiopathic generalized epilepsies. *Hum Mol Genet* 15:1497–1512.